Novel Ligands for the study of Inositol Polyphosphate-Converting Enzymes

Kendall Baker

A thesis submitted to the University of East Anglia for the degree of Doctor of Philosophy

University of East Anglia

School of Biological Sciences

Norwich

September 2016

Abstract

The human genome encodes a number of inositol phosphate phosphatases that act upon inositide or phosphoinositide substrates. Among these, the 5-phosphatases have become targets for therapeutic intervention in human pathologies including cancers and diabetes. Of these, SHIP1 and SHIP2 (SH2-domain-containing inositol 5-phosphatase 1 & 2), which dephosphorylate phosphatidylinositol 3,4,5-trisphophate have received particular attention. In this study, attempts have been made to solve X-ray crystallographic structures of these proteins in complex with physiologically relevant inositide and phosphoinositide ligands or substrate analogs. The substrate analogs that have proved most useful include a family of benzene polyphosphates (BzPs) and biphenyl polyphosphates (BiPhs). This thesis describes the cloning and expression of the catalytic domains of SHIP1 and SHIP2 in *E. coli*, purification of these proteins and structural studies thereon. A structure was solved to 2.75 Å for apo SHIP2cd and from this, and existing literature, a homology model was made for SHIP1cd.

While BiPhs have been reported as ligands of 5-phosphatases, this thesis extends their use to the study of a inositol phosphate kinase; *Arabidopsis thaliana* inositol 1,3,4,5,6-pentakisphosphate (AtIPK1). An enzyme catalysing reversible phosphotransfer between ATP and IP_5. Structures were solved to 2.1 Å of ternary complexes between AtIPK1, BiPh and ADP, the structures reveal the adoption by the protein of a 'half-closed' conformation, reported previously only in the presence of nucleotide alone.

Close scrutiny of the structures of BiPh/protein complexes prompted their examination as potential inhibitors of SHIP1, SHIP2 and AtIPK1. A fluorescence polarisation ligand displacement assay was constructed with a fluorescein-tagged inositol phosphate and comparisons were made of the efficacy of different biphenyl phosphates in displacement of this ligand.

The same polarisation assay was used to screen the NCI Diversity Set II for inhibitors of SHIP2 and AtIPK1. A number of compounds were identified, and characterised for dose response with these proteins. Similar screens, which included SHIP1, were performed with the NCI Approved Oncology Drug Set V. Potential lead compounds were taken forward for characterisation of their ability to inhibit AtIPK1.

Table of Contents

Chapter 2

Structural studies of Human SHIP1 and SHIP2

Chapter 3

Chapter 6

Index of Tables

Index of Figures

Acknowledgements

Firstly, I would like to thank my supervisor Dr Charles Brearley for providing me with such a great opportunity to work and study with him and the rest of lab 1.44. An even bigger thank you for sourcing funding for the project, and the ongoing support and kind patience I have received and am most grateful for at a particularly trying time in my life. My secondary supervisor Dr Andrew Hemmings, who provided unequivocal protein crystallography and structure guidance as well as offering wise words and a place to vent (cry).

Hayley, you guided me in every way possible for the past four years, five if you can include when I was a mere 21 year old undergraduate project student in the lab. It's hard to find a suitable way to ever express my gratitude. You offered me so much understanding, kindness and advice, as well as your brilliant scientific knowledge. It wouldn't have happened without you, and I'm not sure I would have stuck it out. Most of all, you are a brilliant friend who always provided entertainment during long lab hours and it was a pleasure working with you (plus you make good cake!). Megan and I are both very lucky to have had you guide us through our Ph.D. projects.

An ongoing and never-ending thank you is owed to my parents who have always made me feel so proud of myself, and have provided generous and unwavering support throughout my academic studies. They have always encouraged me to do what makes me happy without judgement, pressure or expectation.

I'd also like to thank Megan Gilmartin, Arthur Li, Marcus Edwards for their help, support, advice, and last minute pre-viva preparations. Alexandra Howat, who as an already long standing friend provided invaluable moral support when experiencing post-graduate life together. And finally, Eileen Gallagher who left the lab for pastures new part way through the project but whose PCR skills, cat stories and hilarity were missed for the remainder.

Chapter 1

1.1 Introduction

1.1.1 Inositol polyphosphates and phosphoinositides

All eukaryotic organisms and most archaea contain inositol phosphates (inositides) and/or inositol-containing phospholipids (phosphoinositides) that have diverse roles in biochemical, physiological and developmental processes, and particularly in animal cells in cell proliferation and differentiation (Michell, 2009, Michell, 2011). Though, in the case of inositides (phytate, inositol hexakisphosphate), first identified as a phosphate storage compound in seeds, the remit of these molecules has been extended to include many aspects of cell biology. In recent years, these molecules have been implicated in the control of many nuclear processes including the regulation of chromatin remodeling, gene expression, mRNA export and DNA repair (Irvine, 2003, York, 2006).

1.1.1a myo-inositol structure and nomenclature

Myo-inositol is the simple framework upon which inositol polyphosphates (IPs) are built. IPs exclusively contain just inositol and phosphate, and are water soluble. *Myo*-inositol consists of a six-carbon ring (cyclohexane), each with hydroxyl moieties and a hydrogen atom. It is the most common of the inositol stereoisomers found in nature, with a further eight stereoisomers found in nature in which the axial/equatorial orientation of the hydroxyl groups vary, but they will not be discussed further in this text (Turner et al., 2012). *Myo*-inositol (Ins) has an axial hydroxyl group at the 2-position of the ring with the remainder of the hydroxyl groups positioned equatorially. It assumes a thermodynamically stable chair conformation. To help with its visualisation and nomenclature it is often likened to a turtle in an analogy called Agranoff's turtle (Agranoff, 1978) (Figure 1.1).

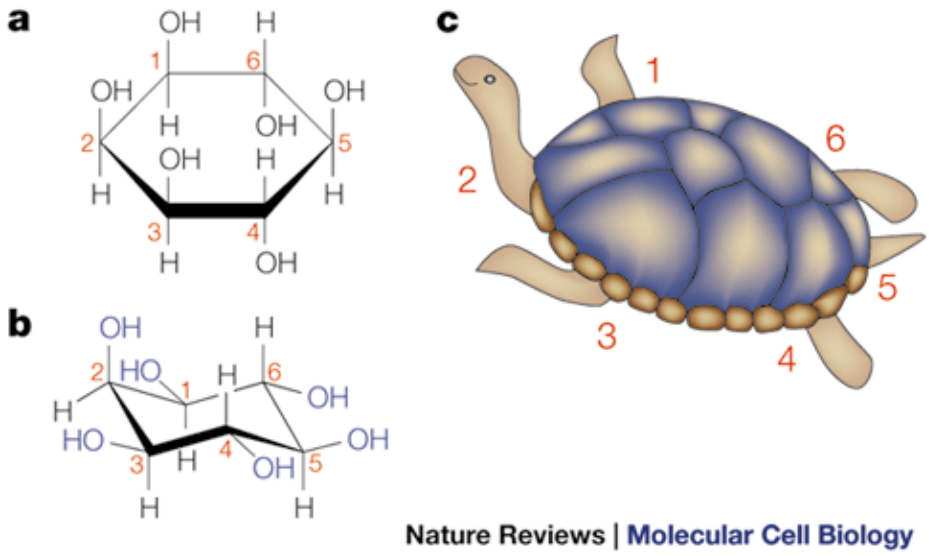

Figure 1.1 – The structure of *myo*-inositol and Agranoff's turtle. Taken from Irvine and Schell, 2001. (a) Haworth projection (b) The thermodynamically stable chair structure (c) Agranoff's turtle analogy.

The carbon positions are analogous to the turtle's extremities and are labeled anticlockwise using the D-numbering system beginning with its front right flipper, the turtle's head is the axial hydroxyl whilst the flippers and tail are the hydroxyl groups that lie in the plane of the ring (equatorial). Ins is achiral due to a plane of reflection within the molecule that lies along the C2 - C5 axis, but substitution of certain hydroxyl groups can make it optically active. Inositol polyphosphates (IPs), as the name suggests, are phosphorylated inositols. There are 63 possible IPs (excluding those with pyrophosphate moieties, more correctly called diphosphoinositol phosphates) and most of these inositol phosphates exist biologically, though only a few have been extensively studied and their metabolisms defined (Irvine and Schell, 2001).

Inositol lipids (phosphoinositides), in addition to inositol and phosphate contain a hydrophobic component usually consisting of two fatty acids esterified to a diacylglycerol moiety, with the 1-hydroxyl of the inositol ring attached through a diester phosphate. For many years, inositol lipid research dominated over inositol phosphates due to their roles in important cellular processes. They can be phosphorylated at the 3, 4, & 5 positions to create an array of 7 molecules that have discrete functions in signalling pathways (Astle et al., 2011).

1.1.1b General synthesis

Before considering the biosynthesis of the physiologically relevant inositol phosphates it is necessary to start with the unit upon which they are built. The route in which Ins is synthesised has been referred to as the Loewus pathway (Eisenberg et al., 1964, Chen and Charalampous, 1966, Sherman et al., 1969b, Loewus and Loewus, 1980, Loewus et al., 1980). The synthesis of Ins begins with the conversion of D-glucose-6-phosphate to 1D-*myo*-inositol 3-phosphate (Ins3P), catalysed by *myo*-inositol-3-phosphate synthase (MIPS) (Eisenberg, 1967, Barnett et al., 1973, Sherman et al., 1969a). This is followed by dephosphorylation by *myo*-inositol monophosphatase (IMP) (Eisenberg, 1967, Gee et al., 1988, Yoshikawa et al., 1997) (Figure 1.2). Although IMP is acting upon Ins3P in this scheme it can also dephosphorylate other isomers of inositol phosphates, excluding inositol 2-phosphate, and cannot dephosphorylate inositol phosphates with additional phosphate moieties (Eisenberg, 1967, Gee et al., 1988, Yoshikawa et al., 1997).

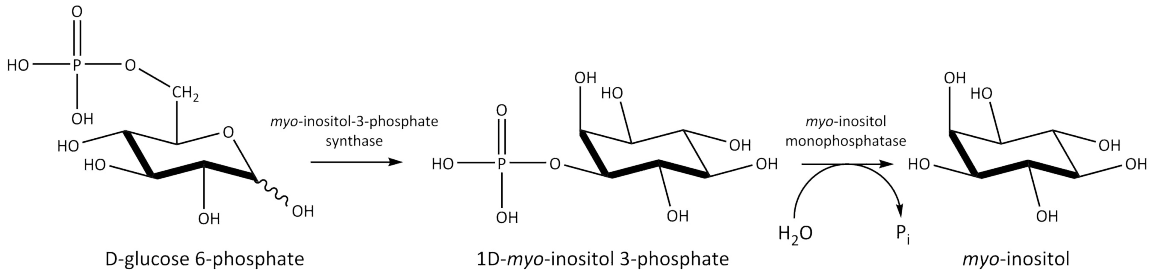

Figure 1.2 – *myo*-inositol biosynthesis

Inositol is incorporated into lipids by the chemical combination of activated phosphatidic acid (CMP-PtdOH) to form phosphatidylinositol (PtdIns). The liberation of Ins(1,4,5)P_3 by the receptor-activated and PtdIns(4,5)P_2-directed phospholipase C (PLC) isoforms, is in eukaryotes, an additional route of production of this specific IP_3 that lends itself to the production of the higher inositol phosphates. Animals and yeast depend on this 'lipid-dependent' pathway to produce the inositol phosphates through IP_3 to IP_6, but plants and slime moulds, and perhaps also animal cells, have an added ability to sequentially phosphorylate from Ins3P through to IP_6, omitting the lipid intermediate (Brearley and Hanke, 1996, Odom et al., 2000, Ongusaha et al., 1998, Saiardi et al., 1999, Stephens and Irvine, 1990, York et al., 1999). Polyphosphoinositides have not been shown to exist in prokaryotes. Although PtdIns has been identified in some prokaryotes, no inositol phosphates derived from membrane lipids have been found so far, nor has the route by which prokaryotes break down inositol lipids been characterised (Irvine, 2005, Lee and Ballou, 1964).

As mentioned previously, Ins3P is generated by MIPS during Ins synthesis, in addition to this it is known that in plants and slime moulds Ins3P can be synthesised from Ins by phosphorylation via an inositol 3-kinase (English et al., 1966, Loewus et al., 1982, Stephens and Irvine, 1990). Furthermore, in animals Ins3P can be produced as a product of dephosphorylation of Ins(3,4)P_2 by inositol-3,4-bisphosphate 4-phosphatase (Howell et al., 1989, Norris et al., 1995, Norris et al., 1997). This enzyme can also hydrolyse Ins(1,3,4)P_3 to Ins(1,3)P_2.

1.1.2 Physiological roles and metabolism of Inositol phosphates and phosphoinositides

1.1.2a Diverse signaling roles of phosphoinositides – regulation of Akt activation and human disease

Following receptor activation (eg. receptor tyrosine kinase) by an agonist, PI3K (phosphoinositide 3-kinase) is recruited to the membrane where phosphorylation of phosphatidylinositol 4,5-bisphosphate (PtdIns(4,5)P_2) occurs to generate PtdIns(3,4,5)P_3. This then recruits proteins with lipid-binding domains to the membrane, for example the serine/threonine kinase Akt (protein kinase B) (Figure 1.3).

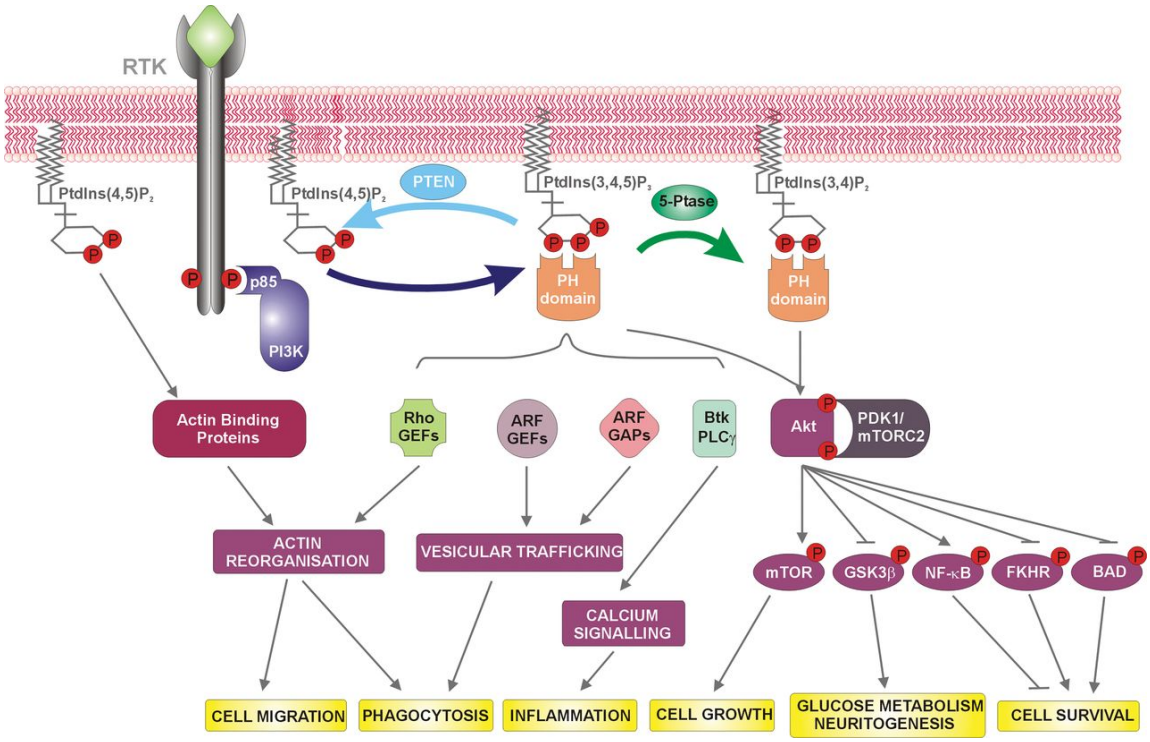

Figure 1.3 – Schematic of signaling pathways dependent on the regulation of phosphoinositides. Taken from Ooms et al., 2009.

The activating protein of Akt, phosphoinositide–dependent kinase (PDK1) is also recruited. The Pleckstrin Homology (PH) domain of Akt can bind to both PtdIns(3,4,5)P_3 and PtdIns(3,4)P_2 and on doing so becomes phosphorylated and activated by PDK1 and mTORC2 (mammalian target of rapamycin complex 2) (Alessi et al., 1997, Sarbassov et al., 2005). Akt then disassociates from the membrane to elicit a variety of responses via the phosphorylation of downstream effectors, eg. GSK3β (glycogen synthase kinase 3β), which goes on to promote glucose uptake. Others include proteins that promote cell growth and cell survival (Ooms et al., 2009, Manning and Cantley, 2007). More widely known, PtdIns(3,4,5)P_3 also promotes the recruitment of phospholipase C (PLC) resulting in IP_3 mediated Ca^{2+} signalling. PtdIns(3,4,5)P_3 levels are not only governed by its synthesis by PI3K, but its degradation by phosphatases. For example, SHIP1 and SHIP2 (chapter 2) and other 5-phosphatases, as well as the 3-phosphatase, PTEN. It is unsurprising given the diversity of second messengers and effector proteins associated with phosphoinositides that their regulation has implications in disease. The relative levels of the different signalling phosphoinositides are dependent on the receptor activated as well as cell type and tissue specific expression of phosphoinositide phosphatases (Ooms et al., 2009).

1.1.2b Inositol hexakisphosate (IP_6)

As well as playing many important roles in cell biology, such as mRNA export, DNA repair, maintenance of basal resistance to plant pathogens, apoptosis, and regulation of chromatin structure (Ives et al., 2000), inositol hexakisphosphate is the most abundant inositol phosphate derivative in plants and provides the main form of phosphorus storage in seeds as the salt, phytate. It allows for the retrieval of phosphorus, inositol and minerals during development and germination. It also accumulates in other plant tissues and organs such as pollen, roots, and tubers (Raboy, 2003). Human grain based diets provide excess of IP_6 which can bring about detrimental effects on health. This is such because it is a potent chelator of essential ions such as Zn^{2+} and Fe^{2+}, which causes deficiencies that can contribute to malnutrition (Raboy, 2001), an issue affecting third world countries in particular. In contrast to this detrimental effect, phytate can act as a powerful antioxidant, which can be advantageous in cancer prevention by preventing the formation of hydroxyl radicals and suppression of lipid peroxidation (Graf et al., 1987). There are also environmental concerns as monogastric animals are unable to digest IP_6, which is excreted as salts that contribute to eutrophication of waterways. It is in the latter steps of inositol synthesis where IP_6 is formed from inositol 1,3,4,5,6-pentakisphosphate (IP5) by 2-phosphorylation of the inositol ring and is catalysed by a family of enzymes called inositol 1,3,4,5,6-pentakisphosphate 2-kinases (IPK1) (see chapter 3).

1.1.3 Inositol polyphosphate surrogates and substrate mimics

1.1.3a Benzene polyphosphates

The long standing interest in Ins(1,4,5)P_3 3-kinases and Ins(1,4,5)P_3 5-phosphatases in the study of disease and cell regulatory processes has led to the synthesis of inositol polyphosphate surrogates as simple alternatives to chemically synthesising complex inositol polyphosphates, which is a time consuming process involving long multistep routes and protecting group chemistry (Ward et al., 1995, Mills et al., 2006, Mills et al., 2007, Mills et al., 2008). Benzene polyphosphates represent achiral polyanionic analogues of inositol phosphates in which the inositol ring is replaced by a planar aromatic core. This ceases any conformational flexibility arising from within the ring, with the only flexibility occurring from the phosphate groups, which provides new and intriguing ligands for inositol phosphate metabolising enzymes. Additionally, the nature of the benzene ring may encourage the formation of new intermolecular ligand-protein interactions such as π–cation interactions that are not observed in inositol polyphosphates (Vandeput et al., 2007). The structures of each of the benzene phosphates that have been provided by collaborators (Potter, B.V.L., Bath, UK) for this study can be seen in Table 1.1.

Studies have shown that such compounds can inhibit PI 3-kinase (PI3K), type I Ins(1,4,5)P_3 5-phosphatase (INPP5A) and the SH2-domain-containing inositol 5-phosphatase, SHIP2. Bz(1,2,4)P_3 (Bz5) in particular was found to inhibit PI3K activity with an IC50 of 25 μM (Ward et al, 1995). In another study it was found to inhibit both PI3K (IC50 6.1 μM) and INPP5A (IC50 32 μM), as well as interacting with the Ins(1,4,5)P_3 receptor and weakly inhibiting Ca^{2+} release (Poitras et al, 1993). Furthermore, both INPP5A and SHIP2 activity is inhibited by Bz(1,2,3,4)P_4 (Bz1), Bz(1,2,3,5)P_4 (Bz2), and Bz(1,2,4,5)P_4 (Bz3) (Vandeput et al, 2007).

Table 1.1 – Structures, chemical names, abbreviations and the references given for the purpose of this text for the benzene phosphates (Mills et al., 2006, Mills et al., 2007, Mills et al., 2008).

Name	Abbreviation	Reference	Structure
benzene 1,2,3,4-tetrakisphosphate	$Bz(1,2,3,4)P_4$	Bz1	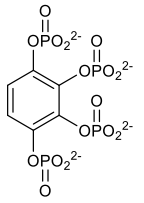
benzene 1,2,3,5-tetrakisphosphate	$Bz(1,2,3,5)P_4$	Bz2	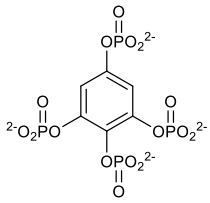
benzene 1,2,4,5-tetrakisphosphate	$Bz(1,2,4,5)P_4$	Bz3	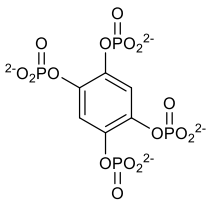
benzene 1,2,3-trisphosphate	$Bz(1,2,3)P_3$	Bz4	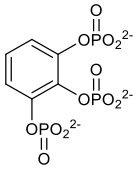
benzene 1,2,4-trisphosphate	$Bz(1,2,4)P_3$	Bz5	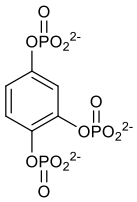
benzene 1,3,5-trisphosphate	$Bz(1,3,5)P_3$	Bz6	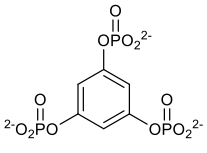
3-hydroxybenzene 1,2,4-trisphosphate	$3\text{-OH-}Bz(1,2,4)P_3$	Bz7	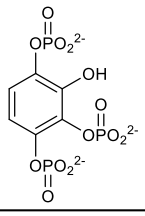

The first crystal structure of a benzene phosphate in complex with a protein was with the PH-domain of protein kinase Bα (Mills et al., 2007). Bz(1,2,3,4)P_4 (Bz1) co-crystallised with the PH-domain and bound with a IC50 of 6.35 μM when compared with 6.22 μM for the natural head group Ins(1,3,4,5)P_4, and therefore was identified as an effective inositol phosphate surrogate even though it is structurally removed from the natural lipid head group.

Since these studies, all of the benzene phosphate compounds 1-7 in Table 1.1 have been shown to inhibit the activity of INPP5A with only Bz 1-6 exhibiting effects on the PH-domain of PKBα (Mills et al, 2008).

Interestingly, 3-hydroxybenzene 1,2,4-trisphosphate (Bz7) has also been characterised as a substrate for INPP5A, which removes the 2-phosphate to yield the symmetrical 2,3-digydroxybenzene 1,4-bisphosphate, and was the first non-inositol based compound to be a substrate for a 5-phosphatase (Mills et al, 2006).

Recently, the crystal structure of type II inositol polyphosphate 5-phosphatase (INPP5B), has been solved to 2.9 Å in complex with Bz(1,2,4,5)P_4 (Bz3), which has offered new insights in to the mechanism of INPP5B-catalysed phosphate group cleavage (Mills et al, 2016). Unlike INPP5A, it is able is hydrolyse both inositol phosphates and inositol phospholipids.

1.1.3b Biphenyl polyphosphates

The benzene polyphosphates were identified as novel inositol 5-phosphatase inhibitors for use as molecular tools for studies within intact cells. This prompted a further pursuit for phosphatase inhibitors of this family of enzymes to facilitate comparison of their catalytic domains. Consequently, a better understanding of their individual functions and control of intracellular levels of inositol phosphates and phosphoinositides would follow (Vandeput et al., 2007).

The discovery of the inhibition of Ca^{2+} release via the Ins(1,4,5)P_3 receptor by Bz(1,2,4)P_3 (Bz5), and the studies that followed between the benzene phosphates and type I Ins(1,4,5)P_3 5-phosphatase (INPP5A) (Poitras et al, 1993, Mills et al, 2006), incited the synthesis of a highly novel and related derivative. The compound biphenyl(2,3',4,5',6)P_5 (BiPh1) consists of five phosphates across two phenyl rings (Table 1.2), and was found to be the most potent inhibitor of INPP5A and SHIP2 across the series of inhibitors at that point. Furthermore, it was found, like the BzPs, to bind to the Ins(1,4,5)P_3 receptor and inhibit Ins(1,4,5)P_3 induced Ca^{2+} release in permeabilised cells (Vandeput et al., 2007). Just like the benzene phosphates they have been shown to substitute for inositol phosphates and phosphoinositides in many incidences since. Four biphenyl polyphosphate compounds exist in this current series of related inositol 5-phosphatase inhibitors (Table 1.2).

Table 1.2 – Structures, chemical names, abbreviations and the references for the purpose of this text of the biphenyl polyphosphates (Vandeput et al., 2007, Mills et al., 2012, Mills et al., 2016). Substituents on the 'lower ring' are represented with a comma.

Name	Abbreviation	Reference	Structure
biphenyl 2,3',4,5',6-pentakisphosphate	BiPh(2,3',4,5',6)P_5	BiPh 1	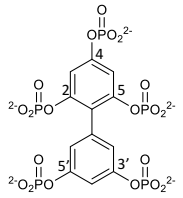
biphenyl 2,2',4,4',5,5'-hexakisphosphate	BiPh(2,2',4,4',5,5')P_6	BiPh 2	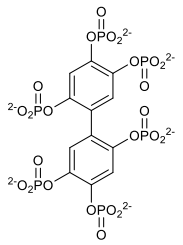
biphenyl 3,3',4,4',5,5'-hexakisphosphate	BiPh(3,3',4,4',5,5')P_6	BiPh 3	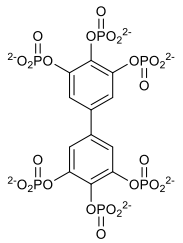
6,6'-difluorobiphenyl 3,3',4,4'-tetrakisphosphate	6,6'-F_2-BiPh(3,3',4,4')P_4	BiPh 4	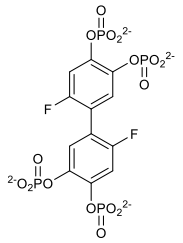

In a subsequent study that focused on the PH domain of PKBα as well as INPP5A, BiPh1 was also identified as an inhibitor alongside the Bz compounds, not including Bz7, that did not bind to the PH domain of PKBα (Mills et al, 2008). This led to molecular modeling of BiPh1 docked in to the active site of the PH-domain of PKBα based on the previous crystal structure in complex with Bz1 (Mills et al, 2007). Where the aryl 2,4,6-trisphosphate motif docks to the same amino acid residues as Bz1, and the 3',5'-bisphosphate motif is potentially implicated in a cation-π interaction with an arginine residue (Mills et al, 2008). These structures, along with PKBα PH domain in complex with Ins(1,3,4,5)P_4, led to the development of a docking protocol to identify drug-like inhibitors by virtual screening (Du-Cuny et al, 2009).

Later came a 2.1 Å resolution crystal structure of BiPh1 coordinated in a shallow pocket, containing the inositol phosphate-binding site, of the 5-phosphatase, SHIP2 (Mills et al, 2012). In this structure the majority of direct protein-ligand interactions are focused on the 6-phosphate of BiPh1 by a region assigned as the 4-phosphate interacting motif (P4IM), named as so because these residues coordinate the 4-phosphate of a natural substrate or product in the active site of type II inositol polyphosphate 5-phosphatase (INPP5B) and SPSynaptoganin (Mills et al, 2012) (Figure 1.4 – A). As discussed in chapter 2.

Recently, alongside the complex with Bz3 noted previously, the crystal structure of BiPh3 bound to the active site of INPP5B has been solved to a resolution of 2.89 Å (Mills et al, 2016). Again, the BiPh is bound in a shallow pocket with most of the interactions focused on the 3-, 4- and 5-phosphates of one ring of the compound (Figure 1.4 – B).

Given the current wealth of inhibitory and structural information on the synthetic benzene and biphenyl phosphates, they could find utility in early stage drug discovery and structure-based inhibitor design of phosphoinositide and inositol phosphate related pathways. This study begins to explore this further by exploiting their novel properties with three inositol phosphate metabolising enzymes.

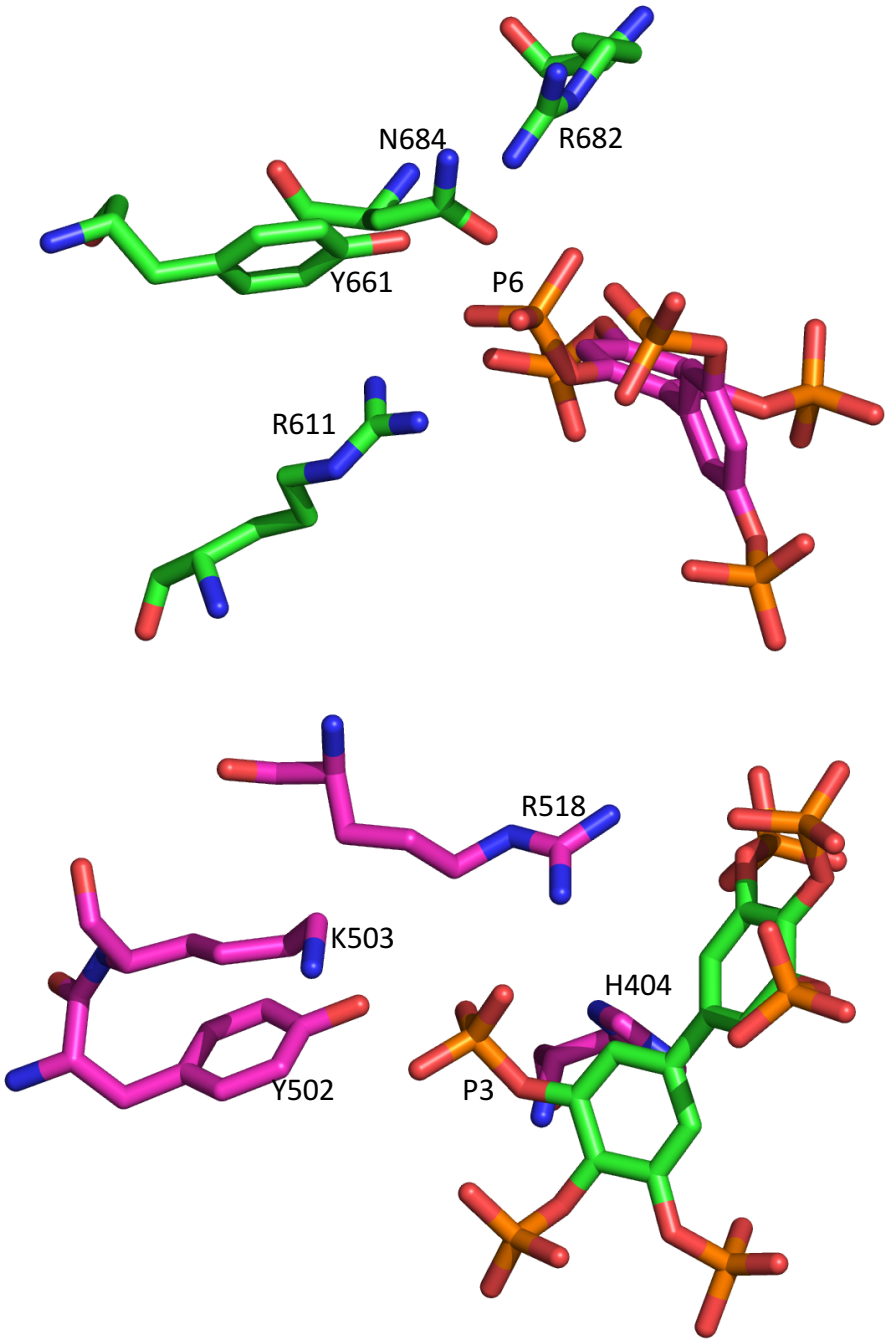

Figure 1.4 – Conserved 4-phosphate position of the 5-phosphatases. (A) P4IM residues within SHIP2 (green) in complex with BiPh1 (magenta). (B) P4IM residues within INPP5B (magenta) in complex with BiPh3 (green). Protein residues and ligands represented as sticks.

Chapter 2 – *Structural studies of Human SHIP1 and SHIP2*

2.1 Introduction

2.1.1 Inositol polyphosphate 5-phosphatases

The human inositol polyphosphate 5-phosphatases consist of ten isozymes, all of which can cleave the 5-phosphate from membrane-bound inositol phospholipids. Asides from type I inositol 5-phosphatase (INPP5A), named as such because it was the first family member to be purified and cloned, which specifically only acts on soluble inositol phosphates and regulates intracellular calcium signalling. The rest are either only able to hydrolyse the former or both (Ooms et al., 2009). The family also contains four yeast enzymes. Many of the 5-phosphatases are able to remove the 5-phosphate from PtdIns(3,4,5)P_3 to yield PtdIns(3,4)P_2, which in turn gets degraded by 4-phosphatases and terminates PI3K/Akt signalling. The pathway is also deactivated by 3-phosphatase PTEN to yield PtdIns(4,5)P_2. Some 5-phosphatases are also active against PtdIns(4,5)P_2, and/or PtdIns(3,5)P_2. For these reasons they are implicated in many disorders such as cancer, diabetes, obesity and neurodegenerative diseases (Majerus and York, 2009). Additionally, the presence of phosphoinositides and inositol phosphates in the nucleus are implicated in the regulation of many cellular processes, including chromatin remodeling, gene expression, mRNA export and DNA repair (Irvine, 2003, York, 2006). Each contains a conserved 300 amino acid catalytic domain which is flanked by various functional domains, which via subcellular localisation and protein-protein interactions targets them for diverse, unique and tissue specific roles (Figure 2.1) (Eramo and Mitchell, 2016).

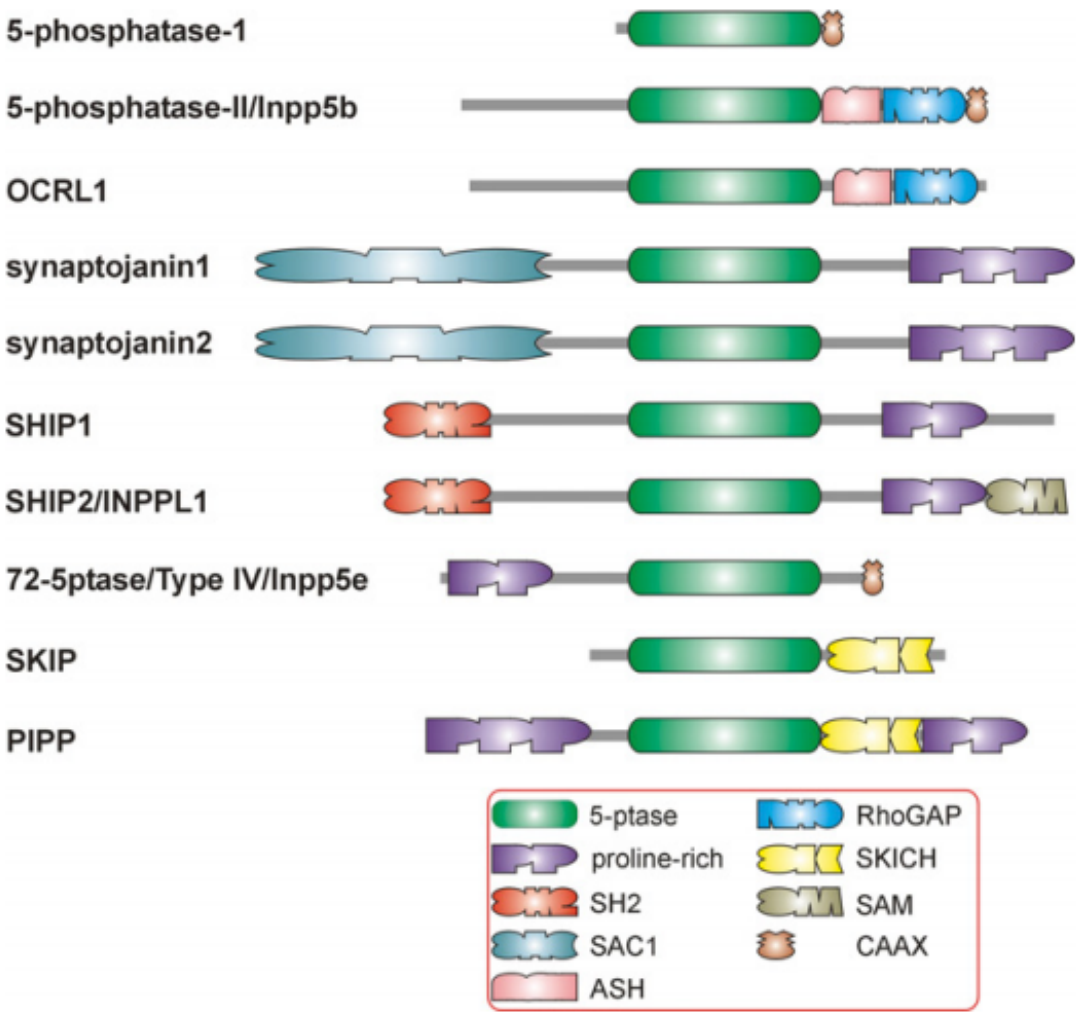

Figure 2.1 – Domain structure of the inositol 5-phosphatases. Taken from Ooms et al, 2009.

The catalytic activity and their substrate specificities for a range of phosphoinositides and inositol phosphates has recently been summerised by Eramo and Mitchell, 2016. The SH2 (Src homology 2)-containing inositol 5-phosphatase (SHIP1) and SHIP2, amongst others, preferentially degrade PtdIns(3,4,5)P_3 (*in vivo*). Whereas others preferentially degrade PtdIns(4,5)P_2, such as type II inositol 5-phosphatase and Synaptojanin 1.

2.1.2 SHIP1 - SH2 (Src homology 2)-containing inositol 5-phosphatase

The SHIP family encompasses SHIP1 and SHIP2. Both contain a SH2 domain N-terminal to their 5-phosphatase domain, NPXY motifs that can be tyrosine phosphorylated, and divergent proline rich domains C-terminal to the catalytic domain (Ooms et al., 2009, Mondal et al., 2012). SHIP1 was first identified as a 5-phosphatase that dephosphorylates PtdIns(3,4,5)P_3 to PtdIns(3,4)P_2, and Ins(1,3,4,5)P_4 to Ins(1,3,4)P_3 (Damen et al., 1996, Lioubin et al., 1996). The 145 kDa protein is expressed in haematopoietic cells and is an established key regulator of the immune system, with known implications in the negative regulation of various cellular processes via the inhibition of PI3K/Akt-dependent processes; including phagocytosis, cell migration, cell survival, proliferation and differentiation (Leung et al., 2009, Parry et al., 2010). SHIP1 $^{-/-}$ B-cells have shown resistance to cell death and possess enhanced proliferative activity due to increased Akt activity following receptor stimulation, attributed by greater PtdIns(3,4,5)P_3 and reduced PtdIns(3,4)P_2 signals (Brauweiler et al., 2000).

2.1.3 SHIP2 - SH2 (Src homology 2)-containing inositol 5-phosphatase 2

SHIP2 is a 142 kDa protein that, in terms of domain structure, is very similar to SHIP1, main differences lie in the fact that SHIP2 contains a SAM (sterile α motif) at its C-terminus and the sequence divergence in their proline rich regions (Backers et al., 2003). SAM domains span 70 residues and form five-helix bundles with two interaction interfaces. They can self-associate forming dimers and possibly more extended structures, with suggested additional abilities in RNA binding. Originally SHIP2 was recognised to dephosphorylate PtdIns(3,4,5)P_3 and Ins(1,3,4,5)P_4, but recently *in vitro* studies suggest a wider and preferred substrate specificity of Ins(1,2,3,4,5)P_5 > Ins(1,3,4,5)P_4 > PtdIns(3,4,5)P_3 ≈ PtdIns(3,5)P_2 ≈ Ins(1,4,5,6)P_4 (Pesesse et al., 1998, Chi et al., 2004). It is more ubiquitous than SHIP1 and is expressed in both haematopoietic and non-haematopoietic tissues, including brain, skeletal muscle, heart, and liver and kidney tissues, the latter to a lesser extent. SHIP2 plays a negative role in insulin signalling as has been demonstrated in many *in vitro* cellular models, where overexpression decreases insulin stimulated PI3K signalling and Akt activation which leads to reduced GLUT4 translocation to the plasma membrane, subsequently reducing

glucose uptake and glycogen synthesis (Blero et al., 2001, Wada et al., 2001). SHIP2 overexpression in mice reduces glucose tolerance and increases body weight due to decreased insulin-stimulated Akt phosphorylation (Kagawa et al., 2008). On the contrary, SHIP2 knockout mice are protected from high fat diet-induced obesity (Sleeman et al., 2005).

Inhibition of SHIP1 and SHIP2 activity, using pan-SHIP1/2 inhibitors and SHIP1 specific 3-α-aminocholestane (3AC), in cancer cell lines decreases Akt phosphorylation. Observations included reduced multiple myeloma (MM) cell growth and viability, and decreased IGF-1-induced phosphorylation of Akt in the presence of 3AC (Brooks et al., 2010). Additionally, pan-SHIP1/2 inhibitors in breast cancer cell lines prohibited SHIP2-mediated PtdIns(3,4,5)P_3 degradation, decreased IGF-1-stimulated phosphorylation of Akt and induced cell cycle arrest and apoptosis in a similar manner (Fuhler et al., 2012).

2.1.4 Structures of inositol polyphosphate 5-phosphatases

Crystal structures of five of the inositol 5-phosphatases are currently available. Four structures are available of type II inositol 5-phosphatase (INPP5B) alone, all in complex with ligands; diC_8PtdIns(4)P_1 (PDB 3MTC), diC_8PtdIns(3,4)P_2 (PDB 4CML), and most recently with biphenyl 3,3',4,4',5,5'-hexakisphosphate and benzene 1,2,4,5-tetrakisphosphate (BiPh3/Bz3- see section 1.1.3) (PDB 5A7I & 5A7J) (Trésaugues et al., 2014, Mills et al., 2016a). The 5-phosphatase domain of yeast *Schizosaccharomyces pombe* SPsynaptojanin in complex with Ins(1,4)P_2 and SHIP2 bound with biphenyl 2,3',4,5',6-pentakisphosphate are also available (PDB, 1I9Z & 4A9C, respectively) (Tsujishita et al., 2001, Mills et al., 2012). The structure of Lowe oculocerebrorenal syndrome protein (OCRL) has been resolved with an inorganic phosphate ion and is the closet structural family member to INPP5B (PDB 4CMN) (Trésaugues et al., 2014), Lastly, the apo-form of phospholipid-specific INPP5E is available (PDB 2XSW) .

No structure is available for SHIP1, but there are two structures available of the catalytic domain of the isozyme SHIP2 (SHIP2cd). One in the apo-form (PDB 3NR8), the other in complex with BiPh1, as mentioned above (Trésaugues et al., 2014, Mills et al., 2016a). The overall structure of this complex can be seen in Figure 2.2.

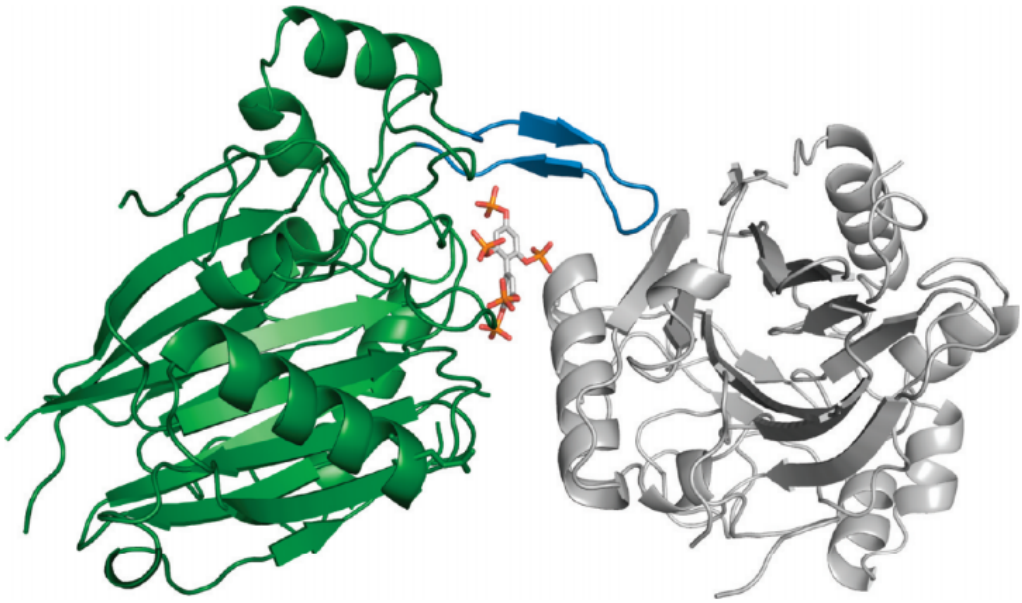

Figure 2.2 – Crystal structure of two SHIP2cd molecules. One molecule (green) has the biphenyl (2,3',4,5',6)P_5 bound in the shallow inositide binding pocket, and has additional interactions with a symmetry related molecule (grey). The flexible loop which is stabilised by interactions with the symmetry mate is shown in blue. Taken from Mills et al, 2012. (PDB 4A9C).

The two published crystal structures of SHIP2cd are in the same conformation and crystallise under similar conditions in the same space group, regardless of the presence of a ligand or not. The protein crystallises with two molecules in the asymmetric unit, with one molecule contacting a symmetry related molecule via a flexible loop that is consequently stabilised, it is disordered in the other molecule as it lacks the same contacts with a symmetry mate. A molecule of BiPh1 was only found in the inositide binding site of the molecule with the stabilised loop. The inositide binding site was originally identified from the complex between the related INNP5B and PtdIns(4)P. BiPh1 binds in to the shallow pocket via multiple interactions between the 3'- ,4- ,5'- and 6-phosphates (Figure 2.3). Nine water molecules are also found in the active site, eight of which mediate hydrogen bonds between phosphates of BiPh1 and SHIP2cd. The role of ligand coordinating residues are discussed in more detail in due course, as well as the role of the flexible loop above the active site that is stabilised and constrained by a symmetry related molecule in the crystal structure.

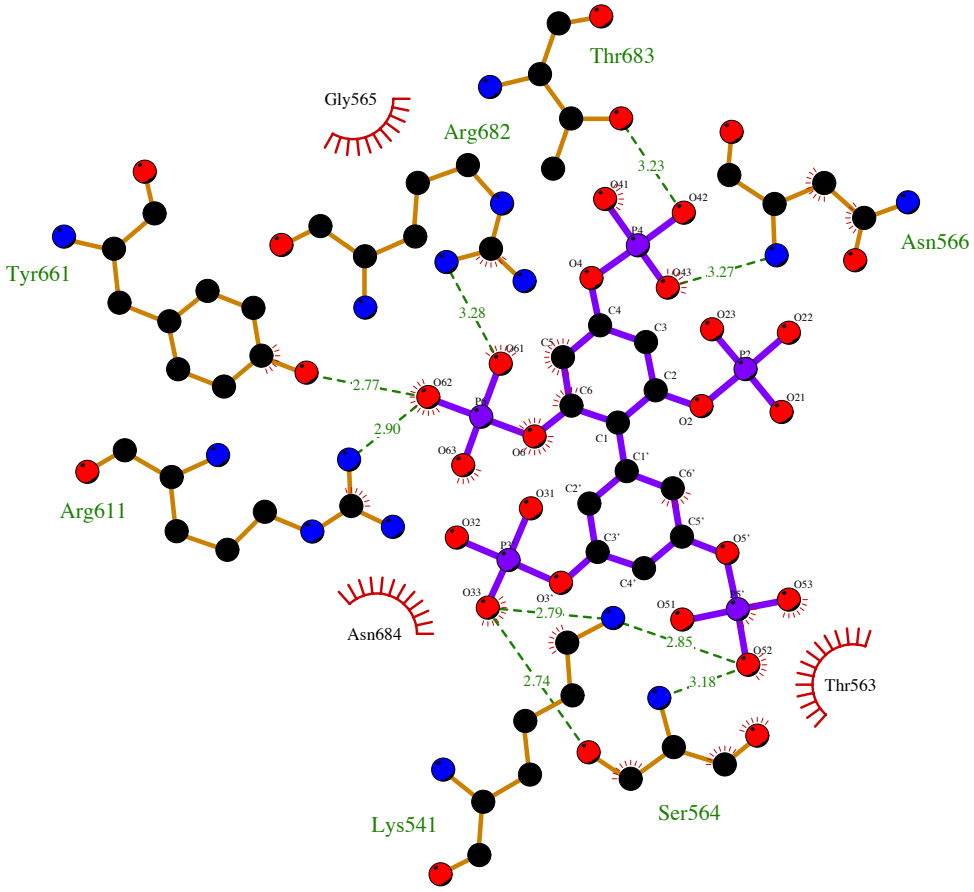

Figure 2.3 – LigPlot ligand interaction diagram of the coordination of biphenyl (3,3',4,4',5,5)P_6 by SHIP2cd.

Much is still left undiscovered when considering the mechanism of SHIP1 and SHIP2, and indeed the rest of the 5-phosphatases, although the first evidence and speculations on the mechanism have recently been revealed. These are based on the structure of INPP5B in complex with BiPh3 containing an inorganic phosphate (P_i) in the active site that is likely to be in the position of a liberated 5-phosphate, and acts directly with the expected catalytic base Asp-447. Arg-451 was for the first time considered as a catalytic residue due to its proximity to the P_i and its conservation across the 5-phosphatases (Mills et al., 2016a).

2.1.5 Experimental aims

No crystal structure of SHIP1 or its catalytic domain is currently available. Additionally there is an added lack of *in vitro* studies, as most characterisation has been done in terms of its regulation and its regulatory influence of the pathways it is implicated in within live cells. Therefore a key objective in this work was to clone *Ship1* (*INPPL1*) and its catalytic domain in to a suitably selected expression vector for overexpression and subsequent protein purification for use in *in vitro* binding and enzymatic assays. Secondly, attempts to crystallise the catalytic domain of SHIP1 (SHIP1cd) were made as it shares high homology with the catalytic domain of SHIP2, of which there is a structure. Comparison of crystal structures would confirm the presence of the extended loop above the active site that is said to be specific only to SHIP1 and SHIP2; in which in the latter it has already been identified (as introduced above). Secondly it may elucidate the mechanisms and residues responsible for their differing substrate specificities.

Furthermore, in light of the current structure of SHIP2cd in complex with BiPh1 and the concerns that come along with it; such as the BiPh1 interactions with a symmetry related molecule, it would be beneficial to gain more structures of SHIP2cd in complex with ligands and inhibitors. A good place to start was with the additional biphenyl- and benzene- phosphate compounds in Tables 1.1 & 1.2.

2.2 Materials and methods

2.2.1 Primers

Primers were designed manually and the necessary flanking sequences for the ligation independent cloning were added (Gileadi et al., 2008, Savitsky et al., 2010) (see Table 2.2). Synthesis was carried out by MWG Eurofins and the lyophilized primers were stored as 100 µM stocks in nuclease free water (Qiagen) at -20 °C. Diluted working stocks at 20 µM were made for use in PCR to prevent degradation of the main stock through repeated freeze-thaw.

2.2.2 PCR amplification using Phusion High Fidelity DNA polymerase

All PCR was carried out in a MJ Research Dyad Thermal Cycler. PCR amplification of *INPP5Dcd* and *INPP5D* was performed using Phusion High Fidelity Polymerase (New England Biolabs) as per manufacturer's instructions and using the primer sequences, annealing temperatures, and elongation times provided in Table 2. . Deoxynucleotide triphosphates; dATP, dTTP, dGTP & dCTP (Roche), were combined at equal concentration to give a working stock of 10 µM.

2.2.3 Agarose gel electrophoresis

A 1 % agaraose gel was used throughout and made by adding 1 g of electrophoresis grade agarose (Melford) to 100 mL 1 x TAE buffer (see Appendix 2). This was heated in a 600 W microwave for approximately 3 min and allowed to cool to 50 °C before addition of 5 µM 10 mg/mL ethidium bromide (Sigma-Aldrich). The gel was cast, adding a well comb, and allowed to set before placing in a Bio-Rad electrophoresis tank containing 1 x TAE buffer. Loading dye was added to the samples, and where appropriate either 10 % of the reaction or the full volume was loaded. Gels were run at 90-100 V until the loading dye had migrated a suitable distance. The resulting gel was imaged using a Bio-Rad Chemidoc Gel Imaging System.

2.2.4 PCR clean up

The appropriately sized band was excised from the gel under UV illumination and the Wizard® SV Gel and PCR Clean-Up System (Promega) used as per the supplied protocol.

2.2.5 Treatment with T4 DNA polymerase

Purified PCR product and/or plasmid were treated T4 DNA polymerase (Clontech) in the presence of the appropriate dNTP for 30 min at 11 °C followed by 20 min at 75 °C.

2.2.6 Plasmid DNA extraction

Plasmid purification from *E. coli* cells was performed using the Wizard® *Plus* SV Miniprep DNA Purification System (Promega) following suppliers standard protocol. Additionally, the sample was incubated at room temperature for 2 min after the addition of the Cell Lysis Solution, and again for 5 min before addition of 50 µL nuclease free water in the final steps of the protocol.

2.2.7 Preparation of chemically competent E. coli cells

Rosetta expression host *E. coli* cells (Novagen) were streaked on to a LB agar plate containing 34 µg/mL chloramphenicol (to maintain the chloramphenicol-resistant pRARE plasmid) from a -80 °C stored glycerol stock and incubated O/N at 37 °C. From the resulting growth, a single colony was selected to inoculate 5 mL of LB medium supplemented with chloramphenicol, and grown in a 37 °C shaking incubator O/N at 220 rpm. The resulting culture was used to inoculate SOB medium in a ratio of 3:500 mL (v/v) and incubated at 30 °C with shaking at 220 rpm until an OD_{595} of ~0.5 was reached. All further steps were carried out on ice or 4 °C, and with ice-cold buffers. A 10 min centrifugation at 5000 rpm of the ice-cold culture was used to obtain a pellet, which after decanting off the supernatant, was gently re-suspended in 100 mL TB buffer before incubation on ice for 10 min. After an identical second centrifugation step the pellet was re-suspend in 18.6 mL of TB buffer, plus an addition of 1.4 mL 1 M DMSO. The cells were then left to rest on ice for at least 10 min before being frozen in 100 µL aliquots in liquid nitrogen and stored at -80 °C in 0.5 mL micro-centrifuge tubes.

2.2.8 Transformation of E. coli standard protocol

Chemically competent *E. coli* cells were thawed on ice for 30 min and 50 µL transferred to a pre-chilled sterile 1.5 mL micro-centrifuge tube. Between 1 to 5 µL of plasmid DNA was added to the cells to obtain successful levels of transformants, and mixed by gentle pipetting before incubation on ice for 30 min. The cells were heat shocked in a 42 °C water bath for 45 sec and immediately returned to the ice for 2 min. Cell recovery and growth was achieved by an addition of 250 µL LB and shaking incubation of the cells at 37 °C for 1 h. The cells were gently centrifuged at 5000 rpm and the pellet re-suspended in 50 µL LB before the entire volume was spread on to a plate containing LB agar media and the appropriate selective antibiotics. The plate was then inverted and incubated O/N at 37 °C. The next day, a single colony was picked from the plate using a sterile pipette tip and used to inoculate 10 mL LB containing selective antibiotics. This was repeated for at least 5 single colonies. The cultures were then grown O/N in a shaking incubator at 37 °C.

2.2.9 Restriction digestion

Plasmid was digested with BsaI-HF restriction enzyme (New England Biolabs) as per manufacturer's guidelines with the appropriate buffer.

2.2.10 Screening of transformants by colony PCR

PCR was performed on 1 µL of O/N culture (section 2.2.8) using GoTaq® G2 Flexi DNA Polymerase (Promega) as per manufacturer's protocol, using the primers and parameters in Table 2. . The reaction mix was first incubated at 98 °C for 5 min to lyse the cells before adding the polymerase.

2.2.11 Plasmid sequencing

Aliquots of extracted plasmid were sent to Source BioScience for sequencing using the pLIC-for and pLIC-rev primers (Gileadi et al., 2008).

2.2.12 Glycerol stocks

Under sterile conditions, cultures were spread on to three plates containing LB agar media plus the appropriate selective antibiotics and incubated O/N at 37 °C. Liquid LB (1 mL) was added to each plate and scraped using a glass spreader to release the bacteria from the plate. The resuspended bacteria was aliquoted in to 1.5 mL microcentrifuge tubes and 330 µL 60 % glycerol (v/v) added before snap freezing in liquid nitrogen in preparation for storage at -80 °C. Bacteria were recovered by scraping the surface of the frozen culture using a sterile loop and streaking on to a selective LB agar plate.

2.2.13 Small scale expression testing of SHIP1cd-His

In sterile 30 mL tubes, 5 mL of LB was inoculated using 20 µL starter culture and grown to OD_{600} 0.5 at 37 °C. The cultures were incubated at 20 °C for 1 hr before addition of 0.2 mM or 0.5 mM IPTG (no addition to control samples) and incubated for a further 16 hrs at 200 rpm.

2.2.14 Preparation of polyacrylamide gels

The resolving gel (see appendix 2) was pipetted between 1 mm glass spacer plates held in casting frames on a casting stand (Bio-Rad), until the gel level was approximately 2 cm from the top of the front plate. Drops of isopropanol were immediately applied to the top of the gel until it was even and free of bubbles, before being left to polymerise for 1 h. The isopropanol was washed off with dH_2O and dried thoroughly with filter paper. The 5 % stacking gel was pipetted on top of the resolving gel up to the very top of the front plate and a 1 mm 10-well comb inserted, and again left to polymerise for 1 h. Gels not for immediate use were stored at 4 °C wrapped in cling film.

2.2.15 Preparation of samples for SDS-PAGE analysis

The relevant protein expression culture was removed from the shaking incubator at the required time-point and a 200 µL sample was transferred to a 1.5 mL microcentrifuge tube. The culture was then returned if necessary. The sample was centrifuged for 1 min at 13000 rpm, and the supernatant discarded. A 300 µL (or 1:1.5 (v/v)) aliquot of 1 x SDS loading buffer (see appendix 2) was used to re-suspend the resulting pellet before boiling for 7 min. Once cooled slightly the sample was pulse centrifuged. If working with purified or partially purified protein, centrifugation was skipped and 1:3 (v/v) of sample to 3 x SDS loading buffer was used.

The comb was removed from a pre-prepared polyacrylamide gel and the wells gently rinsed with dH_2O before being placed in the electrophoresis tank (Bio-Rad) filled with SDS running buffer (see appendix 2) to cover the gel. Typically 10 µL of the sample was loaded in to a well, with a protein molecular weight marker loaded as per manufacturer's instructions in an adjacent well. The gel ran at 150 – 180 V until the dye front was approximately 1 cm from the bottom of the gel. Once extracted from between the glass plates and rinsed with dH_2O, the gel was stained using either InstantBlue (Expedeon) or PageBlue (ThermoFischer scientific), according to the manufacturer's guidelines.

2.2.16 Large scale protein expression

Large-scale expression cultures were 1 L in volume and at least 2 L of expression culture was used per purification. Each 1 L LB plus antibiotic was inoculated using 10 mL of O/N culture and treated as per the small scale expression tests, adding the appropriate amount of IPTG for optimum expression. The 1 L expression cultures were centrifuged at 5000 rpm for 20 min at 4 °C, with each resulting pellet being resuspended in 10 mL cell lysis buffer (see appendix 2) before being snap frozen in liquid nitrogen and stored at -80 °C.

2.2.17 Standard protein purification protocol

The bacterial suspensions of the expression culture pellets were recovered from the freezer and thoroughly thawed on ice. Mechanical cell disruption was achieved by French press at a working pressure of 17000 PSI, with a maximum of 30 mL of suspension being loaded in to the cell at any one time. The suspension and lysate were kept on ice during all steps and each suspension was subjected to 3 passes through the French pressure cell to ensure complete homogenisation. Ultracentrifugation of the lysate at 40000 rpm and 4 °C for 1 h was used to remove the cell debris, and the supernatant carefully decanted in to a pre-chilled tube and stored on ice ready for loading on to a 5 mL Ni-NTA Superflow Cartridge (Qiagen).

Purification was carried out using an ÄKTAprime purification system (GE Lifesciences) at 4 °C. The 5 mL NiNTA superflow cartridge (Qiagen) was equilibrated with buffer A (see Appendix 2) and the supernatant loaded at 0.5 mL/min followed by an 80 mL wash with buffer A. A gradient of imidazole was applied to the column over 50 mL from 20 mM (buffer A) to 500 mM (buffer B) (see Appendix 2), followed by washing with 50 mL buffer B. Fractions were collected throughout; 10 mL during the wash phases and 2 mL during the imidazole gradient. The absorbance of the eluate was monitored at 280 nm, and from the resulting UV absorbance trace fractions containing protein could be identified. A sample was taken of each UV absorbing fraction to be analysed by SDS-PAGE. Fractions confirmed to contain protein were pooled and concentrated using an Amicon® stirred ultrafiltration cell with a 10 kDa cut off membrane to a volume of approximately 2.2 mL in preparation for loading on to a HiLoad 16/60 Superdex 75 column (GE Lifesciences) for size exclusion chromatography.

Again, the column was use in tandem with an ÄKTA prime purification system and equilibrated with 240 mL (two volumes) of sepharose buffer (see Appendix 2). After the concentrated protein was injected, the column was run at 1 mL/min with sepharose buffer for 120 mL. Throughout, 2 mL fractions of eluent were collected and monitored with the UV absorbance detector setting at 280 nm. From the resulting UV absorbance trace, fractions assumed to contain purified protein were first analysed by SDS-PAGE

before being pooled and concentrated. Protein concentration was estimated using a NanoDrop (Thermo Scientific) to measure absorbance at 280 nm together with the extinction coefficient to calculate protein concentration. The purified and concentrated protein was centrifuged at 13000 rpm for 5 minutes at 4 °C before being snap frozen in liquid nitrogen for storage at -80 °C.

2.2.18 Removal of 6xHistidine tag using TEV protease

Pro TEV plus protease (Promega) was used to remove the His-tag from SHIP1cd-His and SHIP2cd-His, following the manufacturers guidelines. In general, the protein was first concentrated to typically 1 – 2.5 mL to reduce the reaction volume, and the suggested volume of the supplied reaction buffer added. The reaction was found to be most effective at an ambient temperature of approximately 18 °C for 16 hr.

2.2.19 SHIP2cd crystal screening and optimisation

Although the conditions for the crystallisation of SHIP2cd were already established (Mills et al., 2012, Trésaugues et al., 2014), and therefore high throughput screening was not required, some optimisation was necessary. Crystals were grown in 96-well plates using a sitting drop method at 16 °C and equilibrated against a 25 µL reservoir of buffer that was used as a precipitant. For the structure presented in this study, optimal conditions were identified as 20 % PEG 6000, 0.1 M citric acid pH 5. Protein at 9 mg/mL, plus 10 mM $MgSO_4$, was incubated at 16 °C prior to setting drops in a 1:2 ratio of protein to precipitant. Crystals formed as needle clusters within 48 hr and were allowed to continue to grow for a further 48-72 hr. The crystals were separated as narrow individual plates and were harvested depending on crystal size and quality.

2.2.20 Crystal cyroprotection

Single crystals were harvested in to 20 % PEG 6000, 30 % ethylene glycol, 0.1 M citric acid pH 5, and flash frozen in liquid nitrogen.

2.2.21 Data collection

X-ray diffraction data was remotely collected at Diamond Light Source (Oxford) on beam line i24.

2.2.22 Data processing and refinement

X-ray diffraction data was indexed and auto processed using Xia2. Molecular replacement was performed using Phaser-MR within the Phenix suite (McCoy, 2007) and structures refined using Phenix refine (Afonine et al., 2005). Coot (Emsley et al., 2010) was used for manual adjustment to models between rounds of automatic refinement.

2.3 Results and Discussion

2.3.1 Expression and purification of SHIP2cd

An expression clone of *INPPL1cd* (SHIP2cd) in the vector pNIC-MBP was purchased via the Structural Genomics Consortium (SGC) from Source BioScience (Clone accession TC124029). The clone was supplied as an *E. coli* stock on an agar slope which was treated as per the supplier's recommendations before purifying the plasmid using the Wizard® *Plus* SV Miniprep DNA Purification System (Promega). To prepare the vector it was transformed into stellar competent *E. coli* cells (Clontech) and single kanamycin resistant colonies selected, from which overnight cultures were grown for high yield plasmid extraction. The plasmid was transformed into expression host, *E. coli* Rosetta2 cells, single kanamycin resistant colonies selected, and the expression of SHIP2cd-His tested via small scale expression tests (see section 2.2.13). Parameters investigated were; temperature, IPTG concentration and length of incubation post IPTG addition (results not shown).

Subsequently, large scale expression cultures were set up for purification of SHIP2cd-His. Two 1 L cultures were set up and expression carried out as outlined in methods (section 2.2.16) using 0.2 mM IPTG to induce protein expression (results not shown). It was later found that 4 L of culture was necessary to produce enough protein for crystallography studies.

SHIP2cd-His protein was purified as per the method described in section 2.2.17. The lysate of the 2 L culture was centrifuged to remove cell debris before loading the supernatant on to a 5 mL Ni-NTA superflow cartridge (Qiagen) for immobilised metal affinity chromatography. Figure 2.4 shows the SDS-PAGE analysis of fractions that were identified as containing SHIP2cd-His from the UV absorbance trace during nickel affinity purification. The overexpressed SHIP2cd-His (38.6 kDa) can be seen most prominently in fractions 16-24 (lanes 6-10), with the most heavy contamination occurring in fractions

16-20 (lanes 6-8). As these contaminated fractions also contained the highest yield of SHIP2cd they were pooled, along with fractions 22-24, for concentrating before size exclusion chromatography on a HiLoad 16/600 Superdex 75 pg column (GE Healthcare Life Sciences), performed according to section 2.2.17. Lane 3 shows the lysate after loading on to the NiNTA column and reveals that some of the SHIP2cd-His protein did not bind to the column, a higher capacity column may be considered for future purifications.

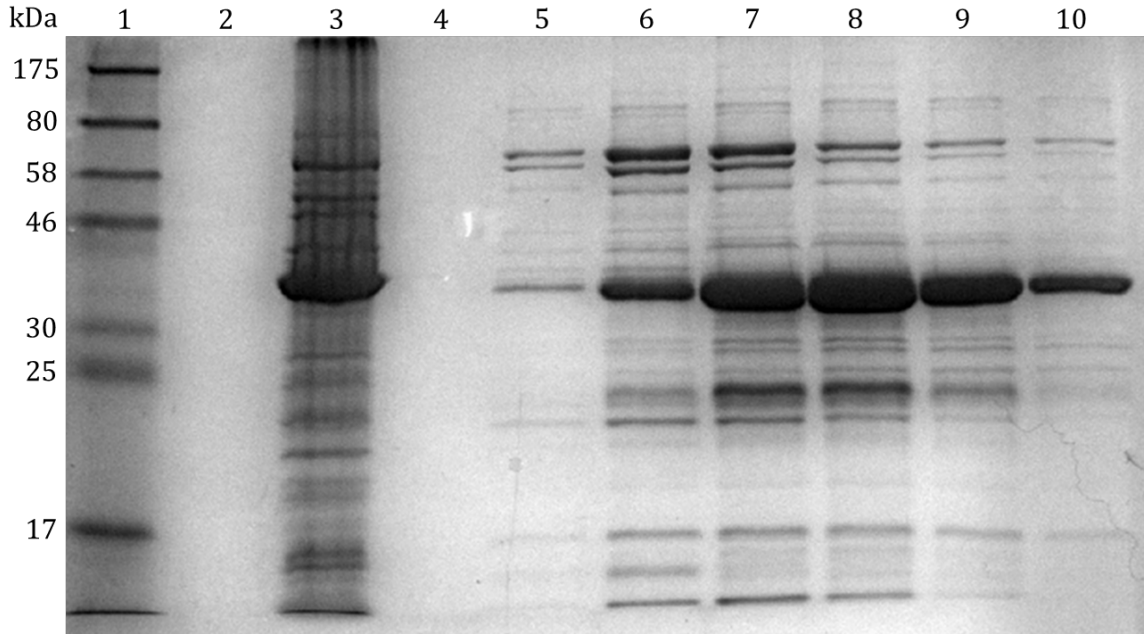

Figure 2.4- Immobilised metal affinity purification of SHIP2cd-His. SDS-PAGE analysis of eluate fractions recovered during NiNTA chromatography. (1) Protein molecular weight marker. (2) Empty. (3) Sample of supernatant post column loading. (4) Empty. (5-10) Fraction number; 14, 16, 18, 20, 22 & 24, respectively.

A sample of the final purified and concentrated protein was analysed by SDS-PAGE and stained with InVision™ His-tag In-gel Stain (Novex by Life Technologies), used as per manufacturer's guidelines. Subsequently, the same gel was stained with a Coomassie blue stain as per section 2.2.15 (Figure 2.5). As the sample was highly concentrated a 1:4 dilution of the protein was used.

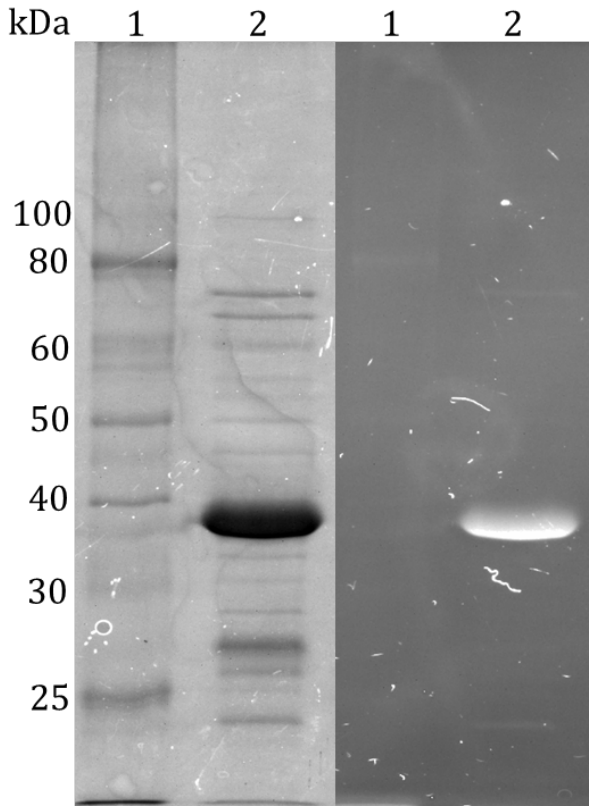

Figure 2.5 - Coomassie blue (left) and InVision staining (right) of purified SHIP2cd-His. (1) Protein molecular weight marker (2) 1:4 (v/v) dilution of purified SHIP2cd-His.

The final purified protein appears to have very little contaminants, bearing in mind the protein is at high concentration on the gel, and does not appear to have truncated protein with His tag which would be made visible by the InVision stain.

Cleavage of the 6xHistidine tag was set up post size exclusion chromatography using Pro TEV plus protease (Promega) after concentrating the protein to 2.5 mL volume. The manufacturer's guidelines were followed and the reaction was incubated for approximately 16 hr at room temperature (18 °C) (section 2.2.18).

A sample was taken prior to cleavage to compare to a post incubation sample, both of which were analysed by SDS-PAGE using a 12.5% acrylamide gel, with the aim to achieve a clear separation of the two samples in order to visualise the change in molecular weight that occurs when the 6xHistide tag is removed (Figure 2.6). The post TEV protease incubation sample is of lower molecular weight indicating the removal of the tag was successful, although some tagged protein still remained. Longer incubation or the use of more TEV protease should be considered to recover a higher yield of SHIP2cd.

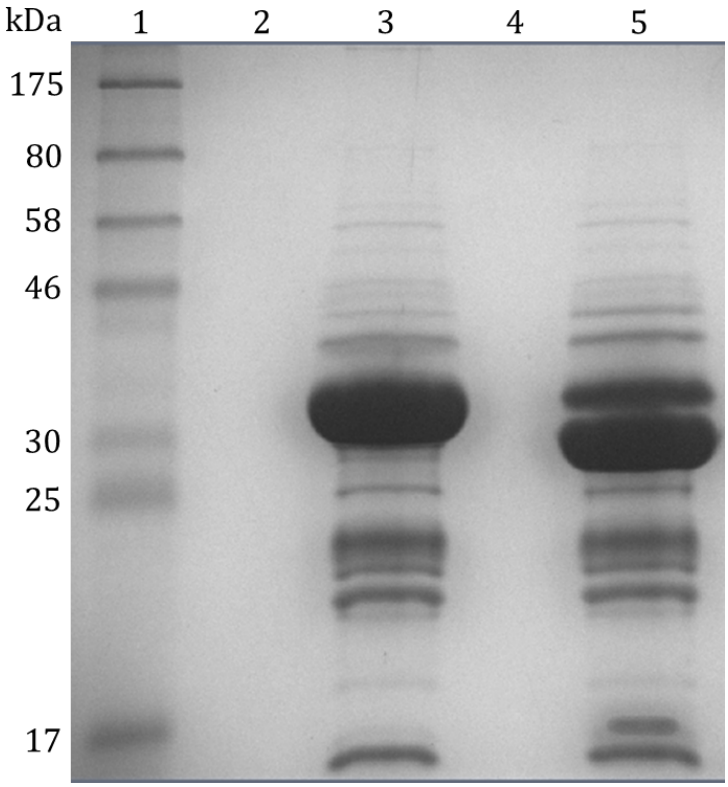

Figure 2.6 - SDS-PAGE analysis on a 12.5 % acrylamide gel of proteolytic cleavage of the N-terminal 6xHis tag from SHIP2cd-His using ProTEV plus protease. (1) Protein molecular weight marker. (2) Empty. (3) SHIP2cd-His. (4) Empty. (5) SHIP2cd post incubation with TEV protease.

The products of the His-tag cleavage reaction were loaded on to a 5 mL NiNTA superflow cartridge (Qiagen), equilibrated with buffer A (see appendix 2), at a flow rate of 0.5 mL/min in a continuous loop for 30 min. Elution of the column with buffer A at 1ml/min yielded SHIP2cd, collected in a 10 mL fraction and five subsequent 2 mL fractions. Subsequently, a single 10 mL fraction was collected in buffer B (results not shown).

The fractions containing SHIP2cd were pooled, concentrated to 2.2 mL and subjected to a final round of size exclusion chromatography (results not shown). Final purified SHIP2cd was concentrated to 9 mg/mL and snap frozen before storage at -80 °C. Figure 2.7 shows a sample of this preparation. The gel is overloaded to visualise the occurrence of contaminants, which are negligible when compared to the concentration of SHIP2cd. Final protein yield approximated to 9 mg/mL obtained from 4 L of expression culture.

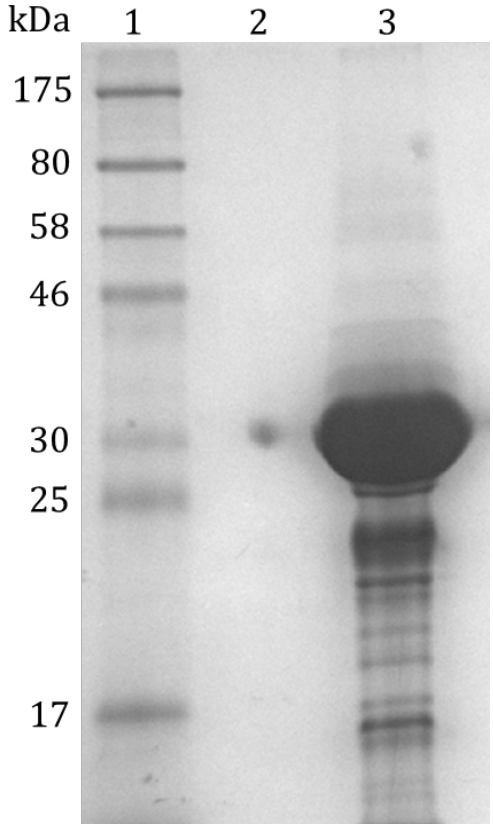

Figure 2.7 - SDS-PAGE analyisis on a 10 % gel of final purified SHIP2cd. (1) Protein molecular weight marker. (2) Empty. (3) Purified SHIP2cd.

2.3.2 Crystallisation of SHIP2cd

SHIP2cd was crystallised as per section 2.2.19, which was adapted from a previous method published by Mills et al, 2012. Crystals grew as individual plates or rods, appearing after 2 days and continued to grow for 3-5 days. Crystallisation was attempted several times and was not consistent, resulting in a lower than hoped for yields of crystals. Nevertheless, individual crystals were harvested into cryoprotectant and stored in liquid nitrogen (section 2.2.20). An example of a SHIP2cd crystal can be seen in Figure 2.8.

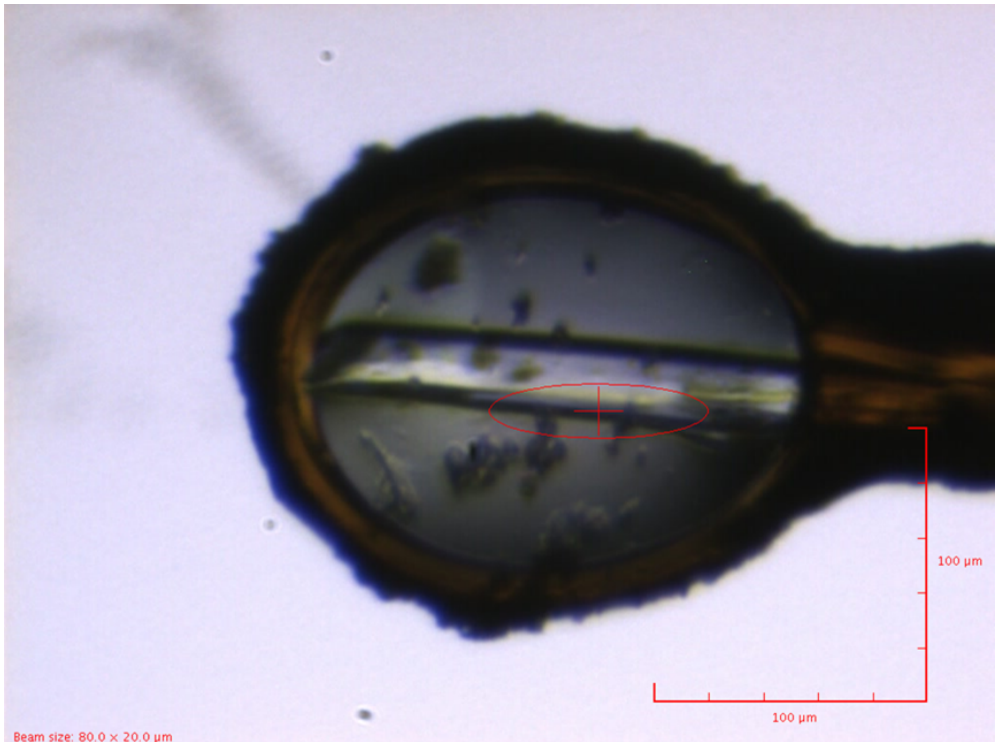

Figure 2.8 – Crystal of SHIP2cd exposed to the beamline for data collection at the Diamond Light Source.

2.3.3 Crystal structure of SHIP2cd

Attempts were made to crystallise SHIP2cd with biphenyl phosphate ligands. The work here was guided by the report of a crystal structure for a catalytic domain of SHIP2 with bound biphenyl 2,3',4,5'-pentakisphosphate ligand resolved to 2.1Å (Mills et al., 2012). Both co-crystallisation and soaking methods were implemented in attempts to obtain crystals of protein/ligand complexes. As well as optimisatisation of the previously published conditions, exploration of alternative conditions via high-throughput screening was also attempted. Prior to the work of Mills and coworkers (2012), the only structure of a 5-phosphatase catalytic domain that had been reported is that of *Schizosaccharomyces pombe* synaptojanin (SPsynaptojanin). The structure was determined in complex with a soluble inositol 1,4-bisphosphate product of 5-phosphatase action on inositol 1,4,5-trisphosphate (Tsujishita et al., 2001). As such, neither structure inform how 5-phosphatases as a class co-ordinate the lipid moieties of their phosphoinositide, particularly PtdIns(3,4,5)P_3, substrates. Since then, the work of Trésaugues et al., 2014, provided a number of structures of the catalytic domains of other 5-phosphatase family members: INPP5B in apo, PtdIns4P-bound and PtdIns(3,4)P_2-bound structures (PDB 3N9V, 3MTC and 4CML at 2.65Å, 2.4Å and 2.3Å respectively), SHIP2 in apo form (3NR8 at 2.8Å), and OCRL in apo form (4CMN at 3.13Å). It is noteworthy that the position of scissile 5-phosphate of substrate is lacking from all these structures.

Although no dataset could be gained here for SHIP2cd with this or any of a number of other biphenyl phosphate compounds, as initially described in the experimental aims, a successful data set for apo SHIP2cd was collected and refined to a resolution of 2.8 Å. Data processing and refinement in the $P2_1$ space group was achieved using the Phenix suite (Adams et al., 2010). Table 2.1 contains data collection and refinement statistics for the apo-protein.

Table 2.1 - X-ray diffraction data processing and model refinement statistics for SHIP2cd.

Data Processing	
Space Group	P 2_1
Unit Cell	
a, b, c (Å)	44.7, 61.1, 114.2
α, β, γ (°)	92.19
Resolution (Å)	57.08-2.75 (2.88-2.75)
R_{merge} (%)	10.7 (39.2)
$\langle I/\sigma(I) \rangle$	7.4 (2.1)
$CC_{1/2}$	0.949 (0.630)
Completeness (%)	97.8 (97.8)
Multiplicity	2.8 (2.7)
Wilson B-factor	6.326

Refinement	
Number of Non-hydrogen atoms	4820
Waters	76
Resolution (Å)	57.08-2.75 (2.92-2.75)
R_{work} (%)	22.8 (27.8)
R_{free} (%)	30.4 (39.2)
Mean B-value ($Å^2$)	25.37
RMSD Bonds (Å)	0.009
RMSD Angles (°)	1.223
RMSD Planes (Å)	0.005

During the course of this study a second structure of SHIP2cd was solved to 2.8 Å, Protein Data Bank Acession 3NR8 (Trésaugues et al., 2014), again in $P2_1$ space group and the same unit cell as the apo structure presented here.

Just like the previously published structures, SHIP2cd crystallised with two molecules (chains A and B) in the asymmetric unit (AU). These align to each other with a RMSD of 0.319 (Figure 2.9 – A). Crystallisation in this space group and unit cell may be expected as the same recombinant protein and very similar crystallisation methods were used. Here, both molecules interact with symmetry related molecules in neighbouring AUs, and these interactions are likely to be required for the stabilisation of the lattice structure (Figure 2.9 B & C).

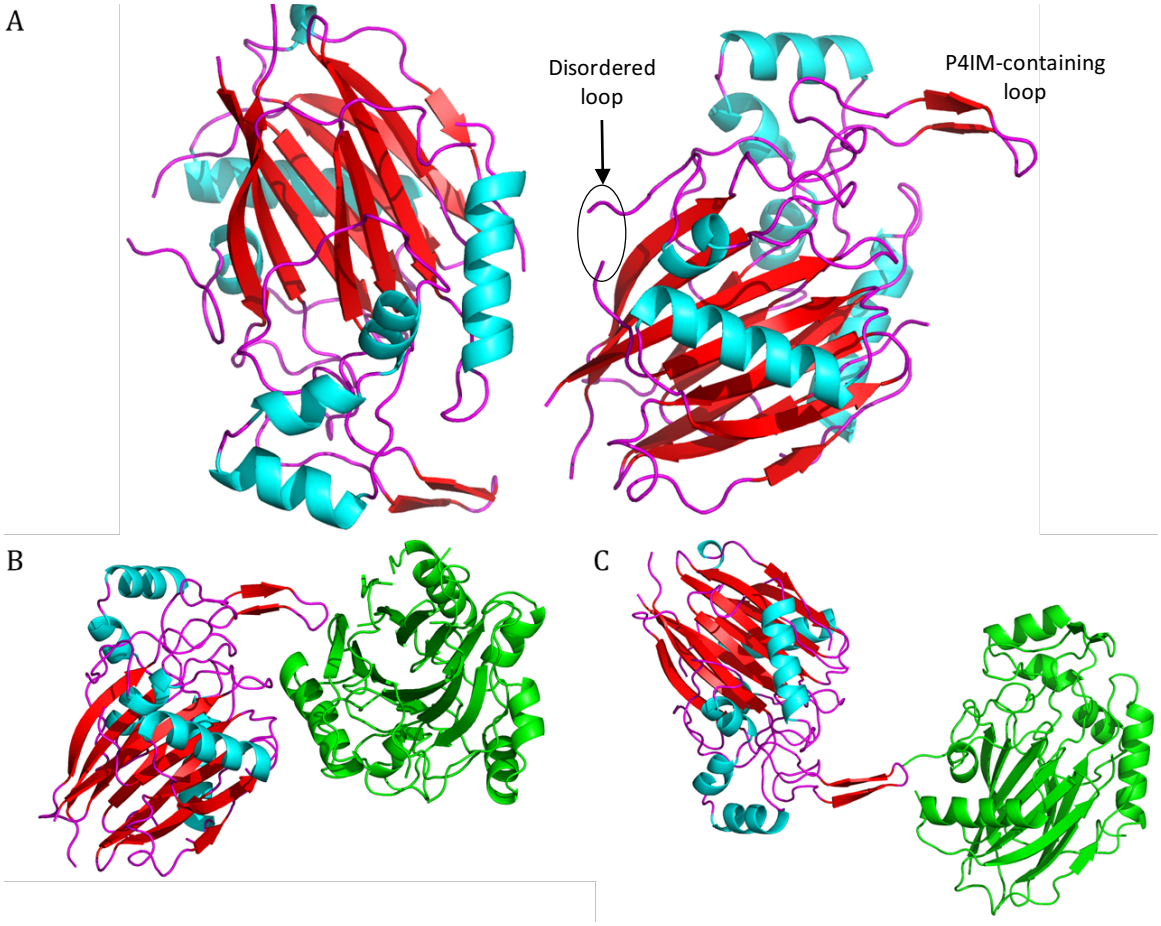

Figure 2.9 – SHIP2cd crystal structure represented as a cartoon and coloured by secondary structure. Symmetry-related SHIP2cd molecules are shown in green. (A) The two molecules in the asymmetric unit. (B) Chain B interaction with a symmetry-related molecule. (C) Chain A interaction with a symmetry related molecule.

Contacts occur via the 4-phosphate interacting motif (P4IM)-containing loop (Figure 2.9), which is thought to be uniquely extended in SHIP1 and SHIP2, and shorter in the other inositol polyphosphate 5-phosphatases (Trésaugues et al., 2014, Mills et al, 2012). The same interactions can be seen in the published structures of SHIP2cd, where chain B interacts with a chain A lattice neighbour, with the converse being true for chain A (Figure 2.2). In chain B, interactions occur at the apex of the extended loop between P678, H-bonded with M502 and with hydrophobic interaction with V525, both of the symmetry related molecule. These interactions, and that of R479 of the neighbour which co-ordinates the 6-phosphate of biphenyl 2,3',4,5',6-pentakisphosphate ligand, likely constrain the loop to this conformation (Figure 2.10).

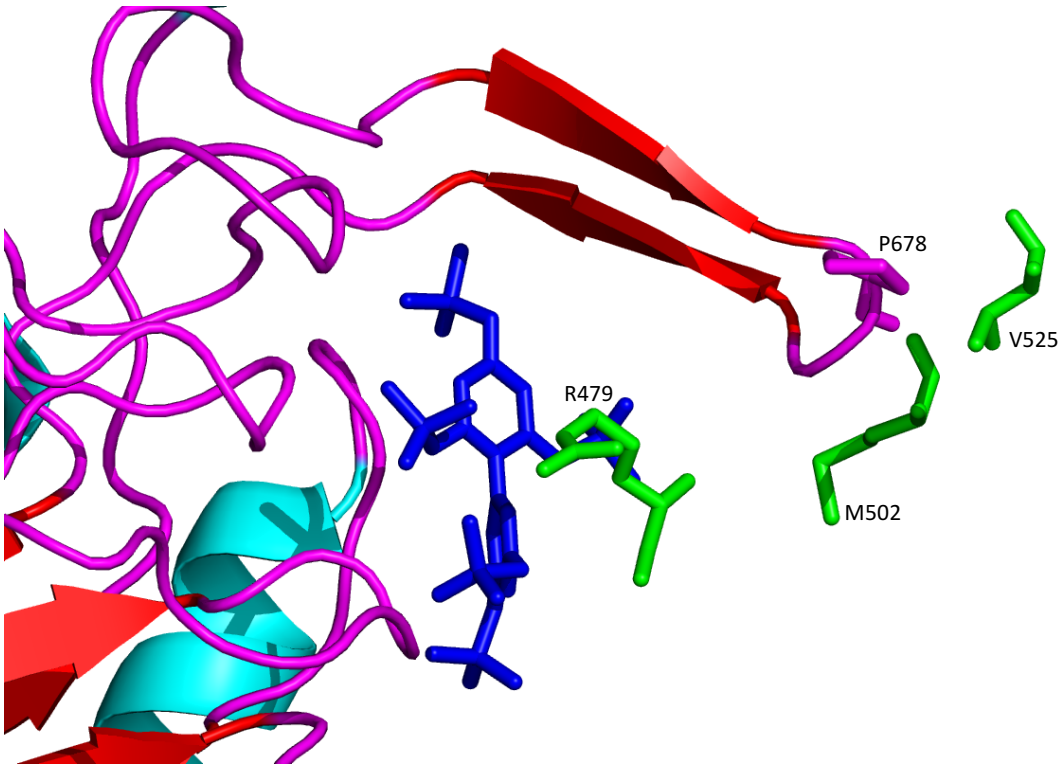

Figure 2.10 – Interactions between the (P4IM)-containing loop of chain B, and a symmetry related lattice neighbour. Chain B is shown as a cartoon representation coloured by secondary structure. BiPh1(blue) and residues that facilitate loop interactions and conformation are shown as sticks. Residues in green arise from the symmetry related chain A.

The P4IM-containing loop of chain A is directed towards a disordered region in the symmetry related molecule, causing consecutive disorder in the loop itself. This disordered region in chain B is indicated in Figure 2.9, and consists of a loop formed by residues 456-460.

As can be seen in Figure 2.11 -B, the electron density for the P4IM-containing loop in chain A is lacking, suggesting flexibility and/or multiple conformations.

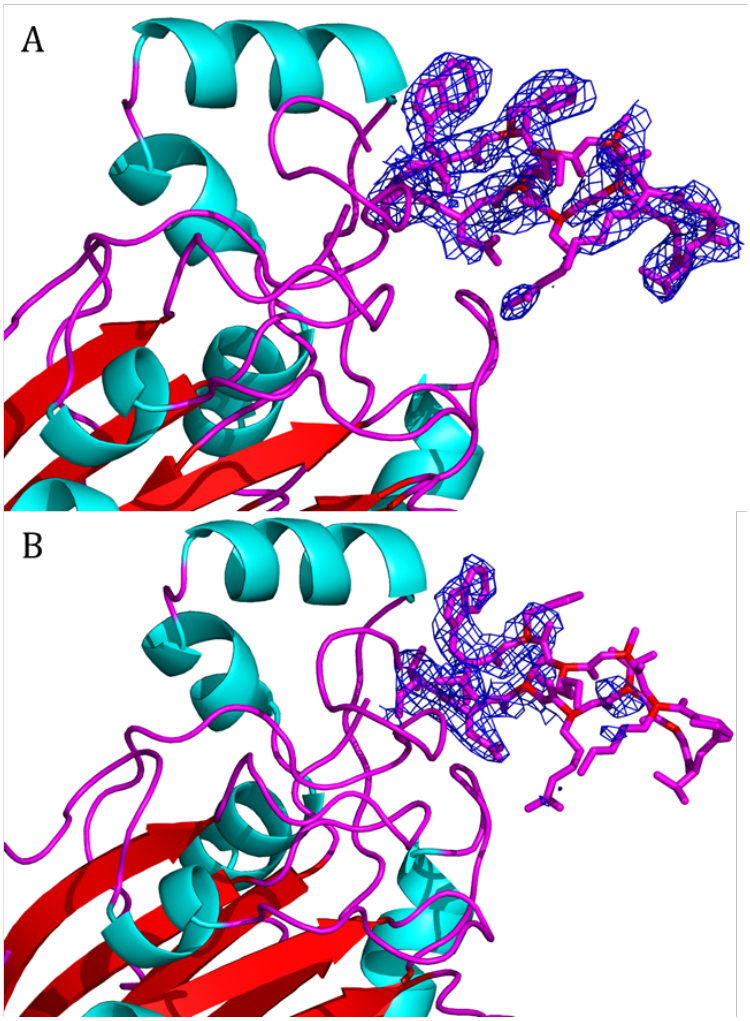

Figure 2.11 – Conformation of the P4IM-containing loop in the SHIP2cd crystal structure. Double difference Fourier electron density is shown as a blue mesh with a map contour of 1.2 σ. (A) Chain B. (B) Chain A.

This loop is thought to be flexible and disordered in the apo-form, but regains order when a substrate or inhibitor is bound resulting in it folding over the active site pocket, as has been postulated by molecular dynamics simulations (Mills et al., 2012). Having said this, the structure of apo SHIP2cd presented here is near identical to the SHIP2cd structure in complex with biphenyl 2,3',4,5',6 pentakisphosphate (BiPh1) (Mills et al., 2012).

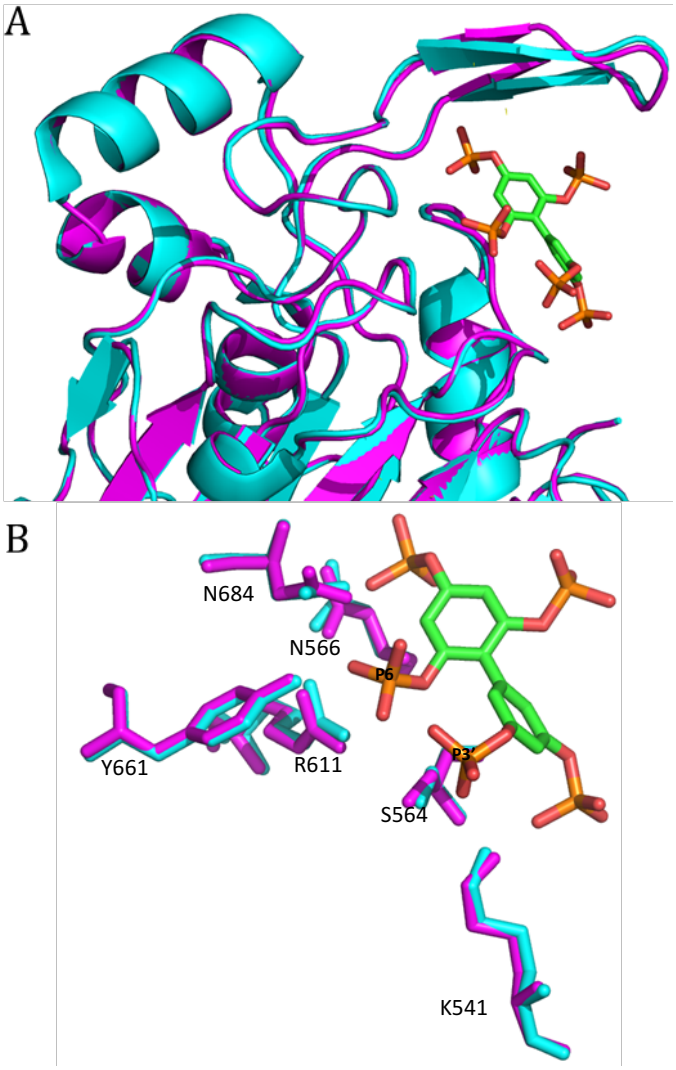

Figure 2.12 –Alignments of apo SHIP2cd (magenta) and SHIP2cd BiPh(2,3',4,5',6)P_5 structures (cyan) (Mills et al., 2012). BiPh(2,3',4,5',6)P_5 is represented as sticks and coloured by element. (A) Cartoon representation of the binding site secondary structure elements. (B) Overlay of side chains that have direct protein-ligand interactions with BiPh(2,3',4,5',6)P_5. Adapted from PDB file 4A9C.

The two structures align with an RMSD of 0.239, with the PI4M-containing loop in seemingly near identical positions regardless of a ligand being present, and appears to be structured. This is reinforced by the double difference electron density around this loop (Figure 2.11 & Figure 2.12 -A), inferring that the P4IM-containing loop must not be essential in coordinating BiPh1 in the active site pocket, but instead is only stabilised by the interactions with the symmetry related molecule in the lattice (chain B only). The structural organisation of this region is also only defined in chain B of a previously published apo-structure of the same space group as well, therefore supporting this notion (Trésaugues et al., 2014).

The interactions that coordinate BiPh1 in the Mills et al. 2012 structure occur with P3', P4, P5' and P6. Regardless of BiPh1 being bound in the active site, the position of the residues that are reported to interact with these phosphates are not altered relative to those in the apo-structure, indicating that no conformational changes in the binding pocket take place upon ligand binding (Figure 2.12 – B). This is supported by the double difference electron density around these residues.

As stated previously, in the crystal environment BiPh1 is coordinated by the symmetry related molecule at its 3', 5'- and 6-phosphates. The true binding orientation of BiPh1 in the active site of SHIP2 remains a concern, even despite the molecular dynamics simulations on the SHIP2cd BiPh1 structure which suggest that the P4IM-containing loop folds over and eliminates interactions with the lattice neighbour (Mills et al., 2012). In consideration of the assumed mobility of the P4IM-containing loop.

In the absence of the identification of novel ligands of SHIP2cd complexes in the work presented in this thesis, the structure reported here does not offer insight to the unanswered question of the co-ordination of the scissile 5-phosphate of inositide or phosphoinositide substrates. To obtain further information, an attempt was made to solve structures of the related, but exclusively hematopoietically-expressed SHIP1 protein.

2.3.4 Ligation independent cloning of INPP5Dcd (SHIP1cd) in to the pNIC28-Bsa4 vector

Unlike the 5-phosphatase domain of SHIP2 (SHIP2cd/*INPPL1cd*) (see section 2.3.3) there was no expression clone available for the SHIP1 protein from the Structural Genomics Consortium (SGC, materials available from Source BioScience). Although the SGC have a selection of plasmids available for purchase, pNIC-MBP, which *INPPL1cd* is in, is not. Therefore, it was necessary to seek out appropriate alternatives that would provide equally successful yields of active protein. As SHIP2 and SHIP1 are close homologues and their 5-phosphatase domains share 63.9 % identity, sensible options would include vectors similar to pNIC-MBP. This plasmid adds a MBP-TVMV-His6-TEV fusion to the N-terminal of the protein, and the MBP tag is cleaved *in vivo* via the TVMV sequence. There is very little information about the plasmid freely available, but it is presumed the MBP tag is necessary to enhance solubility of the target expression protein and/or assist with correct folding and stability.

Firstly, the expression vector pMCSG19 was selected due to its similarity to pNIC-MBP; it also adds a MBP-TVMV-His6-TEV N-terminal fusion to cloned proteins (Donnelly et al., 2006, Eschenfeldt et al., 2009) (DNASU-plasmid repository). The pNIC28-Bsa4 expression vector was also selected due to its extensive use by SGC to successfully clone and express many mammalian proteins; adding a His-TEV N-terminal fusion to the cloned expression target (Gileadi et al., 2008, Savitsky et al., 2010) (GenBank EF198106). Cloning in to pMCSG19 was undertaken in tandem with pNIC28-Bsa4 by a similar ligation independent method (Eschenfeldt et al., 2009) but at first pass did not produce successful clones in the latter stages of cloning and was not pursued further. This may have increased solubility and purity of the protein if pursued and optimised.

Table 2.2 – Primers, annealing temperatures, and elongation times used for the PCR amplification of full length *INPP5D* and its catalytic domain (*INPP5Dcd*) from a cDNA clone template. Flanking sequences required for ligation independent cloning are shown in bold italics.

Gene name	Template IMAGE ID	Forward primer (5' to 3')	Reverse primer (5' to 3')	Fragment size (bp)	Annealing temperature (°C)	Elongation time (sec)
INPP5D	8322634	***TACTTCCAATCCATG***GTC CCCTGCTGGAACCAT	***TATCCACCTTTACTGTCA***CTG CATGGCAGTCCTGCC	3567	57	70
INPP5D-cd	8322634	***TACTTCCAATCCATG***GAG CAGCCGGAGCCCGAC	***TATCCACCTTTACTGTCA***CTG GGAAGTGACTCCTGCCTC	957	64	30

The template used for PCR amplification of *INPP5Dcd* was purchased as a fully sequence cDNA clone (Source BioScience) in the vector pCR4-TOPO and contained the full *INPP5D* sequence (I.M.A.G.E. ID – 8322634) (Accession BC113582). As SHIP1 and SHIP2 share a high percentage identity in their catalytic domains, the sequence for the catalytic domain of SHIP1 (SHIP1cd) was identified via alignment of the full length SHIP1 sequence with the SHIP2cd sequence supplied by the SGC, which is also available in the NCBI database (Accession 3NR8_A).

PCR amplification of *INPP5Dcd* was carried out using Phusion high fidelity polymerase (New England Biolabs) (section 2.2.2) as per manufacturer's instructions and using the primer sequences, annealing temperature and elongation time provided in Table 2.2. The additional sequences required for ligation independent cloning are shown in bold italics (Gileadi et al., 2008). Also shown is a primer set for the amplification of full length SHIP1, but this did not produce successful clones in the final phases of cloning.

To remove primers and other contaminants, the PCR products were purified by gel extraction using the Wizard® SV Gel and PCR Clean-Up System (Promega) after agarose gel electrophoresis (see section 2.2). The PCR products shown in Figure 2.13 were the expected fragment sizes for full length SHIP1 and SHIP1cd; 3567 bp and 957 bp, respectively.

The purified PCR product was treated with T4 DNA polymerase (Clontech) in the presence of dCTP for 30 min at 11 °C followed by 20 min at 75 °C. The exo-nuclease activity of the polymerase hydrolyses nucleotides from the 3' ends until it reaches a C residue, creating a single stranded 5' overhang.

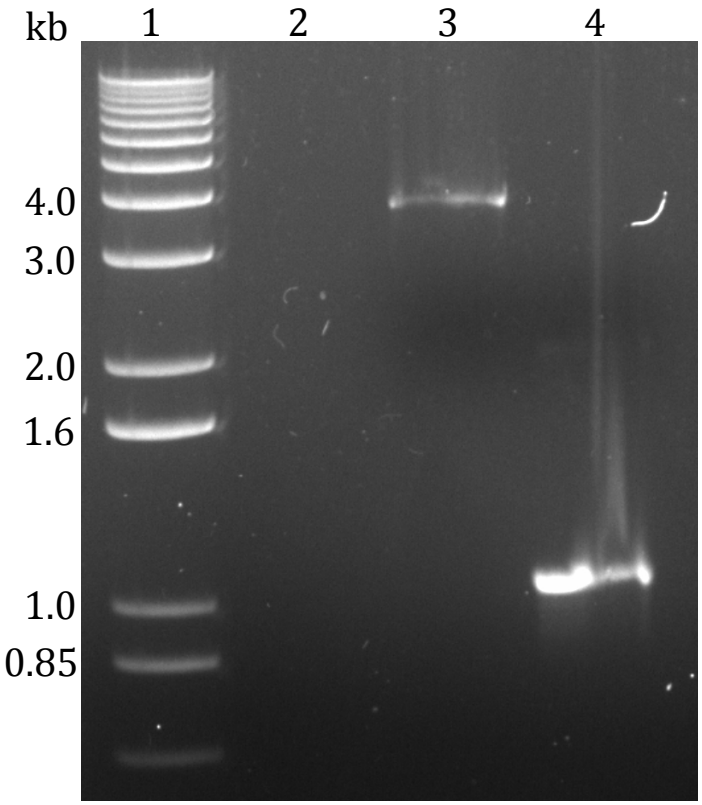

Figure 2.13 – Gel purified PCR amplified products from the pCR4-TOPO-*INPP5D* template analysed on a 1 % agarose gel. (1) 1 kb plus DNA ladder. (2) Empty. (3) Full length *INPP5D.* (4) Catalytic domain fragment of *INPP5D*

The pNIC-Bsa4 vector was purchased from the SGC (Source BioScience) and was supplied as an *E. coli* stock on an agar slope which was treated as per the supplier's recommendations before purifying the plasmid using the Wizard® *Plus* SV Miniprep DNA Purification System (Promega). To prepare vector, it was transformed into Stellar competent *E. coli* cells (Clontech), single kanamycin resistant colonies selected, from which O/N cultures were grown for later plasmid extraction. The plasmid was digested with BsaI-HF restriction enzyme (New England Biolabs) as per the manufacturer's protocol, which subsequently released a 2 kb fragment if digested correctly at both restriction sites. The digested plasmid was analysed by agarose gel electrophoresis and

the linearised ~5.5 kb plasmid extracted. The recovered plasmid was then analysed by agarose gel electrophoresis (Figure 2.14).

To generate the cohesive ends required for ligation independent cloning, the BsaI digested plasmid was treated with T4 DNA polymerase in the presence of dGTP for 30 min at 11 °C followed by 20 min at 75 °C; creating single stranded 5' overhangs complementary to the PCR products.

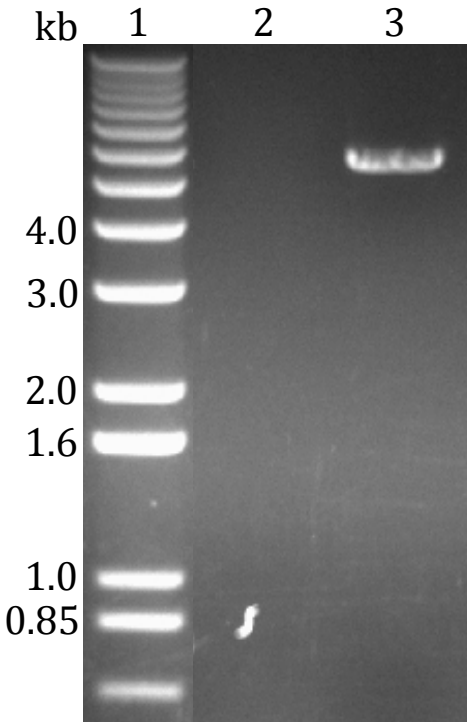

Figure 2.14 – Linearised and gel purified pNIC28-Bsa4 vector analysed on a 1% agarose gel. (1) 1 kb plus DNA ladder. (2) Empty. (3) pNIC28-Bsa4 digested with BsaI.

Annealing of the treated plasmid and insert was achieved by incubating a ratio of 2:1 (v/v) plasmid to insert at room temperature followed by incubation on ice for 10 min before transforming in to stellar competent *E. coli* cells. Only a few transformants were generated for SHIP1cd and none for full length SHIP1. Therefore, only SHIP1cd was pursued due to the time constraints of this project. Changing the ratios of each fragment or higher yields of plasmid and insert may have remedied this. The PCR yield of full length SHIP1 was not as high as SHIP1cd.

Two kanamycin resistant colonies were selected and grown overnight in LB. Colony screening was carried out on the overnight cultures via PCR amplification using GoTaq® G2 Flexi DNA Polymerase (Promega) as per manufacturer's instructions and detailed in materials and methods (section 2.2.10). The primers, annealing temperatures, and elongation times were as Table 2.2.

Both colonies contained the plasmid with the *INPP5Dcd* insert (Figure 2.15), and were extracted using the Wizard® *Plus* SV Miniprep DNA Purification System (Promega). The insert of the final construct (Figure 2. –B (4)) was sequenced using the pLIC-for and pLIC-rev primers (Gileadi et al., 2008), which verified the correct sequence before transformation of the plasmid in to *E. coli* Rosetta2 competent cells and *E. coli* BL21-pRARE2 competent cells for protein expression testing.

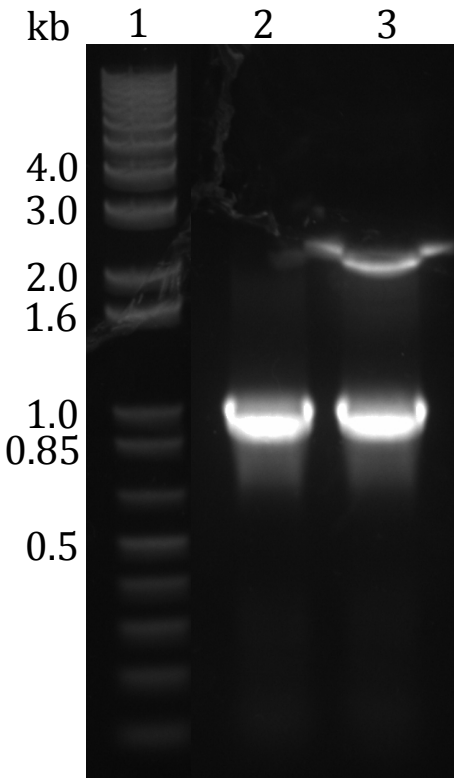

Figure 2.15 – Colony screening by PCR amplification of *INPP5Dcd* from two kanamycin resistant *E. coli* colonies analysed on a 1% agarose gel. (1) 1 kb plus DNA ladder. (2) Colony 1. (3) Colony 2.

2.3.5 Expression of SHIP1cd-His

Two single colonies were selected from the transformation plate to cultivate starter cultures for subsequent expression testing. Expression tests were carried as outlined in methods, and consequently analysed by SDS-PAGE. The estimated protein size for SHIP1cd-His is 39320.5 Da, as computed by ProtParam (Wilkins et al., 1999), from the sequence available on the NCBI database together with the N-terminal fusion sequence.

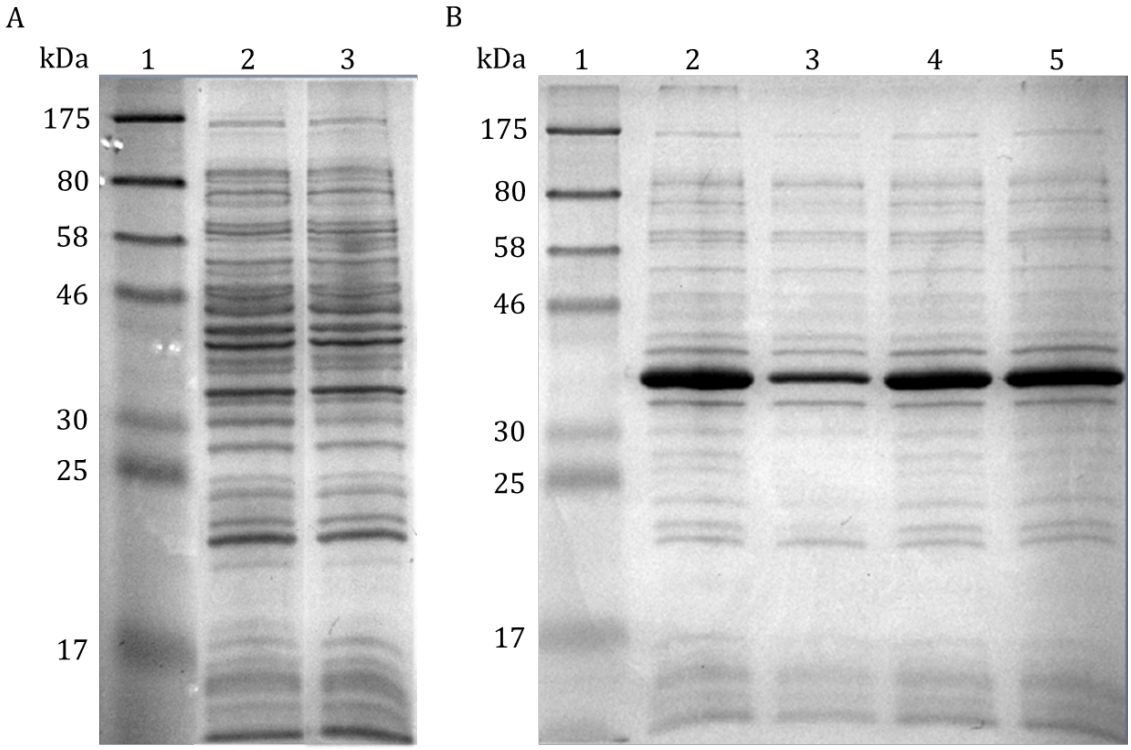

Figure 2.16 – Small scale expression testing of SHIP1cd-His by *E. coli* Rosetta2 cells. SDS–PAGE analysis on a 10% acrylamide gel of whole cell pellets from IPTG induced cultures originating from two separate transformation colonies.

***A* – non-ITPG induced cultures (1) Protein molecular weight marker. (2) Culture A. (3) Culture B.**

***B* – Expression cultures supplemented with IPTG (1) Protein molecular marker. (2) Culture A +0.2 mM IPTG. (3) Culture A +0.5 mM IPTG. (4) Culture B +0.2 mM IPTG. (5) Culture B +0.5 mM IPTG.**

All cultures, including the non-IPTG induced, were left to grow overnight at 20 °C. All the IPTG-induced expression cultures successfully expressed SHIP1cd-His in *E. coli* Rosetta2 cells (Figure 2.16 - *B*). The only notable difference was seen in culture A supplemented with 0.5 mM IPTG, which appeared to give a lower expression yield. In light of these results, culture B was chosen to carry forward for large scale expression and purification because of the apparent strong and consistent expression levels. There appeared to be no basal "leaky" protein expression (Figure 2.16 – *A*) therefore there was no need for glucose supplementation to suppress expression during the growth phase. This is as expected due to Rosetta2 containing the pLysS plasmid (discussed in chapter 3). No expression was observed in BL21-pRARE2 *E. coli* cells (data not shown).

Subsequently, large scale expression cultures were set up that, if successful, would be carried forward to purify SHIP1cd-His. Two 1 L cultures were set up and expression carried out as outlined in methods using 0.4 mM IPTG to induce protein expression (Figure 2.17).

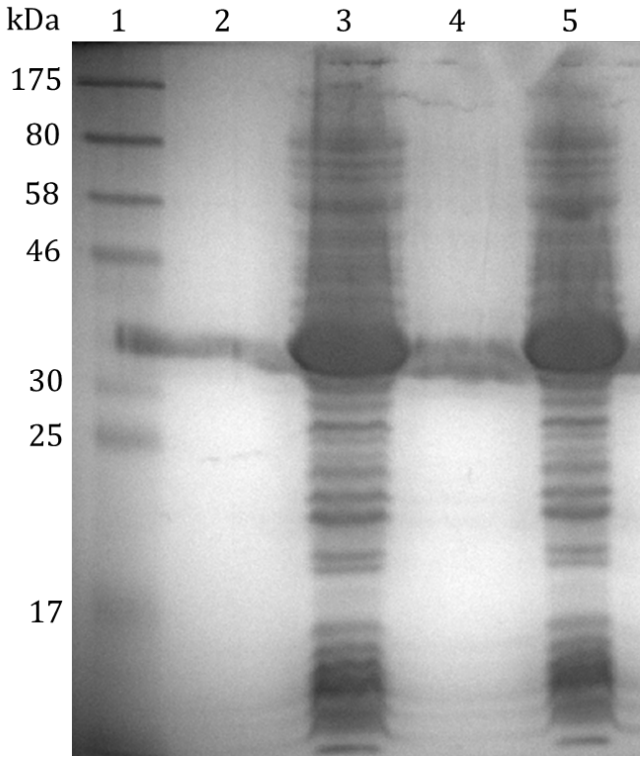

Figure 2.17 – SDS-PAGE analysis of whole cell pellets from the large scale expression of SHIP1cd-His analysed on a 1% agarose gel. (1) Protein molecular weight marker. (2) Empty. (3) 1 L expression culture. (4) Empty. (5) 1 L expression culture.

Both cultures showed high levels of expression under these conditions. Consequently, they were subjected to mechanical cell disruption to be taken forward for purification of SHIP1cd-His.

2.3.6 Purification of SHIP1cd-His

SHIP1cd-His protein was purified as per the method described in section 2.2.17. The lysate of the 2 L culture from section 2.3.2 was centrifuged to remove cell debris before loading the supernatant on to a 5 mL Ni-NTA superflow cartridge (Qiagen) for immobilised metal affinity chromatography.

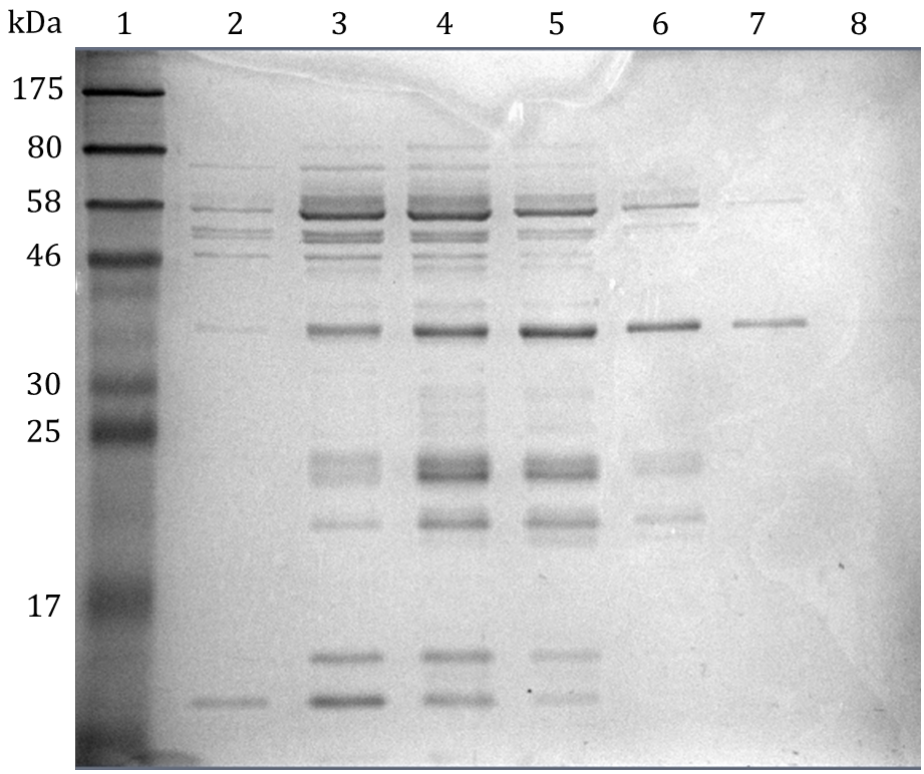

Figure 2.18 - Immobilised metal affinity purification of SHIP1cd-His. SDS-PAGE analysis on a 10% acrylamide gel of eluate fractions recovered during NiNTA chromatography. (1) Protein molecular weight marker. (2-8) Column eluate fractions corresponding to the UV absorbance peak at 280 nm. Fraction number; 14, 16, 18, 20, 22, 24 & 26, respectively.

Figure 2.18 shows the SDS-PAGE analysis of fractions that were identified as containing SHIP1cd-His from the UV absorbance trace during nickel affinity purification. The overexpressed SHIP1cd-His (39.5 kDa) can be seen most prominently in fractions 16-24 (lanes 3-7), with the most heavy contamination occurring in fractions 16-20 (lanes 3-5). As these contaminated fractions also contained the highest yield of SHIP1cd-His they were pooled, along with fractions 21-24, for concentrating before subjection to size exclusion chromatography on a HiLoad 16/600 Superdex 75 pg column (GE Healthcare Life Sciences), performed according to section 2.2.17.

Two peaks were observed on the resulting UV trace from the size exclusion chromatography, albeit not overly distinctive with some observed overlap. As the first peak is expected to be the larger contaminant proteins eluting in the void volume, samples of the fractions from the wide second peak were analysed by SDS-PAGE (Figure 2.19). SHIP1cd-His appeared to be present in fractions 7-17 (lanes 2-7) in varying magnitudes and co-eluted with contaminants. It is likely there is some protein-protein interactions occurring between SHIP1cd and the contaminants, accounting for the wide overlapping peaks on the UV trace. Nevertheless, fractions 10-18, therefore avoiding some of the large and more prominent contaminants observed in lane 3, were pooled and concentrated to approximately 3.5 mg/mL and a volume of 2 mL.

Other attempts at purifying SHIP1cd-His used different buffers, salt concentrations and DTT or TCEP, see section 2.2.9 and appendix 2 for more details. A HiLoad 16/600 Superdex 200 pg (GE Healthcare Life Sciences) was also utilised in an attempt to improve separation between SHIP1cd-His and the contaminating proteins during size exclusion chromatography, much to the same avail. Upon reflection, the pH of the buffers should be adjusted as the next effort to reduce protein-protein interactions by altering the net charge of SHIP1cd-His. ExPASy's ProtParam tool (Wilkins et al., 1999), calculates the pI of SHIP1cd-His to be 6.81 and the buffers were the same as those used for AtIPK1 (Chapter 3), which were pH 7.5. This may have been too close to the isoelectric point of SHIP1cd-His and could have rendered some of the protein insoluble, resulting in aggregation and interactions with contaminating proteins. Nevertheless, as will be seen later on in this text, soluble and catalytically active SHIP1cd protein was obtained.

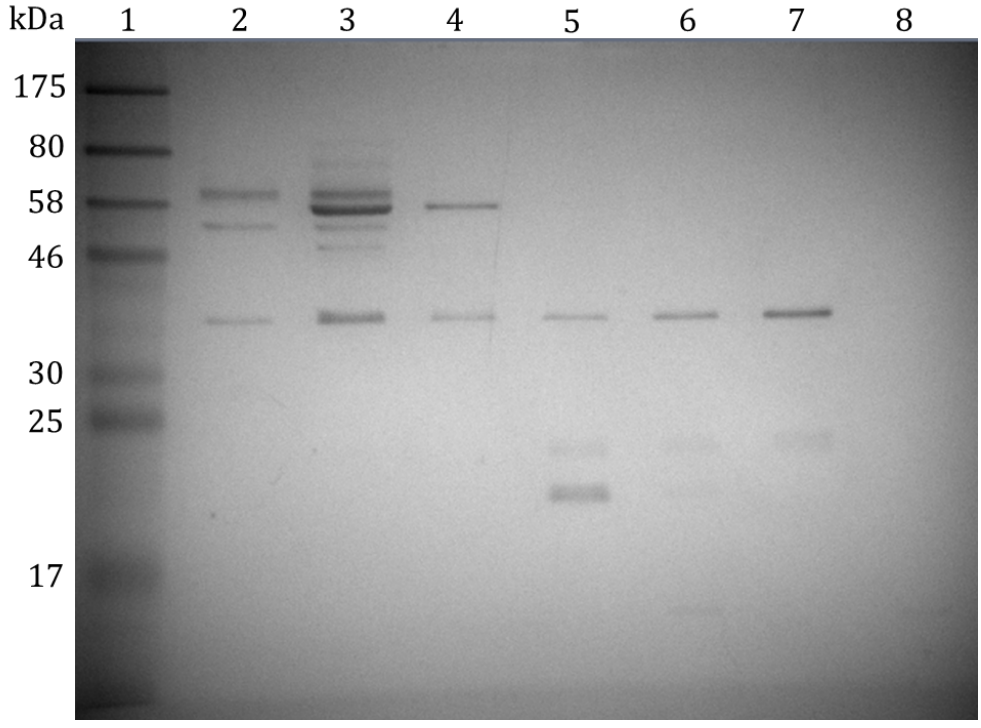

Figure 2.19 - Size exclusion chromatography of SHIP1cd-His. SDS-PAGE analysis on a 10% acrylamide gel of elute fractions recovered from a sepharose gel filtration column. (1) Protein molecular weight marker. (2-8) Column elute fractions corresponding to the UV absorbance peaks at 280 nm. Fraction number; 7, 9, 11, 13, 15, 17 & 19, respectively.

A sample of the final purified and concentrated protein was analysed by SDS-PAGE and stained with InVision™ His-tag In-gel Stain (Novex by Life Technologies), used as per manufacturer's guidelines. Subsequently, the same gel was stained with a Coomassie blue stain as per section 2.2.15 (Figure 2.20). As the sample was highly concentrated a 1:2 dilution of the protein was used. The InVision stain binds specifically to the 6xHistidine tag and can be used to accurately detect the presence of His-tagged fusion proteins due to its fluorescent properties. Its excitation maximum is at a wavelength of 560 nm, and its emission maxima at 590 nm, the parameters pre-set for visualising ethidium bromide sufficed. It can provide a quicker and simpler alternative to a western blot to confirm the presence of His-tagged fusion proteins.

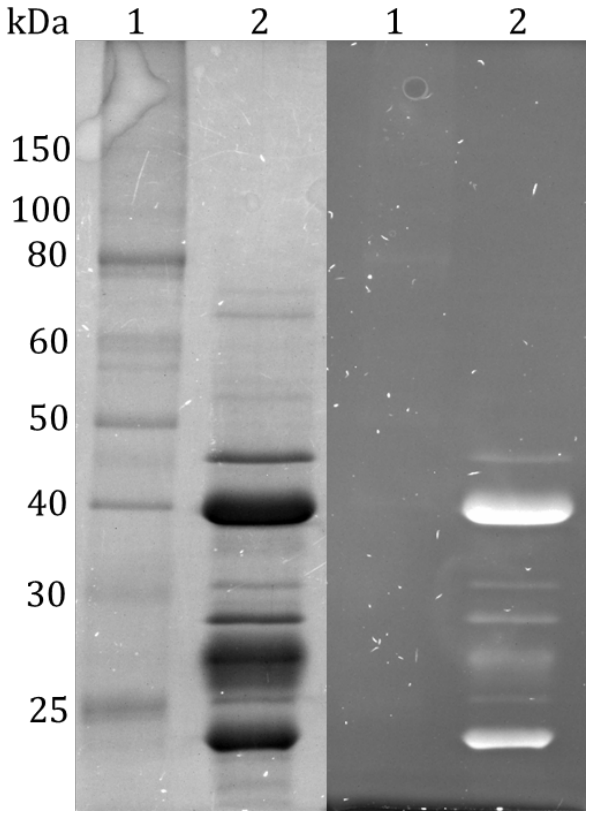

Figure 2.20 - Coomassie blue (left) and InVision staining (right) of purified SHIP1cd-His. (1) Protein molecular weight marker (2) 1:2 (v/v) dilution of purified SHIP1cd-His.

The final purified protein contains contaminants and it appears there are truncated versions of SHIP1cd-His, as can be seen by the right hand side of the gel in Figure 2.20 where only proteins with a histidine-tag are stained. This could be due to the production of truncates during expression, degradation of SHIP1cd-His and/or hydrolysis by proteases. Having these presumably non-folded and truncated versions of SHIP1cd-His present may also reduce the solubility and activity of the protein due to aggregation. Protease inhibitors should be considered during purification.

It is preferential to remove the 6xHistidine tag for the purpose of enzymatic assays to avoid any interference, which could perhaps occur by additional non-canonical interactions. Cleavage of the 6xHistidine tag was set up post size exclusion chromatography using Pro TEV plus protease (Promega) after concentrating the protein to a 1 mL volume. Manufacturers guidelines were followed and the reaction was incubated for approximately 16 hr at room temperature (18 °C).

A sample was taken prior to cleavage to compare to a post incubation sample, both of which were analysed by SDS-PAGE using a 12.5% acrylamide gel, with the aim to achieve a clear separation of the two samples in order to visualise the change in molecular weight that occurs when the 6xHistide tag is removed (Figure 2.21). The post TEV protease incubation sample is of lower molecular weight indicating the removal of the tag was successful, although some tagged protein still remained.

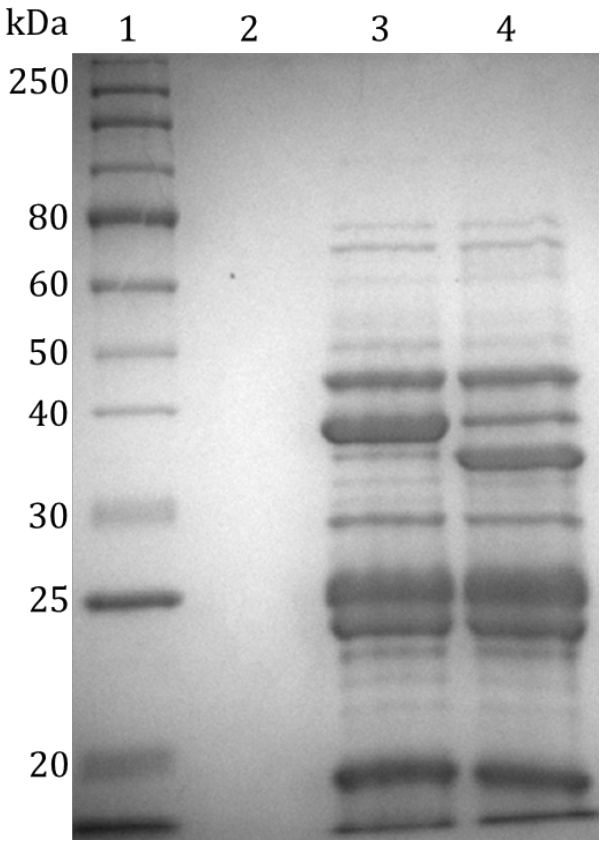

Figure 2.21 - SDS-PAGE analysis on a 12.5 % acrylamide gel of the proteolytic cleavage of the N-terminal 6xHis tag from SHIP1cd-His using ProTEV plus protease. (1) Protein molecular weight marker. (2) Empty. (3) SHIP1cd-His. (4) SHIP1cd post incubation with TEV protease.

The products of the His-tag cleavage reaction were loaded on to a 5 mL NiNTA superflow cartridge (Qiagen), equilibrated with buffer A (see appendix 2), at a flow rate of 0.5 mL/min in a continuous loop for 30 min. The eluate containing SHIP1cd was collected in a 10 mL fraction and five subsequent 2 mL fractions whilst the column was subjected to buffer A at a 1 mL/min flow rate. Subsequently, a final 10 mL fraction was collected when washing the column with buffer B. All fractions were analysed by SDS-PAGE (Figure 2.22). The majority of SHIP1cd was eluted in the initial 10 mL fraction (lane 2) whilst the 6xHistidine tag and TEV protease remained on the column. The final 10 mL fraction contained some SHIP1cd, confirming the removal of the 6xHisidine tag was not 100 % effective (lane 7). The cleaved protein in lanes 2-6 appear to still contain a contaminant larger than SHIP1cd, but some smaller contaminants have been removed as seen in lane 7 which are likely to be those seen in figure 2. Other bands seen in lane 7 are likely to be the 6xHistidine tag and TEV protease, as well as some un-cleaved

SHIP1cd-His. The comparatively small concentration of TEV protease used was reasonably efficient under the conditions tested but perhaps a higher concentration of TEV protease or longer incubation would have remedied this.

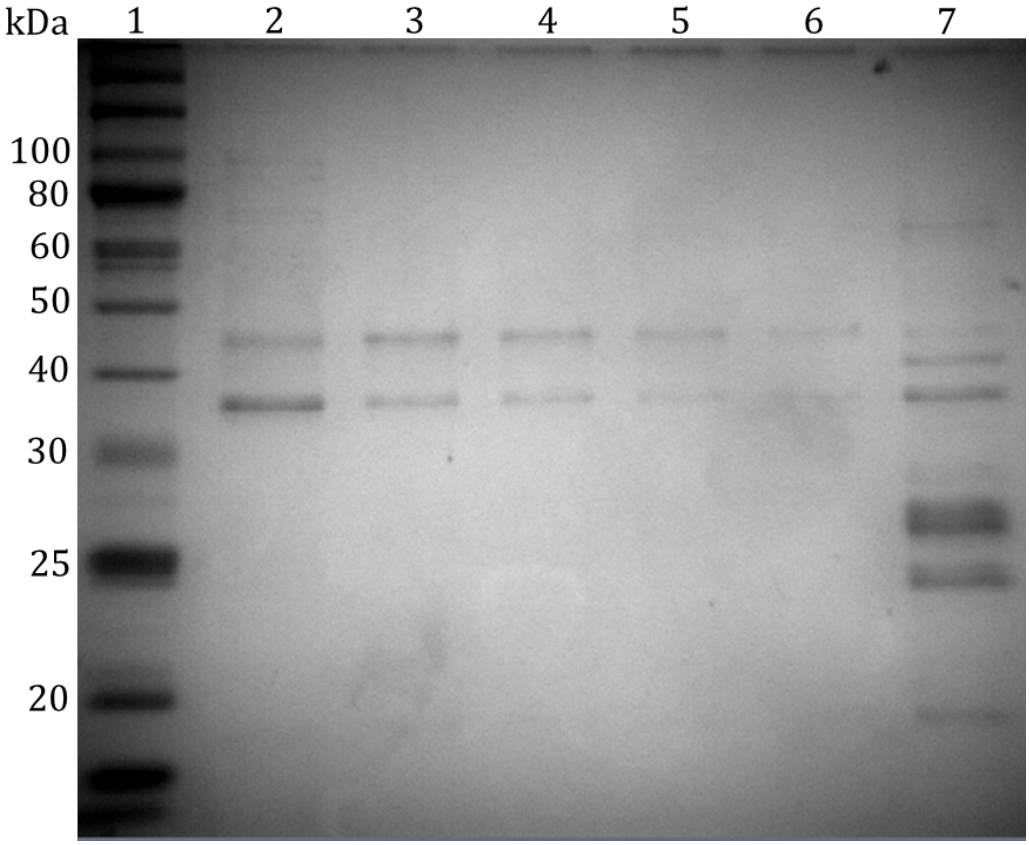

Figure 2.22 - Immoblised metal affinity purification post proteolytic cleavage of SHIP1cd-His with TEV protease. Samples of eluate fractions from the NiNTA column upon washing with NiNTA buffer A, Analysed on a 12.5 % acrylamide gel. (1) Molecular weight marker. (2) Initial 10 mL fraction. (3-6) Subsequent 2 mL fractions. (7) Final 10 mL wash with NiNTA buffer B.

The fractions were pooled, concentrated to 2.2 mL and subjected to a final round of size exclusion chromatography (results not shown). Final purified SHIP1cd was concentrated to 3.2 mg / mL (from 2 L of expression culture) and snap frozen before storage at -80 °C. As can be seen in Figure 2.23, removing the 6xHistidine tag from SHIP1cd-His also removes many of the contaminants when compared to the non-cleaved protein.

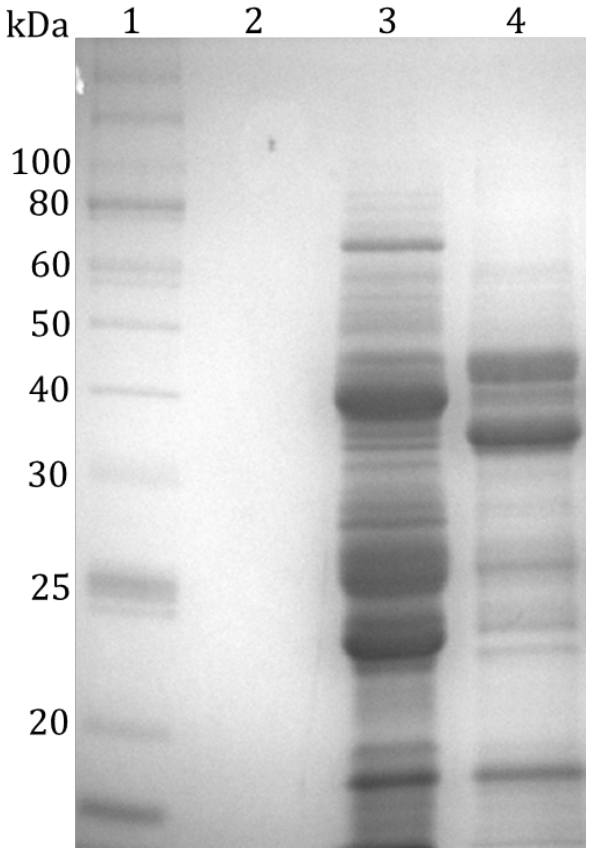

Figure 2.23 – SDS-PAGE analyisis on a 12.5 % gel of final purified SHIP1cd-His and SHIP1cd. (1) Protein molecular weight marker. (2) Empty. (3) Purified SHIP1cd-His. (4) Purified SHIP1cd.

2.3.7 Structure prediction of SHIP1cd

Due to time constraints, suitably pure protein was not obtained in order to submit SHIP1cd in to crystallisation trials as anticipated. As well as the time and effort involved in the execution of crystallisation trials, the purification process would first need to be optimised.

The SWISS-MODEL automated protein structure homology-modelling server is able to generate 3D models for proteins where experimental data is not available. It allows users to; conveniently search for suitable templates using sensitive Hidden Markov Model searches against the SWISS-MODEL Template Library, analyse alternative templates and alignments, perform structural superposition and comparison, explore ligands and cofactors in templates and compare the resulting models using mean force potential based model quality estimation tools (Biasini et al, 2014).

As there are no structures of SHIP1cd available in the PDB, it was submitted for protein structure homology-modelling using the SWISS-MODEL server, which is available via the ExPASy web server. A search for appropriate templates was first carried out against the SHIP1cd sequence used in this study, this resulted in a suggestion that a structure for SHIP2cd (PDB 3NR8) was the top scoring template, closely followed by the SHIP2cd BiPh(2,3',4,5',6)P_5 structure (PDB 4A9C).

The SHIP2cd structure from this study was used as a template for the SHIP1cd model generated by SWISS-MODEL. The resulting model superimposes to the SHIP2cd structure with an RMSD of 0.141, indicating that the model has very minimal changes in structure when compared to its template (Figure 2.24). This is unsurprising considering they share 64 % sequence identity and are isozymes.

Figure 2.24 – Alignment of chain B of the SHIP2cd structure (cyan) to the model of SHIP1cd (magenta), as predicted by SWISS-MODEL homology-modelling server.

As mentioned in previously, there are six available structures of inositol 5-phosphatases in complex with ligands (Mills et al., 2012, Mills et al., 2016b, Tsujishita et al., 2001). These proteins display mutually conserved residues within their binding pockets that coordinate the various ligands. Five of those residues are involved in coordination of BiPh1 in to the active site of SHIP2cd; K541, Y661, R682 & N684 (Figure 2.25). Where K541 coordinates the P1 site; defined according to structures of INPP5B with PtdIns4P and PtdIns(3,4)P_2, and the 5- and 6- hydroxyl site. These positions are occupied by P3' and P5' of BiPh1, respectively. The remaining conserved residues contact the P4 position, P2 of BiPh1. When overlaying these residues from SHIP2cd with the corresponding residues of the SHIP1cd model, they align quite accurately but with one key difference; R682 becomes K682 in SHIP1cd (Figure 2.25). It is one of the residues that contacts the P4 position that is thought to be the position that confers specificity since the 5-phosphatases selectively hydrolyse PI(4,5)P_2 or PI(3,4,5)P_3. Therefore this change of amino acid can be considered to remain viable for ligand binding due to it conferring selectivity towards the substrate, and since arginine and lysine both possess positively charged side chains.

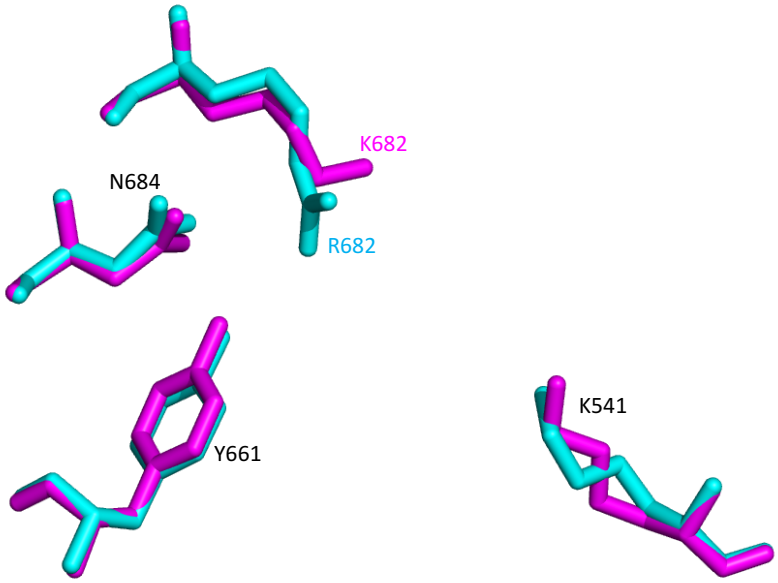

Figure 2.25 – The conserved ligand coordinating residues across all inositol 5-phosphatase structures; alignment of these residues in apo-SHIP2cd (cyan) and the SHIP1cd predicted structure (green).

Out of the ten enzymes in the inositol polyphosphate 5-phosphatase family, only SHIP1cd and SHIP2cd are described to have the extended P4IM-containing loop (Mills et al., 2012). Small changes in this active site loop can be seen between the SHIP1cd model and the SHIP2cd structure. This is also observed in the pre-existing structures of SHIP2cd in the PDB. The homology modelling of SHIP1cd places this loop in the same length of polypeptide as in the SHIP2cd structure, as can be seen by observing the secondary structure (Figure 2.26). The two antiparallel β-sheet, β10 & β11, are connected by a β-turn and are composed of the same number of residues in both structures. However, there is only 50% identity in these secondary structure elements, again supporting the hypothesis that the P4IM-containing loop is not critical in ligand binding and can likely adjust to a variety of ligands interacting with the binding pocket. Conversely, the electron density map for this region in SHIP2cd would ideally be of higher resolution and more whole (section 2.3.6), which may have led to a partial model being built for this region during structure determination. This is also observed in the pre-existing structures of SHIP2cd in the

PDB. Additionally, the loop is constrained at the apex of the β-turn due to interactions with the symmetry related molecule, this would in turn force the P4IM-containing loop of SHIP1cd to this constrained orientation during structure prediction.

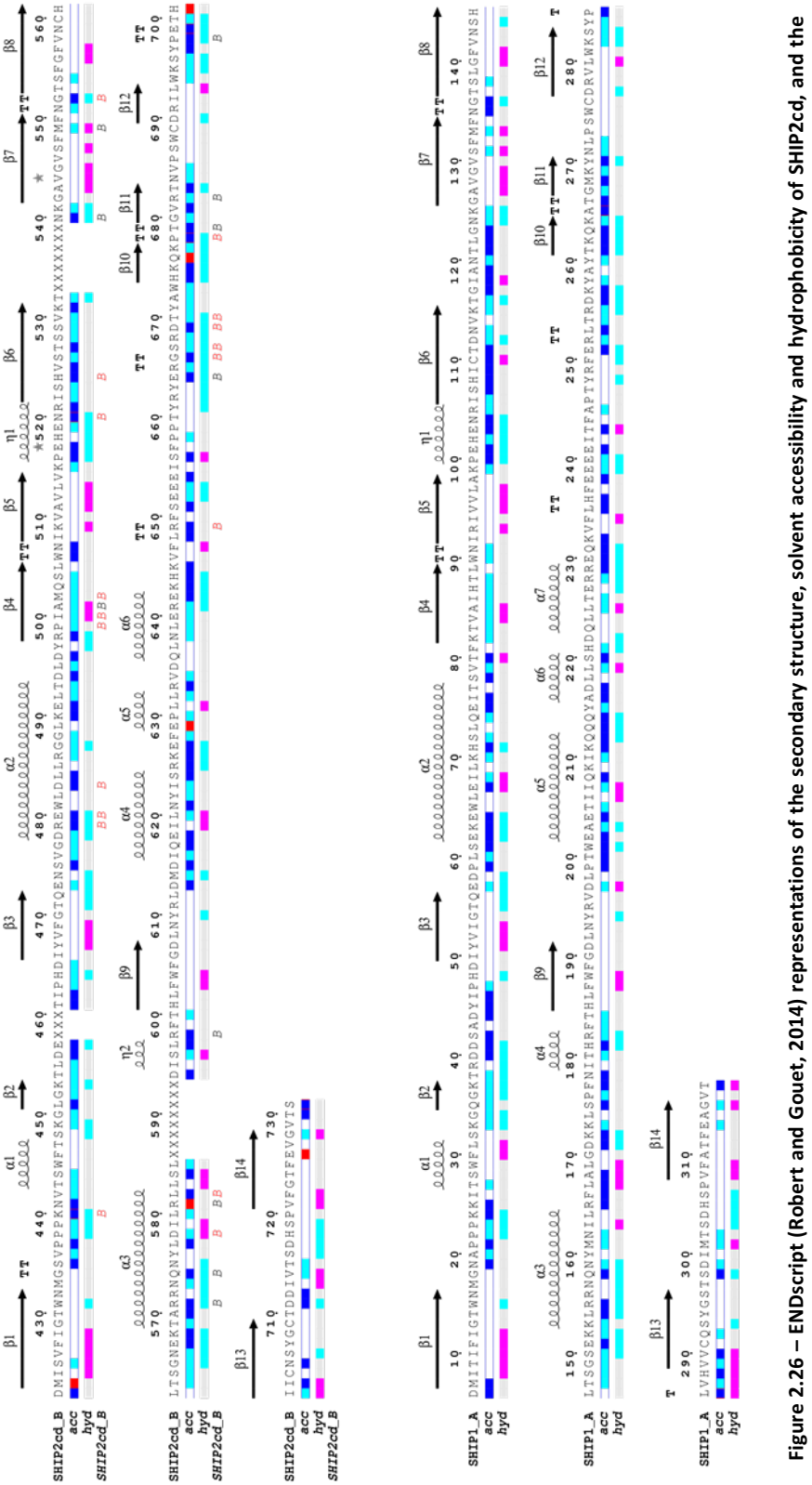

Figure 2.26 – ENDscript (Robert and Gouet, 2014) representations of the secondary structure, solvent accessibility and hydrophobicity of SHIP2cd, and the homology model of SHIP1cd

It is noteworthy to mention the variability of structure prediction and homology modelling methods. When the same SHIP1cd sequence is input in to Phyre2 (Kelley et al., 2015), a different template is suggested as the top scoring suggestion. The result was a model that did not contain the SHIP-specific extension known as the P4IM-conating loop, because the model had skewed towards the arrangement of the template, the 5-phosphatase OCRL-1 (results not shown). This method produced a SHIP1cd model that did not contain the extended P4IM-containg loop that is allegedly unique to SHIP1 and SHIP2.

According to critical assessment of protein structure prediction methods (CASP) (Moult et al., 2014) , it is observed that there are no major differences in accuracy of all widely used web servers for protein modelling. It is therefore surprising that, when processing the same SHIP1cd sequence, SWISS-MODEL and Phyre2 choose different top scoring templates to base the model on. Both methods appear to use very similar algorithms, but employ separate self-assembled databases to search for templates. Although they both use the same sources of information to build the libraries, the subsequent methodology and arrangement within each database must result in altered outcomes.

2.4 Conclusions and future work

No structures of SHIP1cd are yet available, and now that this work has produced a suitable clone that provides soluble SHIP1cd protein, further studies will seek to crystallise this based on what has been learnt from SHIP2cd. This would hopefully clarify the true structure of SHIP1cd and the presence of the P4IM-conating loop that is apparently only present in SHIP1 and SHIP2. Furthermore, the residues responsible for the differing substrate specificities between the isozymes may be revealed. Their specificities towards the biphenyl phosphates is also different (chapter 4). Crystallographic studies should also continue with SHIP2cd to attempt to gain additional structures in complex with the benzene- and biphenyl phosphates. These might include additional mutagenesis studies on the P4IM-containing loop in order to gain structures in which the loop is closed over the inositide binding pocket, as suggested, and not stabilised by interaction with a symmetry related molecule. This would give insight into the true role of this SHIP specific loop. Furthermore, as SHIP1 and SHIP2 are clinical targets for many diseases, structures with additional ligands are likely to provide more information for a framework for rational inhibitor/drug design based on key ligand coordinating and catalytic residues.

Since the experiments performed in this thesis were conducted, the Potter group reported the structure of the related 5-phosphatase INPP5B in complex with a second biphenyl compound, biphenyl 3,3',4,4',5,5'-hexakisphosphate (BiPh3), and a complex with the simpler compound benzene 1,2,4,5-tetrakisphosphate (Bz3) (Mills et al., 2016). INPP5B hydrolyses the 5-phosphate group from water- and lipid-soluble signalling messengers. Crystal structures were resolved to 2.89Å with BiPh3 and to 2.9Å with Bz3; comparisons of the potency of these ligands assayed by phosphate release from Ins(1,4,5)P_3 yielded IC50s of 5.5 and 6.3 μM.

For BiPh3 one of the substituted phenyl rings occupied the binding site occupied by the lipid head group of PtdIns4P in published INPP5B–C_8-PtdIns4P complex (PDB 3MTC) (Trésaugues et al., 2014). The second phenyl ring was solvent-exposed in the structure and was bound to the 6xhistidine tag of another INPP5B molecule, with a molecule of inorganic phosphate (P_i) also present in the active site. The position of this P_i is interpreted to mimic the cleaved 5-phosphate of inositol phosphate substrates and allowed the authors to identify, for the first time, the likely importance to catalytic mechanism of R451 which coordinates this phosphate and an active site water molecule interpreted to initiate hydrolysis of the 'unobserved' 5-phosphate of 5-phosphate-containing inositol phosphate substrates.

Aided by these structures, and the information provided in chapter 4, that benzene and biphenyl polyphosphates are substrates for SHIP1 and SHIP2, it would be possible to construct mutagenesis experiments, modifying individual active site residues, to test the contribution of R451 equivalent in SHIP2 (R611) and the other implicated residues. This endeavor would be greatly assisted by hydroxyl-containing benzene and/or biphenyl polyphosphate standards. 3-Hydroxy benzene 1,2,4-trisphosphate (Bz7) is available, but a lack compounds are available that might represent the dephosphorylation products of e.g. Bz3, solved in the structure of INPP5B (Mills et al., 2016). Of particular interest would be 2-hydroxy benzene 1,4,5-trisphosphate (2-OH Bz(1,4,5)P_3) since Mills and coworkers have shown that in INPP5B complexes, the 2-phosphate of Bz3 interacts with E303, K380 and H400 sidechains of chain A (of the asymmetric unit) and shows longer range interactions with both N449 (3.3 Å) and R451 (3.5 Å). Due to the electron withdrawing effect of the delocalised electrons, a singularly substituted phenol has a pKa of approximately 9.9 when compared to the hydroxyl group moiety of cyclohexanol which is approximately 16 (phosphate substituents would also influence the pKa of a hydroxyl). Such postulation assumed that the lower pKa of the generated phenolic hydroxyl, as compared to an inositol hydroxyl, allows hydrolysis of phosphates from benzene phosphate substrates. Crucially, the data in chapter 4 shows that benzene and biphenyl polyphosphates are substrates for at least two members of the 5-phosphatase family.

Chapter 3 – *Structural studies of Arabidopsis thaliana* inositol *1,3,4,5,6-pentakisphosphate 2-kinase (AtIPK1) in complex with novel inositol phosphate surrogates*

3.1 Introduction

3.1.1 IPK1 classification

Kinase activity leading to the biosynthesis of IP_6 from each of the four separable IP_5's was first detected by ion exchange chromatography from mung bean extracts (Biswas, 1978). Subsequently, a description of IP_5 phosphorylation in mammalian cells was described, along with an account of the complete pathway for the synthesis of IP_6 from Ins(3)P in slime mould in which multiple inositol pentakisphosphate kinases were detected (Stephens et al, 1991). Inositol 1,3,4,5,6-pentakisphosphate (Ins(1,3,4,5,6)P_5) was found to be a prevalent intermediate above the other IP_5 isomers in both animal and plant systems. This observation later led to the isolation and purification of a inositol 1,3,4,5,6-pentakisphosphate 2-kinase (IP52K) (Phillipy et al, 1994). An inositol polyphosphate kinase found to be linked to nuclear mRNA export in yeast, designated with the name Ipk1p, was also identified and characterised as an IP52K (York et al, 1999). Classification of all kinases occurs in to 25 families and 10-folds, where IP52Ks belong to a structural family within the lipid kinase-like family (Cheek et al, 2005). Also in the lipid kinase-like family is inositol 1,4,5-trisphosphate kinase (I3P3K), of which the human and rat crystal structures have been solved (Gonzalez et al., 2004, Miller et al 2004). ATP grasp-like fold proteins also belong in the lipid kinase-like family, with the structure of inositol (1,3,4)-trisphosphate 5/6-kinase adopting such a fold (Miller et al, 2005). Although I3P3K, and other inositol polyphosphate kinases (IPKs), share conserved residues with IP52K at their substrate and cofactor binding sites, IP52K is unique in that it is the only IPK to phosphorylate the axial 2-OH position of *myo*-ins(1,3,4,5,6)P_5 (Phillipy et al, 1994).

3.1.2. IPK1 characterisation

As noted above, the *IPK1* gene was identified when investigating factors that mediate messenger RNA export in a yeast mutant deficient in Gle1P, a protein that associates with the nuclear pore complex (NPC) (York et al, 1999). The gene was found to encode an IP_5 kinase and enzymatic analysis revealed that it was converted Ins(1,3,4,5,6)P_5 to IP_6, thus classifying it as a IP_5 2-kinase. Mutations in *IPK1* led to IP_6 and mRNA export deficiencies, shedding light on essential NPC-factors that contribute to successful nuclear export and demonstrating a requirement for IP_6 in this process. The genetic screen that identified *IPK1* also recognised phospholipase C and an IP_3 kinase as essential for efficient mRNA nuclear export, also due to their involvement in the pathway to IP_6 synthesis.

Not long after, a comprehensive biochemical and functional characterisation of IP_5 2-kinases in fission and budding yeast provided additional evidence that *IPK1* encoded an IP_5 2-kinase (Ives et al, 2000). Many IPK1 orthologs across organisms have been identified since including human (Verbsky et al 2002), *Drosophila* (Seeds et al, 2004), and most pertinent to this study, plants (Stvenson-Paulick et al, 2005, Sweetman et al, 2006).

As introduced in section 1.3, phytate (IP_6) is the main store of phosphate in plant seeds. In *Arabidopsis thaliana*, disruption of *IPK1* (AtIPK1) coincided with a loss in phytate without an accumulation of precursors, therefore reporting a requirement for AtIPK1 in the later steps of seed phytate synthesis (Stevenson-Paulik et al., 2005). When measured in wild type seeds, the major inositol phosphate was IP_6, with levels of IP_4 and IP_5 undetectable (Stevenson-Paulik, Nagy et al, 2009). Conversely, in the mutant AtIPK1 T-DNA insertion line, *atipk1-1*, IP_6 levels were reduced, levels of P_i were higher and lower inositol phosphates such as IP_4 and IP_5 remained low and did not accumulate (Stevenson-Paulik et al., 2005). A desirable trait in cereal crops due to the deleterious effects of phytate in human and animal nutrition (see section 1.3), but has negative influences in

terms of plant growth. If this can be overcome in crop species, the high P_i-low phytate phenotype could be utilised in cereal crop agriculture.

Further characterisation of AtIPK1 and its substrate specificities was provided by Sweetman et al, (2006). Using radiolabelled ATP with thin layer chromatography and HPLC methods, it was confirmed that Ins(1,3,4,5,6)P_5 was a substrate for AtIPK1 along with ATP as a co-substrate, with subsequent kinetic analysis providing a K_M of 22 µM and V_{max} of 35 nmol.min^{-1} (Sweetman et al., 2006). Interestingly, Ins(1,4,5,6)P_4 was also found to be a substrate and yielded an IP_5 product albeit with weak activity, Stevenson-Paulik et al. (2005) had previously reported that it was an equally good substrate of AtIPK1.

3.1.3 The X-ray crystal structure of AtIPK1

As previously eluded to, AtIPK1 is novel in its structural class due to being the only phosphatase with the unique ability to phosphorylate at the 2-OH position, which is directionally axial compared the equatorial phosphates at all other positons of the *myo*-inositol ring (Gonzalez et al, 2010). This leads to striking differences in structure when compared to the remaining family of IPK proteins and renders it a distant family member.

Overall the fold consists of two lobes, designated the N-terminal (N-lobe) and C-terminal (C-lobe) lobes, connected by a hinge (Figure 3.1). The group of features that provide the majority of the interactions that bind the inositide substrate are within the large C-lobe and are referred to as the C_{IP}-lobe (Gonzalez et al, 2010).

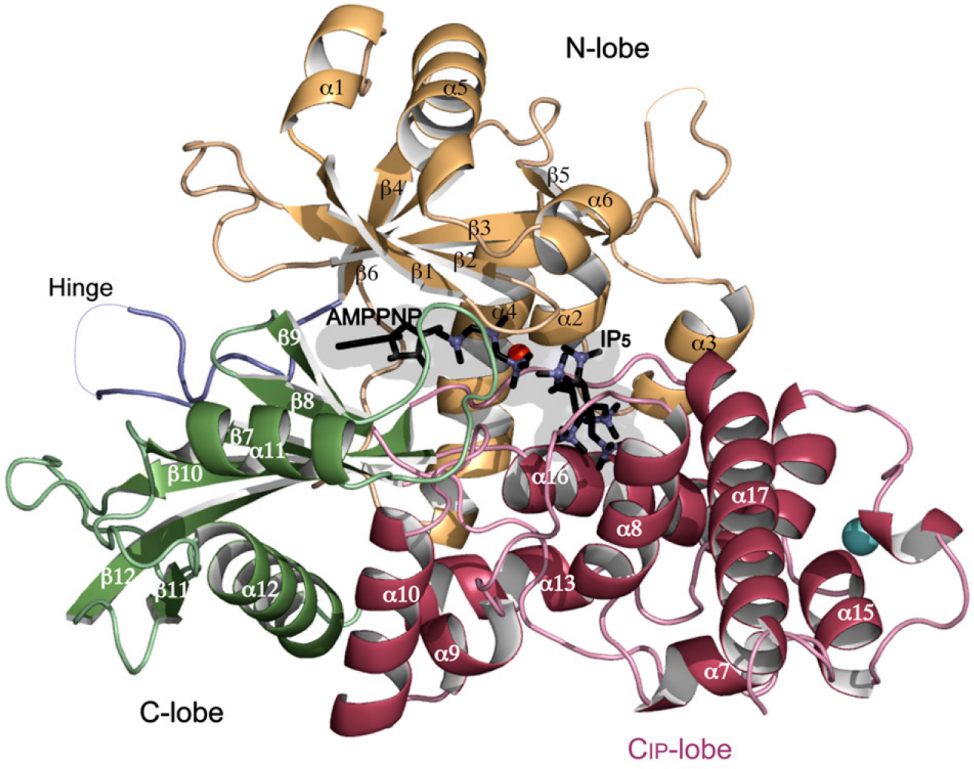

Figure 3.1 – Overall structure of AtIPK1 (taken from Gonzalez et al, 2010). Cartoon representation indicting the different lobes and the hinge that connects them. The N-lobe is orange, and the C-lobe green with the C_{IP} region coloured dark pink. The hinge connecting hinge is blue. The IP_5 substrate and AMPPNP (ATP analogue) are represented as black sticks. Magnesium and zinc ions are red and cyan spheres.

The inositide binding pocket has been identified along with the residues responsible for the recognition of the axial 2-OH that make this enzyme so distinctive amongst the family (Gonzalez et al., 2010). An IP substrate is tightly bound in the binding site through interactions with all phosphate groups, which mostly occur from within the region designated as the C_{IP}-lobe with the exception of the phosphate at the 1 position (P1) that is coordinated via two hydrogen bonds with an arginine from the N-lobe only (R130) (Figure 3.1). All interactions are deemed essential in positionally orienting the IP so the axial 2-OH is bought close to the nucleotide cofactor and magnesium ions for catalysis. The two residues that lend to this enzymes uniqueness are D368 and K168 which contact the P2(2-OH) position and are likely to confer the specificity for this IP_5 conformer.

In light of this structural information providing details on inositol phosphate coordination in to the active site, site directed mutagenesis studies of some of the observed key residues were carried out (Gonzalez et al, 2010). Mutants that replaced K168, the catalytic residue that interacts with the axial 2-OH, were unsurprisingly catalytically inactive. Additionally a D407A mutant, a catalytic residue that recognises the Pγ of the cofactor and the magnesium ion, maintained only 3 % catalytic activity. A mutation in the second residue that contacts the 2-OH, D368, also renders an inactive enzyme. As noted above, R130 is one of only two contacts between the N-lobe and the IP substrate, and the inactivity of a mutant highlights the importance of P1 binding in catalysis and the role of the N-lobe. These mutagenesis studies supported all the observable conclusions for ligand binding from the structure.

3.1.4 Conformational changes of AtIPK1 upon ligand and nucleotide binding

As noted above, residues in both the N- and C-lobes coordinate an inositide in to the active site, this consequently brings the two lobes together and has been termed the "closed form" of the protein. The closed form also features local changes where a clasp is formed between residues of α6 and L3, effectively closing the active site (Figure 3.2). W129 and R130 are the α6 residues that interact with E255 and G254 of L3, respectively. Mutation in R130 results in a 6-fold decrease in activity towards IP_5, but as it also coordinates P1 it is not clear if this is a result of compromised substrate binding and therefore catalytic function, or a hindrance from destruction of the clasp. It was concluded that mutation in W129 does not compromise enzyme function and its role in clasp formation is not critical. Interestingly, shortening L3 increased enzyme activity which is thought to be a result of improved product release, therefore the clasp maybe relevant for modulating kinetics rather than being essential for catalysis.

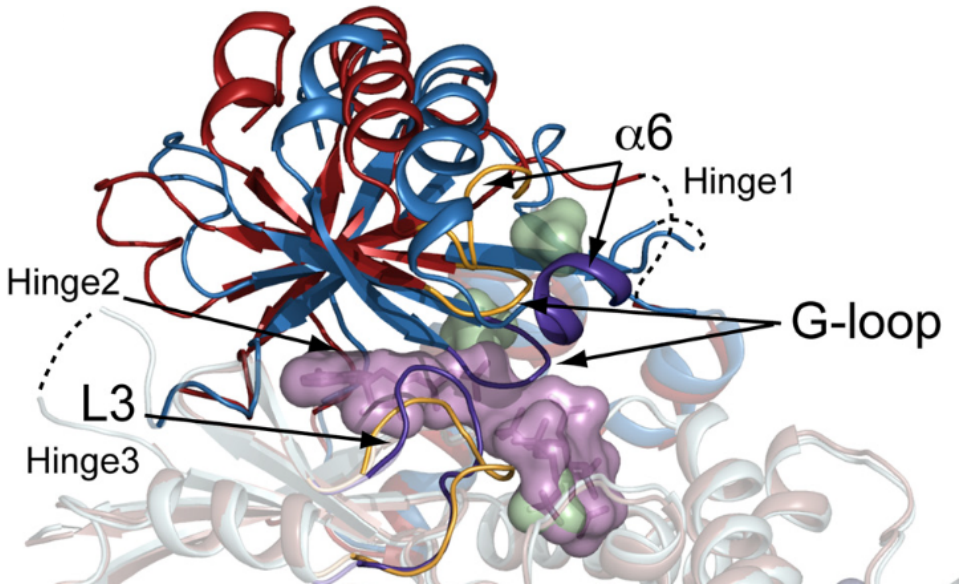

Figure 3.2 – Conformational changes of AtIPK1 upon ligand binding (taken from Banos-Sanz et al, 2012). Superposition of the open (red) and closed (blue) forms. The substrate and co-factor of the closed form are shown as purple surface representations.

The open form of the protein is represented by the apo-protein (W129A mutant), the clasp is unconnected and L3 can be considered mobile. Additionally, α6 shows disorder in this form therefore the conformation and stability of α6 and L3 is dependent on the clasp formation. Furthermore, the N- and C-lobes show a general rigid-body movement and are further apart. Movement occurs via the three hinges that are highly mobile and therefore disordered in the crystal structure. A comparison of the open and closed forms revealed little difference in the inositide binding site. It is mostly pre-formed in the apo-protein apart from the residues that recognise the inositide from within the distant N-lobe; the C_{IP} is the same in both arrangements.

A third conformation is represented by the nucleotide-bound structure of the protein (W129A mutant) and is termed the half-closed form, as it denotes an intermediate state between the apo-form and the closed-form of the protein. In this conformation the N- and C-lobes are closer than in the apo-form (open) but are still too distant to fully form the clasp between α6 and L3. These elements are only fully formed in the closed-form where L3 is also forming a "lid" that closes over the active site pocket. However, it appears to be partly formed through interaction of R130 and G252. The essential elements in the ATP binding site for nucleotide recognition are the same when compared to that of the ternary complex (closed), but Mg^{2+} is missing.

3.1.5 Experimental aims

As crystal structures of other IP_5-binding enzymes have been solved with the biphenyl polyphosphates as novel ligand surrogates (Mills et al., 2016a, Mills et al., 2012), it was intriguing to submit AtIPK1 in to crystallisation trials to see if it could also accommodate these IP analogues. Furthermore, crystal structures of AtIPK1 in complex with three of the benzene polyphosphate compounds had already been solved to good resolution by a colleague (H. Whitfield, unpublished) (section 1.3.1), which had revealed new precedence of essential ligand binding elements when compared to the canonical substrates. Any resulting structures would further reveal the ligand flexibility of AtIPK1, and could provide new notions on substrate coordinating residues as well as provide a well-informed framework for the design of other novel ligands and inhibitors.

3.2 Materials & Methods

Appendix 1 contains supplier addresses. Guidelines for all self-prepared buffers, media, and other additives can be found in appendix 2.

3.2.1 Small scale expression testing AtIPK1

A 1.5 mL aliquot of overnight culture grown in LB containing 0.5 % (w/v) glucose and ampicillin was centrifuged at 5000 rpm and the supernatant discarded. The cells were re-suspended in 5 mL LB with ampicillin plus either; 0, 0.2, 0.5, or 1 mM IPTG. The resulting cultures were incubated at either 18 or 25 °C for up to 16 h with shaking at 200 rpm. Protein expression levels of each culture were analysed by SDS PAGE.

3.2.2 Large-scale expression of AtIPK1 for purification

Large-scale expression cultures were 1 L in volume and at least 2 L of expression culture was used per purification. Per 1 L culture, 300 mL of O/N culture grown in LB containing 0.5 % (w/v) glucose was used to inoculate. The 300 mL culture was centrifuged at 5000 rpm and the supernatant discarded to harvest the cells. The resulting pellet was resuspended in to 1 L LB containing ampicillin. Optimum expression levels were achieved when the culture was supplemented with 0.2 mM IPTG and expressed O/N (approx. 16 h) at 18 °C with shaking at 200 rpm. The 1 L expression cultures were centrifuged at 5000 rpm for 20 min at 4 °C, with each resulting pellet being resuspended in 10 mL cell lysis buffer (see appendix 2) before being snap frozen in liquid nitrogen and stored at -80 °C.

3.2.3 Using 3C protease to remove the 6xHistidine tag

The protein was concentrated to 3 mL and the manufacturers guidelines for the use of HRV3C Protease (Sigma-Aldrich) followed. The reaction was incubated for approximately 16 hr at room temperature (18 °C).

3.2.4 Crystal screening and optimisation

The optimised conditions for the crystallisation of AtIPK1-His had already been established by a colleague and were based upon previously published conditions (Gonzalez et al., 2010). As AtIPK1-His possesses a 6xHistidine tag and was expressed from the pOPINF vector some optimisation upon literature conditions was required. Crystals were grown in 48-well plates using a sitting drop method at 16 °C and equilibrated against a 50 µL reservoir of buffer that was used as precipitant. Initially, crystals were grown in the presence of *myo*-IP_6 and ADP. Optimal conditions were identified as 20 % PEG 3350, 0.1M bis-tris propane pH6 with 2 mM $MgCl_2$. Protein at 10 mg/mL was incubated at 16 °C with 2 mM myo-IP6 and ADP prior to setting drops in a 1:1 ratio of protein to precipitant. Crystals formed as rod clusters within 24 hr and were harvested in to a seed bead (Hampton Research) with 50 µL precipitant to generate a seed stock for downstream microseeding. Using 6 mg/mL protein, drops under the same conditions were set replacing *myo*-IP_6 with the same concentration of the novel ligand. Immediately, approximately 0.1 µL of microseeding solution was added to each drop and the plate sealed. Crystals grew as plate clusters within 2-3 days and were harvested to produce a new seed stock. Fresh and final drops were set in the presence of novel ligand and again microseeded, this step being necessary to avoid the growth of mixed active site occupancy crystals and to improve crystal quality. The crystals grew as individual or clustered plates and were harvested between 2-3 days of growth depending on crystal size and quality.

3.2.5 Crystal cryoprotection

Single crystals were harvested in to 20 % PEG 3350, 25 % EG, 0.1 M bis-tris propane pH 6, 2 mM $MgCl_2$, 1 mM novel ligand and 1 mM ADP, and flash frozen in liquid nitrogen.

3.2.6 Data collection

X-ray diffraction data was remotely collected at Diamond Light Source (Oxford, UK).

3.2.7 Data processing and refinement

Diffraction data was indexed and auto processed by Xia2. Molecular replacement was performed using Phaser-MR within the Phenix suite (McCoy et al., 2007) and structures refined using Phenix refine (Afonine et al., 2005). Coot (Emsley et al., 2010) was used for manual adjustment to models between rounds of automatic refinement. Ligands were built based upon biphenyl 2,3',4,5',6- pentakisphosphate (PDB 4A9C) and edited in REEL before refinement in eLBOW (Moriarty et al., 2009).

3.3 Results and Discussion

3.3.1 Expression and Purification of AtIPK1-His

Cloning of *AtIPK1*-His in to the pOPINF vector was previously accomplished by a colleague and the construct stored as a glycerol stock in *E. coli* Stellar cells. The plasmid was purified using the Wizard® *Plus* SV Miniprep DNA Purification System (Promega) from an O/N culture which had been inoculated using the Stellar glycerol stock, and grown in LB medium supplemented with ampicillin (Section 2.2.6). Once purified, the plasmid was transformed in to chemically competent *E. coli* Rosetta cells (sections 2.2.7 & 8). Two single colonies were selected to inoculate 100 mL cultures in LB containing 0.5 % (w/v) glucose and ampicillin for use as starter cultures for the small scale protein expression testing of AtIPK1-His, as described in section 3.2.1. Parameters investigated were; temperature, IPTG concentration and length of incubation post IPTG addition (results not shown). It is necessary to grow the starter cultures in the presence of 0.5 % glucose to minimise basal or "leaky" expression of AtIPK1-His which can be toxic to the cells when trying to reach the exponential growth phase. This can lead to plasmid instability and/or loss of the plasmid, causing the culture not to grow. Additionally, protein aggregation or expression in to inclusion bodies can occur, affecting the solubility. Cells must be harvested by gentle centrifugation and re-suspended in media without glucose to allow IPTG inducible expression of AtIPK1-His. This step could be avoided by the use of an expression host strain containing the pLysS plasmid, which provides constitutive expression of phage T7 lysozyme to inhibit the T7 RNA polymerase that is expressed from a chromosomal gene and is under the control of the *lacUV5* promoter for IPTG induced expression. Intrinsic inhibition of T7 RNA polymerase like this would eliminate the need for the addition of glucose to repress induction of the *lac* promoter by lactose found in the media. The most efficient expression of AtIPK1-His by the Rosetta expression host cells was achieved using 0.2 mM IPTG to induce protein expression, with incubation at 18 °C plus shaking at 200 rpm for approx. 16 h post IPTG addition.

This was then applied to large scale expression tests with 1 L cultures (Figure 3.3) (Section 3.2.2). A high expression yield in the larger cultures was also observed under these conditions and a strong band the approximate size of AtIPK1-His (51.5 kDa) can be visualised on the SDS-PAGE gel, therefore these were pursued for the purification of AtIPK1-His. A glycerol stock of the original starter culture was made and snap frozen then stored at -80 °C for later use.

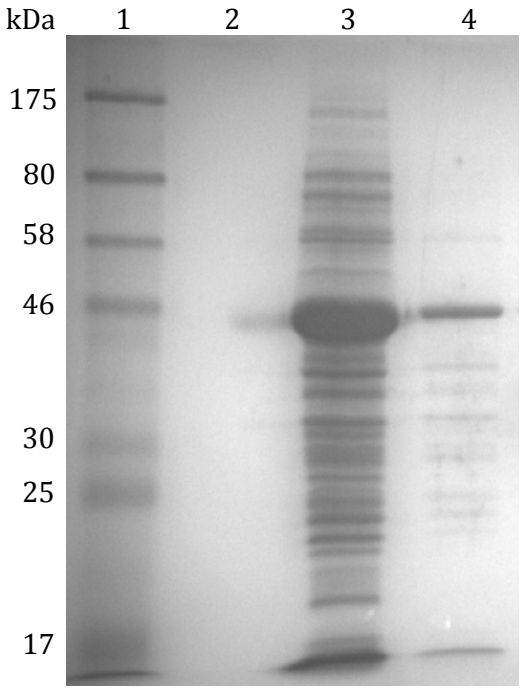

Figure 3.3– SDS-PAGE analysis on a 10 % acrylamide gel of a whole cell pellet originating from a 1 L expression culture of AtIPK1-His. (1) Protein molecular weight marker. (2) Empty. (3) 1:1.5 (v/v) of pelleted culture to SDS-loading buffer. (4) 1:10 (v/v) dilution of lane 3 with SDS-loading buffer.

AtIPK1-His protein was purified in a simple two step purification, as per the method described in section 2.2.17. To obtain a high yield of protein suitable for crystallographic studies at least 2 L of expression culture was required.

Figure 3.4 shows the SDS-PAGE analysis of fractions that were identified as containing AtIPK1-His from the UV absorbance trace during nickel affinity purification. The overexpressed AtIPK1-His can be seen in fractions 15 to 21 (lanes 2-5) but is negligible in fraction 23 (lane 6). Overall, very few contaminants can be seen therefore fraction numbers 14 to 22 were combined and carried forward for subjection to size exclusion chromatography.

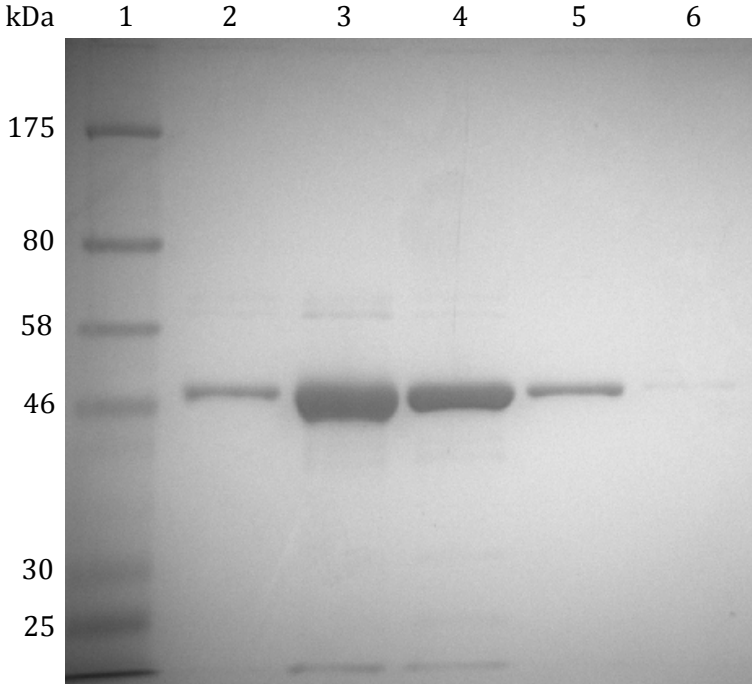

Figure 3.4 – Immobilised metal affinity purification of AtIPK1-His. SDS-PAGE analysis, on a 10 % gel, of eluate fractions recovered during NiNTA chromatography. (1) Protein molecular weight marker. (2-6) Fraction number; 15, 17, 19, 21 & 23, respectively.

Size exclusion chromatography was performed as described in section 2.2.17 on a HiLoad 16/600 Superdex 75 pg column (GE Healthcare Life Sciences) and resulted in a peak on the UV absorbance trace corresponding to fraction numbers 12-16, samples of which were analysed by SDS-PAGE (Figure 3.5). An earlier peak was also detected but was assumed to be larger contaminant proteins eluting in the void volume. It was confidently concluded that fractions 12 to 14 contain purified AtIPK1-His (lanes 3 &5). Fraction 16 also had small amount of purified protein so it can be assumed fraction 15 also contains AtIPK1-His. It is also likely that fraction 11 had a high quantity of AtIPK1-His, therefore fractions 11-16 were subsequently pooled for concentration to 10 mg/mL. A typical protein yield obtained from a 2 L preparation was 20 mg.

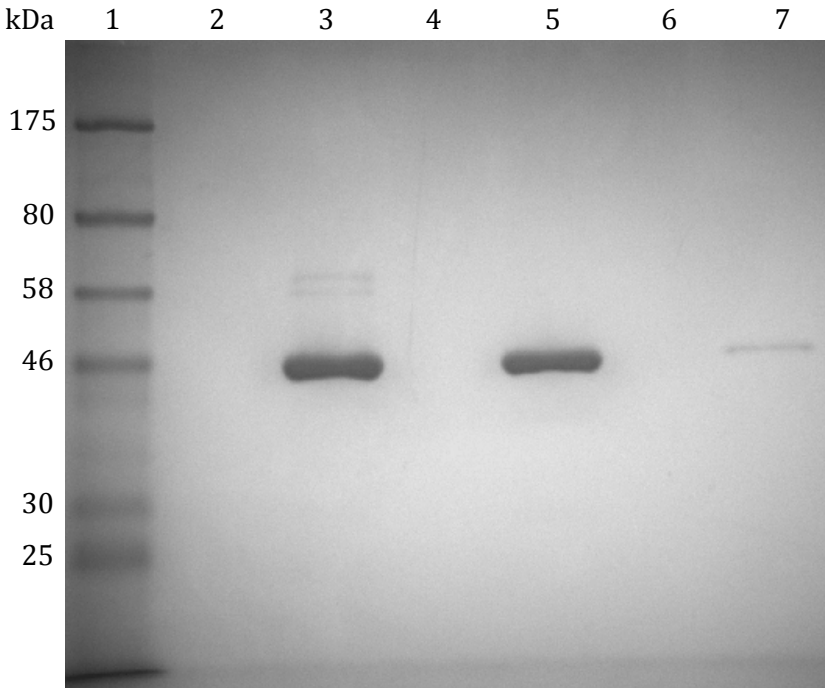

Figure 3.5 – Size exclusion chromatography of His-AtIPK1. SDS-PAGE analysis on a 12.5 % acrylamide gel of the fractions from sepharose gel filtration column eluate that contain His-AtIPK1. (1) Protein molecular weight marker. (3, 5 ,7) Fraction number; 12, 14 & 16, respectively. (2,4,6) Empty.

A sample of the final purified and concentrated protein was analysed by SDS-PAGE and stained with InVision™ His-tag In-gel Stain (Novex by Life Technologies), then subsequently with a Coomassie blue stain as per section 3.2.6 (Figure 3.6). As the sample was highly concentrated, a 1:15 dilution of the protein was used.

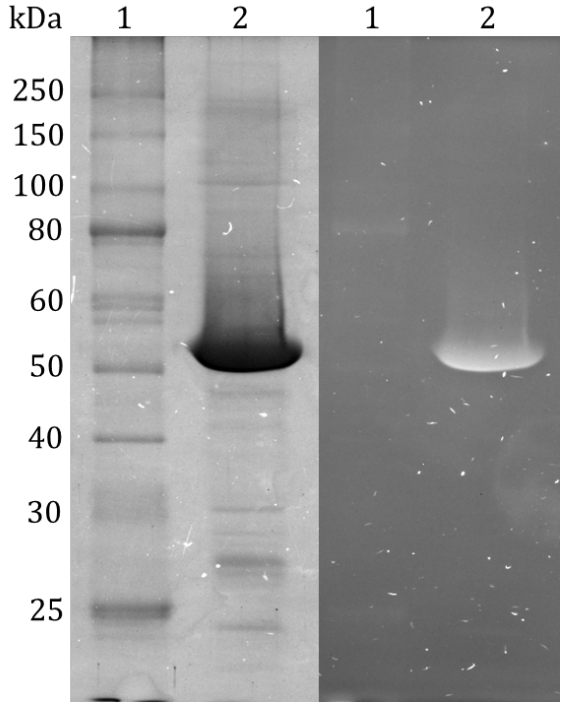

Figure 3.6 – SDS PAGE analysis of purified AtIPK1-His on a 10 % gel. Coomassie blue staining (left) and InVision staining (right). (1) Protein molecular weight ladder (2) 1:15 dilution of purified AtIPK1-His.

The InVision stain binds specifically to the 6xHistidine tag and can be used to accurately detect the presence of His-tagged fusion proteins due to its fluorescence properties at an excitation wavelength of 560 nm, and emission maxima at 590 nm. It can provide a quicker and simple alternative to a western blot to confirm the presence of His-tagged fusion proteins. As can be seen in figure 3, AtIPK1-His can be identified with both staining methods with low levels of contaminant proteins present. The InVision staining also confirms the absence of any 6xHistidine tagged truncates of AtIPK1-His that may have occurred during overexpression, or due to protein degradation or hydrolysis by proteases during purification.

3.3.2 Cleaving the histidine tag and purification of AtIPK1

The original cloning strategy placed a 3C protease recognition site between the N-terminal 6xHistidine tag and the protein coding sequence. Although, as explained later in this study, the 6xHistidine tag is advantageous to successful crystallisation of AtIPK1, it is preferential to remove this tag for the purpose of enzymatic assays and other studies. The protein was purified as previously detailed in 3.3.1, and cleavage of the 6xHistidine tag set up post size exclusion chromatography using HRV3C Protease (Sigma-Aldrich) (Section 3.2.3). The protein was concentrated to 3 mL and the manufacturers guidelines followed. The reaction was incubated for approximately 16 hr at room temperature (18 °C) (results not shown).

The products of the His-tag cleavage reaction were loaded on to a 5 mL NiNTA superflow cartridge (Qiagen), equilibrated with buffer A, at a flow rate of 0.5 mL/min in a continuous loop for 30 min. The eluate containing AtIPK1 was collected in a 10 mL fraction and five subsequent 2 mL fractions whilst the column was subjected to buffer A at a 1 mL/min flow rate. Subsequently, a final 10 mL fraction was collected when washing the column with buffer B. All fractions were analysed by SDS-PAGE (Figure 3.7). The majority of AtIPK1 was eluted in the initial 10 mL fraction whilst the 6xHistidine tag and 3C protease remained on the column. The final 10 mL fraction contained some AtIPK1-His meaning the removal of the 6xHistidine tag was not 100 % effective (lane 8). However, this is a trivial quantity when compared to the successfully cleaved protein (lanes 2-5). Other bands seen in lane 8 are likely to be the 6xHistidine tag and 3C protease. The comparatively small concentration of 3C protease used was very efficient under the conditions tested and produced a high yield of protein recovery.

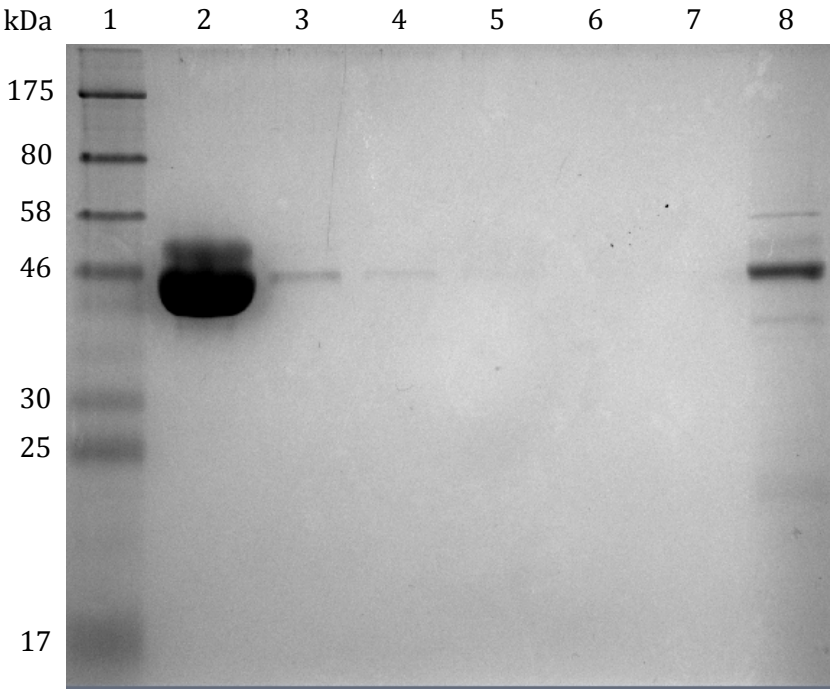

Figure 3.7 – Immoblised metal affinity purification post-proteolytic cleavage of His-AtIPK1 with 3C protease. Samples of eluate fractions from the NiNTA column upon washing with NiNTA buffer A, Analysed on a 12.5 % acrylamide gel. (1) Molecular weight marker. (2) Initial 10 mL fraction. (3-7) Subsequent 2 mL fractions. (8) Final 10 mL wash with NiNTA buffer B.

A final size exclusion chromatography step was added, and performed as described previously, returning the protein to an imidazole free buffer. The protein was concentrated prior to snap freezing in liquid nitrogen and subsequently stored at -80 °C.

3.3.3 Crystallisation of AtIPK1 with biphenyl 2,3',4,5',6-pentakisphosphate, and biphenyl 3,3',4,4',5,5'-hexakisphosphate.

Biphenyl phosphates have been described as synthetic ligands and inhibitors of inositol polyphosphate-converting enzymes, examples of which were discussed in chapters 1 & 2 (Vandeput et al., 2007, Mills et al., 2012, Mills et al., 2016b). AtIPK1 has also been investigated by the Brearley lab for binding of single ring benzene polyphosphates, which are also reported as synthetic substrates and inhibitors of inositol polyphosphate-metabolising enzymes (Ward et al., 1995, Mills et al., 2006, Mills et al., 2008). Structures of AtIPK1-His in complex with three of these inositol polyphosphate mimics have been solved (unpublished). To follow on from this work, AtIPK1 has been investigated for its ability to coordinate the double ringed biphenyl polyphosphate compounds. Four biphenyl phosphate compounds were available from collaborators (Potter, B.V.L.; University of Bath), and are described in section 1.1.3. All of which were utilised in crystallisation trials with AtIPK1.

Crystals were obtained using 6xHistidine tagged AtIPK1 (AtIPK1-His) protein as previous experience in the lab indicated that the tagged version of the recombinant protein resulted in crystals that diffracted to a higher resolution when compared to those grown with AtIPK1 protein that had been cleaved of the 6xHistidine tag. Crystallisation was achieved as described in the section 3.2.4, using buffers and precipitant that had previously proved successful in generating high quality AtIPK1-His crystals. This method differs from the published conditions from the González group, which used a bis-tris methane buffer as opposed to bis-tris propane. Additionally, the González structures of AtIPK1 contain no 6xHistidine tag.

Crystals grew as plate or rod clusters, and after two to three days of growth were separated and individually harvested in to cryoprotectant for storage in liquid nitrogen. The morphology of crystals of AtIPK1 with biphenyl-2,3',4,5',6-pentakisphosphate [BiPh(2,3',4,5',6)P_5] and ADP, and with biphenyl-3,3',4,4',5,5'-hexakisphosphate [BiPh(3,3',4,4',5,5')P_6] and ADP can be seen in Figure 3.8.

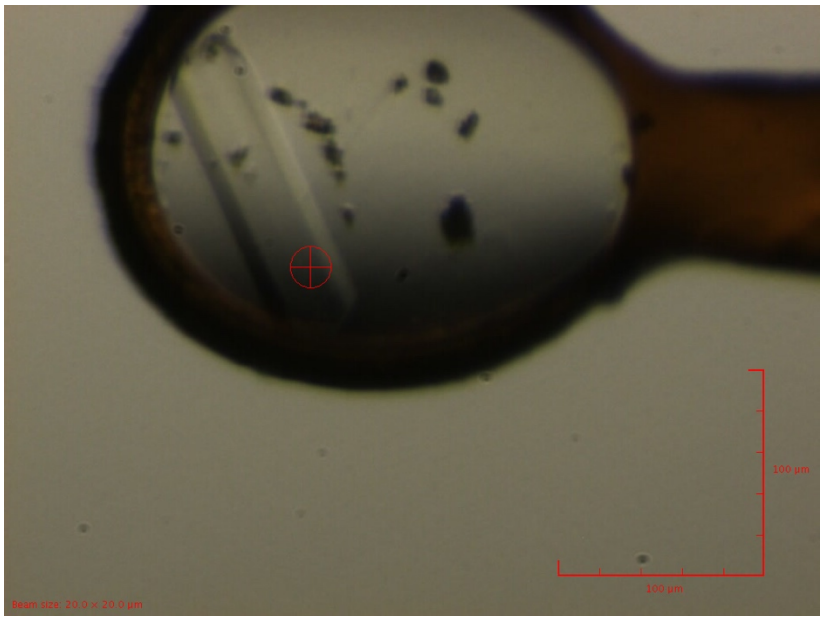

Figure 3.8 – Example of an AtIPK1-His crystal exposed for data collection at the Diamond Light Source. Image is of an AtIPK1-His BiPh(3,3',4,4',5,5')P_6 crystal before exposure to the beamline.

Successful and high quality crystals of AtIPK1-His in complex with BiPh(2,3',4,5',6)P_5 or BiPh(3,3',4,4',5,5')P_6 were only achieved by using the co-crystallisation and micro-seeding method described in the materials and methods.

3.3.4 Crystal structures of AtIPK1 with biphenyl 2,3',4,5',6-pentakisphosphate, and biphenyl 3,3',4,4',5,5'-hexakisphosphate.

The highest resolution data sets collected for AtIPK1-His in ternary complexes with BiPh(2,3',4,5',6)P_5 and BiPh(3,3',4,4',5,5')P_6 (and ADP) were from crystals that diffracted to resolutions of 2.18 Å and 2.07 Å, respectively. Data processing and model refinement in the P1 space group was achieved using the Phenix suite (Adams et al., 2010). Table3.1 contains the data collection and refinement statistics for both ternary complexes, from herein referred to as AtIPK1-His BiPh(2,3',4,5',6)P_5 / BiPh1 and AtIPK1-His BiPh(3,3',4,4',5,5')P_6 / BiPh3.

Table 3.1 – X-ray diffraction data processing and model refinement statistics for AtIPK1-His BiPh(2,3',4,5',6)P_5 / BiPh 1 and AtIPK1-His BiPh(3,3',4,4',5,5')P_6 / BiPh3.

Data Processing		
	BiPh(2,3',4,5',6)P_5	**BiPh(3,3',4,4',5,5')P_6**
Space Group	P1	P1
Unit Cell		
a, b, c (Å)	59.9, 59.8, 85.4	59.6, 59.8, 85.3
α, β, γ (°)	87.7, 87.7, 63.6	87.8, 88.1, 64.0
Resolution (Å)	53.6-2.18 (2.24-2.18)	53.6-2.07 (2.12-2.07)
R_{merge} (%)	0.062 (0.588)	0.050 (0.495)
<I/σ(I)>	8.7 (1.7)	9.3 (1.9)
$CC_{1/2}$	0.991 (0.616)	0.996 (0.721)
Completeness (%)	95.31 (96.0)	96.67 (97.0)
Multiplicity	2.8 (2.9)	2.9 (3.0)
Wilson B-factor	48.22	49.77

Refinement		
	BiPh(2,3',4,5',6)P_5	**BiPh(3,3',4,4',5,5')P_6**
Number of Non-hydrogen atoms	7055	7214
Waters	193	268
Resolution (Å)	53.6-2.18 (2.22-2.18)	53.6-2.07 (2.10-2.07)
R_{work} (%)	18.4 (29.7)	17.9 (27.9)
R_{free} (%)	23.0 (34.5)	22.0 (29.7)
Mean B-value ($Å^2$)	57.5	60
RMSD Bonds (Å)	0.008	0.008
RMSD Angles (°)	1.182	1.117
RMSD Planes (Å)	0.005	0.005
Ligand Occupancy (%)		
Chain A	79	84
Chain B	77	85

Previously published structures of AtIPK1 were obtained in a different space group and unit cell dimension to those in this study, although it should be noted some of these were structures of a W129A mutant of IPK1 (Baños-Sanz et al., 2012; González et al., 2010). The observed space groups for the mutant and native IPK1 in the literature were $P2_12_12$ and $P2_12_12_1$, respectively. However, similarities can be drawn upon; the refined P1 AtIPK1-His BiPh1 and AtIPK1-His BiPh3 structures presented here also have two molecules (A and F) present in the asymmetric unit (AU), comparable to the native protein in both binary and tertiary complexes from the previous studies (Figure 3.9 A). The observed P1 space group is in agreement with all other AtIPK1-His structures generated from the Brearley lab (unpublished data).

The two AtIPK1-His complexes presented have a bis-tris propane molecule associated with molecule A and a tris molecule associated with molecule F. As this appears in both AtIPK1-His structures, bis-tris propane is likely to be critical to crystal packing and stabilisation of the molecules within the unit cell. Additionally, attempts of crystallisation without bis-tris propane, under the conditions that the González group used, were unsuccessful. The density for the tris molecule associated with molecule F in both structures is likely to be another bis-tris molecule, but it could not be confidently modelled to the double difference Fourier electron density, so was left simply as a tris molecule. Although, an argument can be made that as this occurs in both AtIPK1-His structures presented here, it could be a real artifact of crystal packing. Additionally, the tris molecule associated with molecule F is also present in previous AtIPK1 structures produced by the lab (unpublished data), but there is also speculation in this case that it could also be a bis-tris propane, again because it could not be satisfactorily modelled to the electron density maps.

Both refined structures contain the novel ligand (BiPh1/BiPh3), ADP and two magnesium ions in each molecule, as well as a zinc ion coordinated by two cysteines and two histidines in the C-lobe of the protein (Figure 3.9 - B). This is in agreement with previously reported data (Baños-Sanz et al., 2012; González et al., 2010).

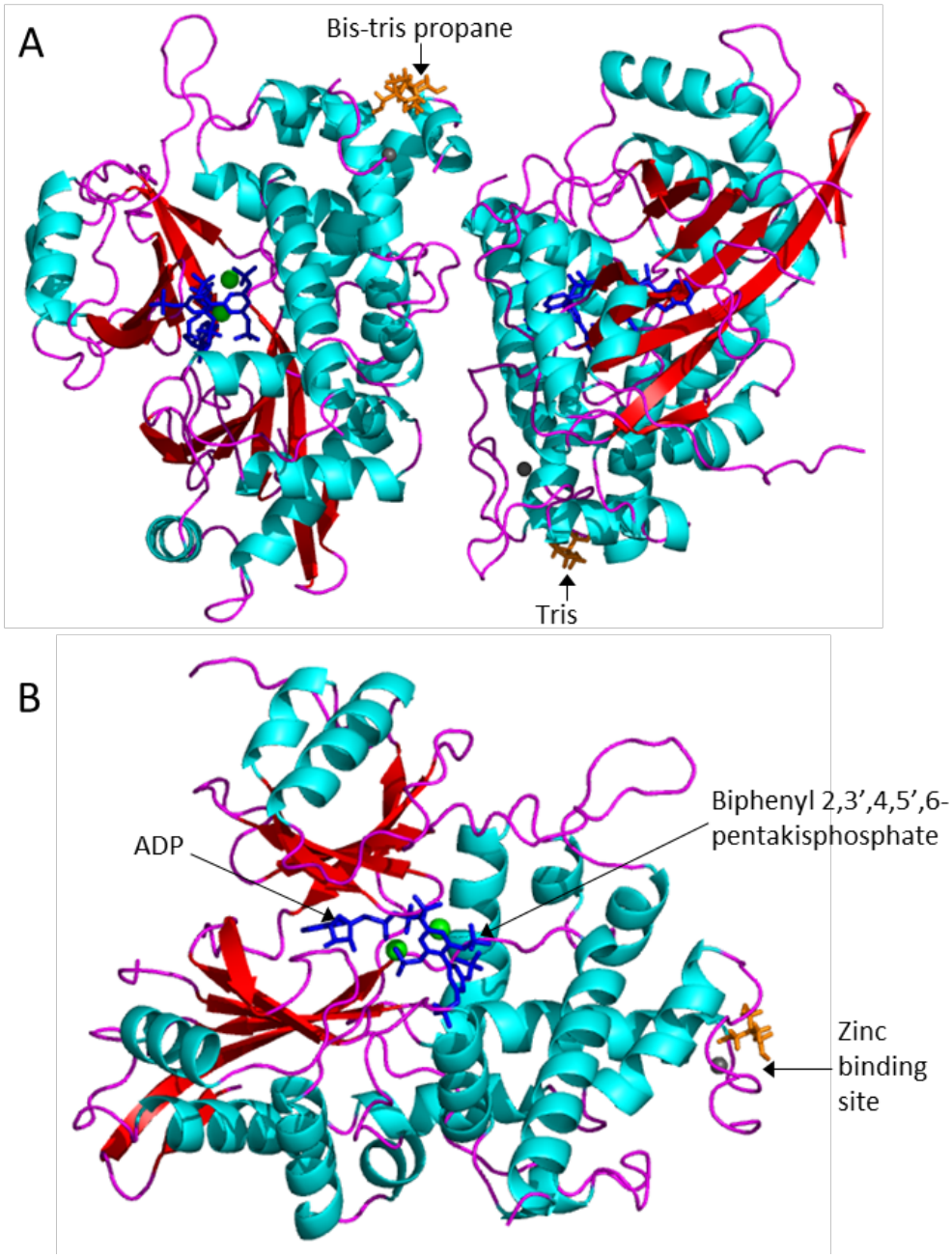

Figure 3.9 – AtIPK1-His BiPh(2,3',4,5',6)P_5 and ADP crystal structure represented as a cartoon and coloured by secondary structure elements. (A) The two molecules in the asymmetric unit. (B) A single molecule of the asymmetric unit - Chain F. The active site is indicated by the presence of BiPh(2,3',4,5',6)P_5 and ADP, and is represented as blue sticks. The two magnesium ions in the active site are shown as green spheres, and zinc as a grey sphere. A tris molecule that associates with the protein upon crystallisation is shown as orange sticks.

Both AtIPK1-His structures present cross AU interactions with neighbouring symmetry related molecules in the lattice via what has been term as a 'fireman's grip'; the 6xHistidine tag from molecule A in the asymmetric unit (AU) 'wraps around' a 6xHistidine tag from molecule F in a neighbouring AU, appearing to stabilise the lattice structure (Figure 3.10). Again, this is in agreement with other AtIPK1-His structure complexes from the group (unpublished data) and is likely to be a reason for the difference in space group observed when compared to the González et al., (2010) and Baños-Sanz et al., (2012) structures, which were crystallised without a histidine tag.

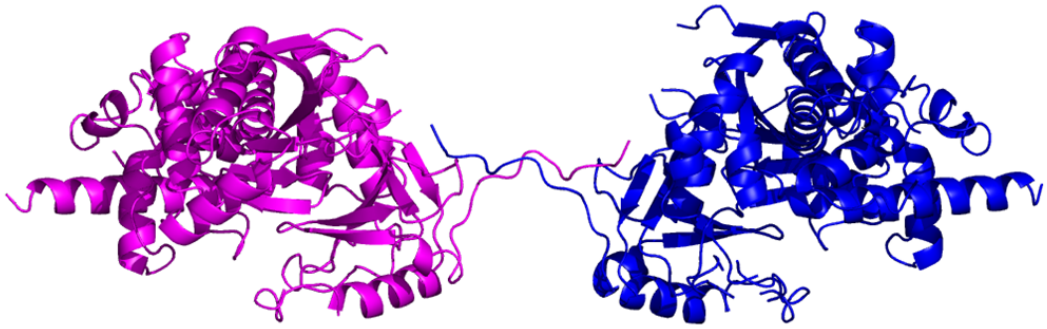

Figure 3.10 – The firemans grip interaction formed by the 6xHis tags from two neighbouring asymmetric units between molecule F (magenta) and molecule A (blue).

The two molecules in the AU for the AtIPK1-His BiPh1 structure globally align to each other with a RMSD of 0.341, and the active site residues 0.176. The near equivalence can be seen for the AtIPK1-His BiPh3 structure where the respective alignment results are 0.331, and 0.155. This reveals that these complexes are likely to have a single conformation within the AU, with reliable models built for both chains but with minor differences which were also revealed in previous structures from the lab (unpublished) and were attributed to the AU-AU interactions between the 6xHistidine tags acting to stabilise an external loop in molecule A when compared to B (results not shown). In the active site region of AtIPK1 BiPh1, Arg45 is in a different position in each molecule, but this is not supported by difference electron density which is of poor quality around this residue, preventing clear interpretation of the position of this residue. Similarly, this also occurs in the two molecules of the AtIPK1 BiPh3 complex. It is also noteworthy that the protein is in complex with much larger ligands when compared to previous structures. As discussed later, it has undergone large conformational changes to accommodate the novel ligands. This may result in differences between the two molecules in the AU during model building and refinement, as parts of the polypeptide were manually built, particularly in flexible regions.

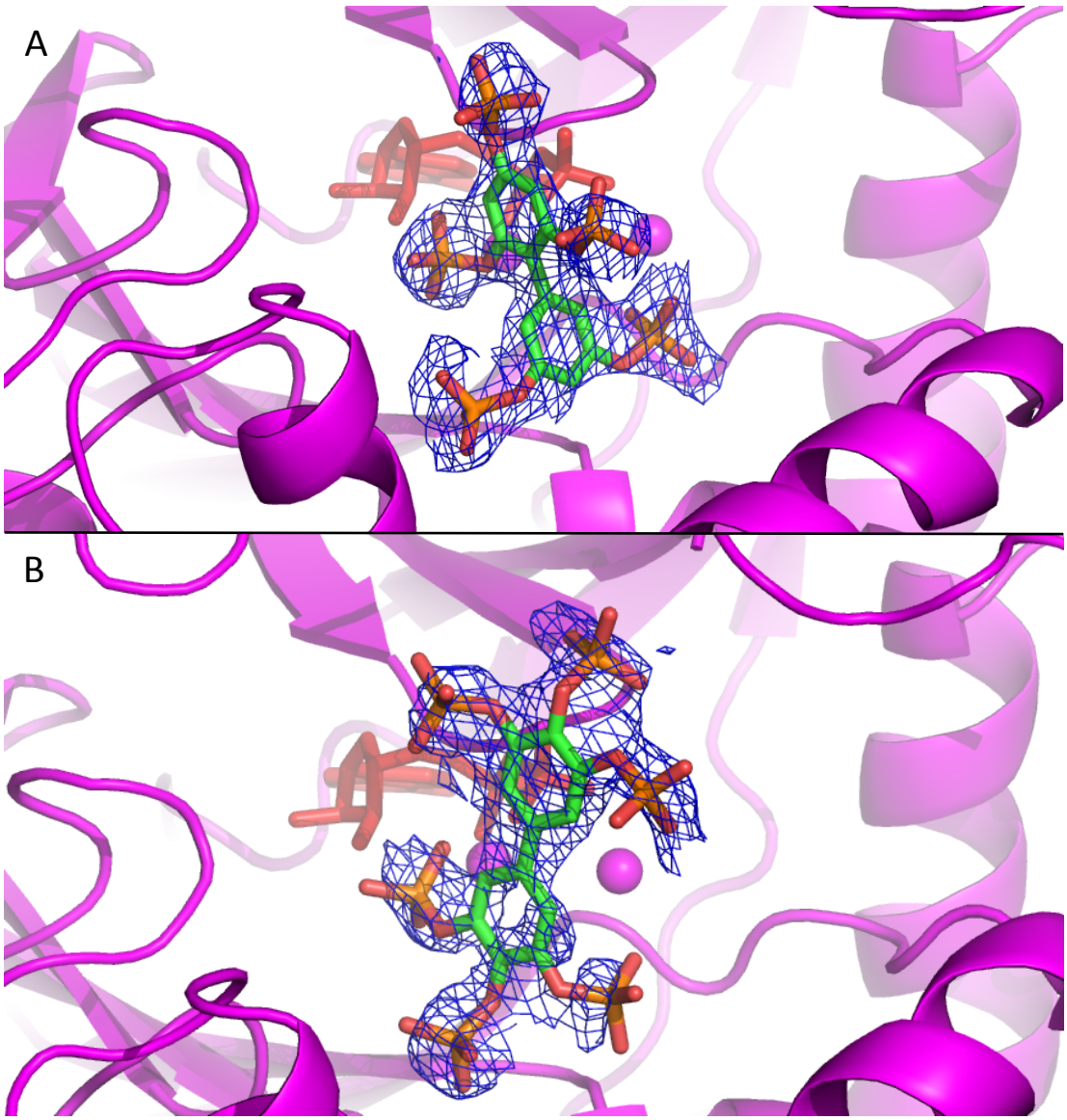

Figure 3.11 – Active sites of AtIPK1-His BiPh(2,3',4,5',6)P_5 and AtIPK1-His BiPh(3,3',4,4',5,5')P_6 showing binding positions and simulated annealing omit maps. (A) AtIPK1-His BiPh(2,3',4,5',6)P_5 (B) AtIPK1-His BiPh(3,3',4,4',5,5')P_6. Ligands are shown as green sticks, ADP as red sticks and magnesium atoms as magenta spheres. The density maps are represented as a blue mesh and are at a contour level of 1.2 σ.

Both BiPh(2,3',4,5',6)P_5 and BiPh(3,3',4,4',5,5')P_6 were found to be bound in the active site of AtIPK1-His; between the N- and C-lobes, where density maps reveal their binding positions (Figure 3.11). The molecules were in the same binding orientation in chains A and F for both BiPh1 and BiPh3, this together with the low RMSD for the superimposition of the active site residues, respectively 0.176 and 0.155, suggest that both ligands possess a single energetically stable binding position within the active site of AtIPK1. However, in respect to one another, the ligands are bound in different orientations.

This is likely to be explained by the differing numbers of phosphates and their spatial positioning on the phenyl rings, as well as the relative planes of each ring in the molecule. The rings of BiPh3 are planar with respect to one another, and slightly rotated in BiPh1. This rotation around the C1-C1' bond allows the phosphate groups to optimise their interactions within the binding site. Due to this there are also differences in the residues that co-ordinate the two ligands (Figure 3.12).

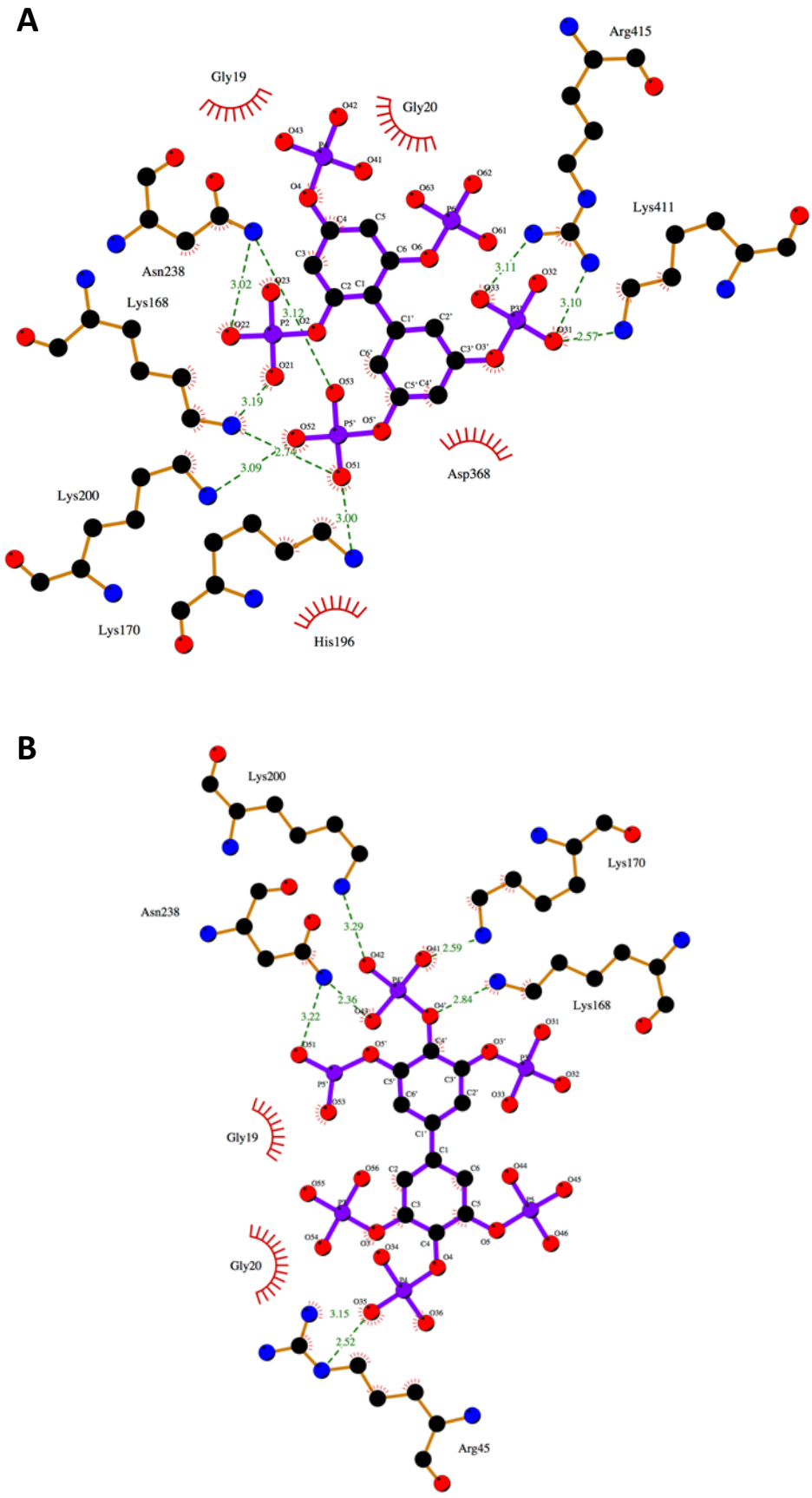

Figure 3.12 Ligplot diagrams of the contacts formed by the BiPh(2,3',4,5',6)P_5 and BiPh(3,3',4,4',5,5')P_6 ligand in the active site of AtIPK1-His. (A) BiPh(2,3',4,5',6)P_5 (B) BiPh(3,3',4,4',5,5')P_6.

Analysis of hydrogen bonding and hydrophobic interactions was achieved using the LigPlot+ program (Laskowski & Swindells, 2011), which automatically generates schematic diagrams of protein-ligand interactions based on the distances between atoms in a given PDB file (Figure 3.12). This revealed that both compounds are coordinated by K200, K170, N238 & K168, suggesting that these residues are likely to be critical to coordinating and positioning substrates in the active site. These mutual residues co-ordinate P5' of BiPh1, and P4' of BiPh3, and shed light on the relative juxtaposed binding orientations of the two ligands. Interestingly, with a physiological substrate (*myo*-IP_5 or -IP_6) the same residues interact with P6 (González et al., 2010). This is also in agreement with structures of AtIPK1-His with benzene polyphosphates where the same residues also provide coordination to a particular phosphate (unpublished data).

Additionally, two of the four 'P6-coordinating residues', K168 and N238, also form secondary contacts with another phosphate, P2, on the 'upper ring' of BiPh1 and P5 on the lower ring of BiPh3 (as orientated in the active site figures). When compared to *myo*-IP_5 / -IP_6 these residues form similar interactions with P1. No additional interactions with the upper rings of the two compounds are present with exception of R45 with P4 of BiPh3, but as discussed previously the position of R45 is not supported by difference electron density therefore its role must be considered with caution. The P3 of BiPh1 is coordinated by K411 and R415, both of which form interactions with the P4 phosphate on the canonical inositol phosphate substrate. It seems that most interactions that coordinate the ligand in the active site occur on the "lower" ring of the biphenyl compounds, with the exception of P2 of BiPh1. This is unsurprising when considering physiological substrates are single ring compounds.

Superposition of chain F of the AtIPK1-His BiPh1 and BiPh3 structures reveals that the positioning of the 'P6 coordinating residues' are conserved between the two structures (Figure 3.13). The two structures globally align with an RMSD of 0.186, indicating that the difference in the spatial positioning of the phosphates between the two ligands does not significantly alter the overall conformation of the AtIPK1. Additionally, there are no significant domain movements and the active site features such as the G-loop, L3 and α6 overlay closely (see section 3.1). There is a small difference in the positioning of one of the magnesium ions. It should also be noted that there is no contact between these ligands and the ADP cofactor via the magnesium ions, unlike structures with traditional substrates.

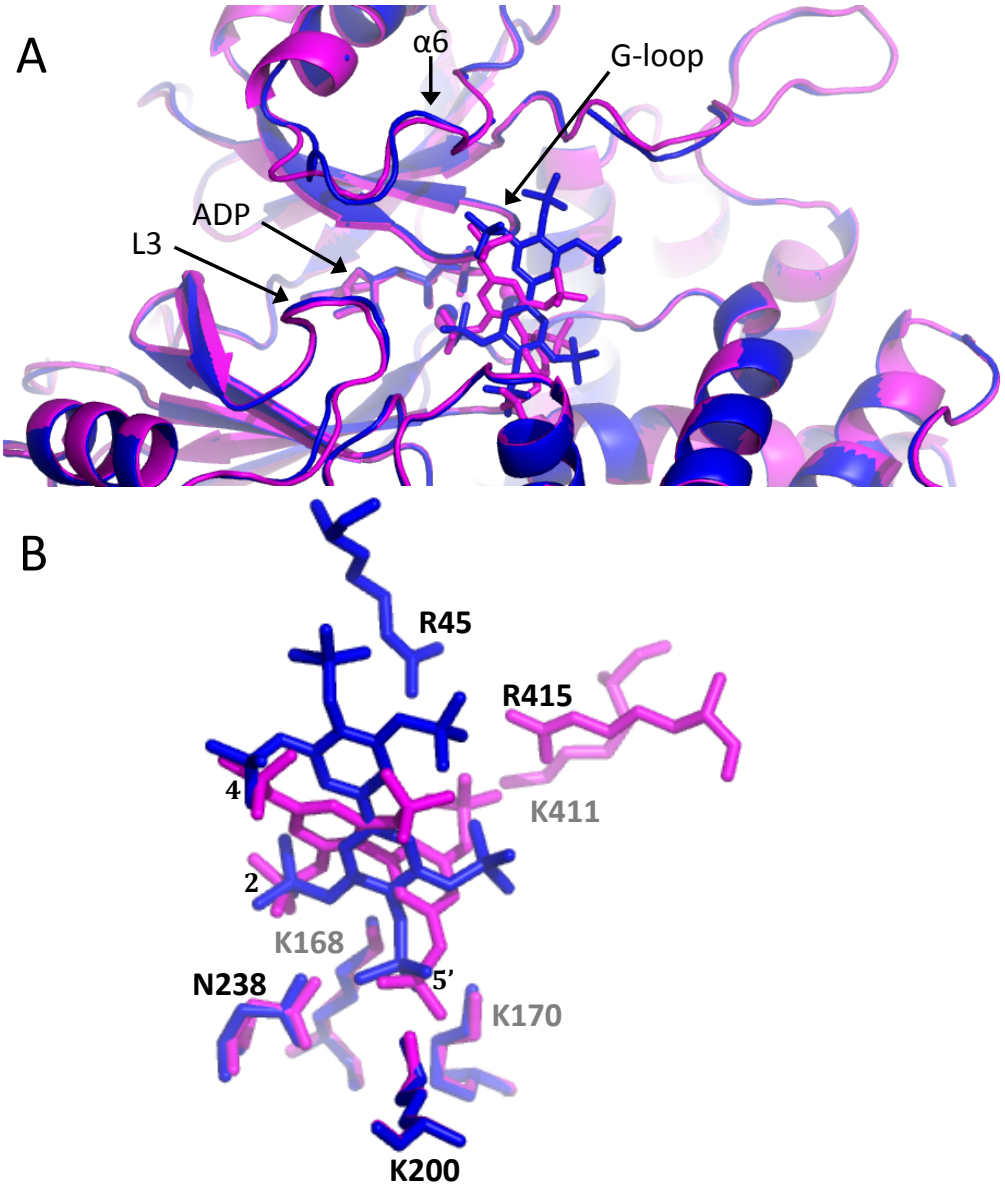

Figure 3.13 - Global alignment of AtIPK1-His BiPh(2,3',4,5',6)P_5 (magenta) and AtIPK1-His BiPh(3,3',4,4',5,5')P_6 (blue) complexes. (A) The overlaid active sites of the two complexes. (B) Active site residues that co-ordinate the ligands. BiPh(2,3',4,5',6)P_5 and BiPh(3,3',4,4',5,5')P_6 can been seen in the active site of the structures in both images, and are represented as sticks. The magnesium ions are shown as spheres and ADP as sticks, coloured according to the complex to which they belong. Phosphate positions are labeled according to BiPh1.

As mentioned previously, comparing the positions of the ligands in the active site shows they are bound in very different orientations despite being structurally similar. This is likely achieved by the differences in the number and spatial arrangement of phosphates, as well the rotation of the C1-C1' bond. The two ligands bear three phosphate positions that are superimposed, and are labeled in according to the numbering of BiPh1 (Figure 3.13). Two of these have already been discussed above and occupy the P1 and P6 positions of a bound *myo*-IP_5 or IP_6. The additional alignment of phosphates occurs between P4 of BiPh1 and P3 of BiPh3 on the upper rings of both compounds. These phosphates appear to have no hydrogen bonding interactions with AtIPK1.However, nearby hydrophobic contacts with G19 and G20 occur with both ligands. This may not be an important artifact of anchoring a substrate in to the active site given the lack of hydrogen bonding between the protein and ligand in this region, but it may provide further stabilisation which in turn allows the protein to accommodate a much larger ligand.

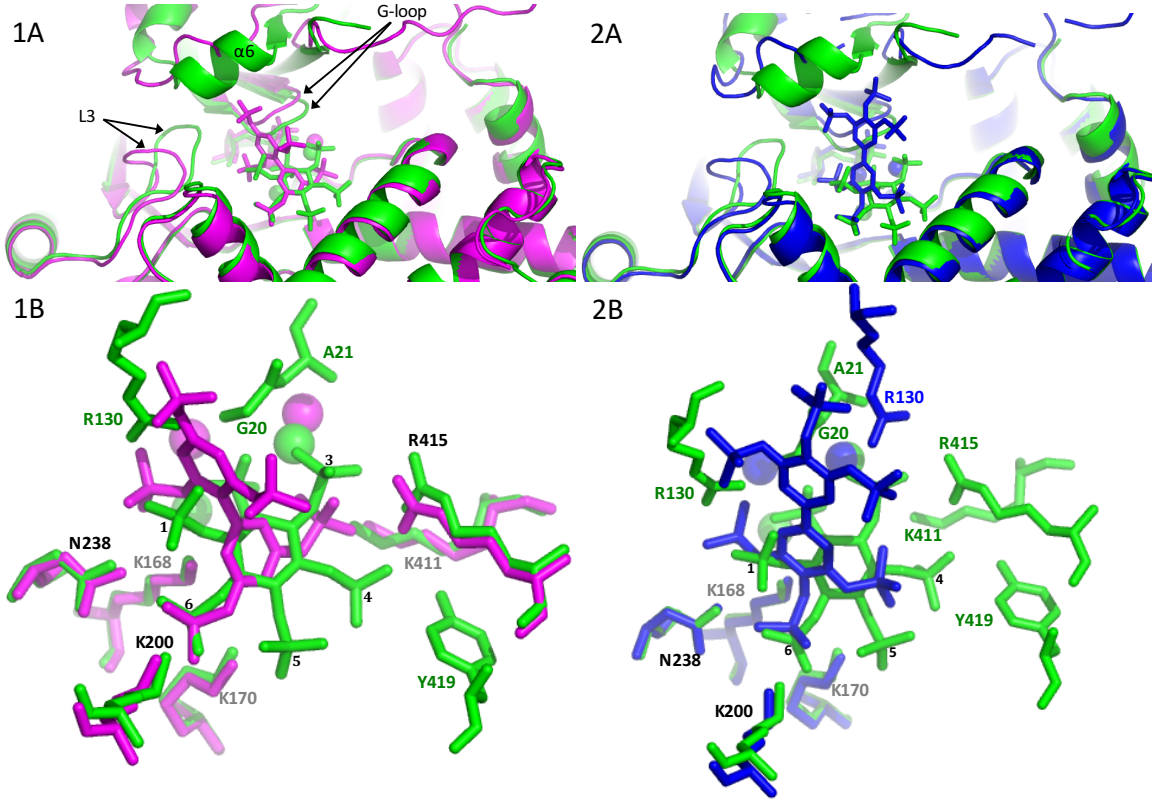

Figure 3.14 – Global alignment of the AtIPK1-His myo-IP_6 (green) with (1) AtIPK1-His BiPh(2,3',4,5',6)P_5 (magenta) and (2) AtIPK1-His BiPh(3,3',4,4',5,5')P_6 (blue); (A) The overlaid active sites of the two complexes. (B) Active site residues that co-ordinate the ligands. Ligands are represented as sticks, magnesium ions as spheres and ADP as sticks, coloured according to the complex to which they belong. *myo*-IP_6 numbering.

Global alignment of both AtIPK1-His BiPh1 and AtIPK1-His BiPh3 to AtIPK1-His *myo*-IP_6 (unpublished data), results in RMSD values of 0.760 and 0.780, respectively. Providing evidence that significant conformational changes are likely to have taken place to accommodate the novel ligands. These changes are isolated to the N-lobe of the protein which appears to have been effectively pushed outward in a near rigid body motion, doing so via the hinge (Section 3.1). These conformational changes and the disorder they cause are discussed in more detail in section 3.2.4.

Upon comparison of the binding orientation of *myo*-IP_6 in the active site to that of BiPh1 and BiPh3 (Figure 3.14), it is apparent that fewer interactions anchor the biphenyl compounds in to the active site than do *myo*-IP_6. This likely arises from the differing spatial arrangement of the phosphates within the compounds, equatorial to the puckered ring of inositol or in the plane of the phenyl rings. This could provide information on which interactions could be more prevalent in determining how and why a compound binds in the active site in a certain manner. The majority of these interactions are provided by the C-lobe in both structures, which unlike the N-lobe, has not undergone any significant conformational changes upon binding the biphenyl compounds. Not only are the two biphenyl compounds in very altered orientations when compared to one another; they bind in an almost orthogonally to *myo*-IP_6, which provides explanation for the large movement of the N-lobe upon biphenyl binding.

It can be clearly seen that the position occupied by P6 of *myo*-IP_6 is satisfied by both ligands, by P5' of BiPh1 and P4' of BiPh3. Additionally, the 'P6-coordinating residues' that surround the phosphate at this P6-equivalent position are shared in all three structures and are in equivalent positions. They provide a pocket in which this phosphate is tightly bound and is likely to be imperative in anchoring the substrate in the active site due to these interactions being ubiquitous across all three structures. Although not entirely overlaid, there is a phosphate in the equivalent *myo*-IP_6 P1 position for both compounds, P2 of BiPh1 and P5' of BiPh3. The interactions are provided by K168 and N238, which together with R130 also coordinate P1 of *myo*-IP_6. The R130 interaction is not present in the structures presented here and may explain why these equivalent phosphates are do not align fully with P1 of *myo*-IP_6. However, they do overlay in each biphenyl compound.

Interestingly, there is no phosphate in the equivalent position of the axial P2 of *myo*-IP_6 for both BiPh1 and BiPh3. This is perhaps not entirely unexpected due to the vast differences in structure between *myo*-IP_6 and the biphenyl compounds, making it impossible to accommodate a phosphate in the 'inositol' P2 binding pocket. This also offers explanation for the lack of interactions between the compound, magnesium ions and cofactor. This further supports that it is the 'inositol' P6 binding pocket, possibly together with the 'inositol' P1 binding pocket, that provides a primary anchoring point for substrates in the active site, and not the residues coordinating the axial P2-positioned hydroxyl group. The structures suggest that the biphenyl compounds act as mimics of inositol substrates but are unlikely to be phosphorylated due to the lack of a hydroxyl group occupying the 'inositol' P2 position or more specifically an axial hydroxyl group. The presence of an axial hydroxyl or phosphate is not required for AtIPK1-His to bind a ligand, evidence of this can also be seen in structures with benzene phosphate compounds (H. Whitfield, UEA, unpublished) which are discussed in due course.

The structures of the same recombinant AtIPK1-His protein in complex with three benzene polyphosphate substrate mimics, and ADP, have previously been solved by a colleague (H. Whitfield, UEA, unpublished). These were benzene 1,2,3,4-tetrakisphosphate (Bz1), benzene 1,2,3,5-tetrakisphosphate (Bz2), and benzene 1,2,4,5-tetrakisphosphate (Bz3). The structure with Bz3 represents the highest resolution structure with these compounds (1.90 Å), of which the alignment with the AtIPK1-His BiPh1 and AtIPK1-His BiPh3 structures can be seen in Figure 3.54. As these mimics closer represent physiological ligands due to their single ring structure, it is unsurprising that the structures with the biphenyl substrate mimics also differ in conformation when compared to AtIPK1 Bz3 as well as to AtIPK1 *myo*-IP_6.

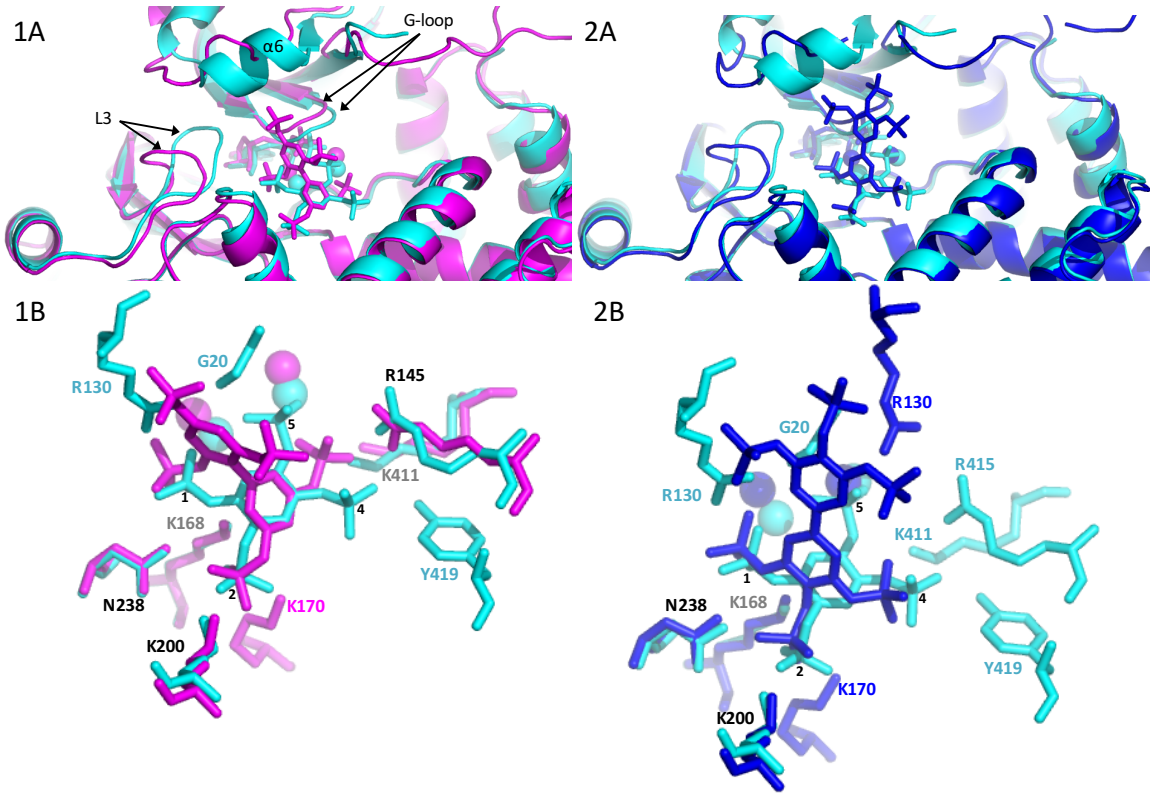

Figure 3.15 - Global alignment of AtIPK1-His Bz(1,2,4,5)P_4 (cyan) with (1) AtIPK1-His BiPh(2,3',4,5',6)P_5 (magenta), and (2) AtIPK1-His BiPh(3,3',4,4',5,5')P_6 (blue); (A) The overlaid active sites of the two complexes. (B) Active site residues that co-ordinate the ligands. Ligands and ADP are represented as sticks & magnesium ions as spheres, coloured according to the complex to which they belong. Phosphates are numbered according to Bz3.

The AtIPK1-His Bz3 complex aligns to the AtIPK1-His BiPh1 & BiPh3 structures with an RMSD of 0.699 and 0.687, respectively, indicating that the protein is in a marginally more similar conformation to AtIPK1-His Bz3 than it is to the AtIPK1-His *myo*-IP_6 structure. Having said this, the N-lobe of the AtIPK1-His Bz3 complex is not as far displaced as it is with a biphenyl ligand and appears to be more ordered, particularly noticeable at α6. It is more akin to the AtIPK1-His *myo*-IP_6 structure than either AtIPK1-His BiPh1 or AtIPK1-His BiPh3, and little conformational changes take place when in comparison with those that arise from the binding of a biphenyl compound. The accommodation of a biphenyl compound not only displaces and disorders the N-lobe significantly, but the positions of L3 and the G-loop are different to those in the AtIPK1-His Bz3 and AtIPK1-His *myo*-IP_6 complexes. The origins of the conformational changes that accommodate a biphenyl polyphosphate are discussed in more detail in section 3.2.4.

Again, in the AtIPK1-His Bz3 structure, the 'inositol' P6 and P1 binding pockets are occupied just like all the previous structures discussed, but with P2 and P1 of Bz3, respectively. This further cements the notion that these binding pockets must be occupied in order to anchor a substrate, and that any novel ligand will orient itself in the active site to satisfy this.

Neither biphenyl compound forms hydrogen bonds with R130 or G20, unlike Bz3 or *myo*-IP_6. As the residues lie within the N-lobe, more specifically α6 and the G-loop, the lack of hydrogen bonding of BiPh1 or BiPh3 by R130 may offer explanation to the de-stabilisation of α6, and may be why it appears disordered in both the structures presented here. Additionally, the G-loop is shifted further from the ligand.

Interestingly, ADP interacts with P5 of Bz3 via a magnesium ion in an interaction similar to that of P2 of *myo*-IP_6, whereas no such interaction exists in either biphenyl structure. However, P5 of Bz3 does not actually reside at the inositol P2 binding pocket, nor does it overlay with P2 of *myo*-IP_6 when the two structures are aligned, yet this interaction between Bz3, a magnesium ion and the cofactor still persists.

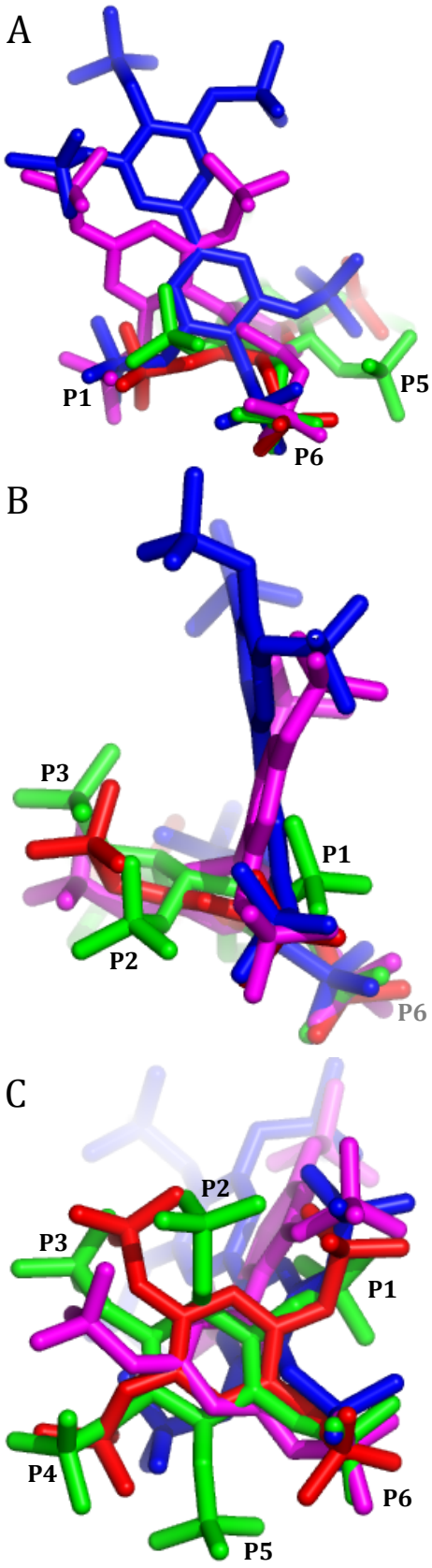

Figure 3.16 Overlay of the binding positions of ligands in complex with AtIPK1-His. (A,B & C) Views of ligand binding from different perspectives; myo-IP_6 (green), Bz3 (red), BiPh(2,3',4,5',6)P_5 (magenta) & BiPh(3,3',4,4',5,5')P_6 (blue). The phosphates (positions) labeled are those of myo-IP_6.

Overlaying all three of the inositol polyphosphate mimics mentioned thus far to *myo*-IP_6 in the active site of AtIPK1-His highlights the conserved positioning of phosphates, with the most striking alignment occurring at the 'inositol' P6 position (Figure 3.16). No other position shows such constricted positioning of a phosphate across all ligands therefore confirming that this phosphate is tightly bound in to the 'inositol' P6 binding pocket. The 'inositol' P1 position is also clearly occupied by all ligands but is not as tightly conserved, especially when comparing the location of the Bz3 phosphate at this position to the phosphate of the other three ligands. The 'inositol' P5 and 'inositol' P3 positions are unlikely to be essential in substrate binding, but the 'inositol' P4 position may have some influence as Bz3 places a phosphate at this position. As mentioned earlier, no novel ligand has a phosphate occupying the 'inositol' P2 catalytic position, confirming that this is not essential in orienting a substrate in the active site, therefore suggesting that none of these inositol polyphosphate mimics would be substrates of AtIPK1. Nevertheless, Bz3 does place a phosphate between the 'inositol' P2 and P3 positions that interact with ADP via magnesium, just like the P2 of *myo*-IP_6 would. Additionally, K168 forms interactions with all the ligands but would normally contact the axial P2 of *myo*-IP_6; suggesting that K168 is critical for ligand binding even though an axial hydroxyl group or phosphate at 'inositol' P2 is not. BiPh1 and BiPh3 also share positioning of a phosphate on their upper rings, P4 and P3 respectively. There is no hydrogen bonding to these phosphates but instead G19 provides hydrophobic contacts nearby. G19 also provides hydrophobic interactions in the *myo*-IP_6 and Bz3 structures despite the phosphates around the single ring molecules being in different positions to those in the biphenyl compounds. Therefore the hydrophobic contacts with G19 may also have to be satisfied when binding a ligand, and may confer substrate specificity and orientation.

It would appear the four residues that form the P6 binding pocket, which have retained positioning across all the structures presented here, primarily determine the orientation of ligand binding. Furthermore, binding position is governed by the 'inositol' P1 position, which is prominently demonstrated by the juxtaposed orientations of the two biphenyl phosphates in the active site.

3.3.5 Conformational changes of AtIPK1 upon ligand binding

Changes in intrinsic tryptophan fluorescence of AtIPK1 upon ligand and cofactor binding, together with structures have revealed that it possesses three distinct conformations when in its apo-form, and inositide and/or nucleotide bound forms (Baños-Sanz et al., 2012(Gosein et al., 2012)). As mentioned in section 3.3.3, residues in both the N- and C-lobes coordinate an inositide in to the active site, which consequently brings the two lobes together, this has been termed the "closed form" of the protein (Figure 3.17 & Figure 3.18 (C)). The closed form also features local changes where a clasp is formed between residues of α6 and L3, effectively closing the active site.

In the "open form", represented by the unbound apo-protein (W129A mutant), this clasp is unconnected and L3 can be considered mobile. Additionally, α6 shows disorder in this form therefore the conformation of α6 and L3 is dependent on the clasp formation. Furthermore, the N- and C-lobes show a general rigid-body movement and are further apart (Baños-Sanz et al., 2012). Movement occurs via three hinges that are highly mobile and therefore disordered in both the closed and open forms of the protein. This disorder is in agreement with both of the structures presented in this study.

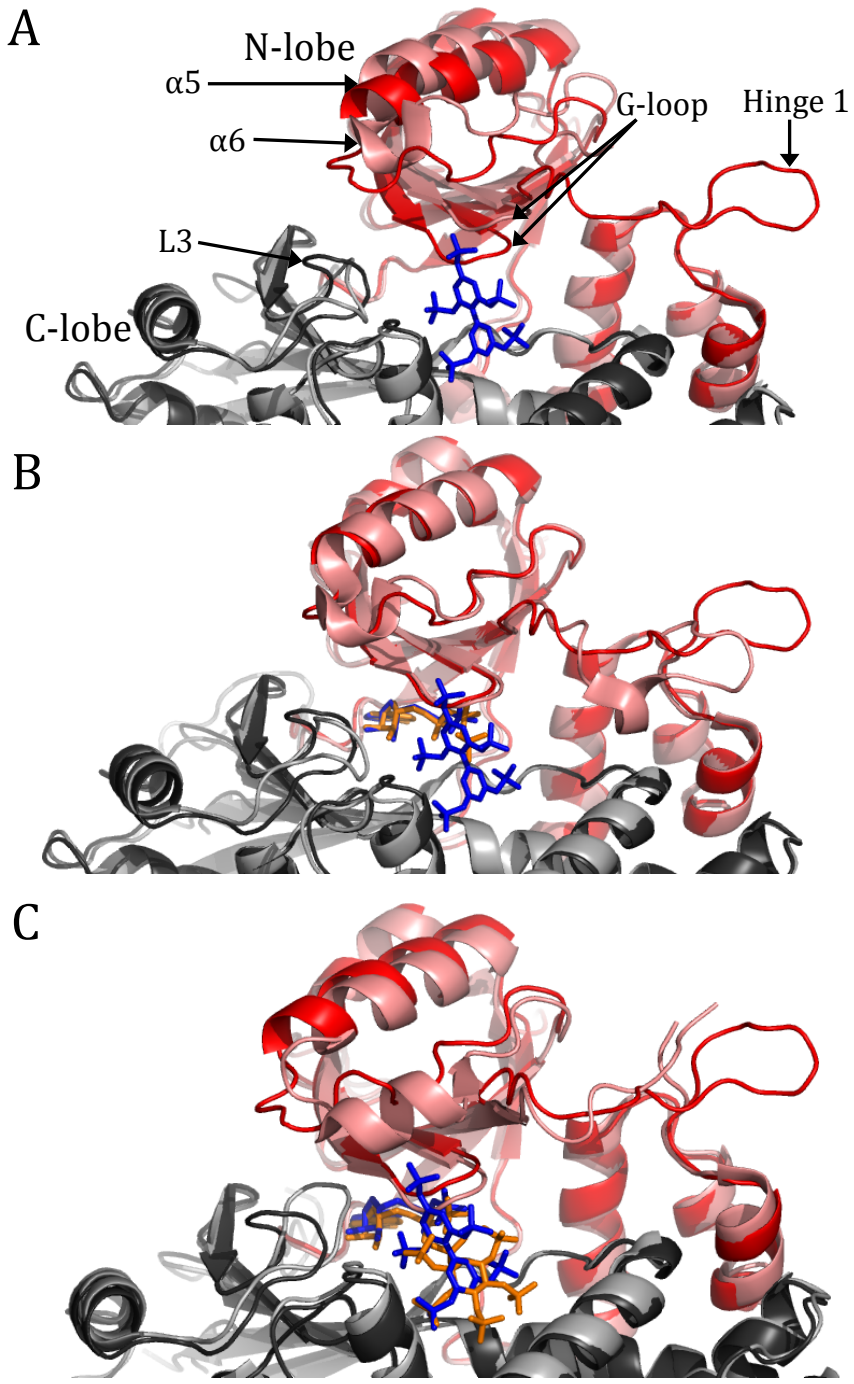

Figure 3.17 – The structure of the AtIPK1-His BiPh(2,3',4,5',6)P_5 active site superimposed on to the three distinct binding conformations of AtIPK1. The N- and C-lobes of AtIPK1-His BiPh(2,3',4,5',6)P_5 (red & black) and the AtIPK1 conformations (pink & grey) are represented as a cartoon, and BiPh(2,3',4,5',6)P_5 (blue) as sticks. (A) The apo-form of a W129A AtIPK1 mutant, which denotes the "open" conformation of the enzyme (PDB 4AXC). (B) The AtIPK1 AMPPNP complex in the "half-closed" conformation. AMPPNP (orange) and ADP (blue) are shown as sticks (PDB 4XAD).(C) The AtIPK1 myo-IP_6 ADP complex that describes the "closed" conformation of the protein (PDB 2XAM). The myo-IP_6 and ADP molecule associated with the complex are shown as orange sticks.

A third conformation is represented by the nucleotide-bound structure of the protein and is termed the "half-closed form", as it denotes an intermediate state between the apo-form and the closed-form of the protein (Baños-Sanz et al., 2012). In this conformation the N- and C-lobes are closer than in the apo-form, but are still too distant to fully form the inositide binding site. Additionally, the clasp observed in the closed-form is not formed and L3 remains flexible, and α6 disordered. These elements are only fully formed in the closed-form where L3 is also forming a "lid" that closes over the active site pocket. When superimposing all three of these conformational states to AtIPK1-His BiPh1 and AtIPK1-His BiPh3, it becomes apparent that both structures are akin to this half-closed form (Figure 3.17 & 3.18). They align with an RMSD of 0.510 and 0.424, respectively, a result which is perhaps surprising given that they are ternary complexes with both nucleotide (ADP) and an inositide mimic bound. Possibly representative of a conformation en-route to product (ADP & *myo*-IP_6) release. For both complexes, L3 is in nearly the exact position as that published for the half-closed structure, and α6 is also disordered. This implies that, despite a ligand being bound in the inositide binding pocket, the inositide binding site is not fully formed and the L3 lid has not closed over the ligand, nor has the clasp formed.

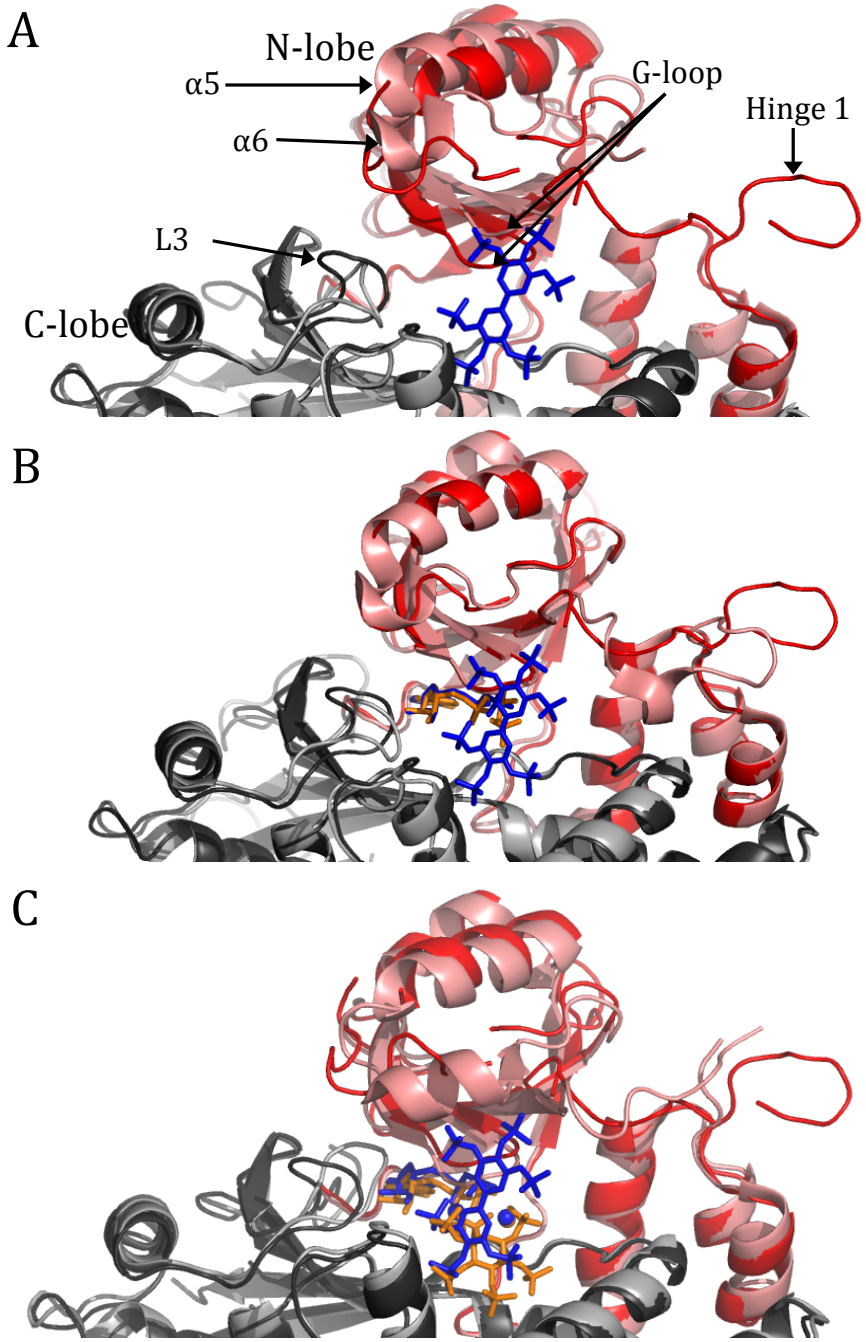

Figure 3.18 – The structure of the AtIPK1-His BiPh(3,3',4,4',5,5')P_6 active site superimposed on to the three distinct binding conformations of AtIPK1. The N- and C-lobes of AtIPK1-His BiPh(3,3',4,4',5,5')P_6 (red & black) and the AtIPK1 conformations (pink & grey) are represented as a cartoon, and BiPh(3,3',4,4',5,5')P_6 (blue) as sticks. (A) The apo-form of a W129A AtIPK1 mutant, which denotes the "open" conformation of the enzyme (PDB 4AXC). (B) The AtIPK1 AMPPNP complex in the "half-closed" conformation. AMPPNP (orange) and ADP (blue) are shown as sticks (PDB 4XAD). (C) The AtIPK1 myo-IP_6 ADP complex that describes the "closed" conformation of the protein (PDB 2XAM). The myo-IP_6 and ADP molecule associated with the complex are shown as orange sticks.

Furthermore, as mentioned in section 3.3.3, BiPh1 and BiPh3 do not form any interactions with residues from the N-lobe with the most obvious absence being the coordination of P1 by R130 from within α6. The lack of interaction from the N-lobe not only explains the failure to form the closed conformation, but also explains how α6 is disordered, lacking interaction with a ligand and therefore L3. In absence of clasp formation, the protein remains in the half-closed form when accommodating a biphenyl polyphosphate rather than transitioning to the closed form. The greater size (volume) of the biphenyl polyphosphates and the different, relative to inositol, spatial positions of their phosphates are likely to preclude achievement of the closed form. It can be assumed that the conformation of a ternary complex between AtIPK1 and a biphenyl polyphosphate is mostly determined by the interaction with bound ADP rather than with the ligand, as the ligand binding site is already fully formed following nucleotide binding and no further conformational changes take place post-biphenyl polyphosphate binding.

3.4 Conclusions and Future work

The work of González (Gonzalez et al., 2010; Banos-Sanz et al., 2012) identified different conformational states representing different stages of the catalytic cycle of AtIPK1. A 'closed' conformation was first described for native protein with inositide and cofactor bound (Gonzalez et al., 2010). Subsequent work with a W129A mutant allowed identification of the apo-form in 'open' conformation and 'half-closed' nucleotide-bound conformation (Banos-Sanz et al., 2012). In the 'open' state there is limited interaction between the N-lobe and the C-IP lobe. In the presence of nucleotide and/or inositide the protein undergoes rigid body motions which in the presence of inositide that culminate in the closing of a clasp formed between R130 of the α6 helix of the N-lobe and G254 of the L3 loop of the C-IP lobe (Baños-Sanz et al., 2012; Gosein and Miller, 2013). The latter study extended understanding of the contribution of the phosphates of Ins(1,3,4,5,6)P5 to catalysis suggesting that the 5-phosphate and the 6-phosphate were key to inositide binding, while the 1-phosphate and 3-phosphate contribute most importantly to enzyme activation. Of the protein residues involved in substrate recognition and enzyme activation, the authors concluded that R130, K170 and K411 were critical to enzyme activity, and that the only N-lobe residue involved in substrate binding is R130 which coordinates the 1-phosphate (Gosein and Miller, 2013; Gonzalez et al., 2010; Banos-Sanz et al., 2012). The outcome of this is that binding of substrate is initiated by binding of the 4-, 5- and 6-phosphates to the C-IP lobe, with closing of the clasp and enzyme activation mediated through the 1-phosphate-mediated interaction of the N-lobe with the C-IP lobe. The structures with the biphenyl phosphates present an argument for a non-essential role of clasp formation in ligand binding and perhaps therefore catalysis, confirmed by the mutagenesis studies by Banos-Sanz et al 2012, where shortening of L3 did not lower enzyme activity but instead increased enzyme efficiently. Rationalised by the idea of a lowered energetic barrier for catalysis, via a more favourable mechanism for the release of products (Banos-Sanz et al, 2012).

Here crystal structures of AtIPK1 were obtained in ternary complex with BiPh(2,3',4,5',6)P_5 (BiPh1) or BiPh(3,3',4,4',5,5')P_6 (Biph3) and ADP. The data clearly show enzyme in 'half-closed' conformation, a conformation previously obtained solely with nucleotide alone. The most basic explanation is that the addition of a second phenyl ring prevents formation of the clasp and closure of N- and C_{IP} lobes. The binding of biphenyl phosphates in the active site and comparison of structures obtained with these and with inositide substrates (Gonzalez et al., 2010; Banos-Sanz et al., 2012; Gosein and Miller, 2013) reveals the major contribution of residues that coordinate the 6-phosphate of inositide substrate, which 'anchor' these ligands in the enzyme. By way of extensive mutagenesis, enzyme assay and isothermal calorimetry of substrate binding, Gosein and Miller have concluded that K170 which coordinates the 5- and 6-phosphate of inositide substrate are critical to enzyme activity, an observation that seems to be supported by the data in this chapter.

Evidently, successful future crystallographic studies of AtIPK1 with the two additional biphenyl compounds presented here, BiPh2 & BiPh4 (Table 1.2), would provide further evidence of the essential features in ligand binding and catalysis. Following this up with mutagenic studies, especially of those residues coordinating the P1 position, could confirm if this and other positions really are essential for binding of the benzene and biphenyl phosphates. Providing these mutations do not compromise crystallisation of the protein, any structural information of mutants that encompass the binding of the BiPh's may aid in the empirical validation of essential binding elements and residues. Design of binding and kinetic assays to support any structural information would be desirable in the quest for elucidating the full mechanism of catalysis of this essential enzyme in the IP_6 synthesis pathway. It has not yet been confirmed that the benzene and biphenyl phosphates are not substrates for AtIPK1. As it currently stands it is unlikely due to the lack of an axial 2-OH or 2-phosphate, and the vacant P2 binding pocket.

Chapter 4 – *Novel fluorescent properties of the benzene- and biphenyl-polyphosphates, and the use of fluorescently tagged inositol phosphates to explore ligand binding*

4.1 – Introduction

4.1.1 – Current applications of the benzene- and biphenyl- polyphosphates

As previously introduced in section 1.1.3, the benzene polyphosphates (BzPs) were first synthesised as a simple alternative to the synthesis of inositol phosphates for use in the study of the enzymes related to PI3K/Akt signalling, PtdIns(1,4,5)P_3 3-kinases and PtdIns(1,4,5)P_3 5-phosphatases. The utility and versatility of the BzPs prompted the synthesis of a second set of related derivatives that also act as inositol phosphate mimics, the biphenyl polyphosphates (BiPhs), also discussed in section 1.1.3. Just like the benzene phosphates they have been shown to substitute for inositol phosphates and phosphoinositides in many of the same incidences since.

As discussed previously (section 1.1.3 & 2.1.4) these compounds have also aided in the pursuit of crystal structures. Those so far include, for the BzPs; Bz(1,2,3,4)P_4 (Bz1) with PKBα PH-domain, and type II inositol polyphosphate 5-phosphatase (INPP5B) with Bz(1,2,4,5)P_4 (Bz3) (Mills et al., 2007, Mills et al., 2016), and for the BiPhs; biphenyl-(2,3',4,5',6)P_5 (BiPh1) with the catalytic domain of SHIP2, and biphenyl (3,3',4,4',5,5')P_6 (BiPh1) with INPP5B (Mills et al., 2012, Mills et al., 2016).

Of particular interest is 3-hydroxybenzene 1,2,4-trisphosphate (Bz7) because it has been characterized as a substrate of INPP5A, where the 2-phosphate is removed to yield 2,3-dihydroxybenzene 1,4-bisphosphate, and currently is the only compound out of the selection used in this study to have been reported as a substrate, the rest are reported exclusively as inhibitors(Mills et al., 2008).

4.1.2 – Current applications of fluorescently tagged inositol phosphates

This chapter discusses the use of a set of fluorescently tagged inositol phosphates as probes for use in fluorescence polarisation binding assays to investigate the binding affinities of SHIP1cd, SHIP2cd and AtIPK1 for various ligands and inhibitors (see table 4.1 for structures). Like the benzene and biphenyl phosphates they were obtained from collaborators at the University of Bath (Potter, B.V.L). One of these is an analogue of IP_3 with a fluorescein 5-isothiocyanate (FITC) at the 2-position of the inositol ring attached via a short linker (2-FITC-IP_3), and was used in similar fluorescence polarisation assays to those in this study to investigate the IP_3 binding core and conformational changes in the N-terminus of IP_3 receptors, which are intracellular Ca^{2+} channels (Ding et al., 2010). Another study has used IP_5 conjugated at the 2-position with 5-carboxyfluorescein (FAM) to yield 2-FAM-IP_5, the probe utilised most frequently in this work (Riley et al., 2014). It was used to visualise the internal visualisation of inositol phosphates by H1229 tumour cells. Most recently, 2-FAM-IP_5 has been used to investigate the binding of inositol phosphates, and subsequent activation, to the HDAC3:SMRT complex which is newly understood to be regulated by certain inositol phosphate stereoisomers (Watson et al., 2016).

4.1.3 – Fluorescence polarisation

Fluorescence polarisation (FP) provides one means of examining ligand binding. When a rigid fluorophore is excited by plane-polarised light, and it remains immobile during its fluorescence lifetime, 60% of the emitted light will be detected in the plane of the exciting light, and the anisotropy will be 0.4. The relationship between anisotropy (r) and the angle (θ) of an oriented fluorophore is shown by equation 4.1.

$$r = (3\langle\cos^2\theta\rangle - 1) / 2 \qquad \text{(Eq. 4.1)}$$

If a single fluorophore is oriented in a single direction $\theta = 0$ and $r = 1$. However it is not possible to obtain a perfectly oriented excited-state population so r is always less than 1. If the molecule rotates during its fluorescence lifetime, less emitted light will be aligned with the excitation plane, and r will be < 0.4. Anisotropy measurements reveal the average angular displacement of the fluorophore that occurs between absorption and emission of a photon. The rate of tumbling is inversely proportional to molecular volume, therefore binding of a small fluorescent probe to a much larger protein would increase anisotropy. FP measures this change in anisotropy as a fluorescent ligand binds. It thereby allows non-destructive quantification of binding without the need to separate bound from free ligand, and is calculated using equation 4.2. It is useful for measurement of low-affinity interactions in which rapid ligand dissociation during separation of bound and free ligand compromises analysis. Additional advantages of FP include the opportunity to make many measurements from the same sample under different conditions, cost-effectiveness, applicability to high-throughput analyses, and avoidance of radio ligands (Ding et al., 2010).

4.1.4 Experimental aims

Upon discovery of the fluorescent properties of the benzene- and biphenyl- phosphates, it was necessary to characterise them further and define their optimal absorption wavelengths, and excitation and emission maxima for fluorescence measurements.

As one of these compounds has been reported as a substrate of 5-phosphatases, and in light of the structures of 5-phosphatases (section 1.1.3 & 2.1), the biphenyl phosphates were tested as substrates in both end-point and real-time kinetic assays by utilisation of changes in their absorbance and novel fluorescent properties.

Further to this, attempts were made to characterise the binding of canonical substrates, known inhibitors and the biphenyl phosphates to SHIP1cd, SHIP2cd and AtIPK1, by use of a fluorescence polarisation method that that utilises inositol phosphates conjugated to fluorescent moieties as novel analogues.

4.2 Materials & methods

4.2.1 UV absorbance wave scans

UV absorbance spectra between 250 – 330 nm of the benzene- and biphenyl-phosphates were performed on a Hidex Sense multimodal microplate reader using a 96-well quartz glass plate (Molecular Devices). Well volume was 40 µL, and each compound at 100 µM in 20 mM HEPES pH 7.3, 1 mM $MgCl_2$.

4.2.2 Fluorescence intensity

Using a Hidex Sense multimodal microplate reader, and in a 384 well Corning low volume black flat bottomed polystyrene plate, finite fluorescence intensity readings of 100 µM benzene- and biphenyl- phosphates in 20 mM HEPES pH 7.3, 1 mM $MgCl_2$ were taken. For the excitation, filters used were; 265±25, 280±10, and 289±10 nm. And for emission, 340±80 nm. Well volume was 20 µL.

4.2.3 Biphenyl phosphate anion exchange chromatography assays; SHIP1cd and SHIP2cd

4.2.3a Preliminary assays

Assays of 1 µM SHIP2cd and 5 µM biphenyl phosphate were set up in 100 µL reaction volumes in 20 mM HEPES pH 7.3, 1 mM $MgCl_2$. Samples were injected on to the column immediately and after overnight incubation at 18 °C.

Biphenyl phosphates and their reaction products from reaction with SHIP2cd were separated by anion exchange chromatography on a 2mm x 250 mm IonPac AS11 column, with 2 mm x 50 mm AG11 guard column, eluted with NaOH. The column was eluted at a flow rate of 0.5 mL / min according to the following gradient: time (min), % B (225 mM NaOH); 0,0; 20,100; 21,0; 30,0. Samples (25 µL volume) were injected by a Thermo Separation Products AS3500 autosampler and peaks were monitored either by tandem fluorescence and suppressed ion conductivity detection, or by tandem UV and

fluorescence detection. The fluorescence detector (Jasco FP-920) was set at 270/10 nm excitation/band width; 330/10 nm emission/bandwidth and gain (photomultiplier voltage) setting of 10. The UV detector (Dionex AD20) was set at 270 nm, while the conductivity detector was set at range 300 µS with 100 mA current on the Dionex 4 mm ASRS-1 suppressor.

4.2.3b Complete assays

Assays of 1 µM SHIP2cd and 5 µM biphenyl phosphate were set up in 200 µL reaction volumes in 20 mM HEPES pH 7.3, 1 mM $MgCl_2$. Samples were injected on to the column immediately, then after incubation at 37 °C for; 15, 30, 60 and 120 min. Before injection, samples were diluted to 0.2 µM biphenyl phosphate with analytical grade water and boiled for 1 min to terminate the reaction.

Biphenyl phosphates and their reaction products from reaction with SHIP1 or SHIP2 were separated by anion exchange chromatography on a 2 mm x 250 mm IonPac AS11 column, with 2 mm x 50 mm AG11 guard column, eluted with NaOH. The column was eluted at a flow rate of 0.4 mL / min according to the following gradient: time (min), % B (225 mM NaOH); 0,0; 20,100; 21,0; 30, 0. Samples (50 µL volume) were injected by Jasco AS-950 autosampler and peaks were monitored either at 265/10 nm excitation/band width; 340/10 nm emission/bandwidth; or 285/10 nm excitation/bandwidth, 340/10 nm emission/bandwidth, in a Jasco FP-920 fluorescence detector at a gain (photomultiplier voltage) setting of 100.

4.2.4 Kinetic assays with the biphenyl polyphosphates

A Corning 96 well half-area black polystyrene flat bottom plate was used with a Molecular devices SpectraMax M5 plate reader. Reactions were followed at an excitation wavelength of 265 nm and emission of 285 nm, reading every 5 seconds for 20 min. Total reaction volume was 100 µL, and were started by addition of 50 µL of the specified concentration of biphenyl phosphate to 2 µM SHIP2cd.

4.2.5 Fluorescence polarisation; dose-response binding and inhibition curves

Polarisation binding assays were carried out in 384 well Corning low volume black flat bottomed polystyrene plate on a Clariostar (BMG LabTech, Germany) plate reader with excitation at 485±5nm and emission at 520±5nm. For saturation curves, 2 nM 2-FAM-IP_5 in 20 mM HEPES pH 7.3 1mM $MgCl_2$, was incubated with increasing protein concentrations (up to 2.5 μM). Aliquots (20 μL) were dispensed in quadruplicate wells and polarisation of the probe was measured at 25°C. All data was averaged and analysed by a 4-parameter fit using GraphPad Prism 6 software allowing dose-response curves to be constructed and EC50 values to be obtained.

Similarly, for inhibition assays, inhibitor (10 nM-100 μM) was titrated against AtIPK1, SHIP2cd or SHIP1cd protein at 200 nM and 2 nM 2-FAM-IP_5 with assay conditions as otherwise described above.

4.3 Results & Discussion

4.3.1 UV absorbance and fluorescence properties of the biphenyl and benzene polyphosphates

As discussed previously (section 1.1.3 & 4.1.1), benzene 1,2,4,5-tetrakisphosphate (Bz(1,2,4,5)P_4 / Bz3) was designed, along with six additional benzene polyphosphates and four biphenyl polyphosphates, as a simple inositol phosphate analogue which can been exploited as novel ligand and inhibitor of inositol phosphate metabolising enzymes (Mills et al., 2008). In a previous assay which followed the conformational changes of AtIPK1 by monitoring its intrinsic tryptophan fluorescence upon ligand binding (results not shown), it became apparent that Bz3 exhibited its own fluorescence properties at similar excitation and emission wavelengths to tryptophan. Before further exploring the fluorescence properties of this inositol phosphate mimic, it was deemed necessary to first investigate the UV absorbance properties of both the benzene and biphenyl phosphates (Figure 4.1). λ_{max} for the biphenyl phosphates are summarised in table 4.1.

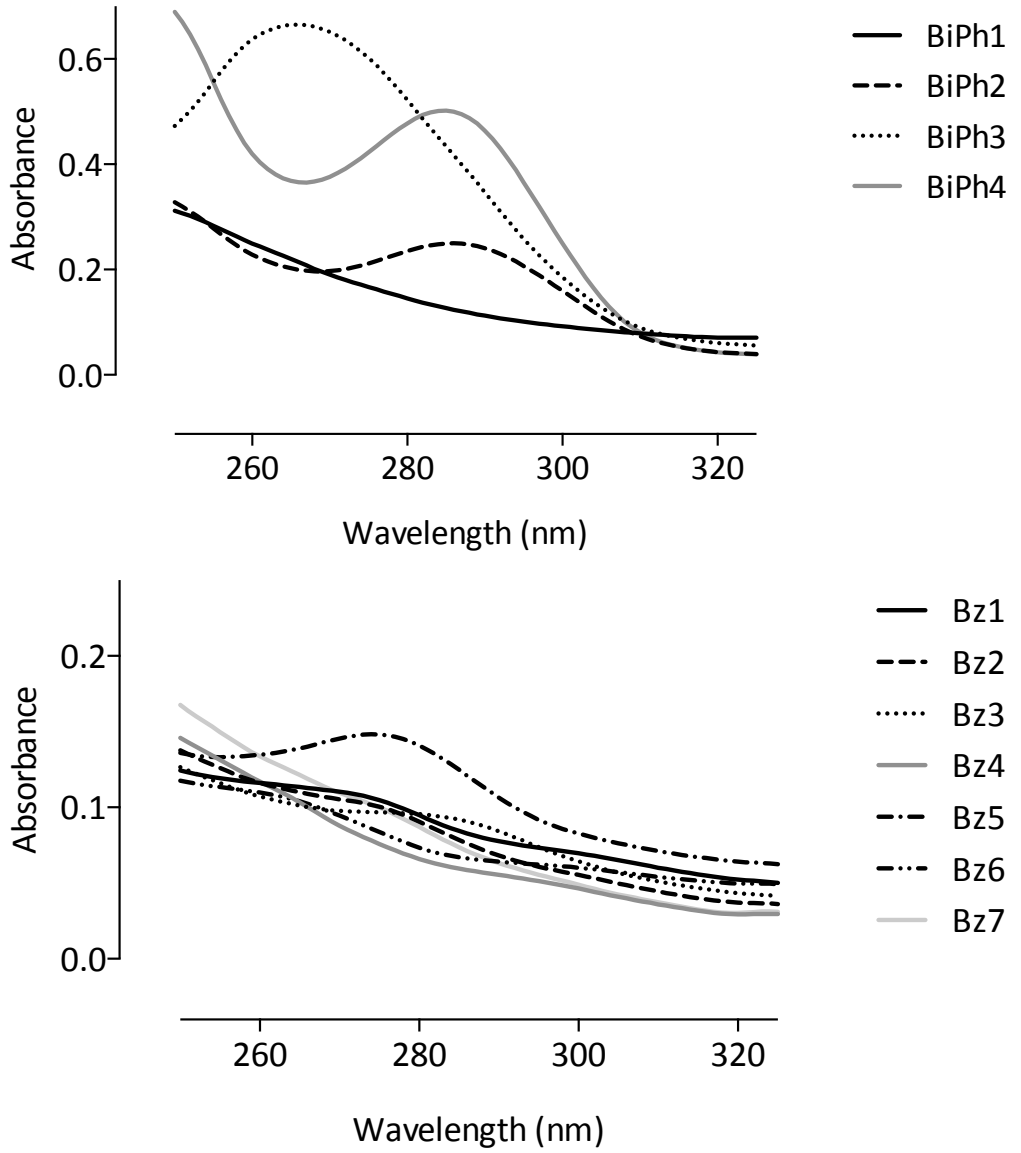

Figure 4.1 – UV absorbance wave scans of 100 µM biphenyl phosphate and benzene phosphate in a 96-well quartz plate.

Table 4.1 – UV absorbance λ_{max} of 100 µM biphenyl phosphate

	λmax
BiPh1	250
BiPh2	286
BiPh3	266
BiPh4	285

Wavelength scans in a 96-well quartz plate revealed the biphenyl polyphosphates had stronger UV absorption properties between 250 – 330 nm than the benzene polyphosphates (Figure 4.1). All the compounds displayed distinctive profiles with clear differences in absorption maxima. Some compounds showed very weak absorption between these wavelengths, with biphenyl 2,3',4,5',6-pentakisphosphate (BiPh1) being the weakest absorbing of the biphenyl phosphates, exhibiting no obvious peak in its absorbance spectra (Figure 4.1 -A). However, it is evident that BiPh1 displays a small absorption peak around 250 nm. Biphenyl 3,3',4,4',5,5'-hexakisphsphate (BiPh3) has the highest absorbance between these wavelengths with a peak maxima at 266 nm. For biphenyl 2,2',4,4',5,5'-hexakisphosphate (BiPh2) and 6,6'-difluorobiphenyl 3,3',4,4'-tetrakisphosphate (BiPh4), absorption maxima occur at approximately 285 nm. The adjacent positioning of the phosphate substituents in BiPh3 may impact on the rotation around the diaryl bond thus effecting electron conjugation between the two equivalent aryl rings, and could offer explanation for the altered and more prominent absorption maxima when compared to the other biphenyl compounds.

Although the benzene phosphates are generally less absorbent, there are still marked differences in their spectra; benzene 1,2,4-trisphosphate (Bz(1,2,4)P_3 / Bz5) has the highest absorbance of the benzene phosphates with a strong absorbance peak at 275 nm, whereas others such as Bz3 are far less UV absorbent and have differing absorbance maxima (Figure 4.1 -B). An absorbance peak for Bz3 occurs at 279 nm. Many have higher absorbance at 260 nm, but this is common to the absorbance spectra of all the compounds. Visually, it is clear from looking at the spectra of the benzene polyphosphates that those with significant absorbance peaks, have maxima occurring at a wavelength longer than 260 nm.

As the majority of the biphenyl polyphosphates displayed large peaks in their UV absorbance spectra, their fluorescence properties were subsequently investigated (Figure 4.2).

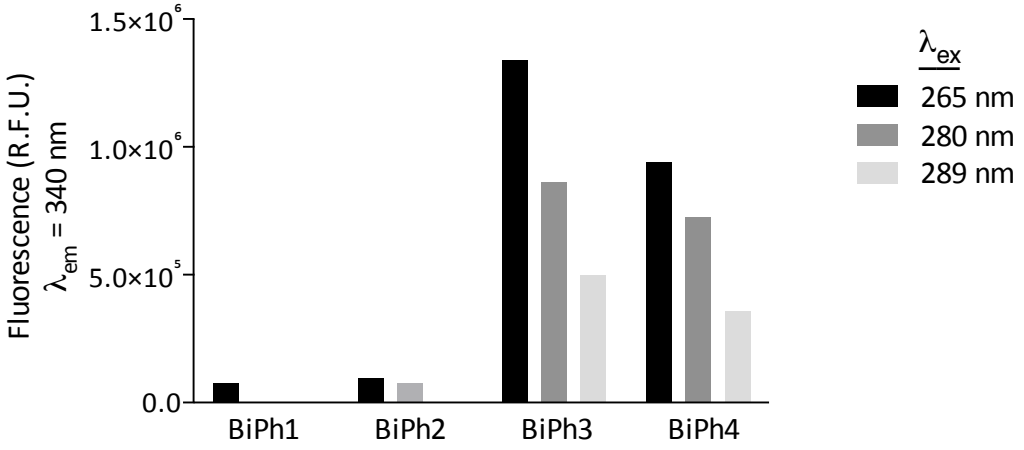

Figure 4.2 – Fluorescence properties of 100 µM biphenyl phosphates. Intensity readings at emission wavelength 340 nm. Values are corrected against the background signal from the buffer.

Using a black 384-well plate and a plate reader with fixed fluorescence filter sets, results agreeably showed that the BiPh's did indeed possess fluorescent properties and the most appropriate emission wavelength to utilise this was 340 nm. After fixing the emission wavelength, their fluorescence intensity at three excitation wavelengths was explored, resulting in the highest intensities being seen at an excitation wavelength of 265 nm (Figure 4.2). BiPh3 and BiPh4 were also strongly fluorescent at 280 and 289 nm, and overall are the most fluorescent across all investigations. Albeit weak in comparison to BiPh3 and BiPh4, BiPh1 and BiPh2 both display fluorescent properties when excited at 265 nm, with BiPh2 also emitting when excited at 280 nm. Therefore consideration must be given to selecting the most appropriate compound when wishing to exploit the fluorescent properties of these inositol phosphate mimics in further investigations.

In a different manner using a fluorimeter and quartz cuvette method, involving collecting excitation and emission spectra rather than single finite readings, the fluorescence properties of the benzene polyphosphates were investigated (Figure 4.3). Most of the Bz's were weakly fluorescent bar Bz3 and Bz5, which displayed fluorescence maxima at an excitation wavelength of 275 nm (Figure 4.3 –A) and emission wavelength of 310 nm (Figure 4.3– B). Both the excitation and emission peaks for Bz3 and Bz5 are wide in nature and span a broad range of wavelengths, therefore expanding the wavelengths at which these compounds could be utilised in further studies exploiting their novel spectral properties as inositol polyphosphate surrogates.

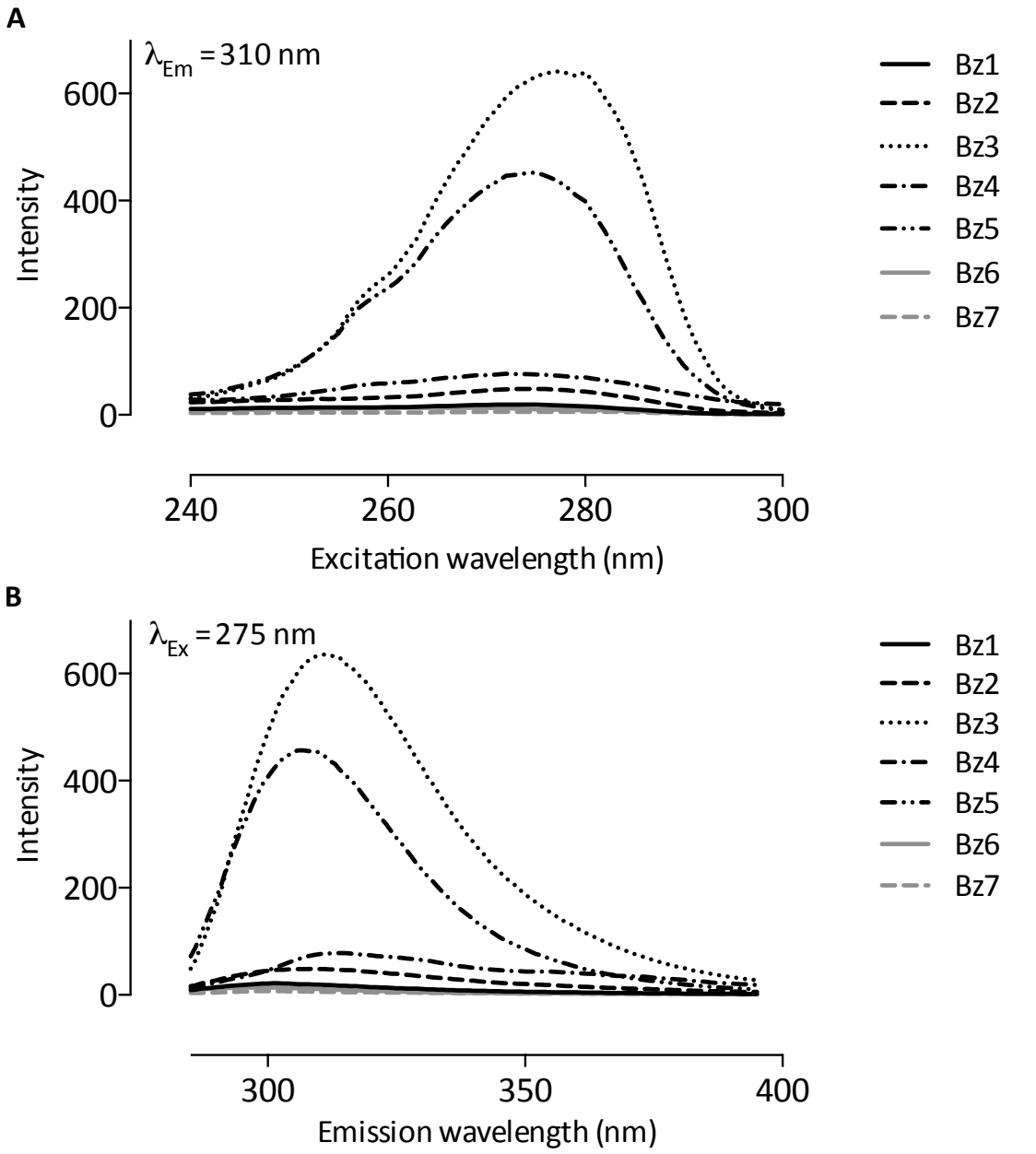

Figure 4.3 – Fluorescence wave scans of 100 µM benzene polyphosphate (A) Excitation spectra at a fixed an emission wavelength of 310 nm. (B) Emission spectra fixed at an excitation wavelength of 275 nm. Spectra are corrected for against buffer background signal.

Following on from this, the same methodology used to investigate the fluorescence of the biphenyl phosphates was applied to Bz3 and Bz5 to supplement the data in figure 4.3, and provides a more direct comparison to the BiPh's (Figure 4.4). Investigation under this method using discreet filter sets at fixed wavelengths revealed that unlike the BiPh's, Bz3 and Bz5 exhibited low fluorescence intensities at an excitation wavelength of 265 nm and emission 340 nm. The most favourable excitation wavelength was 280 nm for both compounds. Bz5 proved to be the most fluorescent at this wavelength, closely followed by exciting at 289 nm whereas Bz3 exhibited a much lower emission exciting at 289 nm.

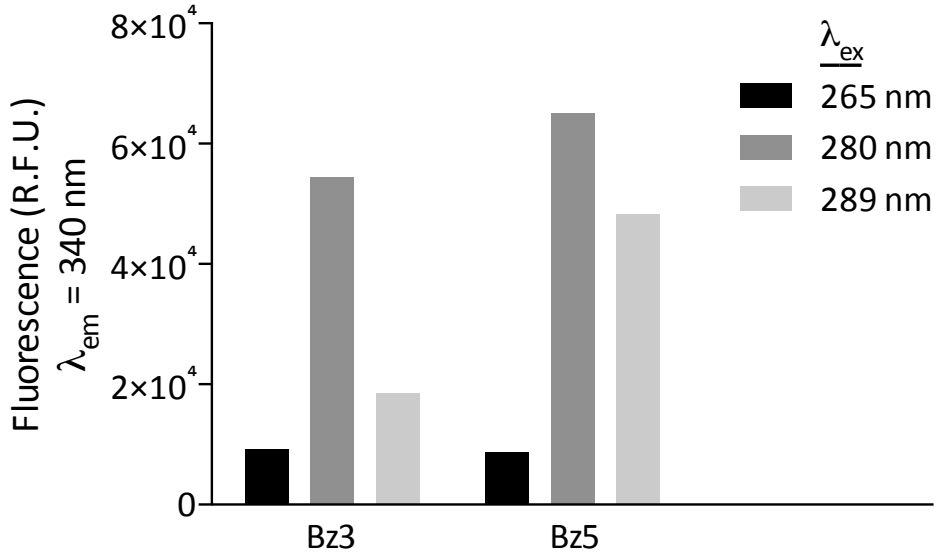

Figure 4.4 - Fluorescence properties of 100 µM benzene polyphosphates. Intensity readings at a fixed emission wavelength of 340 nm. Values are corrected against the background signal from the buffer. Only benzene 1,2,4,5-tetrakisphosphate (Bz3) & benzene 1,2,4-trisphosphate (Bz5) are shown, since only they possess fluorescent properties at these wavelengths.

Currently, only empirical observations can be made when considering why these compounds are fluorescent. As has been seen, some are more fluorescent than others, which can likely be attributed to the different positioning of the phosphate groups around the benzene rings. Looking forward, efforts are focussing on collaboration with physical computational chemists to elucidate the features of these compounds that give them these unique spectral properties. Eventually, this may shed light on which hypothetical products of the turnover of these compounds would also have UV and fluorescent properties and in turn would hopefully allow them to be identified during assays.

Despite having been widely utilised as simple inositol polyphosphate surrogates in inhibition and structural studies (Mills et al., 2008, Mills et al., 2012, Mills et al., 2016), formally the spectral properties of these compounds have been left undiscovered until recently and these results are yet to be published. The unearthing of these novel properties opens up new opportunities to exploit these compounds in enzymatic assays, where they would help interpret the catalytic scope and activity of inositol polyphosphate metabolising enzymes.

4.3.2 Biphenyl polyphosphates are substrates of SHIP1 and SHIP2

As widely introduced previously, the biphenyl phosphates have been reported as inhibitors of the inositol polyphosphate 5-phosphatases, including SHIP2 for which there is also an available structure of the complex formed with biphenyl 2,3',4,5',6-tetrakisposphate (BiPh1) (Mills et al., 2012). Currently there has been no reports of BiPhs as substrates against the proteins that have been demonstrated to accommodate them in their active sites. Characterisation solely as inhibitors of inositol phosphate phosphatases has been described with no reports testing for catalytic activity. However, 3-hydroxybenzene 1,2,4-trisphosphate (Bz7) is an example of a simpler single ringed inositol phosphate mimic (Table 1.1) that has been reported as a substrate for type I Ins(1,4,5)P_3 5-phosphatase (INPP5A), in which its 2-phosphate is removed (Mills et al., 2006). It is then not an unreasonable hypothesis that the biphenyl phosphates may also substitute as substrate mimics of inositol polyphosphate 5-phosphatases.

As a preliminary assay to investigate if the biphenyl polyphosphates could indeed be substrates of SHIP1 and SHIP2, SHIP2cd protein was incubated with biphenyl 2,2',4,4',5,5'-hexakisphosphate (BiPh2) and biphenyl 3,3',4,4',5,5'-hexakisphosphate (BiPh3) overnight, and the products analysed by ion exchange chromatography. Three detection methods in series were used visualise the disappearance of BiPh2, and to monitor to the appearance of any products of the reaction which may or may not exhibit spectral properties like the parent compound. Despite using UV, fluorescence and conductivity detectors, it cannot be guaranteed that new products would be detected, as the detectors were set to fixed wavelengths and new products are likely to have different spectral properties, if any at all, due to the removal of phosphate from the biphenyl rings.

Reaction products were separated by ion exchange chromatography with a gradient of 225 mM NaOH over 20 min. Detection of BiPh2, in Figure 4.5 – A, was achieved by monitoring the UV absorbance of the column eluent at 270 nm. In the overlay of the reactions, a peak of UV absorbing material can be seen eluting at approximately 14 min, which has then disappeared after overnight incubation with SHIP2cd. This peak was confirmed as that of BiPh2 by spiking the sample with a standard of BiPh2. The disappearance of BiPh2 is accompanied by the appearance of a series of peaks of UV absorbance eluting between 5 and 12 min, and an additional peak eluting after the parent material. In the absence of partially dephosphorylated BiPhs as standards, it is not possible to identify the products. Nevertheless, it is compelling evidence that BiPh2 is a substrate of SHIP2 and that several UV absorbing turnover products are generated.

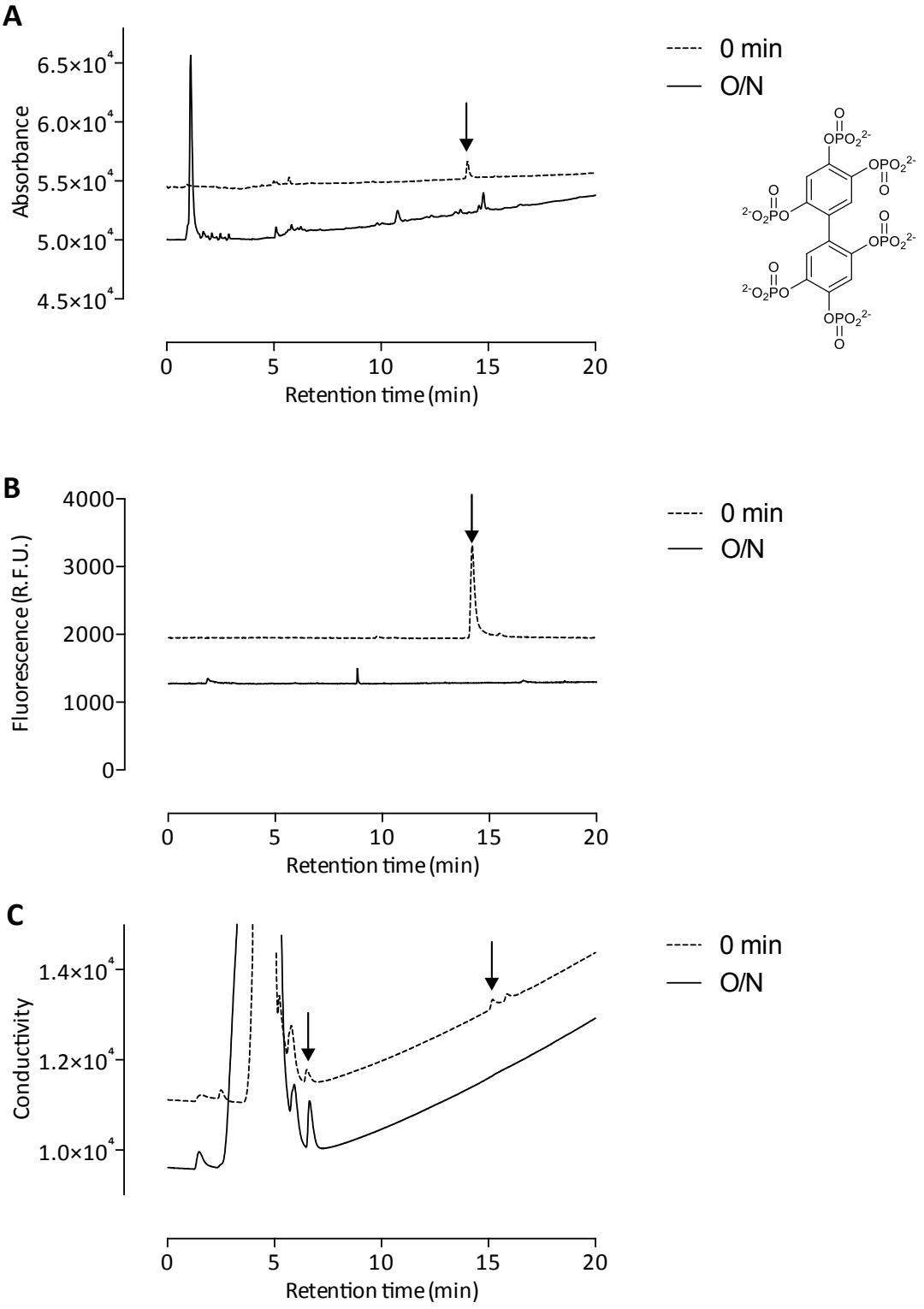

Figure 4.5 – SHIP2cd vs. biphenyl 2,2',4,4',5,5'-hexakisphosphate (BiPh2). Detection of reaction products by; (A) Absorbance at 270 nm (B) Fluorescence at ex 270 nm, em 330 nm (C) Suppressed ion conductivity, left to right the arrows indicate peaks of inorganic phosphate and biphenyl(2,2',4,4',5,5')P_6, respectively. The structure of BiPh2 is shown in the top right.

A more sensitive method of detection is offered by monitoring the fluorescence of the column eluent at excitation of 270 nm and emission 330 nm, and produces a much clearer trace (Figure 4.5 - B). A fluorescence peak of BiPh2 can be seen at approximately 14 min, in agreement with the UV trace, and again is completely diminished after the overnight incubation. The appearance of new fluorescence peaks after incubation is observed but none appear to elute in clear agreement with the UV absorbing peaks in panel A. This suggests that some detectable products from the dephosphorylation of BiPh2 maintain UV properties, but lose fluorescent properties at these wavelengths. Or alternatively, display weak UV absorption but remain detectable by fluorescence, these properties are observed with with Bz3 (Figure 4.1 & 4.3). Again, in the absence of metabolites of BiPh2 by SHIP2 it is unclear what the products could be and therefore why they wouldn't exhibit fluorescent properties. Investigations are hindered by the lack of information about which and how many phosphates are being removed.

Panel C of Figure 4.5 Shows the detection of reaction products monitored by suppressed ion conductivity. The steep gradient of the baseline is a result of the increased conductivity by the gradient of the NaOH solvent; therefore it is not wholly suppressed. Again a peak was detected at approximately 14 min and had disappeared after overnight incubation, supporting the turnover of BiPh2 by SHIP2. A peak at approximately 6.5 min increased in area after overnight incubation with SHIP2cd, and corresponds to an accumulation of inorganic phosphate, likely liberated from BiPh2.

Under the same conditions, the assay was carried out with an additional biphenyl polyphosphate; BiPh3, and analysed by the same anion exchange method (Figure 4.6). With all three detection methods, the peak corresponding to BiPh3 had disappeared after the overnight incubation. The peaks were detected at the same retention time as BiPh2, perhaps not surprising as they possess the same number of phosphates, albeit in different positions. No new UV absorbing metabolites of BiPh3 were visibly detected from the column eluent, unlike for BiPh2 (Figure 4.6 - A).

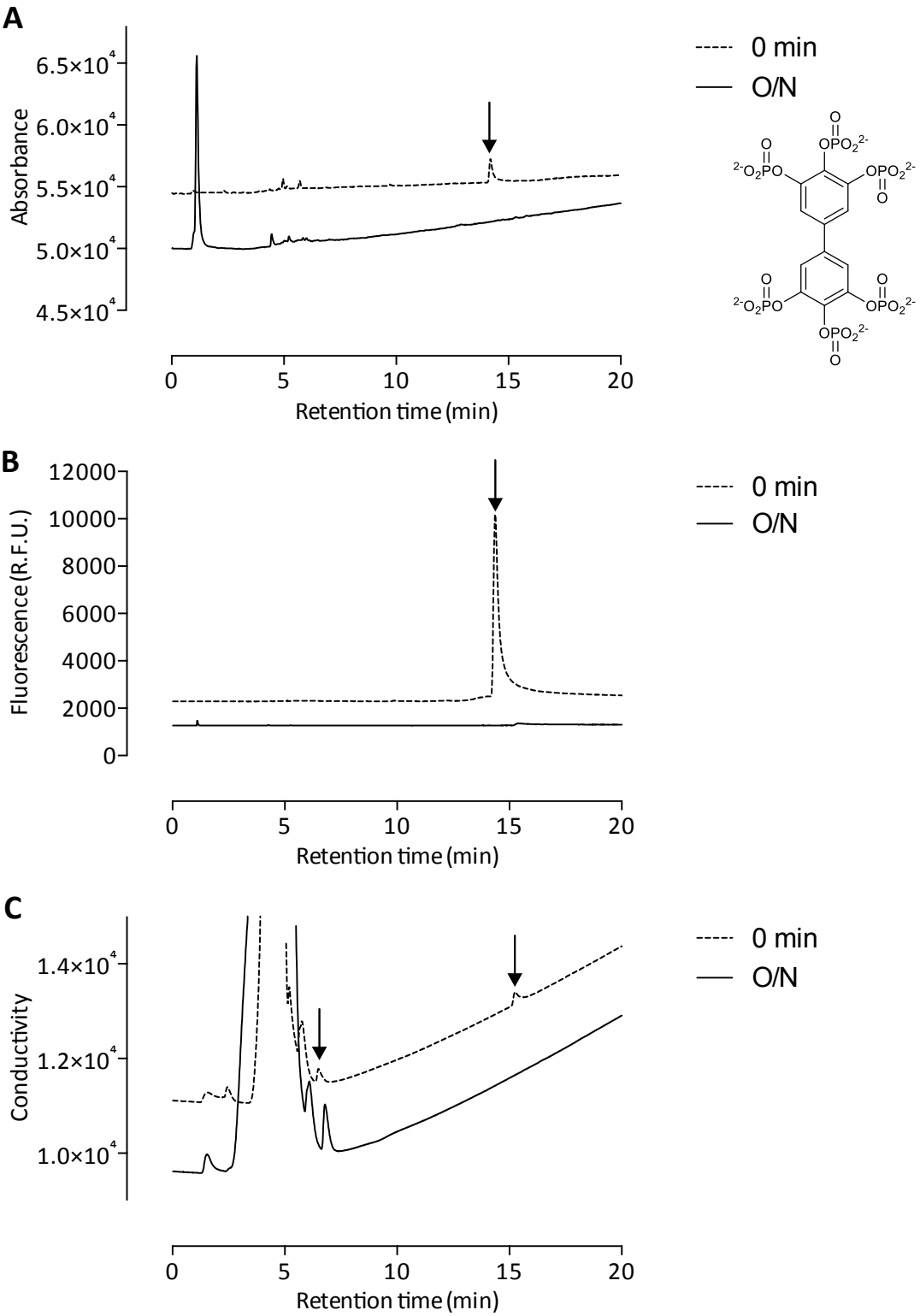

Figure 4.6 – SHIP2cd vs. biphenyl 3,3',4,4',5,5'-hexakisphosphate (BiPh3). Detection of reaction products by; (A) Absorbance at 270 nm (B) Fluorescence at ex 270 nm, em 330 nm (C) Suppressed ion conductivity, left to right the arrows indicate peaks of inorganic phosphate and biphenyl(3,3',4,4',5,5')P_6, respectively.

Similarly, there also was no new fluorescent products of BiPh3 dephosphorylation detected (Figure 4.6- B). Fluorescence is a very sensitive detection method for BiPh3 as it gives a stronger detector response when compared to BiPh2, approximately 10000 to 3200 R.F.U., respectively. This is in agreement with the study of their spectral properties in section 4.3.1, where BiPh3 was found to be far more fluorescent than BiPh2 at those wavelengths tested. Nevertheless, fluorescence is by far the most sensitive method for detecting both BiPh2 and BiPh3 in these types of assays.

Again, the peak corresponding to the accumulation of inorganic phosphate increased in area (Figure 4.6 - C). Though no new products of BiPh3 metabolism were detected by these methods, it can still be assumed that BiPh3 is a substrate for SHIP2 due to the observed loss of the UV, fluorescence and conductivity peaks. Additionally, the area of the inorganic phosphate peak increased post incubation of BiPh3 with SHIP2cd, suggesting an accumulation of phosphate liberated by SHIP2cd from Biph3.

As fluorescence was to be the most sensitive, and therefore the most suitable method for monitoring the biphenyl polyphosphates, further investigations in to the BiPh's as substrates of both SHIP1cd and SHIP2cd were performed based on this fluorescence method. Assays were set up with either SHIP1cd or SHIP2cd, and with each of the four available biphenyl compounds. The reactions were stopped at distinct time points by diluting and boiling the sample for 1 min, before injection on to an ion exchange column for analysis. The two assays presented in Figure 4.7 & 4.8 represent the most efficient turnover of a biphenyl polyphosphate by each of these enzymes, as summarised in figure 4.9 and discussed in due course.

Figure 4.7 shows the disappearance of a fluorescence peak of BiPh2 eluting at approximately 17 min over a time course of 120 minutes in the presence of SHIP2cd. The peak of biphenyl 2,2',4,4',5,5'-hexakisphosphate (BiPh2) decreases in area by 30.4 % in the initial 15 min of the reaction. After 120 min, the peak area had decreased by a total of 80.9 %, confirming that BiPh2 is a substrate for SHIP2.

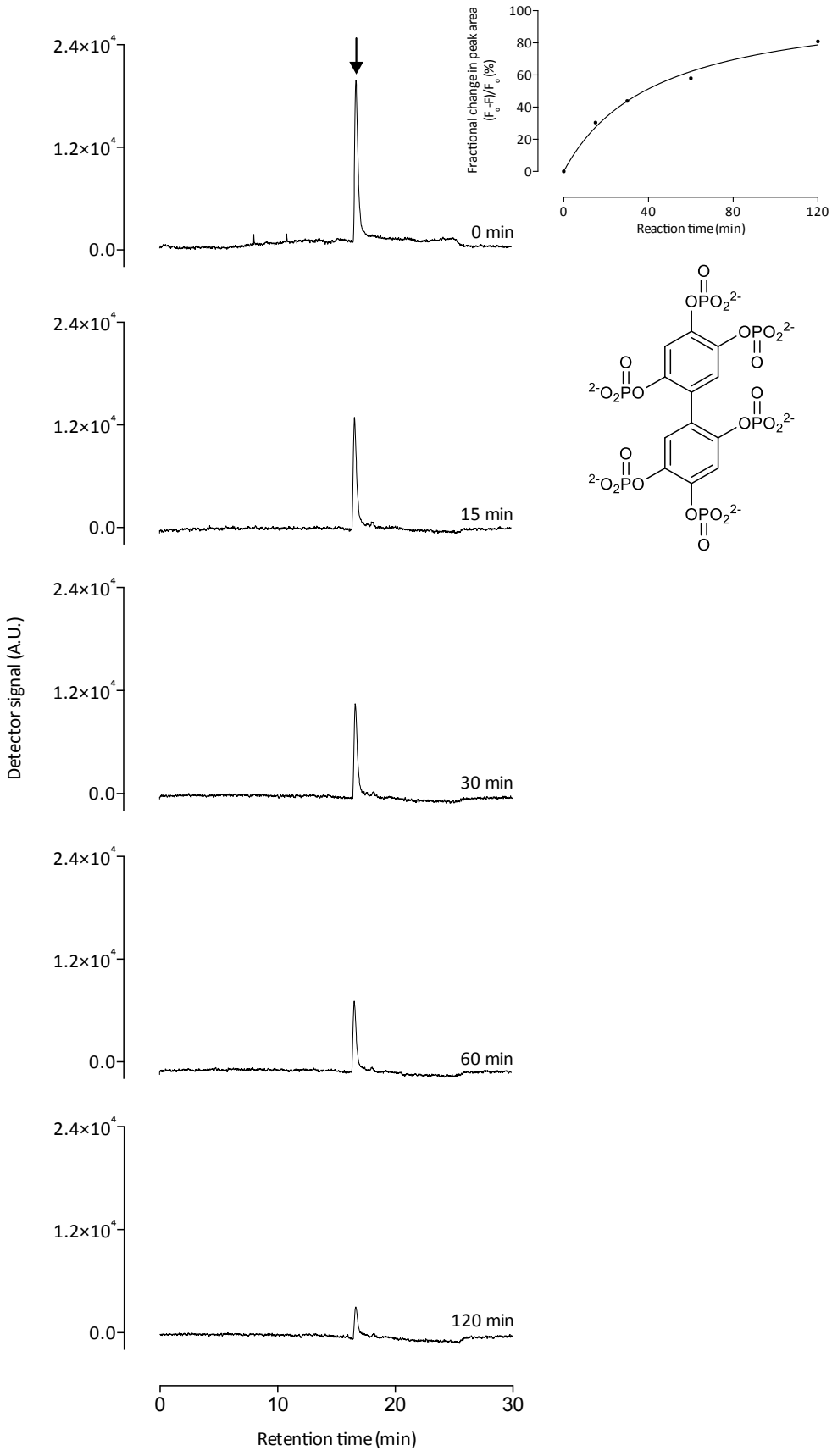

Figure 4.7 – Turnover of biphenyl 2,2',4,4',5,5'-hexakisphosphate (BiPh2) by SHIP2cd analysed by anion exchange chromatography. Elution of BiPh2 from the column was detected by fluorescence at λ_{ex} = 285 nm λ_{em} = 330 nm. Inset in the top right is a progress of reaction curve for the assay and the structure of BiPh2 below.

The SHIP1cd protein was able to hydrolyse 33.5 % of the total biphenyl 3,3’,4,4’,5,5’-hexakisphosphate (BiPh3) in the first 15 minutes of the reaction (Figure 4.8). By the end of the 120 min assay, 96.6 % of the total BiPh3 had been turnover by SHIP1cd, therefore this reaction is marginally faster than the one between SHIP2cd and BiPh2.

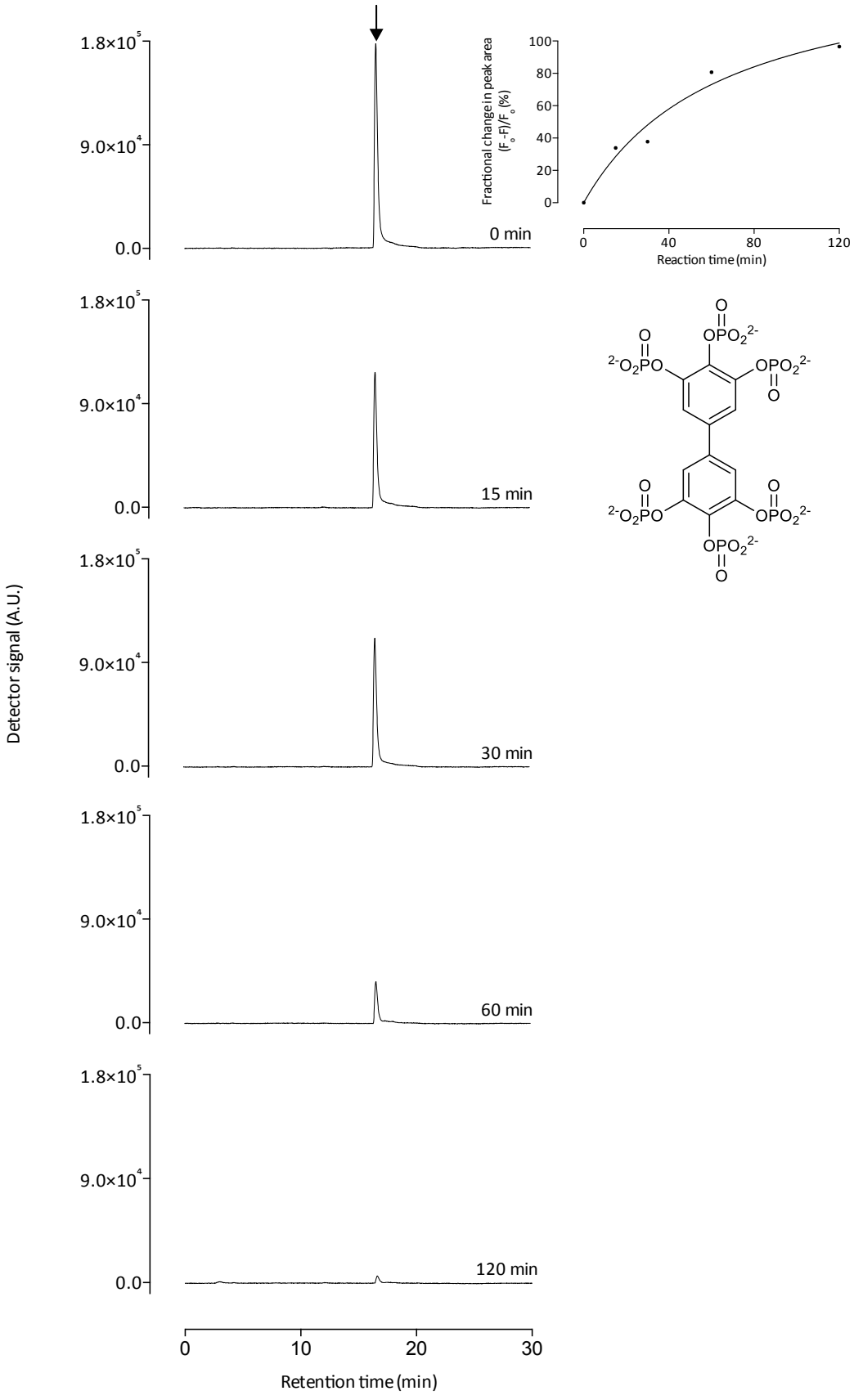

Figure 4.8 – Turnover of biphenyl 3,3',4,4',5,5'-hexakisphosphate (BiPh3) by SHIP1cd analysed by anion exchange chromatography. Elution of BiPh3 from the column was detected by fluorescence at λ_{ex} = 285 nm λ_{em} = 330 nm. Inset in the top right is a progress of reaction curve for the assay and the structure of BiPh3 below.

The two assays presented in Figure 4.7 & 4.8 represent the most efficient turnover of a biphenyl polyphosphate by each of these enzymes. Comparing the progress of reaction profiles for all the biphenyl compounds as substrates corroborates with this, and reveals that the two isozymes may have differing substrate specificities (Figure 4.9). Overall SHIP1cd was more active towards these substrate mimics than SHIP2cd, where all four compounds were hydrolysed by at least 60 % on completion of the assay. In the case of SHIP2cd, only the reaction with BiPh2 progressed to this extent. No enzyme kinetics parameters can be drawn from these investigations as only single concentrations of enzyme and biphenyl polyphosphate were used in this instance. However, the results show an exciting new substrate flexibility of both SHIP1 and SHIP2.

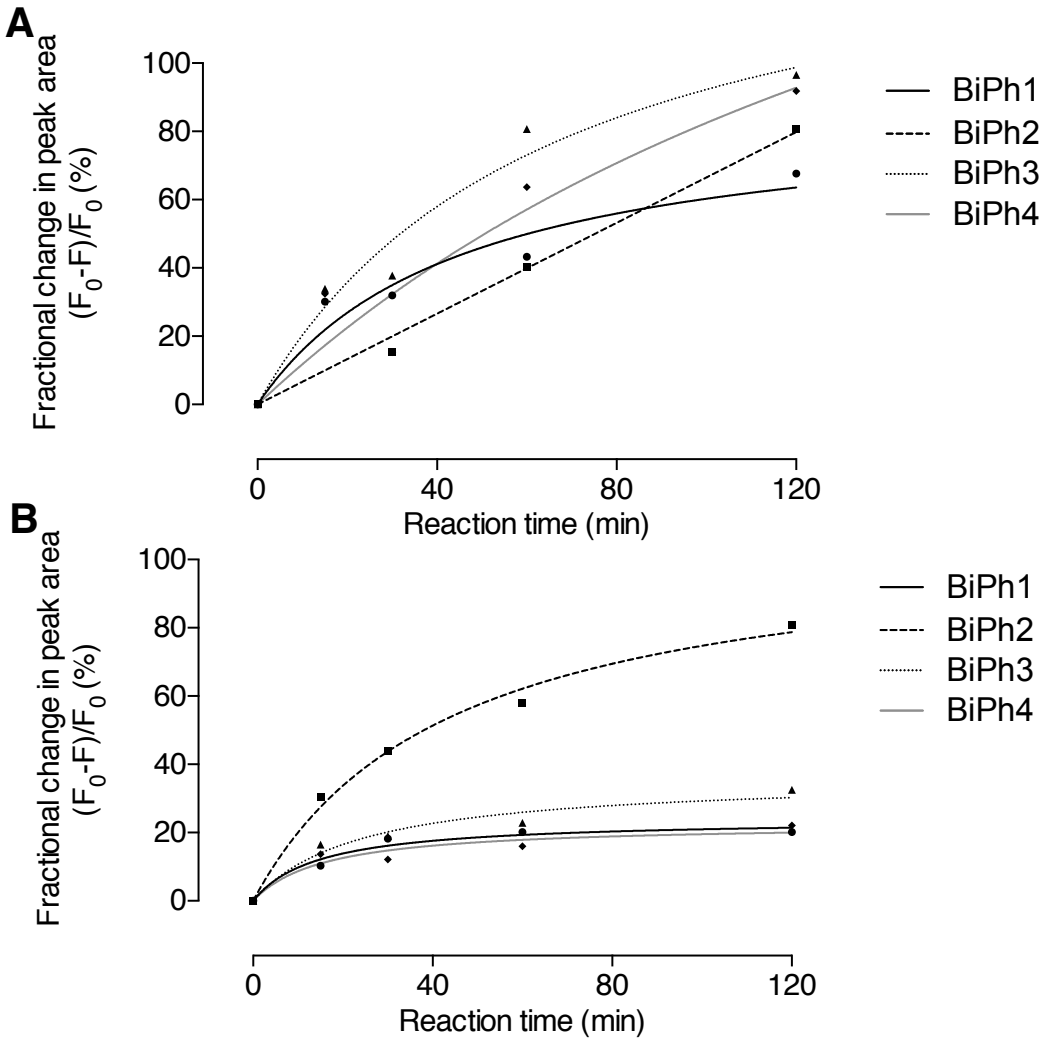

Figure 4.9 – Progress of reaction for the turnover biphenyl phosphates by; (A) SHIP1cd (B) SHIP2cd. Fractional change in peak area (%).

It is evident that the biphenyl polyphosphates are useful in studying the catalytic activity of these proteins by means of end-point reactions, but being able to follow turn-over and subsequent loss in fluorescence in real-time assays would offer further utility and convenience to investigate these enzymes, and perhaps other inositol polyphosphate phosphatases beyond just SHIP1 and SHIP2.

Assays of SHIP2cd and the BiPh's were performed in 96-well black plates, with the reaction being instigated by the addition of a fixed concentration of SHIP2cd. Despite extensive efforts to collect full sets of data, by fine-tuning the method and making use of numerous plate readers, only preliminary data was obtained. This type of instrumentation is generally considered less sensitive when monitoring fluorescence than detectors that are employed with HPLC and IC systems, which made it challenging to gain consistent results with this method. Other parameters such as temperature were also limiting factors. Nevertheless, Figure 4.10 shows the outcome of an assay between SHIP2cd and BiPh3. Where BiPh3 was chosen specifically due to having the strongest fluorescence characteristics of the BiPhs, thus minimising the problems with sensitivity and detection of the loss in fluorescence of these compounds. Three concentrations of BiPh3 were tested and it is evident that the loss of fluorescence which would inevitably be occurring at the lower concentrations, albeit at a slower rate, is not observable under this method, and only the higher concentration (10 µM) results in a visible loss in fluorescence in real-time. This is considerably more substrate than was required in the assay in Figures 4.7 & 4.8, in which the method was able to detect 0.2 µM BiPh3 injection on to a column (50 µL), and therefore presents another limitation to this method.

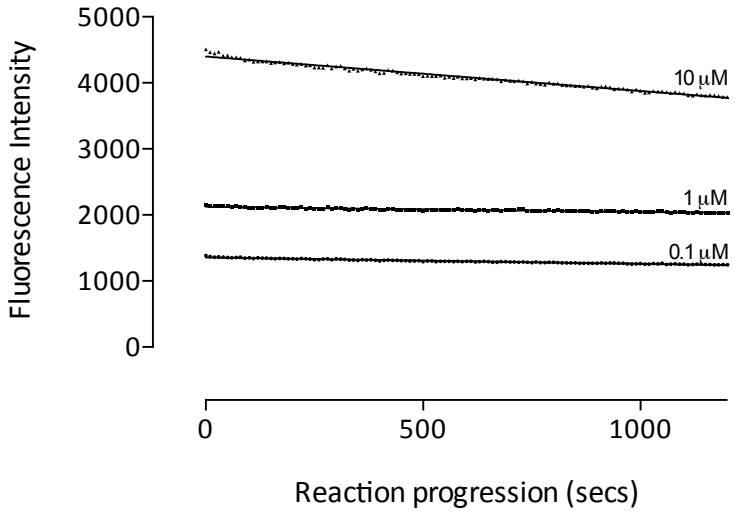

Figure 4.10 – SHIP2 vs. BiPh(3,3',4,4',5,5')P_6 preliminary kinetics data. Loss in fluorescence from BiPh3 followed at λ_{ex} = 265 nm λ_{em} = 330 nm. SHIP2cd fixed at 1.5 μM.

Linear regression was performed on the kinetics data which gave gradients equivalent to the rate of reaction (ΔF.I. / Δtime (s)). As formerly mentioned, there was very little detectable difference in the reaction rate between the assay conducted at 0.1 μM, to that conducted 10-fold higher at 1 μM. The reaction rates were essentially undetectable or too slow for the time course of the assay. The assay performed at 10 μM resulted in a gradient of -0.52 ± 0.006.

Although investigation of the real-time enzyme kinetics of SHIP2cd (and SHIP1cd) with the BiPhs is desirable, this method is not as robust and reproducible as the previous ion chromatography methods. It also lacks the sensitivity which in turn leads to the use of much too high concentrations of compound and inevitably leads to wastage.

4.3.3 Using fluorescently tagged inositol phosphates to explore ligand binding by fluorescence polarisation

A selection of fluorescently tagged inositol polyphosphates were obtained from collaborators (Potter, B.V.L.; University of Bath, UK) and were utilised in creating binding curves with SHIP1cd, SHIP2cd and AtIPK1 via a fluorescence polarisation method (section 4.1 & 4.2.). The curves are constructed by titration of increasing concentrations of protein to a fixed concentration of fluorescent probe while monitoring the emissions in the perpendicular and parallel channels relative to the polarised excitation channel. The method is very robust and reproducible, and offers a high-through put means of conducting these types of investigations because multiple data sets can be analysed at any one time in 384-well microtiter plates.

An EC50 is related to but not equivalent to the disassociation constant (K_d), and is defined simply as the effective concentration of agonist that that provokes a half maximal response; the concentration required to bring the curve to a half way point (50 %) between the bottom and top plateaus of the dose-response curve(0 and 100 %). It is regularly quoted in pharmacological studies when investigating the binding characteristics of drugs to proteins and measures agonist potency, although it is not a direct measure of drug affinity. For most of the fluorescence polarisation dose-response curves presented in this study the bottom baseline was set to 35 mP for free un-bound probe. Additionally, fluorescence polarisation methods have a theoretical maximum of 400 mP. However these values are often not the experimental plateaus, this is recalculated and accounted for when fitting a four parameter fit to the dose-response curves, which actually provides what is referred to as the relative EC50 but the adjective *relative* is usually omitted. The binding of SHIP2cd and AtIPK1 to all the available fluorescent inositol phosphate probes was investigated, and a summary of the EC50 values are shown in Table 4.2.

Table 4.2 – Binding of fluorescently tagged inositol phosphates to AtIPK1 and SHIP2cd.

	EC50 (nM)	
	AtIPK1	SHIP2cd
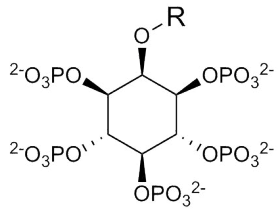 2-FAM-IP$_5$	16.8 ± 1.11	57.2 ± 1.13
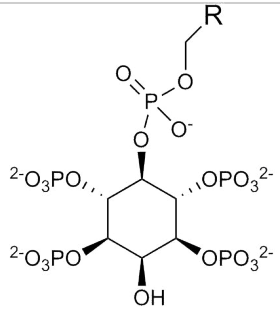 5-FAM-IP$_5$	10.82 ± 1.06	26.51 ± 2.30
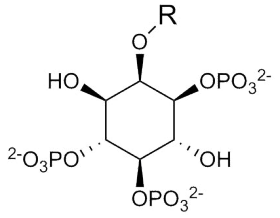 2-FAM-IP$_3$	302.30 ± 1.07	780.6 ± 1.06
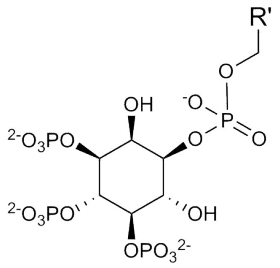 1-FITC-IP$_3$	68.06 ± 2.01	410.50 ± 1.12
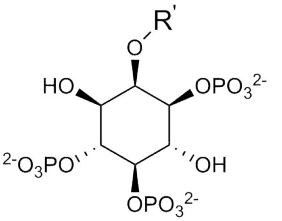 2-FITC-IP$_3$	67.86 ± 1.14	611.3 ± 1.04
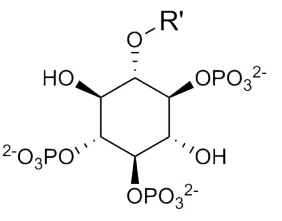 *scyllo*- FITC-IP$_3$	27.3 ± 1.12	1018 ± 2.31

R = 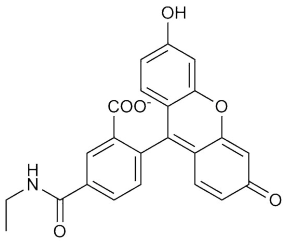

R' = 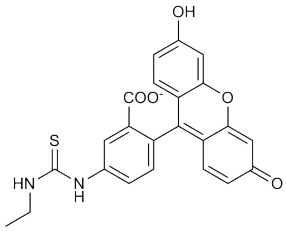

Binding curves and resulting EC50 values for all three proteins with 2-FAM-IP_5, which became the most widely used fluorescence polarisation probe due to being received prior to the other fluorescently tagged inositol phosphates, can be seen in Figure 4.11.

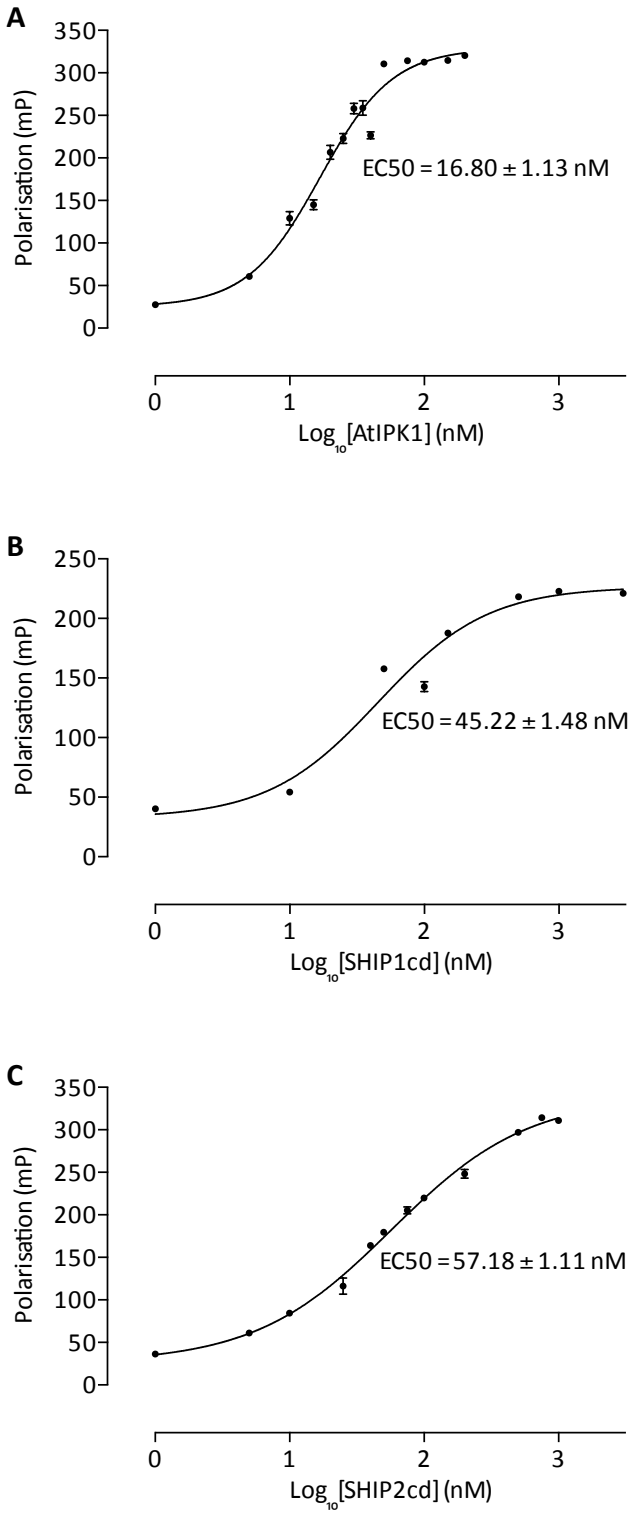

Figure 4.11 – Dose-response binding curves of; (A) AtIPK1, (B) SHIP1cd & (C) SHIP2cd to 2-FAM-IP$_5$. Binding is monitored by the change in polarisation of 2-FAM-IP$_5$ upon increased concentration of protein, λ_{ex} = 485, λ_{em} = 520.

AtIPK1 demonstrates the highest affinity for 2-FAM-IP_5, as it gave the lowest EC50 value of 16.8 ± 1.1 nM (Figure 4.11 - A), when compared to 45.2 ± 1.5 nM and 57.2 ± 1.1 nM for SHIP1cd and SHIP2cd, respectively. Although it should be noted that these values are very similar with very low errors associated with them, which demonstrates that 2-FAM-IP_5 binds tightly to all three proteins.

Though attempted, no structural data is yet available for AtIPK1, SHIP1cd or SHIP2cd in complex with the fluorescent tagged inositol phosphates therefore, though likely, it cannot be confirmed that they are binding in the active sites. Despite this, evidence from the displacement of these polarisation probes from SHIP1cd and SHIP2cd by traditional substrates suggests that they do indeed bind in the active site (Figure 4.12). Inhibition curves are produced using a similar polarisation method where both the probe and protein concentrations are fixed, in this case at 2 and 200 nM respectively. The IC50 is calculated in the same way as the EC50 by a four parameter fit of the dose-response data, and is defined as the concentration of an inhibitor where the response (or binding) is reduced by half. IC50 curves are downwards sloping rather than positive slopes. Just like the EC50 is related to K_d, the IC50 is also indirectly related to the inhibition constant (K_i) and can be arrived at via use of the Cheng-Prusoff equation (Cheng and Prusoff, 1973).

For both proteins, Ins(1,3,4,5,6)P_5 (IP_5) displaced 2-FAM-IP_5 more effectively than Ins(1,2,4,5)P_4 (IP_4). However, displacement by IP_5 in SHIP1cd was more potent than in SHIP2cd with IC50's of 101 ± 1.3 and 4485 ± 1.1 nM, respectively. For SHIP1cd, the data remains at the top plateau of the IP_4 curve up to a higher concentration of 'inhibitor', than with IP_5 (Figure 4.12 - A), also observable with SHIP2cd (Figure 4.12 - B).

The graph fitting software could not fit a complete curve to the IP_4 / SHIP2cd data and the resulting IC50 is ambiguous with a wide confidence interval. However, the value given along with a visual observation provides an insight in to the binding of IP_4 to SHIP2cd, and a reference for comparison to other substrates or inhibitors.

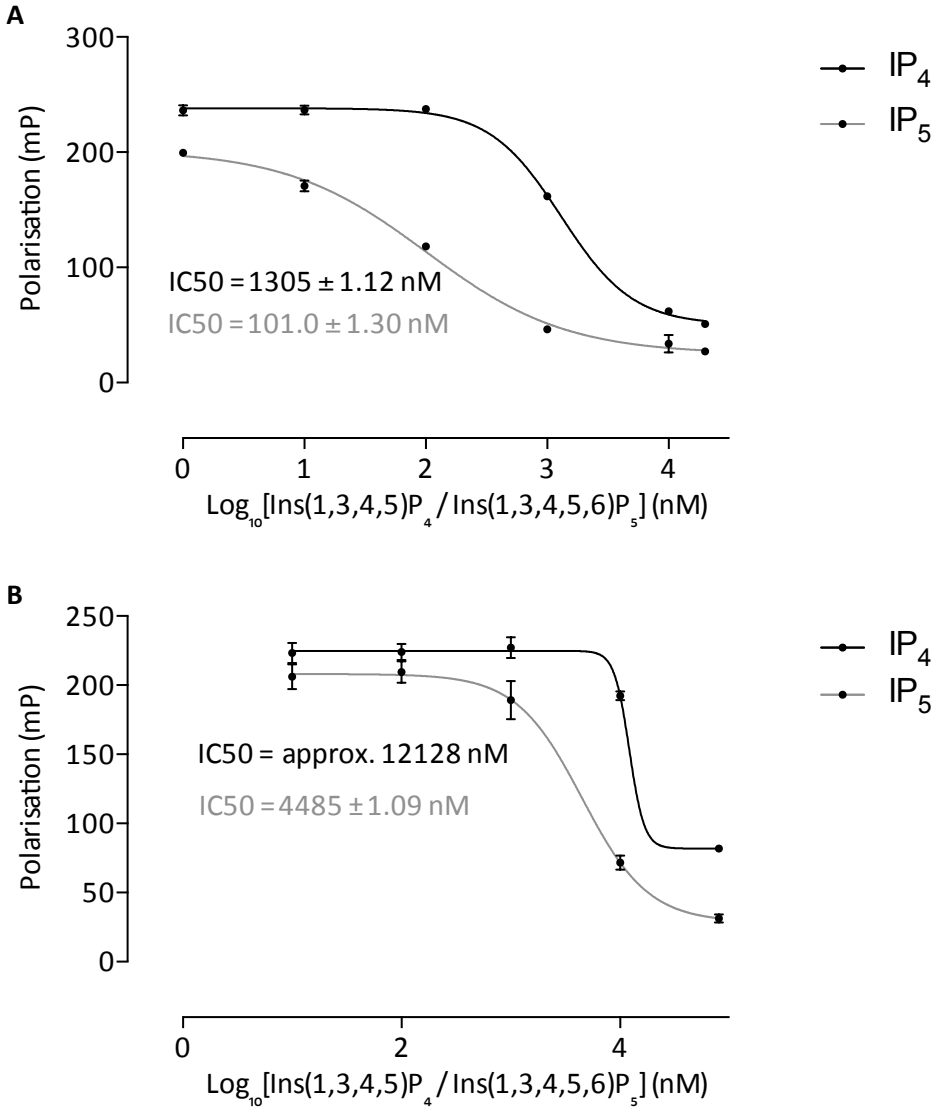

Figure 4.12 – Inhibition curves; Displacement of 2-FAM-IP_5 by inositol 1,3,4,5-tetrakisphosphate and inositol 1,3,4,5,6-pentakisphosphate from (A) SHIP1cd & (B) SHIP2cd. IC50 values are shown in black for displacement with IP_4 and grey for IP_5.

The same method was applied using the biphenyl polyphosphates, previously discussed in detail as inositol phosphate mimics that act as ligand analogues and as substrates of SHIP1cd and SHIP2cd (sections 3.3.4 & 4.3.2); backed up by structural evidence (Mills et al., 2012). All four BiPh compounds (Figure 1.13), were tested for their ability to displace 2-FAM-IP_5 from the active sites of AtIPK1, SHIP1cd and SHIP2cd, at fixed probe and protein concentrations of 2 and 200 nM. As an example of the data obtained, Figure 4.13 shows the results for all three proteins releasing 2-FAM-IP_5 and simultaneously binding to biphenyl (3,3',4,4'5,5')P_6 (BiPh3).

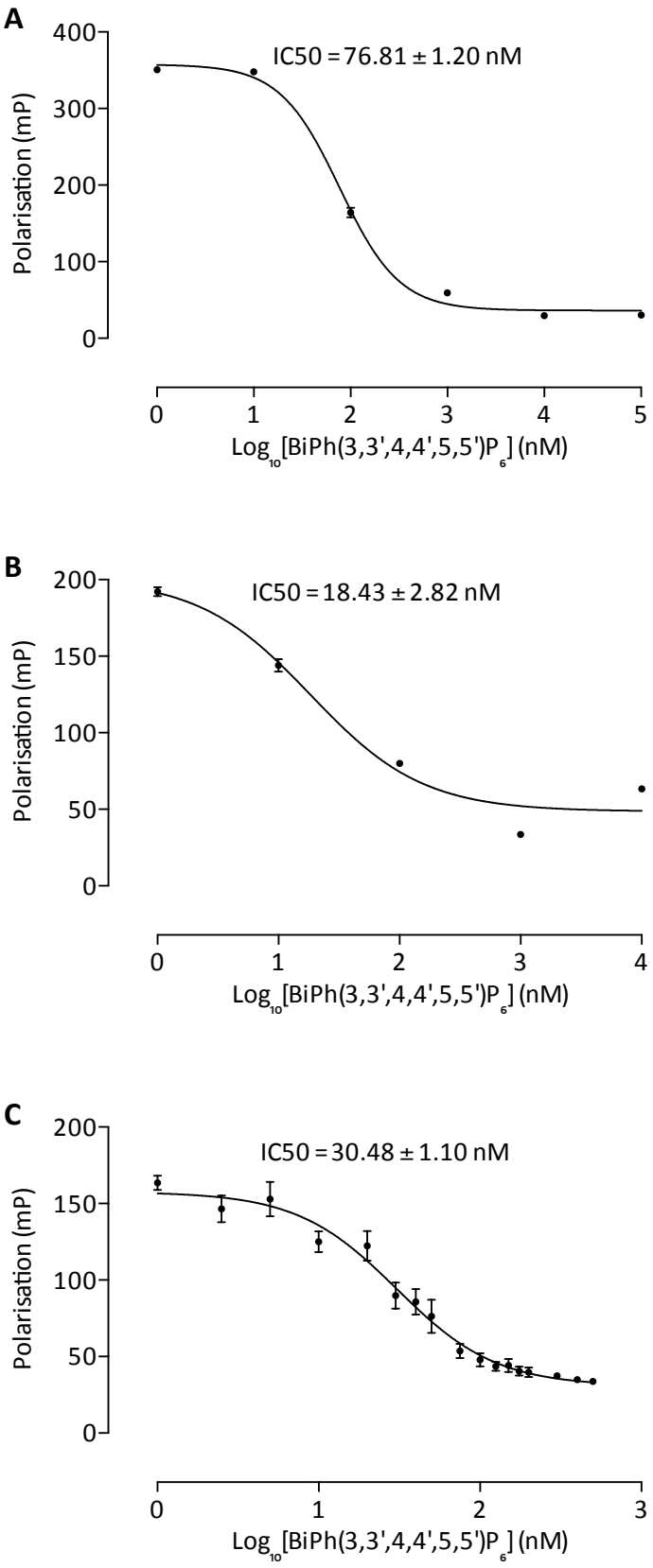

Figure 4.13 – Inhibition curves; displacement of 2-FAM-IP_5 by biphenyl (3,3',4,4',5,5')P_6 (BiPh3) from (A) AtIPK1, (B) SHIP1cd & (C) SHIP2cd. Protein concentration is fixed at 200 nM, probe at 2 nM.

The probe, 2-FAM-IP_5, was displaced the most efficiently with BiPh3 from SHIP1cd with an associated IC50 of 18.4 ± 2.8 nM (Figure 4.13 - B). Fractionally lower than the IC50 values for AtIPK1 and SHIP2cd which were 76.8 ± 1.2 nM and 30.5 ± 1.1 nM.

A summary of the IC50 values for the displacement from AtIPK1, SHIP1cd and SHIP2cd by each of the four biphenyl polyphosphates can be seen in Table 4.3.

Table 4.3– Binding of the biphenyl phosphates to AtIPK1, SHIP1cd & SHIP2cd.

	IC50 (nM)		
	AtIPK1	SHIP1cd	SHIP2cd
BiPh1	101.5	19.31	29.69
BiPh2	66.09	65.53	38.72
BiPh3	76.81	18.43	30.48
BiPh4	51.06	27.35	48.2

It is inherent in the interpretation of experiments performed in this and subsequent sections that 2-FAM-IP_5 is an active site ligand of the proteins tested. For AtIPK1, chapter 3 provides categorical structural data showing the biphenyl phosphates ligands co-ordinate inositol phosphate-coordinating residues in the active site of AtIPK1. Furthermore, structures of SHIP2 and an additional inositol 5-phosphatase, INPP5B, show these surrogate ligands in the active site pocket coordinated by residues that interact with P4 of a canonical substrate (Mills et al., 2012, Mills et al., 2016). Given displacement occurs in all three proteins it is likely that 2-FAM-IP_5 is indeed binding in the active site. Additionally, bona fide substrates were able to displace 2-FAM-IP_5 (Figure 4.12), inositol phosphates have not been shown to bind to these types of proteins elsewhere other than the active site.

Despite high through put screening, SHIP2cd in complex with 2-FAM-IP_5 failed to produce crystals, and due to time constraints SHIP1cd has not yet been subjected to crystallisation screening. Attempts to solve crystal structures of 2-FAM-IP_5 / AtIPK1 did not resolve electron density that could be unambiguously assigned to 2-FAM-IP_5, but did suggest perturbations in the structure of N-lobe of AtIPK1, as seen upon accommodating larger ligands in chapter 3, consequent on inclusion of 2-FAM-IP_5 (personal communication, H. Whitfield, UEA).

4.3.4 Known inhibitors of SHIP1cd & SHIP2cd – validation of 2-FAM-IP_5-based assays

In seeking to confirm the efficacy of 2-FAM-IP_5-based fluorescence polarisation assays it is helpful to test known inhibitors of this class of phosphatase The data shown in Figure 4.14 test the effect of AS1949490, 3-[(4-chlorobenzyl)oxy]-N-[(1S)-1-phenylethyl]-2-thiophenecarboxamide. This compound was identified as a potent SHIP2 inhibitor with an IC50 of 0.62 μM, measured in a phosphate release assay with the catalytic domain of this protein (Suwa et al., 2009). AS1949490 was highly specific for SHIP2 over other 5-phosphatases including SHIP1. The compound increased the phosphorylation of Akt in L6 myotubes and displayed other *in vivo* effects indicative of the activation of insulin signalling pathways.

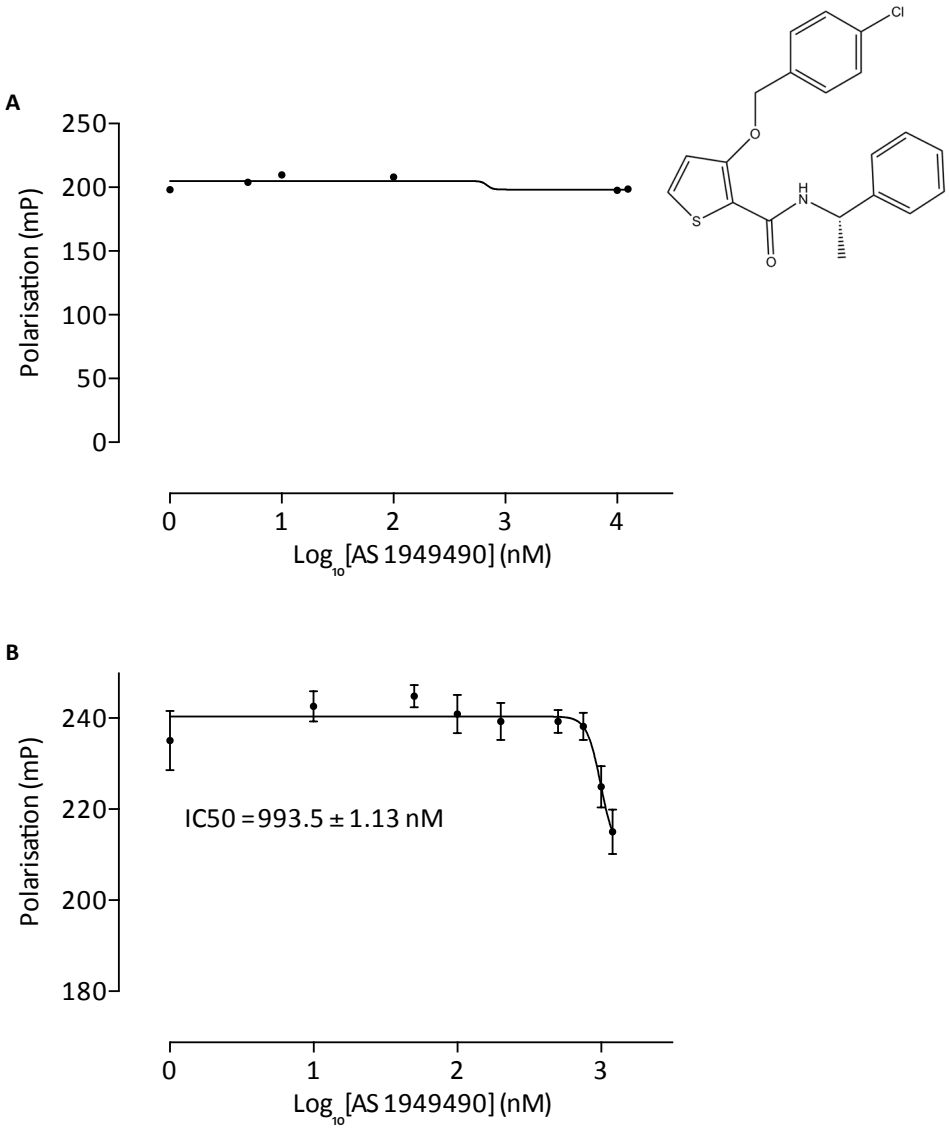

Figure 4.14 – Displacement of 2-FAM-IP_5 by AS 1949490, a SHIP2 inhibitor with a reported 30-fold decreased affinity for SHIP1. (A) SHIP1cd. (B) SHIP2cd.

Like the former study, the polarisation assay confirms the specificity of SHIP2cd over SHIP1cd. The IC50 value of 0.99±1.1 µM, though remarkably similar to that of Suwa et al. (2009), cannot be meaningfully compared with results of assays performed differently in other studies as IC50 does not account for differences in protein and ligand concentration. Nevertheless, the robust discrimination between SHIP isoforms provides validation of polarisation-based assays as tools to study enzymes of this class. AS1949490 was shown to be a competitive inhibitor of SHIP2. The reduction in probe polarisation at concentrations approaching 1 µM seen here may therefore be explained

by progressive displacement of probe from SHIP2, providing indirect evidence, that 2-FAM-IP_5 binds in the active site of 5-phosphatases, or at least in the active site of SHIP2.

3-α-aminocholestane (3AC) was identified by high throughput screening to be a selective inhibitor of SHIP1 (Brooks et al., 2010). The assay used was a commercial assay from Echelon Biosciences, Utah, USA. While the mechanism of action is undefined the similarity of structure with pelorol, an allosteric activator of SHIP1 (Yang et al., 2005) may suggest an allosteric role for 3AC. Interestingly, pelorol, and its synthetic derivatives, AQX-MN100 and AQX-016 (Ong et al., 2007), have been reported to act like PtdIns(3,4)P_2 by binding to the C2 domain of SHIP1 to allosterically modulate (enhance) SHIP1 activity (Blunt and Ward, 2012).

It is remarkable therefore that the experiment shown in Figure 4.15, performed on SHIP1cd, shows that 3AC interacts with SHIP1cd, and not SHIP2cd, and does so with an IC50 of ≈ 2 μM, and increases the binding of 2-FAM-IP_5 to SHIP1cd.

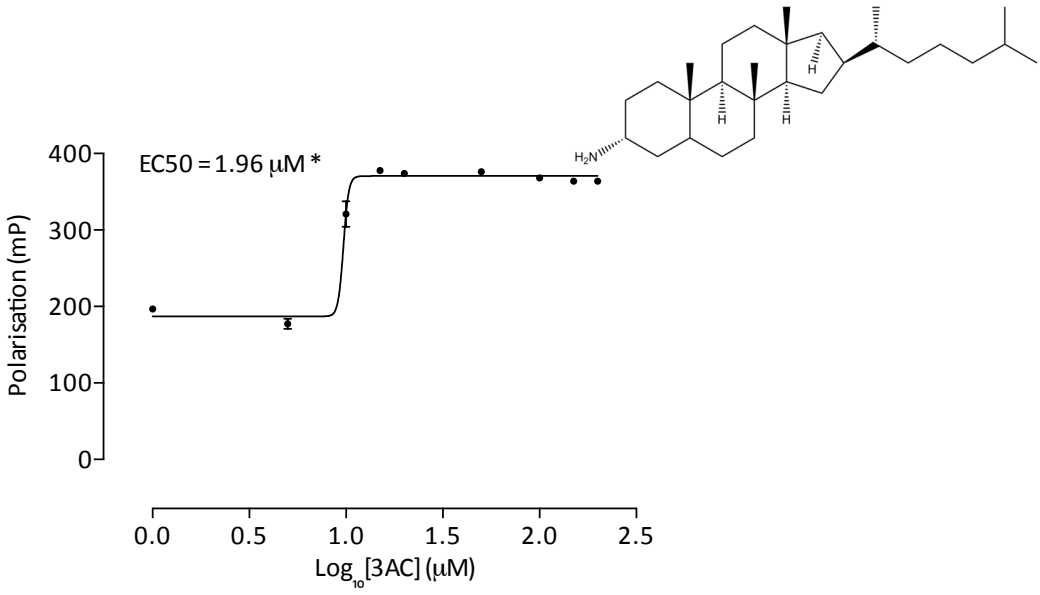

Figure 4.15 – Binding of 3-α-aminocholestane to SHIP1cd

***EC50 stated was calculated in MARS data analysis software (BMG) not from the curve above, this software does not provide a standard error but includes 3AC concentrations below 1 μM. Concentrations are plotted on a log_{10} scale rather than requiring concentrations to be input and plotted in log_{10} (resulting in some negative x-coordinates). Therefore, in this instance it offers a more complete and accurate binding curve and EC50.**

Irrespective of whether 3AC can be considered an analog of pelorol or its synthetic derivatives, these remarkable results strongly indicate that 3AC is an allosteric regulator of SHIP1 that acts on the catalytic domain of the protein. While these results do not directly call into question the reported mode of action of pelorol derivatives that have entered Phase 2 clinical trials for inflammatory disorders (Blunt and Ward, 2012), they do highlight the efficacy of 2-FAM-IP_5-based assays in revealing allosteric as well as competitive (active site) interactions of ligand with this therapeutically important class of phosphoinoisitide 5-phosphatase.

4.4 Conclusions and future work

The UV absorption and novel fluorescence properties of the benzene and biphenyl phosphates have been unearthed and characterised. Work is currently continuing with collaborators as to what attributes give these compounds fluorescent properties via use of density functional theory. This may allow for design of additional fluorescent compounds that could be supplemented with certain moieties that would provide new tools for exploring specificities and functionalities of specific enzymes of this family and perhaps beyond.

The biphenyl phosphates have been shown to be substrates of SHIP1 and SHIP2 as opposed to inhibitors, and have provided a useful tool for the studying the enzymology of these 5-phosphatases via their fluorescent properties. An ion exchange chromatography method provides a sensitive means of detecting the metabolism of the biphenyl phosphates and in future can be extended and refined to extract kinetic parameters for SHIP1 and SHIP2 with the fluorescent substrate mimics. This has also revealed differing substrate specificities between SHIP1 and SHIP2 for the biphenyl phosphates. Both ion chromatography data and subsequent binding analysis reveal a preference for BiPh2 by SHIP2, and BiPh3 by SHIP1. Although no formal comparison of the substrate specificities and affinities of SHIP1 and SHIP2 have been carried out in the same study, the literature does suggest that they possess different substrate ranges as well as affinities for the substrates that they have in common (Eramo and Mitchell, 2016). As described in chapter 2, structural data would greatly aid in the elucidation of this.

A robust high through put fluorescence polarisation method has also been described which allowed the construction of dose-response curves giving descriptions of the binding of fluorescently tagged inositol phosphate analogs to AtIPK1, SHIP1cd, and SHIP2cd.As mentioned earlier, attempts to obtain crystal structures of these proteins with 2-FAM-IP_5 are on-going. It is reasonable to assume that these fluorescent polarisation probes are indeed binding in the active site of the proteins, due to the displacement by canonical substrates, defined inhibitors and the biphenyl phosphates; of which there are structures available and as of now, are substrates.

Further to this, the fluorescence polarisation method has potential in screening inositol phosphate-binding proteins for potential ligands or inhibitors via displacement of 2-FAM-IP_5, or the most suitable probe, from the active site. The search for lead compounds for the design of inhibitors or drugs for clinically relevant IP-kinases and IP-phosphatases is desirable due to the wide range of diseases these family of proteins are implicated in.

Chapter 5 - *Application of fluorescently tagged inositol polyphosphates in novel inhibitor and lead compound discovery*

5.1 Introduction

5.1.1 Screening for lead compounds in drug discovery

During drug discovery, the "hit" identification and lead discovery phase follows an initial process of target identification and validation; a multifaceted process that can take many years to settle on selecting a target for costly drug discovery (Hughes et al., 2011). As opposed to knowledge based screening for hit identification, high throughput screening assumes no prior knowledge of the nature of the chemotype likely to have an effect on the target protein, and involves screening an entire compound library directly against the target. The first potent small molecule inhibitor of SHIP2, AS1949490, was discovered through such a method, which used a standard malachite green assay that measures phosphate release. After identification, AS1949490 was found to be a potent inhibitor (IC50 = 0.62 μM) which increased Akt phosphorylation and reduced blood glucose levels in mice (Suwa et al., 2009). The identification of the SHIP1 inhibitor 3-α-aminocholoestane (3AC) was also identified via a high throughput screen (Brooks et al., 2010). The screen used was the original version of the National Cancer Institute's diversity set (see section 5.3) which is freely available, and a subsequent version has been used in this work. 3AC was identified as a hit by use of a fluorescence polarisation method that detects the 5-phosphatase activity of SHIP1, developed from an assay available from Echelon Biosciences (Drees et al., 2003). More recently, a study has developed an assay and screening strategy that is applicable to 5-phosphatase and phosphoinositide-metabolising enzymes, and from this a specific OCRL/INPP5B inhibitor was identified (Pirruccello et al., 2014). Three assay formats were developed which allowed for the exclusion of false-positives; a fluorescence polarisation assay based on the same principles as Brooks et al, 2010, a less sensitive malachite green assay and a mobility shift assay that was hindered by the speed of detection.

5.1.2 The Z-factor

The Z-factor was defined to as a simple statistical parameter for use in the evaluation and validation of high throughput screening assays, that ultimately can be used to compare the quality of assays and quantify how well the assay works (Zhang et al., 1999). It is a screening window coefficient that reflects the assay signal dynamic range and the data variation associated with single measurement, and has become standard for this type of assay. It defines upper and lower thresholds calculated from the mean of the background/negative control values and the mean of the positive controls. Any true "hits" will be three standard deviations below the mean of the positive control, and three standard deviations above the mean of the negative control. This creates a separation band which is defined by these two thresholds. The difference between the two mean values is called the dynamic range, and dividing the separation band by this computes the Z-factor. A Z-factor of 1.0 is the ideal, but is unobtainable. An excellent assay is signified by a Z-factor between 0.5-1.0.

5.1.4 Lipinski's rule of five

Lipinski's rule of five (or Pfizer's rule of five) is a simple rule of thumb which is commonly cited as a means by which to compare the similarity of compounds with biological activities that might suit them as orally active drugs (Lipinski et al., 2001, Lipinski, 2004).The rule has its origins in the observation that drugs are commonly small hydrophobic molecules whose physicochemical properties are such that they are readily absorbed (pass across membranes). While the field of pharmacokinetics addresses the impact of a potential drug's physicochemical properties on absorption, partition (or distribution), metabolism and excretion, the work described here does not extend to such analysis.

Lipinski's rule rephrased simply states that an orally active drug should have no more than one departure from the following criteria;

- No greater than 5 hydrogen bond donors (for these purposes, hydrogen bonds are N-H or O-H bonds)
- No greater than 10 hydrogen bond acceptors (for these purposes, these are atoms of nitrogen or oxygen)
- A mass of no more than 500 daltons
- A partition coefficient between octanol and water log P not greater than 5

5.1.5 Experimental aims

As high throughput screens are freely available, and a robust and sensitive fluorescence polarisation method has been developed for probing the active sites of inositol phosphate-binding proteins, the proteins in this study were subjected to two high throughput screens. Any inhibitor hits were followed up with binding curves to eliminate false positives and then for AtIPK1, taken forward for binding and inhibition kinetics assays. The screen was approached with proof of concept for the method in mind rather than from a strictly pharmacological point of view.

5.2 Materials and methods

5.2.1 High throughput screening of compound libraries

For high throughput screening of drug discovery screens, assay conditions were as described in 4.2.5, using 5 nM 2-FAM-IP_5, 100 nM protein and 12.5 µM screen compound. The assay was performed in a 96 well plate with a volume of 100 µL per well (Corning 96 well half-area black polystyrene flat bottom plate). Only a single well was each compound was assayed.

5.2.2 Changes in AtIPK1 intrinsic tryptophan fluorescence upon ligand binding

Changes in protein folding consequent on ligand binding or other treatments were reported by the intrinsic fluorescence of 2 µM AtIPK1 protein as described previously (Banos-Sanz et al., 2012). Additions were made of inositol substrate or inhibitor compound (0.25-2 µM) and the fluorescence intensity measured at excitation wavelength of 280 nm and emission of 340 nm using a Hidex Sense plate reader.

5.2.3 Coupled enzyme assay

A Molecular Devices SpectraMax M5 Plate Reader, using Corning flat bottom 96 well plates, was used to monitor the real time absorbance at 340 nm of a coupled enzyme assay. Enzyme (500 ng) was mixed with 20 mM HEPES pH 7.5; 1 mM $MgCl_2$; 20 mM KCl; 0.1 mM ATP; 2 mM PEP; 0.15 mM NADH; 7.5 UmL^{-1} Lactate dehydrogenase; 15 UmL^{-1} Pyruvate kinase along with an inositol phosphate substrate, the concentration of which is specified in each experiment description. The reaction was monitored for 15 minutes at 25 °C along with either a no enzyme or no substrate control. Each experiment consisted of 3 replicates of each condition. Initial linear rates were calculated using Molecular Devices Softmax Pro software for each reaction, normalised against the control reaction rates.

5.3. Results and discussion

5.3.1 Screening compound libraries using fluorescence polarisation

As introduced in section 5.1.1 large compound libraries are frequently used in the search for lead compounds for subsequent optimisation in inhibitor design and discovery of drugs targeted towards proteins whose functions are implicated in human disease. Phosphoinositides and their soluble inositide counterparts, as discussed through-out this text, have been reported in multiple fundamental pathways of cell metabolism and therefore the proteins that govern the levels of these molecules are naturally desirable drug targets for therapeutic intervention of many diseases including cancers and diabetes(Ooms et al., 2009). All three inositol polyphosphate metabolising enzymes discussed in this study have been subjected to two examples of these screens using the fluorescence polarisation method developed in chapter 4. The work demonstrates the versatility of this type of assay and the fluorescent probes at its core.

Libraries were obtained from the National Cancer Institute (NCI) through the Drug Synthesis and Chemistry Branch (DSCB) of the Developmental Therapeutics Program (Maryland, USA), where they are freely available upon request. Two libraries were subsequently screened with both AtIPK1 and SHIP2cd; Diversity set II (DivII) and Approved Oncology Drugs Set V (AODV), 1872 and 114 compounds respectively. SHIP1cd was also screened against AODV.

The libraries were screened with 2-FAMP-IP_5 as a fluorescence polarisation probe in 96-well plates, using the method introduced in chapter 4 (section 4.3.3). Instead of titrating increasing increments of screen compound/potential inhibitor to fixed protein and probe concentrations, a single concentration of compound was used (12.5 µM) to allow for a high-throughput screening method. Observed decreases in polarisation were compared to control samples; fluorescent probe bound to protein and free un-bound

probe, to assess if any change in polarisation was a result of protein binding a potential ligand.

Convention for this type of pharmacological screen is that any given polarisation value below 3 standard deviations from the mean of the negative control is a “hit” and therefore a potential ligand/inhibitor (see section 5.1.2). Due to the robustness of the method developed in this study, and the small errors generated by the plate reader, a small standard deviation was achieved and thus resulted in an elevated number of potential hits. Upon closer inspection, many compounds were discounted due to concerns that they possess their own spectroscopic properties that interfere with the working wavelengths of this assay and hence provided false positive results.

Eventually, potential hits were chosen rather more empirically by assessing which compounds gave a larger and more considerable decrease in polarisation; more akin to approximately 12 standard deviations from the mean of the negative control rather than 3. The Diversity Set II screen contained 1872 compounds and this scrutiny helped simplify the process of finding compounds to follow up and take forward for further investigation. Unfortunately, this means that true hits may have been by-passed.

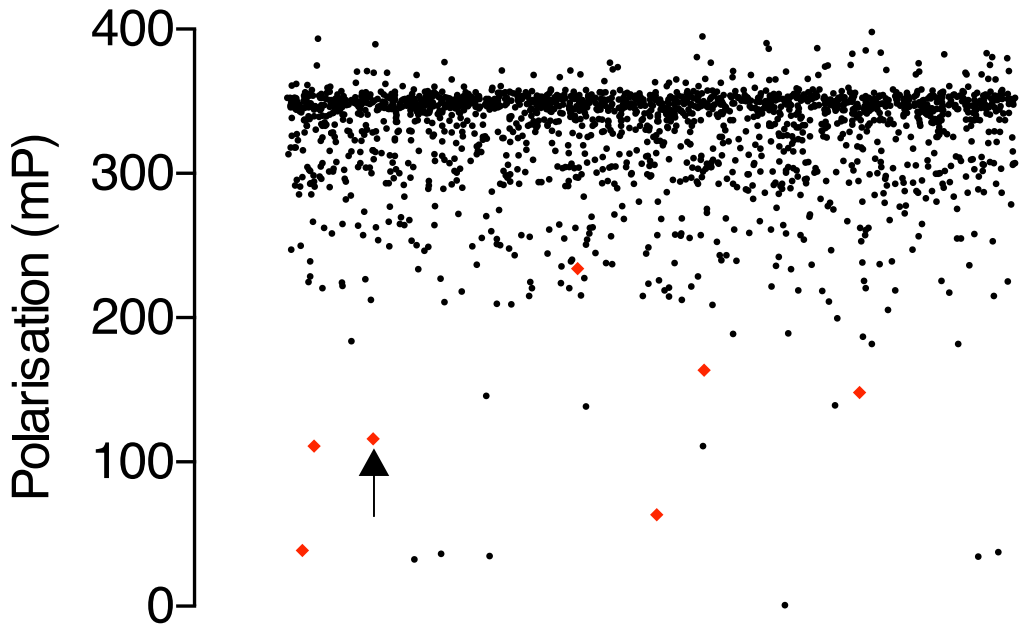

Figure 5.1 – Results of the Diversity Set II screen for AtIPK1, polarisation results for each compound are randomised for visual purposes and raw polarisation values plotted against the y-axis. Points shown in red indicate 'hits' that were chosen for further investigation. The arrow indicates a hit that appeared in results for both AtIPK1 and SHIP2cd.

Across both AtIPK1 and SHIP2cd, nine potential inhibitors from the DivII screen were obtained (Figure 5.1). Four of these were hits for both proteins, an additional four for AtIPK1 only and just one for SHIP2cd only.

The arrow in figure 5.1 indicates a compound that was a hit for both proteins, with an observed decrease in polarisation of 227.43 mP from the mean negative control for AtIPK1.

The AODV screen only contained two plates amounting to 114 compounds and were analysed in the same way as the Diversity Set II screen for AtIPK1, SHIP2cd and SHIP1cd (Figure 5.2). For these 'displacement' assays, the instrument 'target' gain, a parameter set at the polarisation value of maximally bound probe, was set lower than for Diversity Set II since discovering that some compounds/inhibitors caused an increase in polarisation of the probe (chapter 4). The lower value of polarisation of maximally bound probe was achieved with a lower concentration of protein. Increases in polarisation imply an increased affinity between the protein and probe (2-FAM-IP_5), while decreases imply displacement of 2-FAM-IP_5.The arrow in figure 5.2 indicates a compound that appeared to displace the probe from all three proteins tested. Polarisation dropped by 33.5, 19.7 & 24.9 mP for AtIPK1, SHIP2cd & SHIP1cd respectively, approximately 6 to 8 standard deviations from the mean of the maximally bound control. One other compound emerged as a hit for all three proteins. Further to this, AtIPK1 and SHIP2cd also have two additional hits in common from this compound library.

As demonstrated in chapter 4, a reported SHIP1cd inhibitor (3-α-amino-cholestane, 3AC) increased affinity of SHIP1cd for 2-FAM-IP_5. The mechanism of action of 3AC is unknown, but is intriguing, particularly when considering that the binding partner studied here is the catalytic domain not the full-length protein. Consideration of potential mechanisms prompted re-inspection of the screen shown in Fig. 5.2. Some hits that produced increases in polarisation with SHIP1cd were subsequently selected for further scrutiny (Figure 5.2 - C). Overall, screening against SHIP1cd gave 6 additional hits that caused an increase in polarisation that did not emerge with the other two proteins.

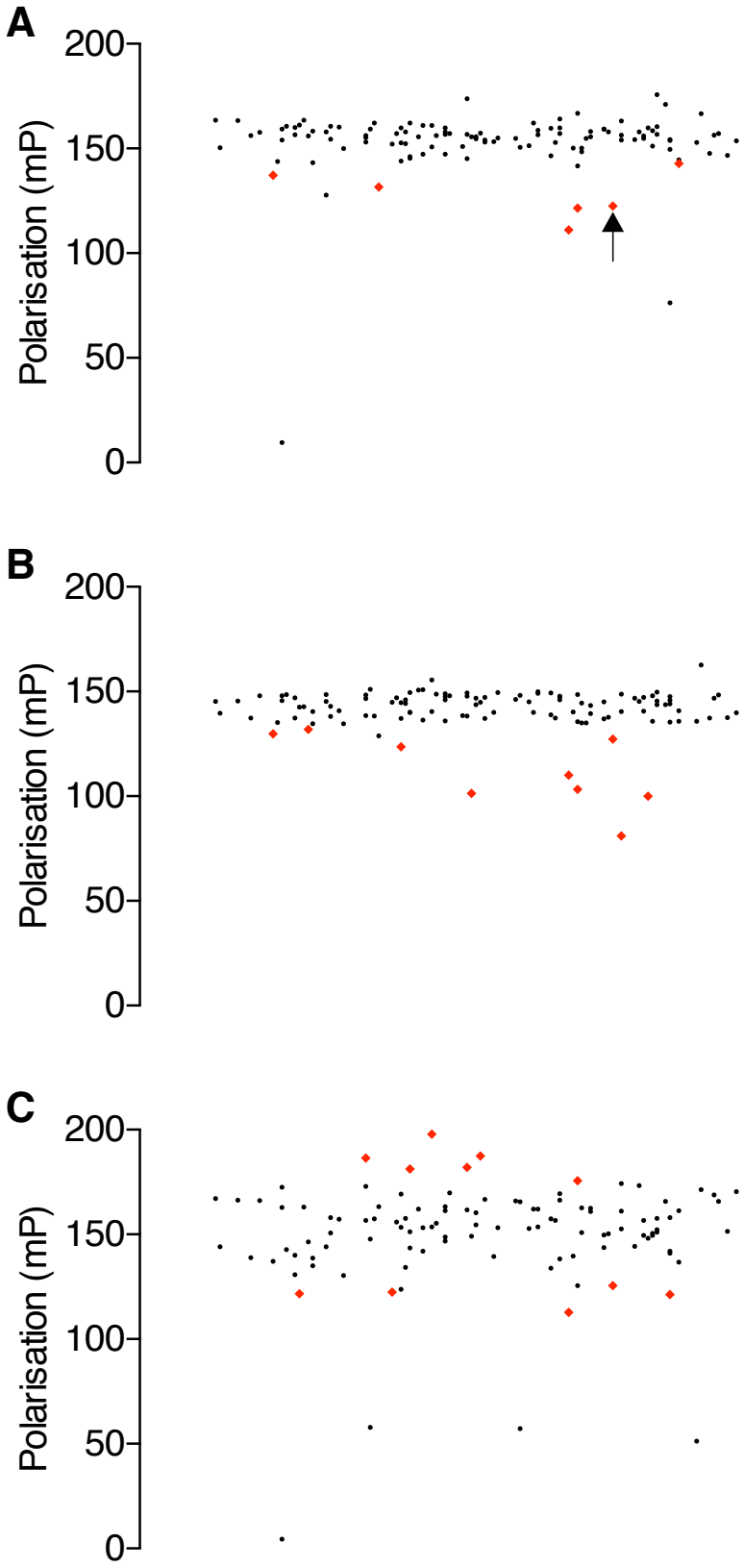

Figure 5.2 – Results of the Approved Oncology Drugs Set V screen for (A) AtIPK1, (B) SHIP2cd & (C) SHIP1cd. Polarisation results for each compound are randomised for visual purposes and raw polarisation values plotted against the y-axis. Points shown in red indicate 'hits' that were chosen for further investigation. The arrow indicates a hit that appeared in results for all proteins.

As stated previously in chapter 4, it is inherent in the interpretation of experiments performed in this chapter that 2-FAM-IP_5 is an active site ligand of the proteins tested. For AtIPK1, chapter 3 provides categorical structural data showing the biphenyl phosphates ligands co-ordinate inositol phosphate-coordinating residues in the active site of AtIPK1. The displacement data presented in chapter 4 also provides compelling evidence that benzene and biphenyl phosphates are active site ligands of SHIP2 and SHIP1, which was first described when biphenyl 2,3',4,5',6 - pentakisphosphate was resolved in the structure of SHIP2 (Mills et al., 2012) That benzene phosphates and biphenyl phosphates displace 2-FAM-IP_5 from AtIPK1, SHIP2cd and SHIP1cd is therefore itself convincing enough evidence that 2-FAM-IP_5 is an active site probe of both classes of protein. Additionally, *bona fide* substrates were able to displace 2-FAM-IP5 (Figure 4.12), inositol phosphates have not be shown to bind to these types of proteins elsewhere other than the active site.

5.3.2 Dose-response curves of the binding of screen hits – Diversity set II

The DIVII screen and the dose-response curves presented in this section pre-date the purification of SHIP1cd, therefore only results for AtIPK1 and SHIP2cd are available thus far. Additionally, all hit compounds were tested on both proteins regardless of providing a positive result with only one of the proteins to validate that the screening method is effective.

The experiments described below are an extension of the unbiased screen shown above (Figure 5.1). They were designed to provide proof of concept that 2-FAM-IP_5 is a useful probe for identifying potential therapeutic agents targeting inositol phosphate kinases and inositol polyphosphate 5-phosphatases.

All compounds identified as 'hits' and taken further for determination of dose-responses were re-inspected for optical properties, UV absorbance and fluorescence, that might give rise to their false identification as 'hits'. UV spectra were run in a 96-well quartz glass plate on a Hidex Sense plate reader at 100 µM concentration, while fluorescence emission spectra were run in 384-well plates on a BMG ClarioStar plate reader with excitation band width 16nm centered on 485nm and emission centered on 515nm (same band width). These wavelengths represent the excitation and emission wavelengths used for the polarisation measurements described here and in chapter 4. The compounds tested in the following all showed absorbances at 485nm that were not considered significant (results not shown).

For determination of dose-responses, probe (2-FAM-IP_5) at 2 nM concentration was incubated with protein at 200 nM and 'hit' compounds were titrated, according to compound, up to concentrations generating a 4-parameter fit sigmoidal curve approaching 'complete' displacement. The highest concentration tested for each compound was 25 µM.

Alternatively, for some compounds the plotted curves were limited to concentration of titrating ligand at which the raw vertical and horizontal polarised emissions of probe were not 'greatly' altered by ligand. Some of the curves do not therefore reach a minimum asymptote.

Where the data allowed, IC50 values were determined. IC50s obtained from such experiments are not intrinsic inhibition constants; that is they reflect the local conditions of the experiment and depend on the concentration of displaced probe and concentration of protein. Nevertheless, in experiments in which different displacing ligands are titrated against a common probe and common protein concentration, the IC50 values obtained do reflect in a meaningful way the affinities of the different titrated ligands for target protein. Such IC50 experiments, polarisation-based or otherwise, are the basis of many pharmaceutical screens commonly performed at the initial stage of screening programs at a single concentration of ligand against fixed probe and protein concentration with millions of individual compounds from chemical libraries far more complex than that tested here. Comparisons of common ligand titrated against different proteins offer meaningful comparisons between the proteins if the probe and protein concentrations are equivalent to all titrations.

Figure 5.3 compares the displacement of 2-FAM-IP_5 from AtIPK1 and SHIP2cd by purpurogallin, an aglycone of various glycosides obtained from oak bark which has been affiliated with antioxidant properties in cardiocytes (Wu et al, 1996). Its structure is related to catechol, 1,2-dihydroxybenzene, and it has been shown to inhibit chatechol-O-methyltransferase (Lambert et al., 2005) as well as innate immunity pathways consequent on activation of the Toll-like receptor 2, in which downstream signaling from TNF-α and IL-1β is repressed (Cheng et al., 2012).

Titration of purpurogallin against IPK1 and SHIP2cd revealed IC50s respectively of 5.5±1.1 and 1.6±1.2 μM, with a smaller Hill Slope for SHIP2cd (Figure 5.3). The range of the assay was 300 mP and 250 mP respectively, the difference in these upper plateaus is likely determined by the differing proteins and their relative starting affinities for 2-FAM-IP_5. They both reach the pre-determined, 'target gain' set at 35 mP, a value representing the intrinsic polarisation of un-bound, free, 2-FAM-$InsP_5$ probe in solution.

Interestingly, purpurogallin has been identified as a ligand occupying the nucleotide binding site of cyclin-dependent kinase 2 (cdk2) by a screening assay, backed-up by structural data (Martin et al., 2012). CDK's are serine/threonine kinases and their deregulation has been implicated in a range of diseases including; cancer, neurodegenerative and inflammatory diseases (Zhang et al., 2009, Bain et al., 2007). A second structure is also available in complex with human thymidylate synthase (Lesa et al., 2012 – to be published). As IPK1 is a reversible nucleotide to inositol phosphate phosphotransferase (Phillippy et al., 1994, González et al., 2010), the identification of purpurogallin as a ligand is perhaps explained by the dual substrate nature of this enzyme. Its identification as a ligand of SHIP2cd is not so readily explained. However, recent preliminary attempts by colleagues in obtaining the crystal structure of AtIPK1 in complex with purpurogallin suggest that it is not occupying the nucleotide binding site.

Inspection of the structure of purpurogallin (Figure 5.3), taken with its molecular mass of 220.2 and logP of 1.06 reveals that purpurogallin meets Lipinski's rule. (see section 5.1.4).

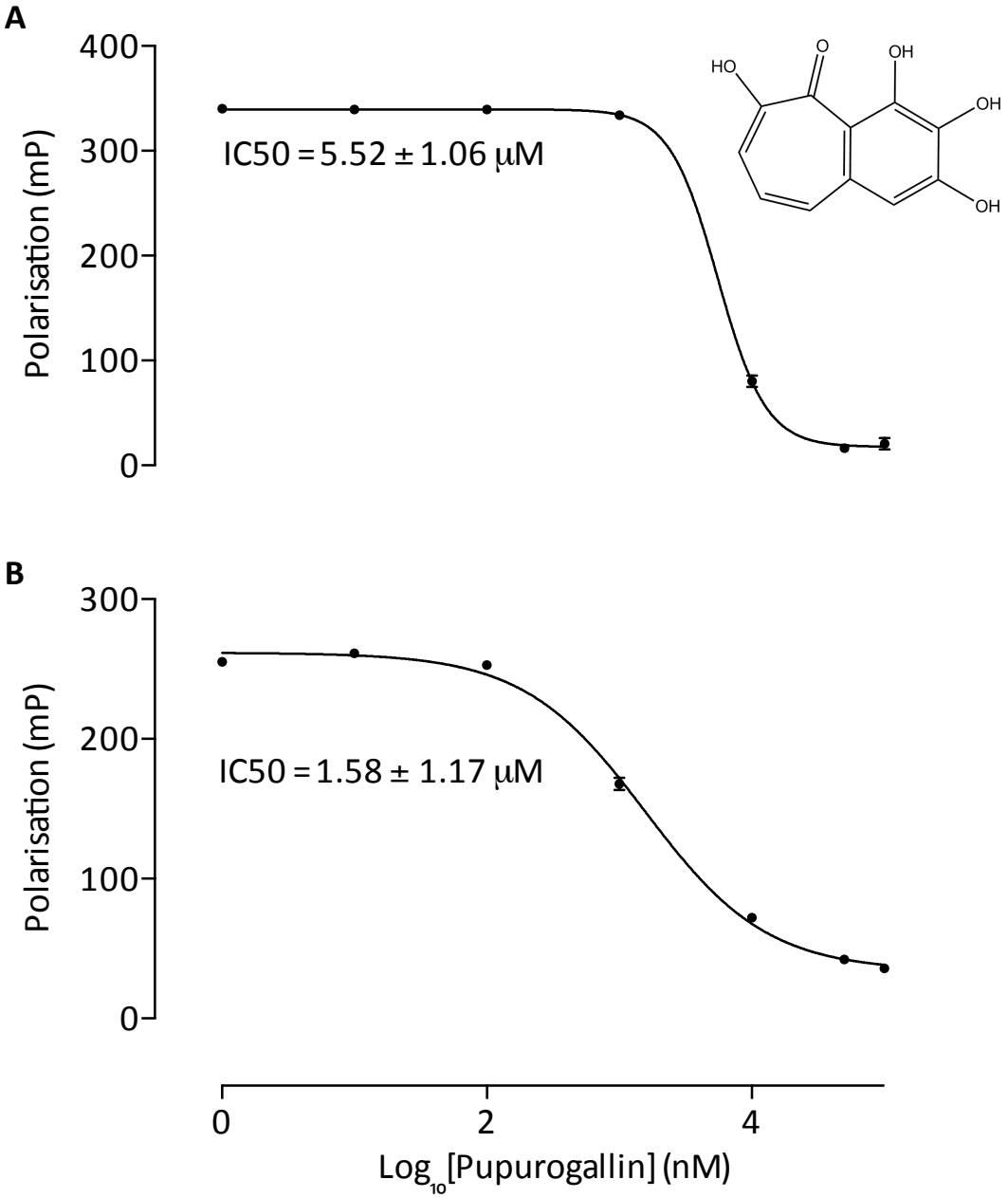

Figure 5.3 – Purpurogallin as a 2-FAM-IP_5 displacing ligand (A) AtIPK1, (B) SHIP2cd. Errors bars (SE) are shown or are smaller than the symbol used.

Figure 5.4 compares the displacement of 2-FAM-IP_5 from AtIPK1 and SHIP2cd by 5,6,7,8,4'-pentahydroxyflavone, also known as nortangeretin. The same compound was identified in a screen of the same library for compounds that bind to the catalytic subunit of casein kinase 2 (Rasmussen et al., 2015) .

Here, titration of 5,6,7,8,4'-pentahydroxyflavone against AtIPK1 and SHIP2cd revealed IC50s respectively of 7.4±1.0 and 1.8±1.1 µM. Similar to purpurogallin, the range of the assay was approximately 300 mP and 250 mP respectively, and both dose-response curves reach the pre-determined lower limit of 35 mP which represents polarisation of the free probe in solution.

With a mass of 302 Da, LogP of 1.64, and seven H-bond acceptors and five donors, 5,6,7,8,4'-pentahydroxyflavone meets the criteria of Lipinski's rule of five.

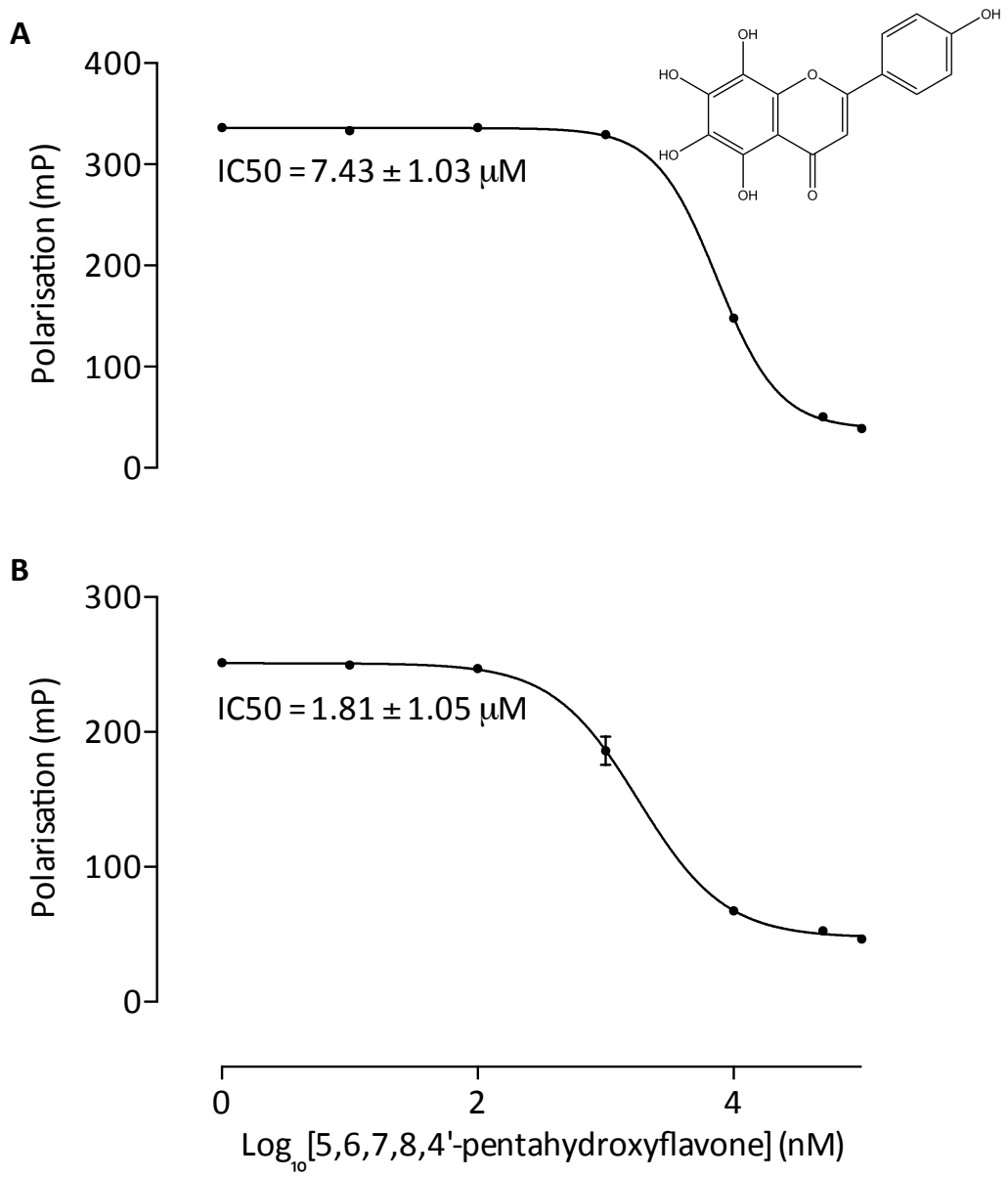

Figure 5.4 –5,6,7,8,4'-pentahydroxyflavone as a 2-FAM-IP_5 displacing ligand (A) AtIPK1, (B) SHIP2cd. Errors bars (SE) are shown or are smaller than the symbol used.

Figure 5.5 compares the displacement of 2-FAM-IP_5 from AtIPK1 and SHIP2cd by Galloflavin, which is commercially sold as a lactate dehydrogenase (LDH) inhibitor that can uniquely exert its effect on both isoforms of the enzyme (Manerba et al., 2012). Galloflavin has recently been shown to reduce lactate levels in adenocarcinoma cells which subsequently decreases their migration ability. This was the result of inhibiting isoform A of LDH which can cause enhanced levels of lactate in tumour tissues when upregulated by pro-inflammatory cytokines (Manerba et al., 2016).

Titration of galloflavin against AtIPK1 and SHIP2cd revealed IC50s respectively of 1.5 and 1.6±1.2 µM. Like the previous dose-response curves, the range of the assay was approximately 300 mP and 250 mP respectively, and both curves approach the pre-determined lower limit of 35 mP for free probe. The curve fitting software could only give an approximation of the IC50 for 2-FAM-IP_5 displacement by galloflavin in SHIP2cd as it claims ambiguity in the data, likely due to the lack of data points on the Hill slope. Nevertheless, a decrease in polarisation down to 35 mP is clearly observed.

With a mass of 278 Da, LogP of 0.88, and eight H-bond acceptors and four donors, galloflavin meets the criteria of Lipinski's rule of five.

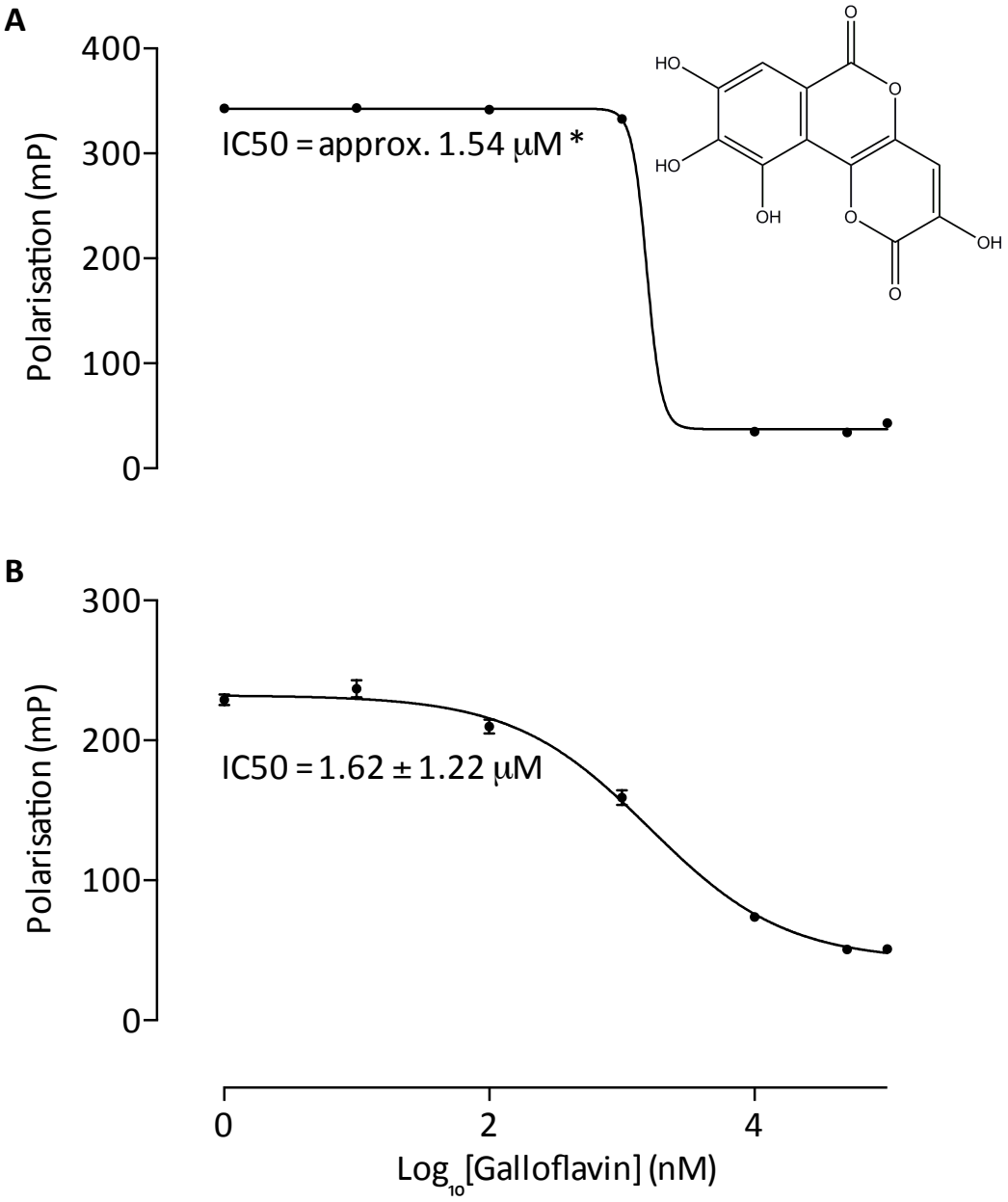

Figure 5.5 –Galloflavin as a 2-FAM-IP_5 displacing ligand (A) AtIPK1, (B) SHIP2cd. Errors bars (SE) are shown or are smaller than the symbol used.

It is clear from the foregoing examples (Figures 5.3 – 5.5) that with such small standard deviations as achieved, this assay with 2-FAM-InsP_5 is robust and shows great potential for discriminating between small structural changes in the displacing ligand. Such chemical modifications are commonly explored when 'hits' are subjected to lead optimisation and subsequent selection of a candidate molecules for clinical development (Hughes et al., 2011).

Even without detailed modeling of the interaction of these 'hits' with the protein subjects, it is clear that there are striking similarities in the structure of the compounds above that may rationalise their ability to yield these effective dose-response curves with AtIPK1 and SHIP2cd. They all share a bicyclic structure, consisting of benzene rings, bar purpurogallin which bears a benzene and cycloheptane. A third ring, a phenol ring moiety, is present in 5,6,7,8,4'-pentahydroxyflavone. All possess at least three adjacent hydroxyl groups on a single benzene ring, and exhibit a carbonyl group on a second distinct ring. Without structures of AtIPK1 or SHIP2cd in complex with these compounds, it is difficult to reason exactly how purpurogallin, 5,6,7,8,4'-pentahydroxyflavone, or galloflavin would coordinate within the active site of these proteins, other than, as mentioned above, it has been shown that purpurogallin is a nucleotide-binding site ligand of cdk2 (Martin et al., 2012).

As introduced previously, SHIP2cd has several commercially available inhibitors including AS1938909 and AS1949490 (Suwa et al., 2009, Suwa et al., 2010). Though in themselves similar, there are no immediately apparent similarities between these inhibitors and the compounds tested here, nor is there currently any mechanistic insight in to how they exert their inhibitory action on SHIP2, therefore at this point no meaningful comparison can be made between them. Nevertheless these papers and that of Ichihara and coworkers (Ichihara et al., 2013) who modified a 4-substituted 2-pyridin-2-ylamide scaffold derived rationally from a comparison of the structures of AS1949490 and NGD-61338, a SHIP2 inhibitor from NeoGenesis Pharmaceuticals Inc (Annis et al., 2009) indicate the kind of medicinal chemistry approach that can be undertaken to improve the affinity of ligand for target protein and to improve

bioavailability of lead compounds. In the case of Ichihara et al. (2013), the primary scaffold incorporated benzyl and (4-chlorobenzyl)oxy groups from AS1949490 and a pyridine-2-amine group from NGD-61338 (Figure 5.6).

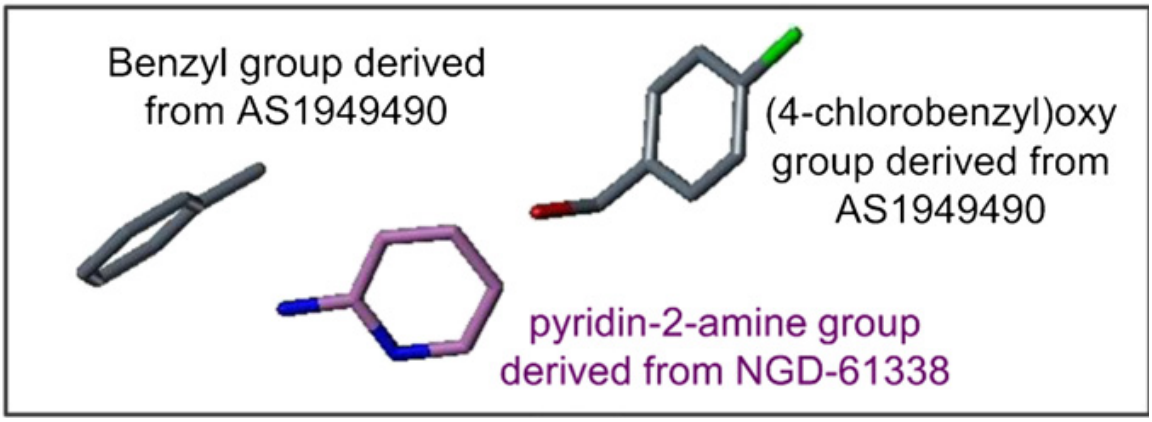

Figure 5.6 – Taken from Ichihara et al., 2013. Example of the incorporation of groups to increase bioavailability and improved affinity for the target protein.

Among the various compounds tested, dose-responsive displacement of 2-FAM-IP_5 from AtIPK1, but not SHIP2cd, was observed with two additional hits from the Diversity Set II screen (results not shown). The first of these identified compounds was cynarin (Figure 5.7 - A), a hydroxycinnamic acid derivative found in artichokes formed from quinic acid and caffeic acid, with postulated antioxidant abilities (Topal et al., 2016). Secondly, chaetochromin (Figure 5.7 - B), a natural product and metabolite of *Chaetomlum gracllе* that has also been found in marine sources (Blunt et al., 2015).

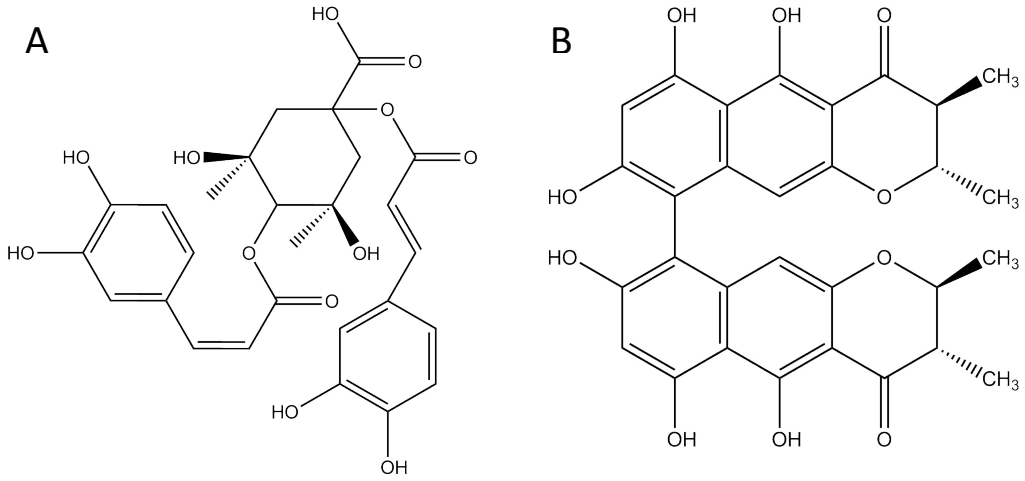

Figure 5.7 – structures of; (A) Cynarin, (B) Chaetochromin

As for the AtIPK1 / SHIP2cd ligands (potential inhibitors) discussed above, both possess alcohol and carbonyl moieties. However, they are much larger and more elaborate. As demonstrated in chapter 3, AtIPK1 accommodates large conformational changes made possible by a global shift of the N-lobe, which may offer explanation to why cynarin and chaetochromin are able to bind within the active site of AtIPK1 and not SHIP2cd. By way of contrast, the inositide binding site is not located between two moveable lobes in SHIP2cd and is consequently a smaller and more restricted binding pocket which appears on the surface of the protein with just small flexible loop that closes over the active site. Other structural features of the two enzymes may account for discrimination of cynarin and chaetochromin ligands, but without further investigation the explanation offered here is speculative at best.

5.3.3 Further investigation of screen hits with AtIPK1, SHIP2cd & SHIP1cd – Approved Oncology Drugs Set V

Of the compounds tested for effects on 2-FAM-IP_5 binding are a number of compounds that have passed all regulatory processes of the Federal Drug Administration (FDA) and some of the EU European Medical Agency. These belong to the National Cancer Institute's Approved Oncology Drugs Set V (AODV).

As for the DivII screen, the experiments described below are an extension of the unbiased screen shown above (Figure 5.2). They were designed to provide proof of concept that 2-FAM-IP_5 is a useful probe for identifying potential therapeutic agents targeting inositol phosphate kinases and inositol polyphosphate 5-phosphatases.

As previously, all compounds identified as 'hits' and taken further for determination of dose-responses were re-inspected for optical properties, UV absorbance and fluorescence, that might give rise to their false identification as 'hits' (results not shown).

For determination of dose-responses, probe (2-FAM-IP_5) at 2 nM concentration was incubated with protein at 200 nM and 'hit' compounds were titrated, according to compound, up to concentrations yielding on 4-parameter fitting sigmoidal curves approaching 'complete' displacement. The highest concentration tested for each compound was 25 µM.

The compound estramustine sodium phosphate was a hit from AODV that was common to AtIPK1, SHIP2cd and SHIP1cd. Dose-dependent response curves up to 100 μM were constructed for each in which the decrease in polarsiation indicates that 2-FAM-IP_5 is being displaced from all three proteins (Figure 5.8). For all three proteins the curves are not complete and did not reach the lower plateau for the free un-bound probe, and in this case accurate IC50s could not be calculated by the graph fitting software. Nevertheless, a clear observation can still be made and the polarisation unarguably decreases. The range of the assay varies between each protein. Most notably for SHIP1cd (Figure 5.8- C), but this is a result of the polarisation gain for the free probe being adjusted to account for any increases in polarisation as observed by SHIP1cd previously (Figure 4.15). The theoretical maximum for polarisation is 400 mP and without adjustment, any increase in polarisation would likely go unresolved. For AtIPK1 and SHIP2cd, (Figure 5.8 - A & B) the assay was identical but the starting polarisation still differs, likely due to the differing nature of the proteins and their relative starting affinities for 2-FAM-IP_5.

All compounds in the AODV screen are approved as oncology drugs, of which estramustine sodium phosphate is a chemotherapeutic agent that has been used in the treatment of prostate cancer across the world. It is a derivative of estradiol with a nitrogen mustard-carbamate ester moiety attached and goes by the brand name Emcyt (Simpson and Wagstaff, 2003, Perry and McTavish, 1995, Fizazi et al., 2007).

An immediate observation when considering a rationale for the binding of estramustine phosphate to these enzymes is the phosphorus containing head group at one end of the molecule. Similarly to the compounds previously discussed it mainly consists of an interconnected multiple ring structure.

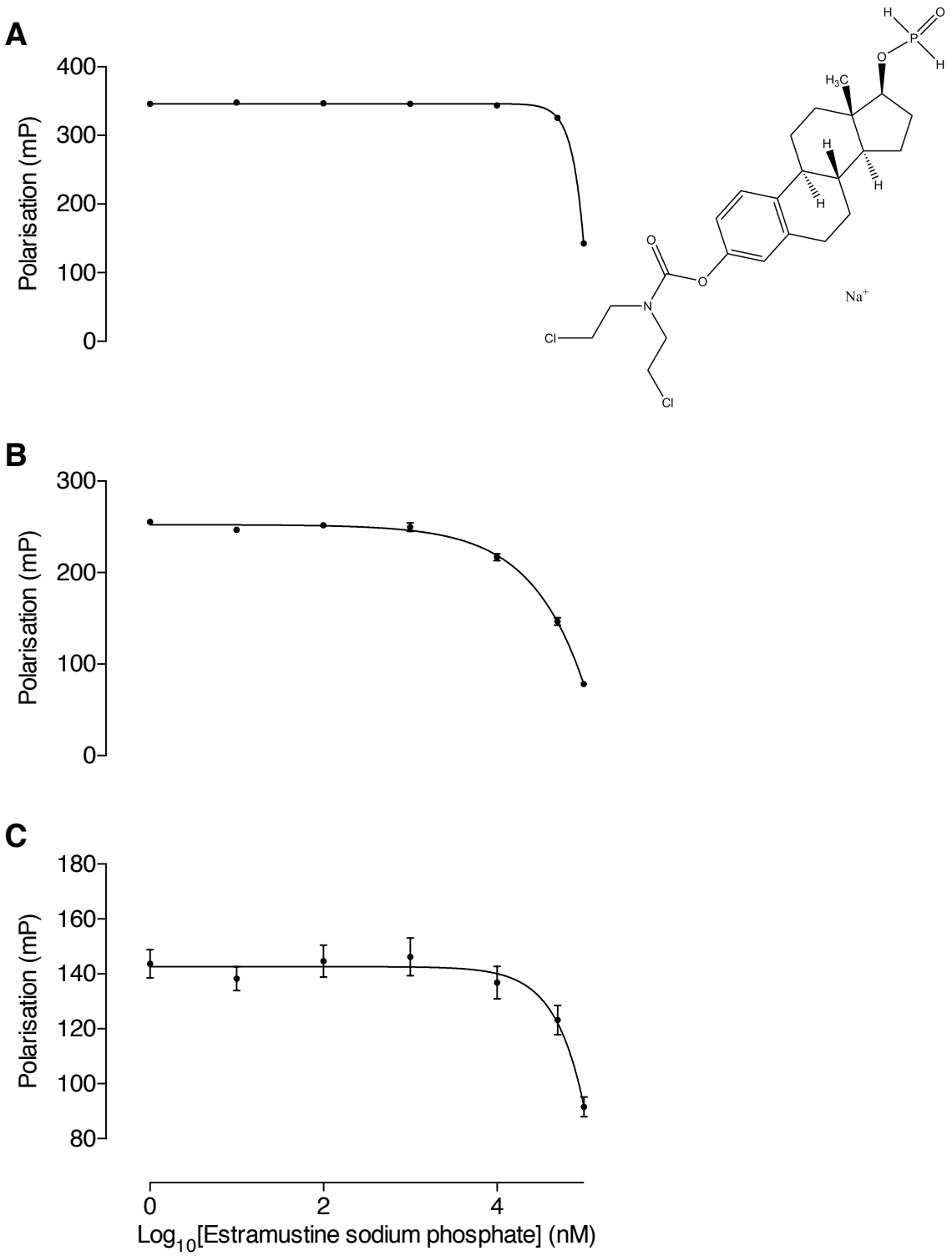

Figure 5.8 –Estramustine sodium phosphate as a 2-FAM-IP_5 displacing ligand (A) AtIPK1, (B) SHIP2cd, (C) SHIP1cd. Errors bars (SE) are shown or are smaller than the symbol used.

From the initial screening process valrubicin emerged as a positive hit for all three proteins tested. However, upon titration against the 2-FAM-IP_5 bound proteins no decrease in polarisation was observed for SHIP1cd, only with AtIPK1 and SHIP2cd (Figure 5.9). As with estramustine phosphate, the curves are not complete and did not reach the lower plateau for the free un-bound probe, and accurate IC50s could not be calculated by the graph fitting software. Nevertheless, a clear observation can still be made and the polarisation unarguably decreases. For SHIP2cd, the polarisation has decreased further indicating that at the highest concentration of valrubicin tested 2-FAM-IP_5 is more readily displaced from SHIP2cd than AtIPK1. The starting polarisation value differs, which is likely due to the differing nature of the proteins and their relative starting affinities for 2-FAM-IP_5, and this appears to have been consistent through-out the construction of all comparable dose-response curves of AtIPK1 and SHIP2cd.

Valrubicin is a derivative of anthracycline doxorubicin and is a cytotoxic chemotherapy drug to treat bladder cancer (Onrust and Lamb, 1999). Again, in common with the previous compounds, valrubicin mainly consists of an interconnected multiple benzene ring structure with hydroxyl and carbonyl moieties.

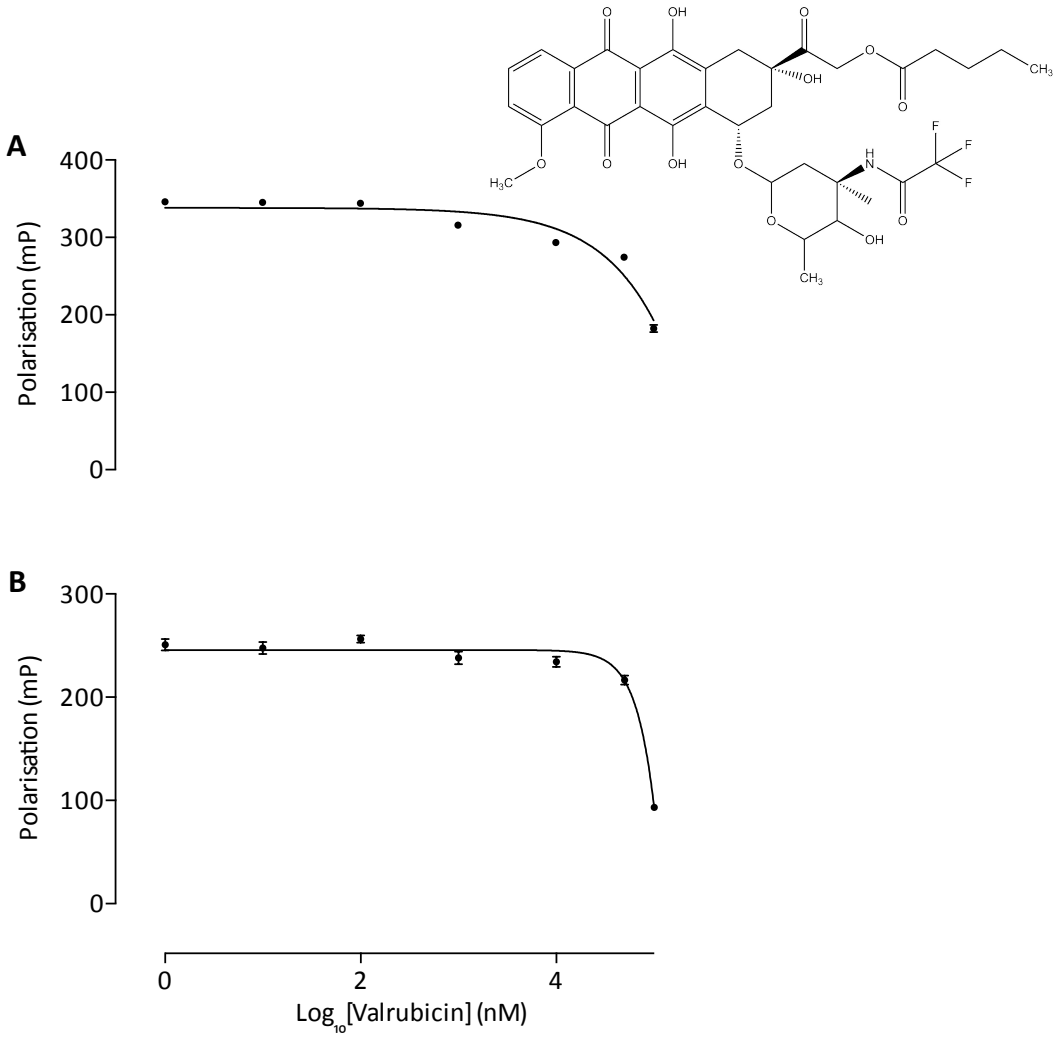

Figure 5.9 –Valrubicin as a 2-FAM-IP_5 displacing ligand (A) AtIPK1, (B) SHIP2cd. Errors bars (SE) are shown or are smaller than the symbol used.

Pomalidomide from the AODV screen was revealed as a positive hit for AtIPK1 only, a titration of which against 2-FAM-IP_5 bound AtIPK1 can be seen in Figure 5.10. Unlike with other dose-response curves presented in this section, it is more complete and is approaching the lower limit of 35 mP for the free un-bound probe. An IC50 of 97.4 ± 1.3 µM was calculated even though the lower plateau was not fully reached.

Thalidomide, the parent compound of pomalidomide, was originally discovered to inhibit angiogenesis and then followed up in clinical trials for cancer which resulted in its approval by the FDA for use multiple myeloma (D'Amato et al., 1994). Pomalidomide is amino substituted and has improved anti-tumor activity (D'Amato et al., 2001).

Again, it has an interconnected ring structure, consisting of a benzene and a cyclopentane ring with carbonyl groups. However, it is considerably smaller than the other compounds that appeared as hits from this screen.

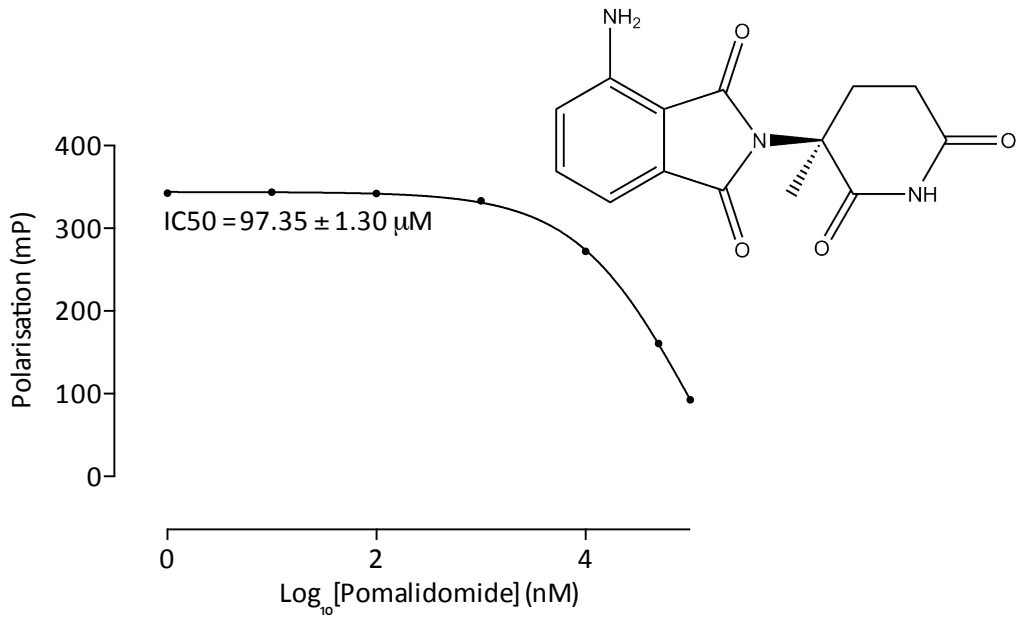

Figure 5.10 –Pomalidomide displacing 2-FAM-IP_5 from AtIPK1.

There were two drugs from this screen that displayed striking effects when titrated against SHIP1cd (Figure 5.11) but not IPK1 or SHIP2 (data not shown).

Bosutinib, originally synthesised by Wyeth and developed by Pfizer is a tyrosine kinase inhibitor (Vultur et al., 2008) that has found use in treatment of chronic myeloid leukemia (Cortes et al., 2011). Crizotinib (Forde and Rudin, 2012) is an aminopyridine that is a competitive inhibitor, within the ATP-binding pocket, of the c-Met/Hepatocyte growth factor receptor (HGFR) tyrosine kinase. Both these compounds when tested in a 2-FAM-IP_5 displacement assay elicited increases in the affinity of 2-FAM-IP_5 binding, just like 3AC (Figure 4.15), albeit with an approximate IC50, as the curves did not reach an upper asymptote, that is 10-fold higher than that of 3AC. While the 5-phosphatase family, or certainly the catalytic domain of this family, lack obvious nucleotide binding sites, the similarity of effect of two FDA approved drugs when compared to a known allosteric regulator of SHIP1, shown here to act on the catalytic domain of the enzyme, is a notable result and one which highlights potential therapeutic opportunity or at least the identification of alternative targets for known and approved drugs.

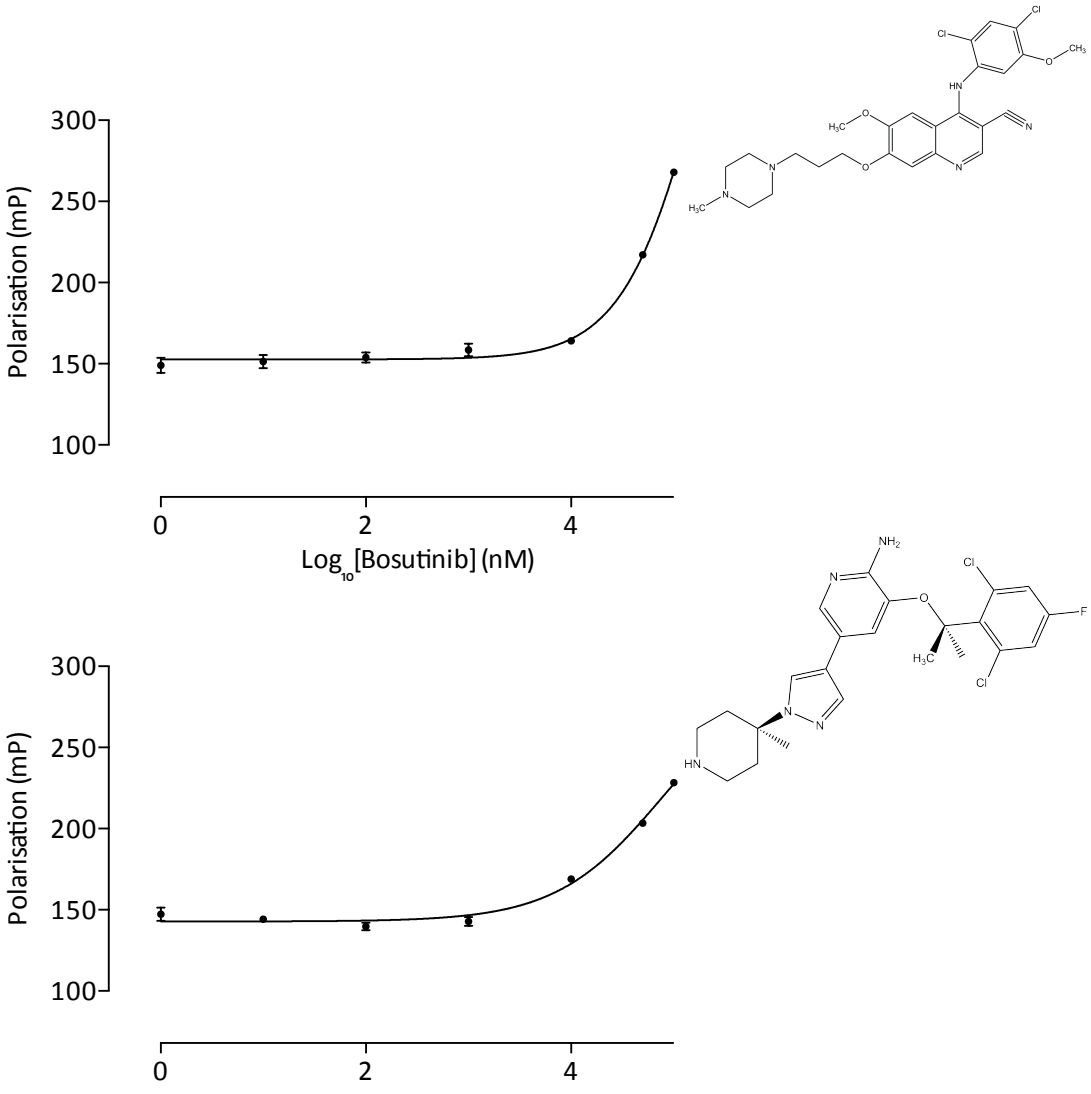

Figure 5.11 – SHIP1cd exhibiting increased affinity for 2-FAM-IP_5 upon titration with two AODV screen compounds; (A) Bosutinib & (B) Crizotinib.

5.3.4 Utilising the intrinsic tryptophan fluorescence of AtIPK1 to investigate binding of potential inhibitors, validation of polarisation screens

As reported in chapter 3, AtIPK1 undergoes large conformational changes upon ligand binding, most notably in the N-lobe of the protein. The use of the intrinsic tryptophan fluorescence of AtIPK1 to monitor protein folding consequent on ligand binding or other treatments has previously been reported (Banos-Sanz et al., 2012). AtIPK1 has four tryptophan residues; W13, W69, W129 and W381. As a ligand binds, the environment of the local residues can change and this in turn can affect the fluorescence properties of the aromatic amino acids. Conformational changes can affect these residues discretely, or quenching of fluorescence can occur as an influence of other residues.

Previous to this study, probing of the structure of AtIPK1 and the accessibility of its tryptophan residues was achieved by fluorescence quenching using potassium iodide, and concluded that the quenching mechanism was collisional (temperature dependent) (Baños-Sanz et al., 2012). Additionally, two tryptophan residues are found partially in a hydrophobic pocket (W13 & W69) and the other two are fully solvent exposed (W129 & W381), where W129 is in the active site. This work was followed by titration of inositol phosphates and a nucleotide substrate analogue (AMP-PNP) to assess the changes in tryptophan fluorescence in the binary and ternary complexes of AtIPK1 and a W129A mutant (data not shown). Changes in intrinsic fluorescence upon ligand binding were attributed to changes in the local environment of W13 & W69, and not W129 or fully solvent exposed W381.

Figure 5.12 demonstrates the average fractional loss in intrinsic tryptophan fluorescence when increasing concentrations of IP_5 are titrated against a fixed concentration of AtIPK1. In this instance, a one site-binding model was fitted to the data and the dissociation constant (K_d) calculated 2.8±0.8 μM. In the previous work mentioned above, the K_d for IP_5 binding was calculated as 0.35±0.12 μM. Gosein and Miller obtained a value for In(1,3,4,5,6)P5 binding of 0.6 μM by isothermal calorimetry (Gosein and Miller, 2013). Although not far removed from these values, the method used by the authors was different; it used a fluorimeter fitted with a 1 mL quartz cuvette rather than a 384-well black plate in a BMG ClarioStar plate reader as used in the results presented here.

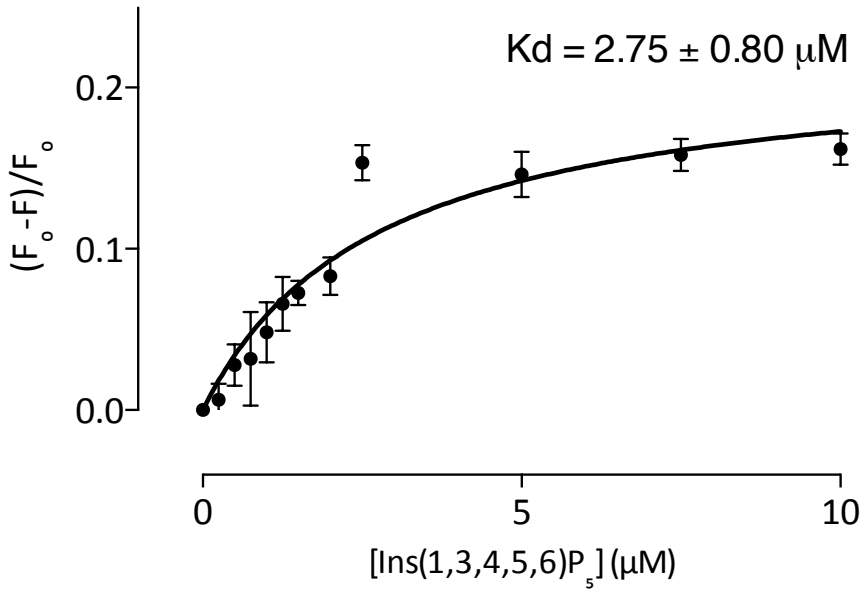

Figure 5.12 – Fractional change in fluorescence intensity of AtIPK1 upon binding inositol 1,3,4,5,6 pentakisphosphate (IP_5). Error bars show the standard errors in that data.

The same fluorescence titration method was performed on AtIPK1 with the compounds that manifested as hits from DivII (section 5.3.1) and that were successful in subsequent dose-dependent response curves (section 5.3.2), as supporting evidence of the efficacy of this high through put screening method in the search for true inhibitors of proteins that act upon inositol phosphates. The excitation wavelength was limited to 295 nm to avoid excitation of tyrosine and phenylalanine.

The average fractional change in the decrease in fluorescence intensity was plotted and one site binding model curves fitted which generated dissociation constants for each compound. Figure 5.13 Shows the resulting curves and K_d for the three compounds from DivII that appeared as hits for both AtIPK1 and SHIP2cd. Unfortunately this method does not work with SHIP2cd, due to a surplus of tryptophan residues and their associated solvent exposures.

The curves revealed that AtIPK1 has the highest affinity for 5,6,7,8,4'-pentahydroxyflavone out of the three compounds with a K_d of 4.8±1.5 µM. At 50 µM, the upper limit of this assay, the fluorescence intensity had decreased by 50 % (Figure 5.13). The K_d for the binding of purpurogallin and galloflavin are not dissimilar, 8.0±1.7 µM and 7.7±1.9 µM respectively. At the highest concentration of compound, purpurogallin appeared to almost completely diminish the intrinsic fluorescence intensity of AtIPK1, whereas galloflavin reduced fluorescence by approximately 60 % at 50 µM.

As a rule of thumb, various authors suggest limiting the absorbance of extrinsic fluorophore probes to values < 0.05 to minimise inner filter effects, or the use of short path length cuvettes to reduce the effect. Clearly, the low (single figure µM) concentration of AtIPK1 protein and the low extinction coefficient of aromatic amino acids are unlikely contributors to inner filter effects in these experiments, but the extinction coefficient of purpurogallin ε420nm is 2640 $M^{-1}.cm^{-1}$ in 50 mM pH 7.0 phosphate buffer (Wang et al., 2007), with an extinction coefficient approximately

double this value at 290 nm. The possibility remains that, at least for purpurogallin, some of the effect on tryptophan fluorescence is an absorbance effect.

This said, the considerably reduced absorbances of these compounds at wavelengths > 420 nm makes clear that the effects of these compounds observed in 2-FAM-$InsP_5$ polarisation experiments are minimal, particularly when the extremely short pathlength of the 384 well plate and 485 nm/515 nm excitation and emission wavelengths are considered.

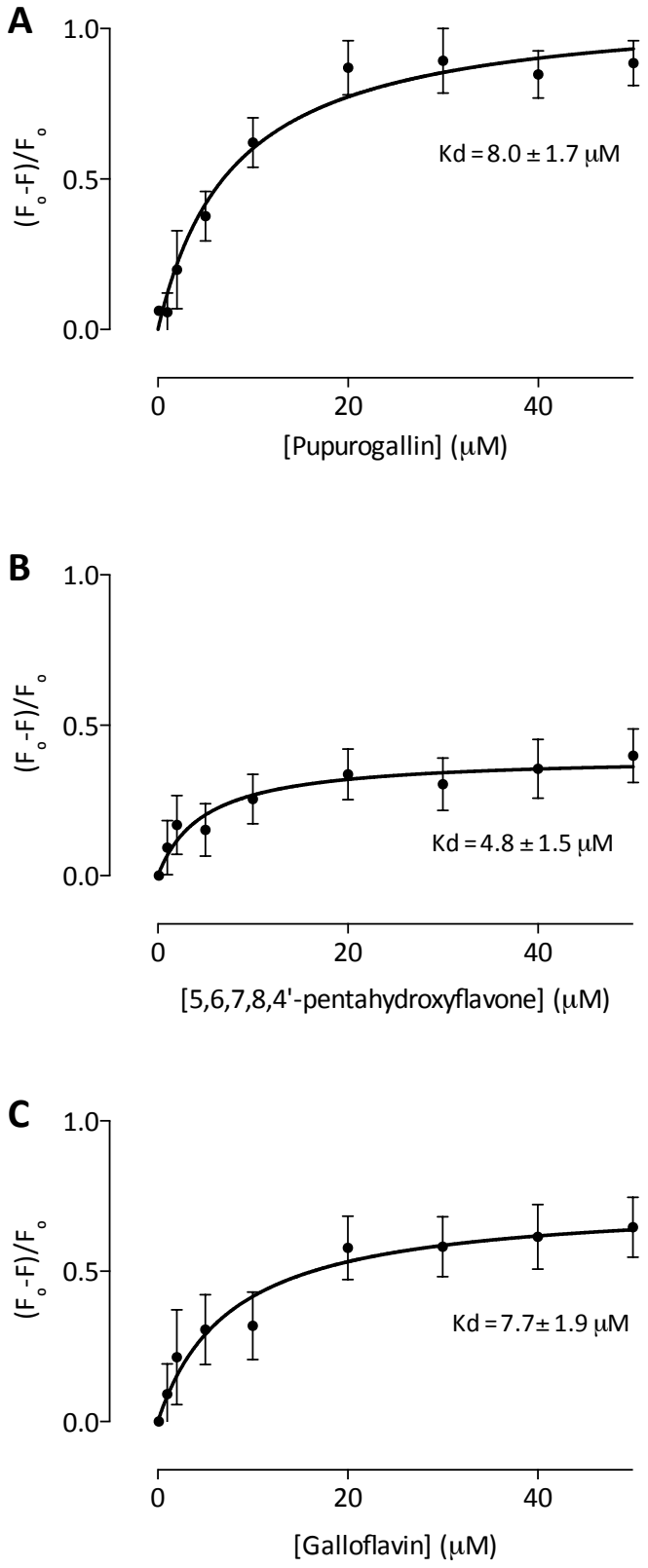

Figure 5.13 – Fractional change in the intrinsic fluorescence intensity of AtIPK1 upon binding compounds were positive hits as potential inhibitors from the diversity set II library. (A-C); Purpurogallin, 5,6,7,8,4'-pentahydroxyflavone & galloflavin. Error bars show the standard errors in that data.

As previously described in section 5.3.2, cynarin and chaetochromin were also from the DivII screen but only emerged as hits for AtIPK1. The same fluorescence titration and one site binding model analysis was carried out with these compounds (Figure 5.14).

Chaetochromin produced the lowest K_d, 3.8±1.6 µM, and therefore exhibited the tightest binding of all compounds tested using this method. At the higher concentrations it diminished the fluorescence intensity by approximately 90 %, whereas cynarin only elicited around a 50 % response with a larger K_d of 9.4±3.6 µM.

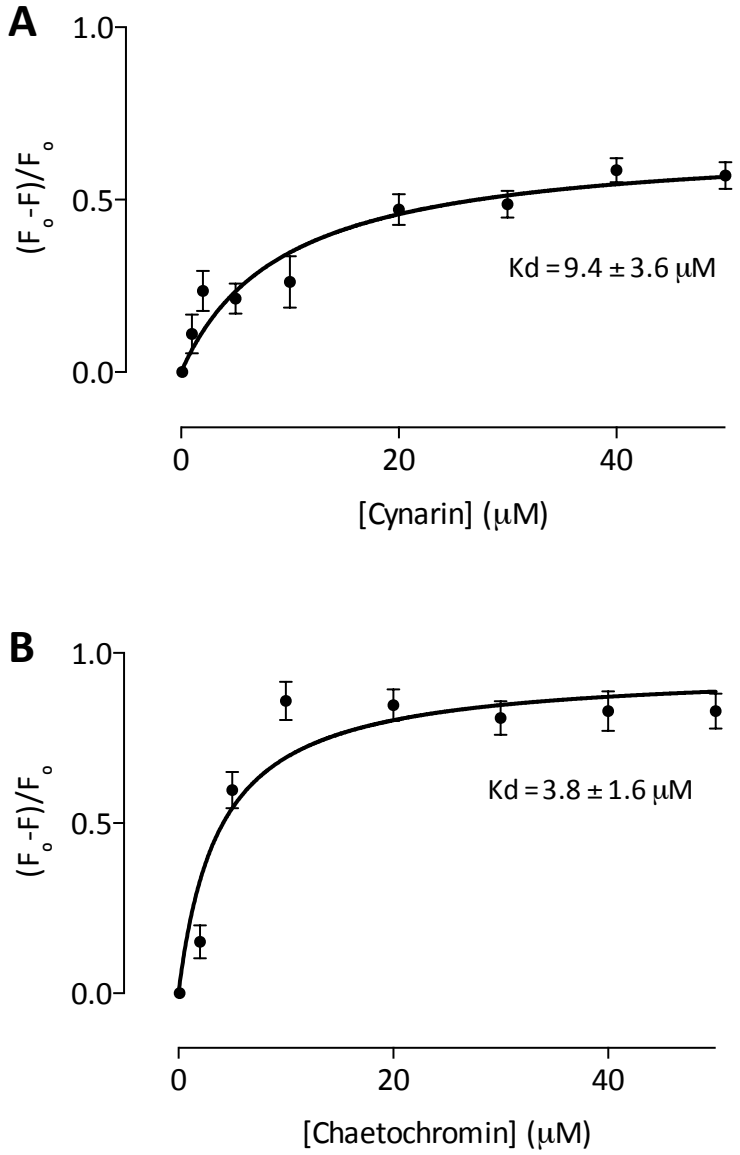

Figure 5.14 – Fractional change in the intrinsic fluorescence intensity of AtIPK1 upon binding compounds that were positive hits as potential inhibitors for AtIPK1 only from the diversity set II library. (A) Cynarin (B) Chaetochromin. Error bars show the standard errors in that data.

5.4.5 Inhibiting the kinase activity of AtIPK1 - coupled assay

A coupled enzyme assay was used to report the real time enzyme activity of AtIPK1 in the presence of purpurogallin. The coupled assay follows the loss in absorption of NADH at 340 nm when it is converted to NAD^+. Upon IP_5 phosphorylation, conversion of ATP to ADP occurs which is then used by pyruvate kinase (PK) to convert phosphoenolpyruvate (PEP) to pyruvate. The pyruvate is then converted to lactate by lactate dehydrogenase (LDH) using a hydrogen atom from NADH. The conversion of NADH to NAD^+ is representative of the turnover rate of ATP to ADP by AtIPK1, and the rate of reaction can be determined from the gradient of the initial (linear) loss of absorption (Δabs / Δtime (s)).

An example of this reaction is shown in Figure 5.15, in which the conversion of IP_5 to IP_6 is inhibited by the addition of 100 μM IP_6. The traces are normalised against a no AtIPK1 control. The gradient between 20 and 120 seconds for the non-inhibited reaction is 21.6 s^{-1} with the reaction going to completion by 150 seconds. In the presence of IP_6, the gradient is 11.2 s^{-1}.

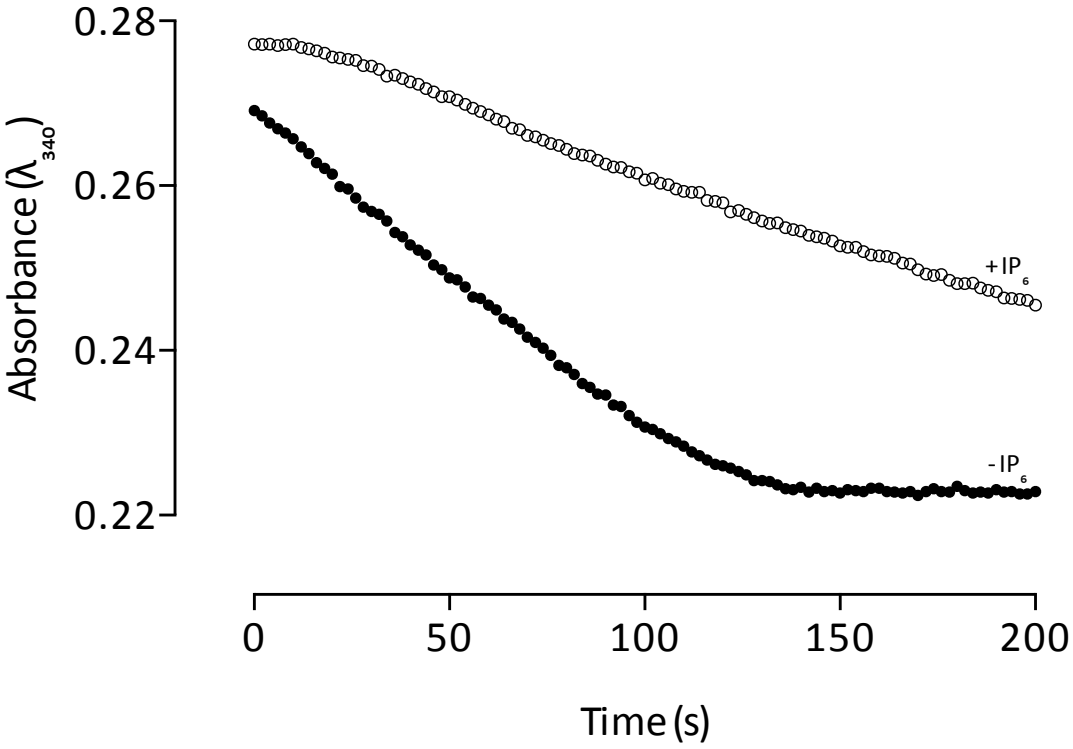

Figure 5.15 – Coupled enzyme assay; phosphorylation of inositol 1,3,4,5,6 pentakisphosphate by AtIPK1 and inhibition of phosphorylation by 100 µM IP_6.

Figure 5.16 shows preliminary data for the inhibition of AtIPK1 via this assay by increasing concentrations of purpurogallin. The calculated reaction rates were normalised by subtracting the inhibited rate from the rate of the non-inhibited reaction that was followed in tandem, and divided by the non-inhibited reaction to give a fractional change in reaction velocity. Upon increasing concentrations of purpurogallin the turnover of IP_5 to IP_6 by AtIPK1 is clearly inhibited, with the reaction being slowed by almost 60 % in the presence of 50 µM purpurogallin. Because in any measurement the 'inhibitor' concentration is constant, the slopes of the reaction curves are meaningful. Nevertheless, the extinction coefficient of purpurogallin at 340nm is approximately half that at 420 nm. These preliminary data provide further supporting evidence for purpurogallin being a positive inhibitor hit for AtIPK1.

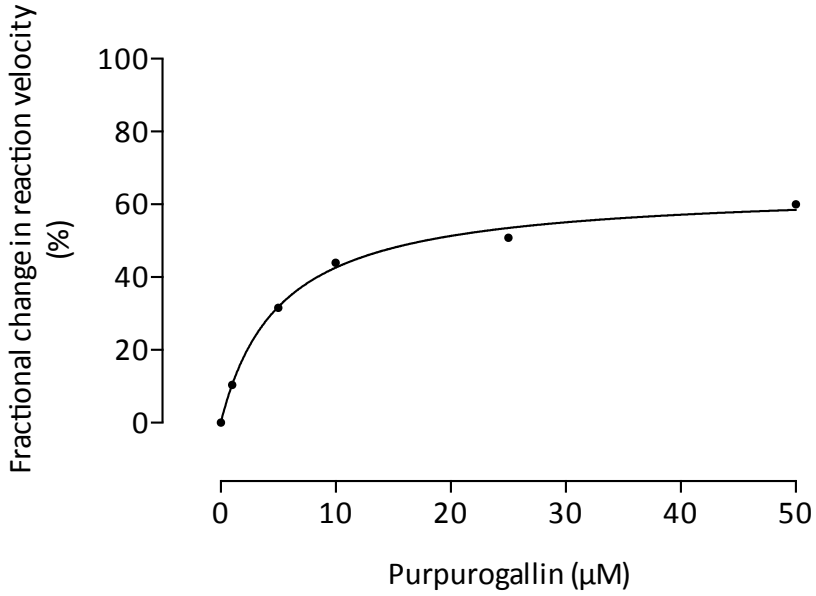

Figure 5.16 – Fractional change in velocity of the phosphorylation of inositol 1,3,4,5,6 pentakisphosphate by AtIPK1 upon increasing concentrations of purpurogallin.

5.4 Conclusions and future work

The experiments described in this chapter and chapter 4 demonstrate the utility of 2-FAM-IP_5 as an active site ligand of inositol phosphate-converting enzymes which are either inositol phosphate – nucleotide phosphotransferases (AtIPK1) or inositol phosphate 5-phosphatases (SHIP1cd and SHIP2cd). The latter belong to a family of 10 enzymes in humans that are the subject of considerable pharmaceutical interest (Blunt and Ward, 2012), and SHIP1 and SHIP2 share a conserved 5-phosphatase domain with the rest of the family; INPP5A, INPP5B, INPP5E, INPP5J, OCRL, SKIP, Synaptojanin 1 and Synaptojanin 2 (Ooms et al., 2009, McCrea and De Camilli, 2009). While the physiological substrates of these enzymes are not all clearly defined, some e.g., SHIP1 and SHIP2 which act physiologically on PtdIns(3,4,5)P_3 have become therapeutic targets, not least because of the restricted expression of SHIP1 in blood cell lineages (Hamilton et al., 2011). Because of the considerable therapeutic interest in phosphoinositide metabolising enzymes, there remains considerable interest in tools enabling identification of small molecules that influence the activity of specific enzymes (Blunt and Ward, 2012). These small molecules may represent modulators including inhibitors or activators, and may represent active site or allosteric modulators. Inhibitors and/or activators have been identified for SHIP1 and SHIP2, as well as for OCRL and the related enzyme INPP5B (Yang et al., 2005, Suwa et al., 2009, Brooks et al., 2010, Pirruccello et al., 2014).

The efficacy of inhibition or activation of these enzymes is commonly tested in assays which measure the ability of compounds to inhibit or activate the release of phosphate from a substrate in vitro. Phosphate is itself commonly measured using malachite green- or molybdate-based assays (Pirruccello et al, 2014). The same authors used an indirect polarisation based assay in which the action of 5-phosphatases on PtdIns(3,4,5)P_3 yield a PtIns(3,4)P_2 product which competes with a fluorescent PtdIns(3,4)P_2 for a post –reaction added binding protein. While such assays are readily performed on plate readers, they are end point assays which require stopping of reactions and subsequent additions of reagent before measurement.

In consideration of the search for allosteric modulators and irrespective of the mode of inhibition or activation of inositide- or phosphoinositide-metabolising enzymes, the efficacy of inhibitors or activators reflects binding and subsequent effect on the catalytic processing of bound inositide/phosphoinositide substrate. There remains opportunity and need for the development of assays which interrogate the binding of substrates, substrate analogs, inhibitors, and distal binding of allosteric regulators on enzymes.

The strategies identified here for high-throughput screening of ligand binding, whether substrate, substrate analog, inhibitor, activator or modulator, are relevant to inositide- and phosphoinositide-binding enzymes. More generally, these enzymes include inositide-kinases, inositide phosphotransferases, inositide phosphatases, phosphoinositide kinases and phosphoinositide phosphatases. The strategy revealed is likely applicable to enzymes which phosphorylate inositides and phosphoinositides at single or multiple positions and to enzymes which dephosphorylate inositides and phosphoinositides at single or multiple positions.

The identification of small molecules, approved oncology drugs, such as Bosutinib and Crozotinib, as ligands of SHIP1cd is intriguing. What is more remarkable is that both these compounds share with 3-α-aminocholestane (chapter 4), a known specific inhibitor of SHIP1cd, but not active on SHIP2. That all three ligands increase the affinity of SHIP1cd for 2-FAM-InsP_5, but not SHIP2 or AtIPK1, implies a potential common mechanism of modulation of SHIP1. That they increase the affinity for the polarisation probe suggests that they are not active site competitors, rather that they have an allosteric role. This observation is remarkable, particularly in light of the identification for pelorol (a natural compound isolated from the marine sponge Dactylospongia elegans) which exerts an allosteric role as an activator of SHIP1 catalytic activity. This allostery has been attributed to interaction with the C2 domain, not the catalytic domain (Yang et al., 2005), SHIP2 possesses a C2-domain but is not sensitive (Blunt and Ward, 2012). Derivatives of pelorol, include AQX-016A, AQX-MN100 and AQX-1125, which, produced by Aquinox Pharmaceuticals, have been taken forward to Phase II

clinical trials (Blunt and Ward, 2012). Interest in pelorol derivatives is current with other groups undertaking medicinal chemistry approaches. The identification here of catalytic domain–limited allostery of SHIP1, but not SHIP2, is fascinating. It remains to be tested whether Bosutinib and Crozotinib are inhibitors, like 3-α-aminocholestane, or are activators, like pelorol and its derivatives.

Chapter 6 – *Concluding Remarks*

6.1 *Cloning, purification and structures of the catalytic domains of SHIP1 and SHIP2*

The human SHIP proteins are amongst the 5-phosphatases responsible for the attention of signalling from activated Akt (PKB), and therefore they are implicated in many cell regulatory pathways that led to diseases such as cancers and diabetes (Kagawa et al., 2008, Yu et al., 2008). SHIP1 and SHIP2 are isoenzymes expressed in different cell types, and exhibit varying affinities and specificities (Ooms et al., 2009).

The catalytic mechanism of the 5-phosphatases is far from understood and only recently, on the basis of new structural data, there have been encouraging speculations on which conserved residues account for coordination of the scisscile bond (Mills et al., 2016).. In light of a structure of SHIP2cd in complex with biphenyl 2,3',4,5',6- pentakisphosphate (BiPh1) (Mills et al., 2102), attempts were made here at obtaining complexes with the rest of the benzene and biphenyl phosphates. Due to time constraints and the need for a refined purification method, SHIP1cd has not yet been subjected to crystallisation trials. Although, a successful ligation independent cloning method has been used to obtain overexpression of soluble recombinant protein for *in vitro* assays.

An apo-structure of SHIP2cd was obtained that was in agreement with those already published (Mills et al., 2012, Trésaugues et al., 2014). The P4IM-containing loop that has been postulated (by molecular dynamics) to close over the active site post inositide binding was constrained in the same position as described in the published structures confirming, in the lack of the ligand, that the loop is not essential for binding of BiPh1. SHIP1cd was subjected to structure prediction by use of the SWISS-MODEL homology-modelling server, which suggested the use of apo SHIP2 (PDB 3NR8) as a template. With this guidance in mind, modelling was undertaken using the SHIP2cd structure from the present study (chapter 2) as a template and resulted in a SHIP1cd structure similar to that of SHIP2cd, RMSD of 0.141. Small changes in this active site loop can be seen between the SHIP1cd model and the SHIP2cd structure, supporting the evidence for it being flexible and disordered. The homology modelling of SHIP1cd gives a loop of the same length (with similar numbers of residues) as in the SHIP2cd structure, as can be seen by

observing the secondary structure prediction by use of the ENDscript web server. There is, however, only 50% sequence identity in these secondary structure elements, again supporting the hypothesis that the P4IM-containing loop is not critical in ligand binding and can likely adjust to a variety of ligands interacting with the binding pocket. Moreover, although it is not the primary structural feature that anchors a ligand in to the active site, it is not unreasonable to hypothesise that the differences in substrate affinity between SHIP1cd and SHIP2cd could be accounted for by variations within this loop. Of course, without any available structures of SHIP1cd and considering the potential bias caused by homology-modelling, this is only speculation, therefore future efforts should concentrate on obtaining structures of SHIP1cd, or indeed the full length protein. As well as subjection of SHIP2cd to further crystallisation trails to explore conditions in which crystals with complexed protein can be obtained. Future efforts will be focused on the elucidation of the substrate specificities and mechanism of SHIP1, SHIP2 and the physiologically relevant 5-phosphatase family.

6.2 AtIPK1 in complex with large inositol phosphate surrogates insights large conformational changes

Previous to this study, structures have been obtained of AtIPK1 in complex with the single ringed benzene phosphates (unpublished data, Hayley Whitfield). Additionally, structures of the apo-protein (W129A mutant), nucleotide-bound (W129A mutant), and the ternary complex with nucleotide (ADP/ATP) and inositol polyphosphates (IP_6/IP_5), led to the characterisation of three conformational states; the open, half-closed and closed conformation, respectively (Banos-Sanz et al., 2012). The benzene and biphenyl phosphates have emerged as useful tools in both determining the specificity of an enzyme, since they can be designed to test various phosphate binding positions in an active site pocket, and in prospective design of inhibitors. This has led to the elucidation of the complexes with the biphenyl phosphates presented here. Complexes with BiPh(2,3',4,5',6)P_5 (BiPh1) and BiPh(3,3',4,4',5,5')P_6 (BiPh3) confirmed the importance of the P6 binding pocket that anchors all ligands into the active site. The ubiquitous occupation of this pocket across all structures suggests it is the primary determinant of binding orientation and forces the orientation of the biphenyl phosphate ligands to an almost perpendicular (orthogonal) pose compared to the benzene phosphates and canonical inositol phosphate substrates. Additionally, despite having a similar two ringed structure with only the phosphate substitutions to distinguish between them, they are bound in juxtaposed orientations because of the need for the P6 position to be satisfied.

The almost perpendicular mode of binding compared to previous structures has caused knock on conformational changes within AtIPK1. Overlaying the BiPh complexes with the defined conformational states from the literature revealed that the BiPh complexes are akin to the half-closed structure complexed with nucleotide alone, despite being ternary complexes. There are large conformational global changes occurring where the N- and C-lobes are further apart to accommodate the volume of the ligand, as well as more local changes. The distancing of the N-lobe (from the C-lobe) has the consequence that the BiPh is mostly coordinated by C-lobe residues with a key interaction missing from the N-lobe that is usually mediated by R130 in the closed form of the protein. The clasp that forms in the closed conformation of the protein has not been formed, L3 has not folded over the active site and α6 is disordered similar to the reported half-closed structure. In

absence of clasp formation, the protein remains in the half-closed form when accommodating a biphenyl polyphosphate rather than transitioning to the closed form. The greater size (volume) of the biphenyl polyphosphates and the different, relative to inositol, spatial positions of their phosphates are likely to preclude achievement of the closed form. Since, crystallisation screening has resulted in the collection of successful high quality data sets for complexes between AtIPK1 and BiPh2 / BiPh4, although the presence of compound in the inositide binding site has been confirmed the structures are not yet fully refined. Continued work is concentrating on elucidation of inhibitory characteristics of these compounds toward AtIPK1 to extract inhibition constants.

6.3 Revealing the fluorescent properties of the benzene- and biphenyl- phosphates, - substrates of SHIP1 and SHIP2.

As discussed, the benzene and biphenyl phosphates have been utilised in both enzymology and structural studies with inositol phosphate-binding enzymes, and are mostly reported as inhibitors (Mills et al., 2008, Vandeput et al., 2007, Mills et al., 2016, Swarbrick et al., 2015, Ward et al., 1995, Mills et al., 2007, Mills et al., 2012). One, however, was reported as an unusual substrate of type I Ins(1,4,5)P_3 5-phosphatase (INPP5A) (Mills et al., 2006).

Following discovery of the fluorescent properties of the biphenyl phosphates (chapter 4), assays were performed against SHIP1cd and SHIP2cd as alternative members of the 5-phosphatase family, for one of which there is a structure in complex with BiPh1, as discussed previously (Mills et al., 2012). The assays revealed firstly that biphenyl phosphate are substrates, and that the biphenyl phosphates provide a very sensitive method of detection via their fluorescent properties. Here, when resolved by anion exchange chromatography. Very little BiPh was required to gain a full time course of end-point reaction results, when compared to attempts at less sensitive real-time, enzyme-coupled, assays, which commonly require substrate inositol phosphate in the high tens of micromolar concentration. The use of these fluorescent BiPh substrates allowed the construction of progress of reaction curves. Both SHIP1 and SHIP2 were able to turn over all BiPh as visualised by a decrease in fluorescence of an hplc peak of parent compound. However, differing substrate specificities were revealed towards the BiPhs. Additionally,

new UV absorbant hplc peaks were visualised in the preliminary O/N only experiments, revealing the appearance of products of BiPh dephosphorylation. In the absence of partially dephosphorylated BiPhs as standards, it is not possible to identify the products. Nevertheless, these data provide compelling evidence that BiPhs are substrates of SHIP1 and SHIP2. Work in due course would likely focus on extracting enzymology constants of the turnover of these compounds by SHIP1cd and SHIP2cd, and subsequently data describing the inhibition of their turnover either by bone fide substrates and standard or potential inhibitors. As mentioned above, efforts will focus on the attainment of structural data in complex with these substrates. Additionally, site-directed mutagenesis of postulated key residues of the 5-phosphatases in substrate and inhibitor binding prior to subjection of this assay could reveal mechanisms of ligand binding and catalysis. The assays should also be tested on the fluorescent benzene phosphate compounds, of which there are two; benzene 1,2,4,5-tetrakisphosphate (Bz3) & benzene 1,2,4-trisphosphate (Bz5). These compounds are ever increasing in utility for the characterisation and structure elucidation of this family of enzymes.

6.4 A robust fluorescence polarisation assay to explore ligand binding and its application in high throughput screening for lead compounds

Large compound libraries are now available, often free of charge, to both private and academic sectors for the use in screening methods against proteins that are usually targets for therapeutic intervention. High throughput screening is one of the initial stages of lead compound discovery and is commonly used over partial rational design methods. The methods in which these screens are utilised in the search for dose-responses vary, but many consist of time consuming end-point assays, such as the malachite green phosphate release assay (Suwa et al., 2009). Fluorescently tagged inositol phosphates were used to explore the binding of inhibitors and the biphenyl phosphates to AtIPK1, SHIP1cd and SHIP2cd in fluorescence polarisation assays. Dose-reponse binding curves were constructed for binding of 2-FAM-IP_5 to SHIP1cd and SHIP2cd, and subsequently IC50s for displacement by BiPh ligands were obtained, again revealing the substrate specificities of SHIP1cd and SHIP2cd for the biphenyls that were in agreement with the anion exchange chromatography assays. The fluorescence polarisation method allowed

for the collection of large data sets, in 384-well plates with minimal errors associated. As all the enzymes in this study present various physiologically important roles, and a robust high throughput method was now available for probing the active sites of inositol phosphate-converting enzymes, they were subjected to two screens obtained from the NCI. Hits from the fluorescence polarisation screens that appeared in the separation band, were subjected to further investigation via completion of full dose-response inhibition curves.

Because of the availability of assays of AtIPK1 function developed already in the laboratory, compounds identifed to have effects in fluorescence polarisation screens were further tested on AtIPK1 for effect on intrinsic tryptophan fluorescence which has been shown to accompany conformational changes induced on substrate binding (Banos-Sanz et al., 2012). Additionally, hits identified in fluorescence polarisation screen were tested for effect on catalytic turnover using a coupled enzyme. One such compound that stood out from these assays was purpurogallin, which has subsequently been entered in to crystallisation trails with AtIPK1. A successful high resolution data set for co-crystallised purpurogallin and ADP has been collected since, and although there is no strong electron density for purpurogallin in the active site, structural perturbations suggest the presence of a ligand. In sumary, the fluorescence polarisation assay has produced a high throughput robust method for the discovery of novel inhibitors of inositol phosphate-binding proteins, and provides a proof of concept for the method rather than being approached from a strictly pharmacological point of view.

Appendices

Appendix 1 – Supplier addresses

Company	Location
Bio-Rad Laboratories Ltd	Hemel Hempstead, UK
BMG Labtech	Aylesbury, UK
Clontech	Saint-Germain-en-Laye, France
Corning	Amsterdam, The Netherlands
Dionex	Sunnyvale, USA
DNASU – Plasmid repository	Arizona, USA
Echelon	Utah, USA
Expedeon	Harston, UK
GE Healthcare Life Sciences	Little Chalfont, UK
Hidex	Turku, Finland
Invitrogen Ltd	Paisley, UK
Life technologies (Novex)	Paisley, UK
Melford Laboratories Ltd	Ipswich, UK
Merck Millipore	Billerica, USA
Molecular Devices	California, USA
MWG Eurofins	Ebersberg, Germany
National Cancer Institute	Maryland, USA
New England Biolabs Ltd (NEB)	Hitchin, UK
Promega	Southampton, UK
Qiagen	Crawley, UK
Sigma-Aldrich	Gillingham, UK
Source BioScience	Nottingham, UK
Thermo Scientific Ltd	Loughborough, UK

Appendix 2.1- Bacterial culture (For 1 L)

Luria-Bertani (LB) broth	10 g Tryptone 5 g Yeast extract 10 g NaCl
LB-Glucose (LB-G)	10 g Tryptone 5 g Yeast extract 10 g NaCl 5 g Glucose
LB-Agar	10 g Tryptone 5 g Yeast extract 10 g NaCl 15 g Agar
TB buffer	10 mM HEPES pH6.7 15 mM $CaCl_2$ 55 mM $MnCl_2$ 250 mM KCl

Appendix 2.2 –Antibiotics and Additives

Ampicillin	100 µg / mL
Kanamycin	50 µg /mL
Isopropyl β-D-1-thiogalactopyranoside (IPTG)	0.2 -0.4 mM

Appendix 2.3 – Buffers for protein purification

2.3.1 SHIP1 and SHIP2

Cell Lysis Buffer	20 mM HEPES pH 7.5 500 mM NaCl 10 mM Imidazole 10 % Glycerol 0.5 mM TCEP 0.5 % Triton
NiNTA Buffer A	20 mM HEPES pH 7.5 500 mM NaCl 25 mM Imidazole 10 % Glycerol 0.5 mM TCEP
NiNTA Buffer B	20 mM HEPES pH 7.5 500 mM NaCl 500 mM Imidazole 10 % Glycerol 0.5 mM TCEP
Sepharose Buffer (1)	20 mM Tris-HCl pH7.5 200 mM NaCl 2 mM DTT 10 % Glycerol (Add EDTA for tag cleavage buffer)
Sepharose (2) - For crystallograpghy	20 mM HEPES pH 7.5 300 mM NaCl 10 % Glycerol 0.5 mM TCEP

2.3.2 AtIPK1 (Also tried with SHIP1 – see results)

Cell Lysis Buffer	50 mM NaH_2PO_4 pH 7.5 300 mM NaCl 20 mM imidazole 0.5 % Triton
NiNTA Buffer A	50 mM NaH_2PO_4 pH7.5 300 mM NaCl 20 mM imidazole
NiNTA Buffer B	50 mM NaH_2PO_4 pH7.5 300 mM NaCl 500 mM imidazole
Sepharose Buffer	20 mM Tris-HCl pH7.5 200 mM NaCl 2 mM DTT

References

AFONINE, P. V., GROSSE-KUNSTLEVE, R. W. & ADAMS, P. D. 2005. A robust bulk-solvent correction and anisotropic scaling procedure. *Acta Crystallogr D Biol Crystallogr,* 61**,** 850-5.

ALCAZAR-ROMAN, A. R. & WENTE, S. R. 2008. Inositol polyphosphates: a new frontier for regulating gene expression. *Chromosoma,* 117**,** 1-13.

ALESSI, D. R., JAMES, S. R., DOWNES, C. P., HOLMES, A. B., GAFFNEY, P. R., REESE, C. B. & COHEN, P. 1997. Characterization of a 3-phosphoinositide-dependent protein kinase which phosphorylates and activates protein kinase Balpha. *Curr Biol,* 7**,** 261-9.

ANNIS, D. A., CHENG, C. C., CHUANG, C. C., MCCARTER, J. D., NASH, H. M., NAZEF, N., ROWE, T., KURZEJA, R. J. & SHIPPS, G. W., JR. 2009. Inhibitors of the lipid phosphatase SHIP2 discovered by high-throughput affinity selection-mass spectrometry screening of combinatorial libraries. *Comb Chem High Throughput Screen,* 12**,** 760-71.

ASTLE, M. V., HORAN, K. A., OOMS, L. M. & MITCHELL, C. A. 2007. The inositol polyphosphate 5-phosphatases: traffic controllers, waistline watchers and tumour suppressors? *Biochem Soc Symp***,** 161-81.

BACKERS, K., BLERO, D., PATERNOTTE, N., ZHANG, J. & ERNEUX, C. 2003. The termination of PI3K signalling by SHIP1 and SHIP2 inositol 5-phosphatases. *Adv Enzyme Regul,* 43**,** 15-28.

BAIN, J., PLATER, L., ELLIOTT, M., SHPIRO, N., HASTIE, C. J., MCLAUCHLAN, H., KLEVERNIC, I., ARTHUR, J. S., ALESSI, D. R. & COHEN, P. 2007. The selectivity of protein kinase inhibitors: a further update. *Biochem J,* 408**,** 297-315.

BANOS-SANZ, J. I., SANZ-APARICIO, J., WHITFIELD, H., HAMILTON, C., BREARLEY, C. A. & GONZALEZ, B. 2012. Conformational changes in inositol 1,3,4,5,6-pentakisphosphate 2-kinase upon substrate binding: role of N-terminal lobe and enantiomeric substrate preference. *J Biol Chem,* 287**,** 29237-49.

BLERO, D., DE SMEDT, F., PESESSE, X., PATERNOTTE, N., MOREAU, C., PAYRASTRE, B. & ERNEUX, C. 2001. The SH2 domain containing inositol 5-phosphatase SHIP2 controls phosphatidylinositol 3,4,5-trisphosphate levels in CHO-IR cells stimulated by insulin. *Biochem Biophys Res Commun,* 282**,** 839-43.

BLUNT, M. D. & WARD, S. G. 2012. Targeting PI3K isoforms and SHIP in the immune system: new therapeutics for inflammation and leukemia. *Curr Opin Pharmacol,* 12**,** 444-51.

BRAUWEILER, A., TAMIR, I., DAL PORTO, J., BENSCHOP, R. J., HELGASON, C. D., HUMPHRIES, R. K., FREED, J. H. & CAMBIER, J. C. 2000. Differential regulation of B cell development, activation, and death by the src homology 2 domain-containing 5' inositol phosphatase (SHIP). *J Exp Med,* 191**,** 1545-54.

BREARLEY, C. A. & HANKE, D. E. 1996. Metabolic evidence for the order of addition of individual phosphate esters in the myo-inositol moiety of inositol hexakisphosphate in the duckweed Spirodela polyrhiza L. *Biochem. J.,* 314**,** 227-233.

BROOKS, R., FUHLER, G. M., IYER, S., SMITH, M. J., PARK, M. Y., PARAISO, K. H., ENGELMAN, R. W. & KERR, W. G. 2010. SHIP1 inhibition increases immunoregulatory capacity and triggers apoptosis of hematopoietic cancer cells. *J Immunol,* 184**,** 3582-9.

CHEEK, S., GINALSKI, K., ZHANG, H. & GRISHIN, N. V. 2005. A comprehensive update of the sequence and structure classification of kinases. *BMC Struct Biol,* 5**,** 6.

CHEN, I. W. & CHARALAMPOUS, C. F. 1966. Biochemical studies on inositol. IX. D-Inositol 1-phosphate as intermediate in the biosynthesis of inositol from glucose 6-phosphate, and characteristics of two reactions in this biosynthesis. *J Biol Chem,* 241**,** 2194-9.

CHENG, K., WANG, X., ZHANG, S. & YIN, H. 2012. Discovery of Small-Molecule Inhibitors of the TLR1/TLR2 Complex. *Angewandte Chemie International Edition,* 51**,** 12246-12249.

CHENG, Y. & PRUSOFF, W. H. 1973. Relationship between the inhibition constant (K1) and the concentration of inhibitor which causes 50 per cent inhibition (I50) of an enzymatic reaction. *Biochem Pharmacol,* 22**,** 3099-108.

CHI, Y., ZHOU, B., WANG, W. Q., CHUNG, S. K., KWON, Y. U., AHN, Y. H., CHANG, Y. T., TSUJISHITA, Y., HURLEY, J. H. & ZHANG, Z. Y. 2004. Comparative mechanistic and substrate specificity study of inositol polyphosphate 5-phosphatase Schizosaccharomyces pombe Synaptojanin and SHIP2. *J Biol Chem,* 279**,** 44987-95.

CORTES, J. E., KANTARJIAN, H. M., BRUMMENDORF, T. H., KIM, D. W., TURKINA, A. G., SHEN, Z. X., PASQUINI, R., KHOURY, H. J., ARKIN, S., VOLKERT, A., BESSON, N., ABBAS, R., WANG, J., LEIP, E. & GAMBACORTI-PASSERINI, C. 2011. Safety and efficacy of bosutinib (SKI-606) in chronic phase Philadelphia chromosome-positive chronic myeloid leukemia patients with resistance or intolerance to imatinib. *Blood,* 118**,** 4567-76.

D'AMATO, R. J., LENTZSCH, S., ANDERSON, K. C. & ROGERS, M. S. 2001. Mechanism of action of thalidomide and 3-aminothalidomide in multiple myeloma. *Semin Oncol,* 28**,** 597-601.

D'AMATO, R. J., LOUGHNAN, M. S., FLYNN, E. & FOLKMAN, J. 1994. Thalidomide is an inhibitor of angiogenesis. *Proc Natl Acad Sci U S A,* 91**,** 4082-5.

DAMEN, J. E., LIU, L., ROSTEN, P., HUMPHRIES, R. K., JEFFERSON, A. B., MAJERUS, P. W. & KRYSTAL, G. 1996. The 145-kDa protein induced to associate with Shc by multiple cytokines is an inositol tetraphosphate and phosphatidylinositol 3,4,5-triphosphate 5-phosphatase. *Proc Natl Acad Sci U S A,* 93**,** 1689-93.

DING, Z., ROSSI, A. M., RILEY, A. M., RAHMAN, T., POTTER, B. V. & TAYLOR, C. W. 2010. Binding of inositol 1,4,5-trisphosphate (IP3) and adenophostin A to the N-terminal region of the IP3 receptor: thermodynamic analysis using fluorescence polarization with a novel IP3 receptor ligand. *Mol Pharmacol,* 77**,** 995-1004.

DONNELLY, M. I., ZHOU, M., MILLARD, C. S., CLANCY, S., STOLS, L., ESCHENFELDT, W. H., COLLART, F. R. & JOACHIMIAK, A. 2006. An expression vector tailored for large-scale, high-throughput purification of recombinant proteins. *Protein Expr Purif,* 47**,** 446-54.

DREES, B. E., WEIPERT, A., HUDSON, H., FERGUSON, C. G., CHAKRAVARTY, L. & PRESTWICH, G. D. 2003. Competitive fluorescence polarization assays for the detection of phosphoinositide kinase and phosphatase activity. *Comb Chem High Throughput Screen,* 6**,** 321-30.

EISENBERG, F., BOLDEN, A. H. & LOEWUS, F. A. 1964. Inositol formation by cyclization of glucose chain in rat testis. *Biochem Biophys Res Commun,* 14**,** 419-24.

EMSLEY, P., LOHKAMP, B., SCOTT, W. G. & COWTAN, K. 2010. Features and development of Coot. *Acta Crystallogr D Biol Crystallogr,* 66**,** 486-501.

ENGLISH, P. D., DIETZ, M. & ALBERSHEIM, P. 1966. Myoinositol kinase: partial purification and identification of product. *Science,* 151**,** 198-9.

ERAMO, M. J. & MITCHELL, C. A. 2016. Regulation of PtdIns(3,4,5)P3/Akt signalling by inositol polyphosphate 5-phosphatases. *Biochem Soc Trans,* 44**,** 240-52.

ERNEUX, C., EDIMO, W. E., DENEUBOURG, L. & PIRSON, I. 2011. SHIP2 multiple functions: a balance between a negative control of PtdIns(3,4,5)P(3) level, a positive control of PtdIns(3,4)P(2) production, and intrinsic docking properties. *J Cell Biochem,* 112**,** 2203-9.

ESCHENFELDT, W. H., LUCY, S., MILLARD, C. S., JOACHIMIAK, A. & MARK, I. D. 2009. A family of LIC vectors for high-throughput cloning and purification of proteins. *Methods Mol Biol,* 498**,** 105-15.

FIZAZI, K., LE MAITRE, A., HUDES, G., BERRY, W. R., KELLY, W. K., EYMARD, J. C., LOGOTHETIS, C. J., PIGNON, J. P. & MICHIELS, S. 2007. Addition of estramustine to chemotherapy and survival of patients with castration-refractory prostate cancer: a meta-analysis of individual patient data. *Lancet Oncol,* 8**,** 994-1000.

FORDE, P. M. & RUDIN, C. M. 2012. Crizotinib in the treatment of non-small-cell lung cancer. *Expert Opin Pharmacother,* 13**,** 1195-201.

FRECH, M., ANDJELKOVIC, M., INGLEY, E., REDDY, K. K., FALCK, J. R. & HEMMINGS, B. A. 1997. High affinity binding of inositol phosphates and phosphoinositides to the pleckstrin homology domain of RAC/protein kinase B and their influence on kinase activity. *J Biol Chem,* 272**,** 8474-81.

FUHLER, G. M., BROOKS, R., TOMS, B., IYER, S., GENGO, E. A., PARK, M. Y., GUMBLETON, M., VIERNES, D. R., CHISHOLM, J. D. & KERR, W. G. 2012. Therapeutic potential of SH2 domain-containing inositol-5'-phosphatase 1 (SHIP1) and SHIP2 inhibition in cancer. *Mol Med,* 18**,** 65-75.

GILEADI, O., BURGESS-BROWN, N. A., COLEBROOK, S. M., BERRIDGE, G., SAVITSKY, P., SMEE, C. E., LOPPNAU, P., JOHANSSON, C., SALAH, E. & PANTIC, N. H. 2008. High throughput production of recombinant human proteins for crystallography. *Methods Mol Biol,* 426**,** 221-46.

GONZÁLEZ, B., SCHELL, M. J., LETCHER, A. J., VEPRINTSEV, D. B., IRVINE, R. F. & WILLIAMS, R. L. 2004. Structure of a Human Inositol 1,4,5-Trisphosphate 3-Kinase: Substrate Binding Reveals Why It Is Not a Phosphoinositide 3-Kinase. *Molecular Cell,* 15**,** 689-701.

GOSEIN, V., LEUNG, T. F., KRAJDEN, O. & MILLER, G. J. 2012. Inositol phosphate-induced stabilization of inositol 1,3,4,5,6-pentakisphosphate 2-kinase and its role in substrate specificity. *Protein Sci,* 21**,** 737-42.

GOSEIN, V. & MILLER, G. J. 2013. Conformational stability of inositol 1,3,4,5,6-pentakisphosphate 2-kinase (IPK1) dictates its substrate selectivity. *J Biol Chem,* 288**,** 36788-95.

GOSEIN, V. & MILLER, G. J. 2013. Roles of phosphate recognition in inositol 1,3,4,5,6-pentakisphosphate 2-kinase (IPK1) substrate binding and activation. *J Biol Chem,* 288**,** 26908-13.

GRAF, E., EMPSON, K. L. & EATON, J. W. 1987. Phytic acid. A natural antioxidant. *J. Biol. Chem.,* 262**,** 1164-1150.

HAMILTON, M. J., HO, V. W., KURODA, E., RUSCHMANN, J., ANTIGNANO, F., LAM, V. & KRYSTAL, G. 2011. Role of SHIP in cancer. *Exp Hematol,* 39**,** 2-13.

HUGHES, J. P., REES, S., KALINDJIAN, S. B. & PHILPOTT, K. L. 2011. Principles of early drug discovery. *Br J Pharmacol,* 162**,** 1239-49.

ICHIHARA, Y., FUJIMURA, R., TSUNEKI, H., WADA, T., OKAMOTO, K., GOUDA, H., HIRONO, S., SUGIMOTO, K., MATSUYA, Y., SASAOKA, T. & TOYOOKA, N. 2013. Rational design and synthesis of 4-substituted 2-pyridin-2-ylamides with inhibitory effects on SH2 domain-containing inositol 5'-phosphatase 2 (SHIP2). *Eur J Med Chem,* 62**,** 649-60.

IRVINE, R. F. 2003. Nuclear lipid signalling. *Nat Rev Mol Cell Biol,* 4**,** 349-60.

IRVINE, R. F. 2005. Inositide evolution - towards turtle domination? *The Journal of physiology,* 566**,** 295-300.

IRVINE, R. F. & SCHELL, M. J. 2001. Back in the water: the return of the inositol phosphates. *Nat Rev Mol Cell Biol,* 2**,** 327-38.

IVES, E. B., NICHOLS, J., WENTE, S. R. & YORK, J. D. 2000. Biochemical and Functional Characterization of Inositol 1,3,4,5,6-Pentakisphosphate 2-Kinases. *Journal of Biological Chemistry,* 275**,** 36575-36583.

KAGAWA, S., SOEDA, Y., ISHIHARA, H., OYA, T., SASAHARA, M., YAGUCHI, S., OSHITA, R., WADA, T., TSUNEKI, H. & SASAOKA, T. 2008. Impact of transgenic overexpression of SH2-containing inositol 5'-phosphatase 2 on glucose metabolism and insulin signaling in mice. *Endocrinology,* 149**,** 642-50.

LAMBERT, J. D., CHEN, D., WANG, C. Y., AI, N., SANG, S., HO, C.-T., WELSH, W. J. & YANG, C. S. 2005. Benzotropolone inhibitors of estradiol methylation: kinetics and in silico modeling studies. *Bioorganic & Medicinal Chemistry,* 13**,** 2501-2507.

LEE, Y. C. & BALLOU, C. E. 1964. Structural Studies on the Myo-Inositol Mannodides from the Glycolipids of Mycobacterium Tuberculosis and Mycobacterium Phlei. *J Biol Chem,* 239**,** 1316-27.

LEUNG, W. H., TARASENKO, T. & BOLLAND, S. 2009. Differential roles for the inositol phosphatase SHIP in the regulation of macrophages and lymphocytes. *Immunol Res,* 43**,** 243-51.

LIOUBIN, M. N., ALGATE, P. A., TSAI, S., CARLBERG, K., AEBERSOLD, A. & ROHRSCHNEIDER, L. R. 1996. p150Ship, a signal transduction molecule with inositol polyphosphate-5-phosphatase activity. *Genes Dev,* 10**,** 1084-95.

LIPINSKI, C. A. 2004. Lead- and drug-like compounds: the rule-of-five revolution. *Drug Discovery Today: Technologies,* 1**,** 337-341.

LIPINSKI, C. A., LOMBARDO, F., DOMINY, B. W. & FEENEY, P. J. 2001. Experimental and computational approaches to estimate solubility and permeability in drug discovery and development settings. *Adv Drug Deliv Rev,* 46**,** 3-26.

LOEWUS, M. W. & LOEWUS, F. A. 1980. The C-5 hydrogen isotope-effect in myo-inositol 1-phosphate synthase as evidence for the myo-inositol oxidation-pathway. *Carbohydr Res,* 82**,** 333-42.

LOEWUS, M. W., LOEWUS, F. A., BRILLINGER, G. U., OTSUKA, H. & FLOSS, H. G. 1980. Stereochemistry of the myo-inositol-1-phosphate synthase reaction. *J Biol Chem,* 255**,** 11710-2.

LOEWUS, M. W., SASAKI, K., LEAVITT, A. L., MUNSELL, L., SHERMAN, W. R. & LOEWUS, F. A. 1982. Enantiomeric Form of myo-Inositol-1-Phosphate Produced by myo-Inositol-1-Phosphate Synthase and myo-Inositol Kinase in Higher Plants. *Plant Physiol,* 70**,** 1661-3.

MAJERUS, P. W. & YORK, J. D. 2009. Phosphoinositide phosphatases and disease. *J Lipid Res,* 50 Suppl**,** S249-54.

MANERBA, M., DI IANNI, L., GOVONI, M., ROBERTI, M., RECANATINI, M. & DI STEFANO, G. 2016. Lactate dehydrogenase inhibitors can reverse inflammation induced changes in colon cancer cells. *Eur J Pharm Sci*.

MANNING, B. D. & CANTLEY, L. C. 2007. AKT/PKB signaling: navigating downstream. *Cell,* 129**,** 1261-74.

MARTIN, M. P., ALAM, R., BETZI, S., INGLES, D. J., ZHU, J. Y. & SCHONBRUNN, E. 2012. A novel approach to the discovery of small-molecule ligands of CDK2. *Chembiochem,* 13**,** 2128-36.

MCCOY, A. J. 2007. Solving structures of protein complexes by molecular replacement with Phaser. *Acta Crystallogr D Biol Crystallogr,* 63**,** 32-41.

MCCREA, H. J. & DE CAMILLI, P. 2009. Mutations in phosphoinositide metabolizing enzymes and human disease. *Physiology (Bethesda),* 24**,** 8-16.

MICHELL, R. H. 2009. First came the link between phosphoinositides and Ca2+ signalling, and then a deluge of other phosphoinositide functions. *Cell Calcium,* 45**,** 521-6.

MICHELL, R. H. 2011. Inositol and its derivatives: their evolution and functions. *Adv Enzyme Regul,* 51**,** 84-90.

MILLER, G. J. & HURLEY, J. H. 2004. Crystal Structure of the Catalytic Core of Inositol 1,4,5-Trisphosphate 3-Kinase. *Molecular Cell,* 15**,** 703-711.

MILLER, G. J., WILSON, M. P., MAJERUS, P. W. & HURLEY, J. H. 2005. Specificity Determinants in Inositol Polyphosphate Synthesis: Crystal Structure of Inositol 1,3,4-Trisphosphate 5/6-Kinase. *Molecular Cell,* 18**,** 201-212.

MILLS, S. J., DOZOL, H., VANDEPUT, F., BACKERS, K., WOODMAN, T., ERNEUX, C., SPIESS, B. & POTTER, B. V. 2006. 3-hydroxybenzene 1,2,4-trisphosphate, a novel second messenger mimic and unusual substrate for type-I myo-inositol 1,4,5-trisphosphate 5-phosphatase: Synthesis and physicochemistry. *Chembiochem,* 7**,** 1696-706.

MILLS, S. J., KOMANDER, D., TRUSSELLE, M. N., SAFRANY, S. T., VAN AALTEN, D. M. & POTTER, B. V. 2007. Novel inositol phospholipid headgroup surrogate crystallized in the pleckstrin homology domain of protein kinase Balpha. *ACS Chem Biol,* 2**,** 242-6.

MILLS, S. J., PERSSON, C., COZIER, G., THOMAS, M. P., TRESAUGUES, L., ERNEUX, C., RILEY, A. M., NORDLUND, P. & POTTER, B. V. 2012. A synthetic polyphosphoinositide headgroup surrogate in complex with SHIP2 provides a rationale for drug discovery. *ACS Chem Biol,* 7**,** 822-8.

MILLS, S. J., SILVANDER, C., COZIER, G., TRESAUGUES, L., NORDLUND, P. & POTTER, B. V. 2016. Crystal Structures of Type-II Inositol Polyphosphate 5-Phosphatase INPP5B with Synthetic Inositol Polyphosphate Surrogates Reveal New Mechanistic Insights for the Inositol 5-Phosphatase Family. *Biochemistry,* 55**,** 1384-97.

MILLS, S. J., VANDEPUT, F., TRUSSELLE, M. N., SAFRANY, S. T., ERNEUX, C. & POTTER, B. V. 2008. Benzene polyphosphates as tools for cell signalling: inhibition of inositol 1,4,5-trisphosphate 5-phosphatase and interaction with the PH domain of protein kinase Balpha. *Chembiochem,* 9**,** 1757-66.

MONDAL, S., SUBRAMANIAN, K. K., SAKAI, J., BAJRAMI, B. & LUO, H. R. 2012. Phosphoinositide lipid phosphatase SHIP1 and PTEN coordinate to regulate cell migration and adhesion. *Molecular Biology of the Cell,* 23**,** 1219-1230.

MOULT, J., FIDELIS, K., KRYSHTAFOVYCH, A., SCHWEDE, T. & TRAMONTANO, A. 2014. Critical assessment of methods of protein structure prediction (CASP)--round x. *Proteins,* 82 Suppl 2**,** 1-6.

NAGY, R., GROB, H., WEDER, B., GREEN, P., KLEIN, M., FRELET-BARRAND, A., SCHJOERRING, J. K., BREARLEY, C. & MARTINOIA, E. 2009. The Arabidopsis ATP-binding Cassette Protein AtMRP5/AtABCC5 Is a High Affinity Inositol Hexakisphosphate Transporter Involved in Guard Cell Signaling and Phytate Storage. *The Journal of Biological Chemistry,* 284**,** 33614-33622.

ODOM, A. R., STAHLBERG, A., WENTE, S. R. & YORK, J. D. 2000. A role for nuclear inositol 1,4,5-trisphosphate kinase in transcriptional control. *Science,* 287**,** 2026-2029.

ONG, C. J., MING-LUM, A., NODWELL, M., GHANIPOUR, A., YANG, L., WILLIAMS, D. E., KIM, J., DEMIRJIAN, L., QASIMI, P., RUSCHMANN, J., CAO, L. P., MA, K., CHUNG, S. W., DURONIO, V., ANDERSEN, R. J., KRYSTAL, G. & MUI, A. L. 2007. Small-molecule agonists of SHIP1 inhibit the phosphoinositide 3-kinase pathway in hematopoietic cells. *Blood,* 110**,** 1942-9.

ONGUSAHA, P. P., HUGHES, P. J., DAVEY, J. & MICHELL, R. H. 1998. Inositol hexakisphosphate in Schizosaccharomyces pombe: synthesis from Ins(1,4,5)P3 and osmotic regulation. *Biochem J,* 335 (Pt 3)**,** 671-9.

ONRUST, S. V. & LAMB, H. M. 1999. Valrubicin. *Drugs Aging,* 15**,** 69-75; discussion 76.

PARRY, R. V., HARRIS, S. J. & WARD, S. G. 2010. Fine tuning T lymphocytes: a role for the lipid phosphatase SHIP-1. *Biochim Biophys Acta,* 1804**,** 592-7.

PERRY, C. M. & MCTAVISH, D. 1995. Estramustine phosphate sodium. A review of its pharmacodynamic and pharmacokinetic properties, and therapeutic efficacy in prostate cancer. *Drugs Aging,* 7**,** 49-74.

PESESSE, X., MOREAU, C., DRAYER, A. L., WOSCHOLSKI, R., PARKER, P. & ERNEUX, C. 1998. The SH2 domain containing inositol 5-phosphatase SHIP2 displays phosphatidylinositol 3,4,5-trisphosphate and inositol 1,3,4,5-tetrakisphosphate 5-phosphatase activity. *FEBS Lett,* 437**,** 301-3.

PIRRUCCELLO, M., NANDEZ, R., IDEVALL-HAGREN, O., ALCAZAR-ROMAN, A., ABRIOLA, L., BERWICK, S. A., LUCAST, L., MOREL, D. & DE CAMILLI, P. 2014. Identification of inhibitors of inositol 5-phosphatases through multiple screening strategies. *ACS Chem Biol,* 9**,** 1359-68.

POITRAS, M., BERNIER, S., BOULAY, G., FOURNIER, A. & GUILLEMETTE, G. 1993. Interaction of benzene 1,2,4-trisphosphate with inositol 1,4,5-trisphosphate receptor and metabolizing enzymes. *Eur J Pharmacol,* 244**,** 203-10.

RABOY, V. 2001. Seeds for a better future: 'low phytate' grains help to overcome malnutrition and reduce pollution. *Trends Plant Sci,* 6**,** 458-62.

RABOY, V. 2003. myo-Inositol-1,2,3,4,5,6-hexakisphosphate. *Phytochemistry,* 64**,** 1033-43.

RASMUSSEN, T. D., GUERRA, B. & ISSINGER, O.-G. 2015. Screening of DTP Compound Libraries for CK2 Inhibitors with Focus on Natural Products. *In:* AHMED, K., ISSINGER, O.-G. & SZYSZKA, R. (eds.) *Protein Kinase CK2 Cellular Function in Normal and Disease States.* Cham: Springer International Publishing.

RILEY, A. M., WINDHORST, S., LIN, H. Y. & POTTER, B. V. 2014. Cellular internalisation of an inositol phosphate visualised by using fluorescent InsP5. *Chembiochem,* 15**,** 57-67.

SAIARDI, A., ERDJUMENT-BROMAGE, H., SNOWMAN, A. M., TEMPST, P. & SNYDER, S. H. 1999. Synthesis of diphosphoinositol pentakisphosphate by a newly identified family of higher inositol polyphosphate kinases. *Curr. Biol.,* 9**,** 1323-1326.

SARBASSOV, D. D., GUERTIN, D. A., ALI, S. M. & SABATINI, D. M. 2005. Phosphorylation and regulation of Akt/PKB by the rictor-mTOR complex. *Science,* 307**,** 1098-101.

SAVITSKY, P., BRAY, J., COOPER, C. D., MARSDEN, B. D., MAHAJAN, P., BURGESS-BROWN, N. A. & GILEADI, O. 2010. High-throughput production of human proteins for crystallization: the SGC experience. *J Struct Biol,* 172**,** 3-13.

SHERMAN, W. R., STEWART, M. A. & ZINBO, M. 1969. Mass spectrometric study on the mechanism of D-glucose 6-phosphate-L-myo-inositol 1-phosphate cyclase. *J Biol Chem,* 244**,** 5703-8.

SIMPSON, D. & WAGSTAFF, A. J. 2003. Estramustine Phosphate Sodium. *American Journal of Cancer,* 2**,** 373-390.

SLEEMAN, M. W., WORTLEY, K. E., LAI, K. M., GOWEN, L. C., KINTNER, J., KLINE, W. O., GARCIA, K., STITT, T. N., YANCOPOULOS, G. D., WIEGAND, S. J. & GLASS, D. J. 2005. Absence of the lipid phosphatase SHIP2 confers resistance to dietary obesity. *Nat Med,* 11**,** 199-205.

STEPHENS, L. R., HAWKINS, P. T., STANLEY, A. F., MOORE, T., POYNER, D. R., MORRIS, P. J., HANLEY, M. R., KAY, R. R. & IRVINE, R. F. 1991. myo-inositol pentakisphosphates. Structure, biological occurrence and phosphorylation to myo-inositol hexakisphosphate. *Biochem J,* 275 (Pt 2)**,** 485-99.

STEPHENS, L. R. & IRVINE, R. F. 1990. Stepwise phosphorylation of myo-inositol leading to myo-inositol hexakisphosphate in Dictyostelium. *Nature,* 346**,** 580-583.

STEVENSON-PAULIK, J., BASTIDAS, R. J., CHIOU, S.-T., FRYE, R. A. & YORK, J. D. 2005. Generation of phytate-free seeds in Arabidopsis through disruption of inositol polyphosphate kinases. *Proceedings of the National Academy of Sciences of the United States of America,* 102**,** 12612-12617.

SUN, Y., THOMPSON, M., LIN, G., BUTLER, H., GAO, Z., THORNBURGH, S., YAU, K., SMITH, D. A. & SHUKLA, V. K. 2007. Inositol 1,3,4,5,6-Pentakisphosphate 2-Kinase from Maize: Molecular and Biochemical Characterization. *Plant Physiology,* 144**,** 1278-1291.

SUWA, A., KURAMA, T., YAMAMOTO, T., SAWADA, A., SHIMOKAWA, T. & ARAMORI, I. 2010. Glucose metabolism activation by SHIP2 inhibitors via up-regulation of GLUT1 gene in L6 myotubes. *European Journal of Pharmacology,* 642**,** 177-182.

SUWA, A., YAMAMOTO, T., SAWADA, A., MINOURA, K., HOSOGAI, N., TAHARA, A., KURAMA, T., SHIMOKAWA, T. & ARAMORI, I. 2009. Discovery and functional characterization of a novel small molecule inhibitor of the intracellular phosphatase, SHIP2. *Br J Pharmacol,* 158**,** 879-87.

SWARBRICK, J. M., RILEY, A. M., MILLS, S. J. & POTTER, B. V. 2015. Designer small molecules to target calcium signalling. *Biochem Soc Trans,* 43**,** 417-25.

SWEETMAN, D., JOHNSON, S., CADDICK, SAMUEL E K., HANKE, DAVID E. & BREARLEY, CHARLES A. 2006. Characterization of an Arabidopsis inositol 1,3,4,5,6-pentakisphosphate 2-kinase (AtIPK1). *Biochemical Journal,* 394**,** 95-103.

TOPAL, M., GOCER, H., TOPAL, F., KALIN, P., KOSE, L. P., GULCIN, I., CAKMAK, K. C., KUCUK, M., DURMAZ, L., GOREN, A. C. & ALWASEL, S. H. 2016. Antioxidant, antiradical, and anticholinergic properties of cynarin purified from the Illyrian thistle (Onopordum illyricum L.). *J Enzyme Inhib Med Chem,* 31**,** 266-75.

TRÉSAUGUES, L., SILVANDER, C., FLODIN, S., WELIN, M., NYMAN, T., GRÄSLUND, S., HAMMARSTRÖM, M., BERGLUND, H. & NORDLUND, P. 2014. Structural Basis for Phosphoinositide Substrate Recognition, Catalysis, and Membrane Interactions in Human Inositol Polyphosphate 5-Phosphatases. *Structure,* 22**,** 744-755.

TSUJISHITA, Y., GUO, S., STOLZ, L. E., YORK, J. D. & HURLEY, J. H. 2001. Specificity determinants in phosphoinositide dephosphorylation: crystal structure of an archetypal inositol polyphosphate 5-phosphatase. *Cell,* 105**,** 379-89.

TURNER, B. L., CHEESMAN, A. W., GODAGE, H. Y., RILEY, A. M. & POTTER, B. V. 2012. Determination of neo- and D-chiro-inositol hexakisphosphate in soils by solution 31P NMR spectroscopy. *Environ Sci Technol,* 46**,** 4994-5002.

VANDEPUT, F., COMBETTES, L., MILLS, S. J., BACKERS, K., WOHLKONIG, A., PARYS, J. B., DE SMEDT, H., MISSIAEN, L., DUPONT, G., POTTER, B. V. & ERNEUX, C. 2007. Biphenyl 2,3',4,5',6-pentakisphosphate, a novel inositol polyphosphate surrogate, modulates Ca2+ responses in rat hepatocytes. *FASEB J,* 21**,** 1481-91.

VERBSKY, J. W., WILSON, M. P., KISSELEVA, M. V., MAJERUS, P. W. & WENTE, S. R. 2002. The Synthesis of Inositol Hexakisphosphate: CHARACTERIZATION OF HUMAN INOSITOL 1,3,4,5,6-PENTAKISPHOSPHATE 2-KINASE. *Journal of Biological Chemistry,* 277**,** 31857-31862.

VULTUR, A., BUETTNER, R., KOWOLIK, C., LIANG, W., SMITH, D., BOSCHELLI, F. & JOVE, R. 2008. SKI-606 (bosutinib), a novel Src kinase inhibitor, suppresses migration and invasion of human breast cancer cells. *Mol Cancer Ther,* 7**,** 1185-94.

WADA, T., SASAOKA, T., FUNAKI, M., HORI, H., MURAKAMI, S., ISHIKI, M., HARUTA, T., ASANO, T., OGAWA, W., ISHIHARA, H. & KOBAYASHI, M. 2001. Overexpression of SH2-containing inositol phosphatase 2 results in negative regulation of insulin-induced metabolic actions in 3T3-L1 adipocytes via its 5'-phosphatase catalytic activity. *Mol Cell Biol,* 21**,** 1633-46.

WANG, H., GODAGE, H. Y., RILEY, A. M., WEAVER, J. D., SHEARS, S. B. & POTTER, B. V. 2014. Synthetic inositol phosphate analogs reveal that PPIP5K2 has a surface-mounted substrate capture site that is a target for drug discovery. *Chem Biol,* 21**,** 689-99.

WANG, Q., YANG, Z., ZHANG, X., XIAO, X., CHANG, C. K. & XU, B. 2007. A supramolecular-hydrogel-encapsulated hemin as an artificial enzyme to mimic peroxidase. *Angew Chem Int Ed Engl,* 46**,** 4285-9.

WARD, S. G., MILLS, S. J., LIU, C., WESTWICK, J. & POTTER, B. V. 1995. D-myo-inositol 1,4,5-trisphosphate analogues modified at the 3-position inhibit phosphatidylinositol 3-kinase. *J Biol Chem,* 270**,** 12075-84.

WATSON, P. J., MILLARD, C. J., RILEY, A. M., ROBERTSON, N. S., WRIGHT, L. C., GODAGE, H. Y., COWLEY, S. M., JAMIESON, A. G., POTTER, B. V. & SCHWABE, J. W. 2016. Insights into the activation mechanism of class I HDAC complexes by inositol phosphates. *Nat Commun,* 7**,** 11262.

WILKINS, M. R., GASTEIGER, E., BAIROCH, A., SANCHEZ, J. C., WILLIAMS, K. L., APPEL, R. D. & HOCHSTRASSER, D. F. 1999. Protein identification and analysis tools in the ExPASy server. *Methods Mol Biol,* 112**,** 531-52.

WU, T.-W., ZENG, L.-H., WU, J., FUNG, K.-P., WEISEL, R. D., HEMPEL, A. & CAMERMAN, N. 1996. Molecular structure and antioxidant specificity of purpurogallin in three types of human cardiovascular cells. *Biochemical Pharmacology,* 52**,** 1073-1080.

YANG, L., WILLIAMS, D. E., MUI, A., ONG, C., KRYSTAL, G., VAN SOEST, R. & ANDERSEN, R. J. 2005. Synthesis of pelorol and analogues: activators of the inositol 5-phosphatase SHIP. *Org Lett,* 7**,** 1073-6.

YORK, J. D. 2006. Regulation of nuclear processes by inositol polyphosphates. *Biochim Biophys Acta,* 1761**,** 552-9.

YORK, J. D., ODOM, A. R., MURPHY, R., IVES, E. B. & WENTE, S. R. 1999. A Phospholipase C-Dependent Inositol Polyphosphate Kinase Pathway Required for Efficient Messenger RNA Export. *Science,* 285**,** 96-100.

YU, J., RYAN, D. G., GETSIOS, S., OLIVEIRA-FERNANDES, M., FATIMA, A. & LAVKER, R. M. 2008. MicroRNA-184 antagonizes microRNA-205 to maintain SHIP2 levels in epithelia. *Proc Natl Acad Sci U S A,* 105**,** 19300-5.

YUAN, F.-J., ZHAO, H.-J., REN, X.-L., ZHU, S.-L., FU, X.-J. & SHU, Q.-Y. 2007. Generation and characterization of two novel low phytate mutations in soybean (Glycine max L. Merr.). *Theoretical and Applied Genetics,* 115**,** 945-957.

YUAN, F.-J., ZHU, D.-H., TAN, Y.-Y., DONG, D.-K., FU, X.-J., ZHU, S.-L., LI, B.-Q. & SHU, Q.-Y. 2012. Identification and characterization of the soybean IPK1 ortholog of a low phytic acid mutant reveals an exon-excluding splice-site mutation. *Theoretical and Applied Genetics,* 125**,** 1413-1423.

ZHANG, J., YANG, P. L. & GRAY, N. S. 2009. Targeting cancer with small molecule kinase inhibitors. *Nat Rev Cancer,* 9**,** 28-39.

ZHANG, J. H., CHUNG, T. D. & OLDENBURG, K. R. 1999. A Simple Statistical Parameter for Use in Evaluation and Validation of High Throughput Screening Assays. *J Biomol Screen,* 4**,** 67-73.